METABOLIC REPROGRAMMING SUPPORTS MICROGLIAL SURVIVAL AND IMMUNE FUNCTION

by

Elisa York

B.Sc., University of Western Ontario, 2012

A THESIS SUBMITTED IN PARTIAL FULFILLMENT OF

THE REQUIREMENTS FOR THE DEGREE OF

DOCTOR OF PHILOSOPHY

in

THE FACULTY OF GRADUATE AND POSTDOCTORAL STUDIES

(Neuroscience)

THE UNIVERSITY OF BRITISH COLUMBIA

(Vancouver)

June 2019

© Elisa York, 2019

The following individuals certify that they have read, and recommend to the Faculty of Graduate and Postdoctoral Studies for acceptance, the dissertation entitled:

Metabolic reprogramming supports microglial survival and immune function

submitted by Elisa York in partial fulfillment of the requirements for

the degree of Doctor of philosophy

in Neuroscience

Examining Committee:

Dr. Brian MacVicar
Supervisor

Dr. Lynn Raymond
Supervisory Committee Member

Dr. Catharine Winstanley
University Examiner

Dr. Robert Nabi
University Examiner

Additional Supervisory Committee Members:

Dr. Cheryl Wellington
Supervisory Committee Member

Dr. James Johnson
Supervisory Committee Member

Abstract

In addition to energy production, metabolic pathways, such as glycolysis and mitochondrial metabolism, are important in regulating peripheral immune cell activity. This thesis examines whether cellular metabolism also regulates the immunological functions of microglia, the brain's resident immune cells. The metabolic and anatomical complexity of the brain provides unique challenges for these studies, which required the development of two new methodological approaches. The first, 3DMorph, allows automatic and unbiased quantification of microglial morphology in three dimensions, improving the efficiency, accuracy, and reproducibility of microglial morphology analyses. The second establishes the use of fluorescence lifetime imaging of endogenous nicotinamide adenine dinucleotide (NADH-FLIM) within single microglia of acute hippocampal slices. This work demonstrates that GFP exhibits blue emission with short fluorescence lifetimes, which contaminates the metabolic signal, and alternatively validates microglial identification using tomato lectin to allow metabolic measurements by NADH-FLIM *in situ*.

Using these techniques, microglial metabolism was investigated at baseline, as was their metabolic flexibility following nutrient depletion. Relative to the surrounding neuropil, microglia are highly glycolytic in control conditions. However, upon removal of glucose, microglial glutaminolysis is sufficient to support mitochondrial metabolism, cell viability, and immune surveillance. This flexibility may permit microglial survival and function during metabolic perturbations, such as stroke or hypoglycemia. Changes in cellular metabolism also regulated microglial immune activity. Lipopolysaccharide (LPS) application to acute hippocampal slices triggered an increase

in microglial glycolysis, which was inhibited by co-incubation with 2-deoxy-D-glucose (2DG), a glycolysis inhibitor. LPS stimulation also increased production of the pro-inflammatory cytokines IL-1β and TNFα. LPS-induced production of these cytokines was decreased in the presence of 2DG, confirming a role for glycolysis in regulating microglial immune function.

These data indicate that microglia exhibit remarkable metabolic flexibility that exceeds the ability of neurons. In addition, the activity of metabolic pathways impacts microglial immune function by altering IL-1β and TNFα production. The microglial morphology and metabolism tools presented here will continue to provide insights into metabolic signals regulating brain immune function. Both microglial and metabolic dysregulation are implicated in neurodegeneration following trauma or disease, making metabolic manipulations for therapeutic intervention or disease prevention a promising area of study.

Lay Summary

The brain's environment is kept separate from the body's by a tightly regulated blood-brain barrier, which excludes cells of the immune system from entering brain tissue. To protect itself, the brain has its own immune system, made of a group of cells called microglia. In immune cells of the body, cellular metabolism (whether the cells burn sugars, proteins, or fats for energy) can control if these cells become inflammatory. We show that microglia preferentially consume sugar, but surprisingly, when sugar is removed, microglia are flexible in their nutrient choice and instead rely on protein. Like the body's immune system, microglia are regulated by the nutrients they consume, and preventing these cells from burning sugar also prevents their immune activation. These findings will be important in understanding, and potentially treating, brain damage or neurodegenerative diseases, as these are conditions where cellular metabolism and microglial activity have gone awry.

Preface

The work presented in Chapter 2 was designed with input from Dr. Brian MacVicar and Jeffrey LeDue. I performed all MATLAB programming and scientific experiments, with the exception of *in vivo* imaging (Figure 2.6), which was done jointly by Jasmin Hefendehl and Lasse Dissing-Olesen, and neuronal patch-filling and imaging (Figure 2.7), which was done by Dr. Nicholas Weilinger. I performed all morphological processing, statistical analyses, and manuscript writing. This work has been published as: **York E.M.**, LeDue J.M., Bernier LP., and MacVicar B.A. (2018). 3DMorph Automatic Analysis of Microglial Morphology in Three Dimensions from *Ex Vivo* and *In Vivo* Imaging. **eNeuro** 5(6) 1-12.

The work presented in Chapter 3 was designed with input from Dr. Brian MacVicar, Dr. Nicholas Weilinger, and Jeffrey LeDue. All experiments and data analyses were performed myself, with assistance from Dr. Nicholas Weilinger in imaging recombinant GFP (Figure 3.2 and Figure 3.3). I wrote the manuscript and received edits from Dr. Brian MacVicar, Dr. Nicholas Weilinger, and Jeffrey LeDue. This work has been accepted for publication in Biomedical Optics Express as: **York E.M.**, Weilinger N.L., LeDue J.M., and MacVicar B.A. Green Fluorescent Protein emission obscures metabolic fluorescent lifetime imaging of NAD(P)H.

Chapter 4 was performed in collaboration with Dr. Louis-Philippe Bernier, and Alireza Kamyabi, with input from Dr. Brian MacVicar. I performed all NAD(P)H-FLIM experiments and Seahorse metabolic assays, and associated analyses. Alireza Kamyabi performed the MTT and *in vitro* phagocytosis assays, as well as 3DMorph quantification (Figure A.2.1, Figure A.2.2, and Figure

A.2.3). Dr. Louis-Philippe Bernier performed all microglial two-photon imaging (Figure A.2.1, Figure A.2.3, and Figure A.2.4).

Chapter 5 was performed jointly with Dr. Jingfei Zhang, with input from Dr. Brian MacVicar. I performed all experiments and analyses associated with NAD(P)H-FLIM, HIF-1α measurements, and *in situ* cytokine measurements. Dr. Zhang performed all electrophysiology experiments (Figure B.2.1).

In both chapter 4 and 5, I was the sole author of the text, and all works not performed by myself have been included as appendices.

All animal procedures performed for this dissertation were approved by the University of British Columbia Animal Care Committee under certificates A15-0209 and A15-0086.

Table of Contents

Abstract ..... **iii**

Lay Summary ..... **v**

Preface ..... **vi**

Table of Contents ..... **viii**

List of Tables ..... **xv**

List of Figures ..... **xvi**

List of Abbreviations ..... **xviii**

Acknowledgements ..... **xxii**

Dedication ..... **xxiv**

Chapter 1: Introduction **1**

1.1 Microglial physiology 3

1.1.1 Microglial roles in development 4

1.1.2 Microglial morphology 8

1.2 Microglia-neuron communication 11

1.2.1 Microglia sense neuronal activity 13

1.2.2 Microglia modify neuronal activity 17

1.3 Key pathways of cellular metabolism 21

1.3.1 Glycolysis 24

1.3.2 Mitochondrial metabolism 28

1.3.3 Measuring cellular metabolism in the brain 30

1.4 Immunometabolism 35

1.4.1 Increased aerobic glycolysis 37
1.4.2 Broken TCA cycle 39
1.4.3 Glutaminolysis support of TCA cycle metabolites 43
1.5 Rationale and hypotheses 44
Chapter 2: 3DMorph automatic analysis of microglial morphology in three dimensions from *ex vivo* and *in vivo* imaging 52
2.1 Introduction 52
2.2 Materials and Methods 54
2.2.1 Animal protocols 54
2.2.2 Acute hippocampal slice preparation 54
2.2.3 Treatment conditions and SNAPSHOT 54
2.2.4 Acute hippocampal slice image acquisition 55
2.2.5 Cranial window surgery 55
2.2.6 *In Vivo* image acquisition 56
2.2.7 Neuronal dye loading 56
2.2.8 3DMorph Workflow 57
2.2.9 Threshold images 59
2.2.10 Identify and segment cells 61
2.2.11 Total territorial area of microglia 61
2.2.12 Identify full cells 61
2.2.13 Distance between cell centroids 63
2.2.14 3D skeletonization and branch tracing 63
2.2.15 Export data 64

2.2.16 Statistics 65
2.3 Results 65
2.3.1 Accuracy of 3DMorph results 65
2.3.2 Microglial morphology changes in response to local cues 68
2.3.3 Microglial morphology *in vivo* 71
2.3.4 Morphology of neurons 72
2.4 Discussion 73
2.5 Troubleshooting 75
2.5.1 Errors when running the script 75
2.5.1.1 Mex file error, or all output data for full cells is “0”: 75
2.5.1.2 ThresholdGUI: 75
2.5.1.3 numObjMg = numel(FullMg): 76
2.5.1.4 “waitbar” error: 76
2.5.1.5 GMModel: nuc must be a positive integer: 76
2.5.2 Unsatisfactory data processing 76
Chapter 3: Green fluorescent protein emission obscures metabolic fluorescent lifetime imaging of NAD(P)H 78
3.1 Introduction 78
3.2 Materials and Methods 82
3.2.1 Animal protocols 82
3.2.2 Acute hippocampal slice preparation 82
3.2.3 Recombinant GFP 83
3.2.4 Imaging parameters 83

3.2.5 NAD(P)H Fluorescence Lifetime Data 84
3.2.6 Single-cell NAD(P)H lifetime analysis 85
3.3 Results 85
3.3.1 Recombinant GFP lifetime under NAD(P)H imaging parameters 85
3.3.2 NAD(P)H measurements in Thy1-EGFP neurons 90
3.3.3 Cell-specific metabolism in EGFP-negative systems 92
3.3.4 NAD(P)H measurements in CX3CR1-EGFP microglia 94
3.3.5 Reactive oxygen species and protein load on NAD(P)H measurements 95
3.4 Discussion 97
Chapter 4: Microglial glutamine metabolism maintains viability and immune surveillance during glucose deprivation 102
4.1 Introduction 102
4.2 Materials and Methods 105
4.2.1 Animal protocols 105
4.2.2 Acute hippocampal slice preparation 105
4.2.3 Two-photon NAD(P)H imaging 106
4.2.4 NAD(P)H fluorescence lifetime data 107
4.2.5 Primary microglia culture and Seahorse assays 108
4.2.6 Reagents 109
4.2.7 Data analysis and statistics 109
4.3 Results 109
4.3.1 Microglia maintain baseline and immune surveillance in 0 mM glucose *in situ* 109
4.3.2 Microglial mitochondrial metabolism is maintained during aglycemia *in situ* 111

4.3.3 Microglia are capable of metabolizing glutamine *in vitro* 115
4.3.4 During aglycemia, glutaminolysis supports microglial metabolism *in situ* 118
4.3.5 Glutaminolysis maintains microglial motility and immune function in 0 glucose . 121
4.3.6 Microglial metabolic switch to glutaminolysis is dependent on mTOR 122
4.4 Discussion 123
4.4.1 Microglia maintain metabolism, motility, and immune surveillance in the absence of glucose 123
4.4.2 Microglial glutaminolysis maintains mitochondrial metabolism during aglycemia 124
4.4.3 Glutaminolysis supports microglial surveillance during aglycemia 125
4.4.4 mTOR-mediated metabolic flexibility 127
4.4.5 Microglial metabolic flexibility 128
Chapter 5: TLR4-mediated increase of microglial glycolysis inhibits expression of LTP through IL-1β 129
5.1 Introduction 129
5.2 Materials and Methods 132
5.2.1 Animal protocols 132
5.2.2 Acute hippocampal slice preparation 132
5.2.3 Primary microglia culture 133
5.2.4 Two-photon imaging 133
5.2.5 Microglial morphology analysis 135
5.2.6 NAD(P)H fluorescence lifetime data 135
5.2.7 Pro-inflammatory cytokine, HIF-1α, and NADPH measurement 136
5.2.8 Data analysis and statistics 137

5.2.9 Drugs and reagents 137
5.3 Results 137
5.3.1 LPS increases microglial glycolysis, which can be blocked by 2DG 137
5.3.2 Metabolic adaptation prior to morphological changes 140
5.3.3 LPS stabilizes HIF-1α through glycolysis-mediated pathways 141
5.3.4 LPS triggers glycolysis-dependent pro-inflammatory cytokine production 144
5.3.5 LPS inhibits LTP in acute hippocampal slices 145
5.3.6 LPS inhibits LTP through IL-1β signalling 146
5.3.7 LPS-induced LTP impairment is mediated by the TLR4 pathway 147
5.3.8 LPS inhibition of LTP is mediated by metabolically regulated IL-1β 147
5.4 Discussion 148
5.4.1 Microglial metabolism is important for proper response to immune stimulation by LPS 148
5.4.2 LPS inhibits LTP through an IL-1β dependent pathway 151
5.4.3 LPS stimulation inhibits LTP through TLR4-mediated IL-1β release 152
5.4.4 LPS-mediated LTP inhibition is rescued by blocking increased glycolysis 153
Chapter 6: Conclusion 154
6.1 Summary of research findings 154
6.1.1 3DMorph microglial morphology analysis 154
6.1.2 GFP contamination of NAD(P)H-FLIM 155
6.1.3 Microglial metabolic flexibility 156
6.1.4 Immunometabolic reprogramming of microglia 159
6.2 Overall significance 163

6.2.1 Microglia in acute metabolic disruptions 163
6.2.2 Microglia in chronic metabolic disruptions 165
6.2.3 Microglia and metabolism in neurodegenerative diseases 167
6.3 Future Directions 172
6.3.1 Mechanistic investigation of microglial metabolic reprogramming 172
6.3.2 A role for astrocytes in metabolic regulation 174
6.3.3 Clinical relevance 175
References 177
Appendices 234
Appendix A 234
A.1 Chapter 4 additional methods 234
A.2 Chapter 4 additional figures 236
Appendix B 240
B.1 Chapter 5 additional methods 240
B.2 Chapter 5 additional figures 242

List of Tables

Table 1.1 Overview of mechanisms of metabolic reprogramming in immune cells.....36

Table 2.1 67

List of Figures

Figure 1.1: Mechanisms of communication between microglia and neurons in the healthy brain to maintain homeostatic activity. 12

Figure 1.2: Key pathways of cellular metabolism. 23

Figure 1.3: Overview of 3DMorph platform. 47

Figure 1.4: Hypothesized microglial metabolic reprogramming. 51

Figure 2.1 3DMorph workflow. 58

Figure 2.2 Select threshold and identify cells. 60

Figure 2.3 Analysis of individual full cells. 62

Figure 2.4 Validation and comparison of 3DMorph with current analysis tools 66

Figure 2.5 Microglia morphology changes in response to local cues. 70

Figure 2.6 Morphology analysis of *in vivo* microglia images. 72

Figure 2.7 Morphology analysis of dye-loaded neuron. 73

Figure 3.1 NAD(P)H-FLIM. 79

Figure 3.2 Recombinant GFP lifetime across excitation and emission settings. 87

Figure 3.3 Recombinant GFP emission lifetime and intensity spectra. 89

Figure 3.4 NAD(P)H measurements of Thy1-EGFP neurons *in situ*. 91

Figure 3.5 EGFP-expressing microglia have shorter NAD(P)H mean lifetimes. 93

Figure 3.6 ROS scavengers do not increase NAD(P)H lifetimes in EGFP expressing microglia. 95

Figure 3.7 Exogenous protein expression does not cause short NAD(P)H lifetime measurements. 96

Figure 4.1 NAD(P)H-FLIM photons are mainly from NADH. 112

Figure 4.2 Microglia maintain mitochondrial metabolism in 0 mM glucose *in situ*. 114

Figure 4.3 Microglia metabolize glutamine *in vitro* to maintain OCR. 118

Figure 4.4 Microglia metabolize glutamine *in situ*. 120

Figure 5.1 LPS increases microglial glycolysis. 139

Figure 5.2 LPS increases microglial glycolysis prior to morphological changes. 141

Figure 5.3 LPS stabilizes HIF-1α and increases pro-inflammatory production through glycolysis-mediated pathways. 143

Figure A.2.1 Microglia maintain baseline and immune surveillance in 0 mM glucose *in situ*. . 236

Figure A.2.2 Microglia metabolize glutamine *in vitro* to maintain viability and function. 237

Figure A.2.3 Microglial motility and immune surveillance are supported by glutaminolysis in 0 mM glucose. 238

Figure A.2.4 Microglial metabolic switch to glutaminolysis is dependent on mTOR. 239

Figure B.2.1 LPS inhibits LTP through IL-1β in a TLR4-mediated and metabolically-dependent manner 242

List of Abbreviations

2DG	2-deoxy-D-glucose
2PLSM	2-photon laser scanning microscopy
α-KG	α-ketoglutarate
AA	Ascorbic acid
aCSF	Artificial cerebral spinal fluid
AD	Alzheimer's disease
ATP	Adenosine triphosphate
BBB	Blood-brain barrier
BDNF	Brain-derived neurotrophic factor
C1q	Complement receptor 1q
CNS	Central nervous system
CSF-1	Colony stimulating factor-1
Cpt1a	Carnitine palmitoyltransferase 1a
CR3	Complement receptor
DAMP	Damage associated molecular patterns
DMF	Dimethyl fumarate
DMOG	Dimethyloxaloylglycine
ECAR	Extracellular acidification rate
EGCG	Epigallocatechin gallate
EGFP	Enhanced green fluorescent protein

ELISA	Enzyme-linked immunosorbent assay
ETC	Electron transport chain
EV	Extracellular vesicle
FAO	Fatty acid oxidation
fEPSP	Field excitatory postsynaptic potentials
FLIM	Fluorescence lifetime imaging
GABA	γ-Aminobutyric acid
GAPDH	Glyceraldehyde 3-phosphate dehydrogenase
GDH	Glutamate dehydrogenase
GFP	Green fluorescent protein
GLS	Glutaminase
HD	Huntington's disease
HFS	High-frequency stimulation
HIF-1α	Hypoxia-inducible factor 1α
HK	Hexokinase
IFNγ	Interferon γ
IKKε	I kappa B kinase-epsilon
IL-1β	Interleukin-1β
IL-1R	Interleukin-1 receptors
IL-1Ra	Interleukin-1 receptor antagonist
IL-1RAcP	Interleukin-1 receptor accessory protein
IL-34	Interleukin 34

iGluR	Ionotropic glutamate receptors
IRF	Instrument response function
LPS	Lipopolysaccharide
LTD	Long-term depression
LTP	Long-term potentiation
LRRK2	Leucine-rich repeat kinase 2
mGluR	Metabotropic glutamate receptors
MSD	Meso Scale Discovery
mtHtt	Mutant Huntington protein
mTOR	Mammalian target of rapamycin
MyD88	Myeloid differentiation primary response gene 88
NADH	Nicotinamide adenine dinucleotide
NADPH	Nicotinamide adenine dinucleotide phosphate
NMDA	N-methyl-d-aspartate
NO	Nitric oxide
NOX	NADPH oxidase
OCR	Oxygen consumption rate
OXPHOS	Oxidative phosphorylation
PAMP	Pathogen associated molecular patterns
PD	Parkinson’s disease
PDH	Pyruvate dehydrogenase
PFK	Phosphofructokinase

PGC-1α	proliferator-activated receptor gamma coactivator 1α
PHD	Prolyl hydroxylase
PINK1	PTEN-induced kinase 1
PPP	Pentose phosphate pathway
PRR	Pattern recognition receptors
ROS	Reactive oxygen species
Runx1	Runt-related transcription factor 1
SDH	Succinate dehydrogenase
SNT	Simple Neurite Tracer
TBK1	Tank-binding kinase-1
TCA cycle	Tricarboxylic acid cycle
TCSPC	Time-correlated single photon counting
TLR	Toll-like receptor
TNFα	Tumor necrosis factor α
WT	Wild type

Acknowledgements

I would like to thank my thesis advisor, Dr. Brian MacVicar, for his tremendous support and encouragement. I am exceedingly grateful for your willingness to discuss results, your assurance that the data's the data, and your foresight in guiding future experiments. Your motivation and patience as a mentor, and your unending passion as a scientist have been instrumental to both the successful completion of this work, and to my ambition to continue in academia. Thank you for everyday being the kind of scientist I aspire to become.

Thank you also to the members of my thesis committee, Dr. Lynn Raymond, Dr. Cheryl Wellington, and Dr. James Johnson, who were always enthusiastic in discussing my work, and have provided indispensable feedback. Your input has shaped and improved the work in this dissertation, and our interactions have enriched my training experience.

I would also like to gratefully acknowledge that my research was funded by the Canadian Institutes of Health Research Doctoral Award, and the University of British Columbia Four Year Doctoral Fellowship.

Throughout my degree, I have had the pleasure of working with a brilliant and stimulating group of colleagues and collaborators. Thank you to all members of the MacVicar lab, past and present, for your assistance, camaraderie, and enlightening discussions (scientific and otherwise). Your advice and motivation were valued when experiments were going well, and invaluable when they were not. In particular, I would like to express my gratitude to LP Bernier, Nick Weilinger, and

Jeff LeDue. You have each acted as a mentor to me, providing moral support, career and training advice, scientific expertise, and always patiently answered my relentless questions. You have taught me so much.

Finally, a huge thank you to my friends and family for your patience, support, and on occasion, therapy. I really could not have done it without you.

To York Road, and the people who make it home.

Chapter 1: Introduction

Often referred to as the brain's resident macrophage, microglia are the primary immune cells within the central nervous system (CNS) (Hines et al., 2009; Kettenmann et al., 2011). These cells originate in the yolk sac, migrating into the developing brain and populating it by embryonic day 9.5 in mice (Ginhoux et al., 2010; Prinz & Priller, 2014). Microglia are ubiquitous throughout the brain and spinal cord, showing highly territorial process movement such that no two cells overlap in area (Hines et al., 2009). Like neurons, microglia are extremely long-lived cells, and their population appears to be locally maintained (Ajami et al., 2007; Füger et al., 2017; Prinz & Priller, 2014; Réu et al., 2017).

Mature microglia have small, compact cell bodies with long, thin processes, which are highly dynamic and constantly survey their microenvironment (Hines et al., 2009; Nimmerjahn et al., 2005). This morphology, referred to as 'resting' or 'ramified', paired with their expression of immune and neurotransmitter receptors (Kettenmann et al., 2011) makes microglia ideal candidates for maintaining protection, extracellular homeostasis, and neuronal health. As evidence of their importance, microglia have been associated with neuronal development (Kaneko et al., 2010; Paolicelli et al., 2011; Roumier et al., 2008; Squarzoni et al., 2014), synaptic pruning (Kettenmann et al., 2013; Schafer et al., 2012), and regulation of neurotransmission (Kettenmann et al., 2013; Parkhurst et al., 2013; Stellwagen et al., 2005; Stellwagen & Malenka, 2006; Y. Wu et al., 2015; J. Zhang et al., 2014). Through their pattern recognition receptors (PRRs; including Toll-like receptors, TLRs), microglia are able to respond to damage or pathogen associated molecular patterns (DAMPs, or PAMPs, respectively), and inflammatory cytokines (Kettenmann et al., 2011; Lehnardt, 2009; Takeuchi & Akira, 2010).

In response to immune activation, microglia rapidly withdraw their processes to become amoeboid, enhancing their phagocytic activity and migration to sites of damage (Kettenmann et al., 2011). Microglia also proliferate, and increase their production and secretion of inflammatory cytokines and chemokines. For proper immune resolution after an insult is cleared, microglia are expected to phagocytose any remaining damaged or apoptotic cells and produce anti-inflammatory cytokines (Buckley et al., 2014), eventually re-establishing tissue homeostasis.

Cellular senescence or chronic inappropriate activation have been implicated in many neurodegenerative diseases including Parkinson's disease, Alzheimer's disease, Huntingtin's disease, and many others (Crotti & Glass, 2015; Kettenmann et al., 2013; Perry & Holmes, 2014; Phani et al., 2012). In addition, sustained immune activation can lead to secondary damage from inflammation, cytokine exposure, or excitotoxic damage. This is commonly seen in cases of stroke, traumatic brain injury, or spinal cord injury (Allison & Ditor, 2015; David & Kroner, 2011; Kumar & Loane, 2012; Loane, Kumar, et al., 2014; Walberer et al., 2014). Clearly, the ability to properly regulate the CNS immune response (both activation and resolution) is critical for host defense, as well as long-term neuronal health.

In cells of the peripheral immune system, cellular metabolism pathways have emerged as regulators of activation (Buck et al., 2015; EL Kasmi & Stenmark, 2015; B. Kelly & O'Neill, 2015). These highly conserved pathways, classically considered as only a means of energy production, consist of many enzymes and intermediate metabolites that also form a signalling network influencing cellular function. Upon pro-inflammatory stimulation, increased aerobic

glycolysis, alterations in the tricarboxylic acid (TCA) cycle, and repurposing of the electron transport chain (ETC) for reactive oxygen species (ROS) production allow cellular polarization to enhance pro-inflammatory immune functions. Conversely, resolution and anti-inflammatory functions are associated with increased oxidative phosphorylation (OXPHOS) and fatty acid metabolism (Buck et al., 2016, 2015; EL Kasmi & Stenmark, 2015; B. Kelly & O'Neill, 2015; Newton et al., 2016).

Therefore, alterations in cellular metabolism may act as signalling platforms necessary to regulate immune phenotype. The role of these alterations are unclear in the brain, where glucose is considered the obligate energy source with dramatic neuronal impairments seen in glucose-deprived conditions such as vascular dementias (Daulatzai, 2017), stroke (Sims & Muyderman, 2010), or hypoglycemic episodes (Meneilly & Tessier, 2016; Rehni & Dave, 2018). It is important that microglia survive throughout these metabolic challenges because they perform important immunological and phagocytic functions in brain regions that are injured. How microglial cellular metabolism and immune activity are maintained or altered in these highly disrupted environments is not known.

The purpose of this dissertation was to investigate the metabolic flexibility of microglia, and to determine the contribution of metabolic pathways in regulation of microglial immune function.

1.1 Microglial physiology

Typically studied in association with disease, damage, or post-mortem pathologies, microglia have historically been viewed as cells that are damaging and even toxic to neurons. However, the past

decades of work have revealed a more complex range of roles for these cells. Microglia are now known to exhibit highly dynamic morphologies and functions with important roles for immune response to damage and infection, as well as in the regulation of baseline neuronal activity and developmental changes. While they continue to be associated with disease and damage, a more nuanced view is now taken, with an understanding that microglia first and foremost have a role in neuronal protection. It may even be a lack of basal neurotrophic or defense activity by microglia that contributes to onset and progression of disease. Their role in development has also become widely appreciated, as has their contribution to ageing, with clear evidence of their importance for synaptic pruning at both time points. With more studies into their diversity and homeostatic functions, it is certain that the importance and breadth of microglial roles will only continue to increase.

1.1.1 Microglial roles in development

Unlike most cells of the neural parenchyma, which are derived from the neural ectoderm, microglia originate from erythro-myeloid progenitor cells in the embryonic yolk sac. They migrate into the developing brain at embryonic day E9.5 in mice, possibly following chemokine gradients such as interleukin 34 (IL-34). While colony stimulating factor-1 (CSF-1) is largely responsible for the differentiation of most macrophage populations, CSF-1 knockout animals maintained normal adult microglia, but they were absent in animals lacking the receptor, CSF-1R (Ginhoux et al., 2010). A likely explanation for the survival of microglia in the absence of CSF-1 is that IL-34, which is expressed in mouse and human brain, can function as a ligand for the CSF-1R to maintain brain microglia (H. Lin et al., 2008; Wei et al., 2010).

During migration and development, embryonic microglia retain the same amoeboid phenotype seen in yolk sac precursors (Ginhoux et al., 2010), as this likely enables their migratory and phagocytic functions at this time point (Perez-Pouchoulen et al., 2015). As development continues and the function and activity of neural tissue changes, microglia begin to adopt their classic mature morphology of a small cell body (~10 μm diameter) with many fine processes. Transformation into this ramified morphology begins around two postnatal weeks, and is accompanied by a decrease in the expression of the Runt-related transcription factor 1 (Runx1) (Zusso et al., 2012). The developmental amoeboid morphology is recapitulated in disease and damage where microglial immune function is stimulated to again trigger proliferation, migration, and phagocytosis, and is also associated with an increased expression of Runx1 (Zusso et al., 2012).

Once in the developing brain, microglia have been shown to influence neuronal wiring. This was shown by Squarzoni et al., (Squarzoni et al., 2014) who reported that embryonic microglia are not homogenously distributed throughout the brain, but accumulate in hotspots and avoid other regions. Squarzoni et al. discovered that the location of microglia at this critical time point in neurodevelopment plays a role in axonal guidance and circuit formation. In E18.5 mice, when microglia were depleted, TH-positive axonal outgrowth was observed into the subpallium, whereas microglia stimulation by maternal immune activation with LPS reduced this pattern of axonal outgrowth. In addition, they found no effect on thalamic axon invasion, whereas either microglial depletion or maternal immune activation resulted in early entry into the cortical plate and a lack of layer V focalization of Lhx6-expressing interneurons (Squarzoni et al., 2014). These data convincingly show that the timing and location of microglial migration into the developing brain is important for proper neural wiring.

Microglia are also essential modulators of neuronal circuitry refinement after birth. Through the classical and alternative complement cascade, fractalkine, and purinergic signalling, neuronal activity instructs microglia on which synapses should be removed by pruning (Hong, Dissing-Olesen, et al., 2016; Kettenmann et al., 2013; Y. Wu et al., 2015). Developmental synaptic pruning is specific and activity dependent. In studies of monocular deprivation, inactive synapses were contacted more frequently and associated with microglial alterations in motility, morphology, and phagocytosis. Disrupting the purinergic receptor, P2Y12, inhibited the ability of microglia to sense ATP release from activated synapses, and resulted in mice that were unable to form ocular dominance columns during the critical period (Sipe et al., 2016). It is commonly thought that ATP and ADP release form a local gradient, acting as 'find me' signals to attract microglial processes while synapse removal is mediated by 'eat me' signals. These 'eat me' signals appear to be mediated largely by the complement cascade pathways, traditionally associated with innate immune response. Investigated primarily in the development and ocular dominance specification of the retinogeniculate circuit, microglia have been observed to engulf synapses, and evidence of presynaptic membranes have been found inside microglial lysosomes. Through complement receptor 3 (CR3), microglia preferentially engulf synapses tagged with the eat me signal, C1q (Schafer et al., 2012; Stevens et al., 2007). In addition to stimulating synapse engulfment, it is important that functional synapses are maintained, which is in part mediated by the 'don't eat me' signal, CD47 and its receptor expressed on microglia, SIRPα. Mice lacking CD47 or SIRPα showed increased synaptic pruning in the retinogeniculate system, and a lack of preferential removal of inactive synapses (Lehrman et al., 2018). Thus, it is clear that microglia remain important throughout postnatal neuronal development for pruning of inactive synapses to mediate

circuit refinement. Several neurodevelopmental or neurodegenerative diseases have been associated with aberrant synaptic pruning. Specifically, overactive pruning may be a potential risk or cause for development of schizophrenia (Sellgren et al., 2019), while increased pruning later in life is seen in Alzheimer's disease and may be a molecular abnormality early in disease causing later cognitive impairment and memory loss (Hong, Beja-Glasser, et al., 2016).

After successfully migrating into the developing brain, maturing, and performing synaptic pruning during circuit refinement, the microglia are very long-lived, persisting in the brain for months to years (Füger et al., 2017; Réu et al., 2017). In contrast to most adult tissue macrophages, whose local population is maintained by replenishment from blood monocytes, resident microglia appear to self-renew within the brain, although the contribution of peripheral hematopoietic cells during healthy, homeostatic conditions is still hotly debated (Ajami et al., 2007; Bruttger et al., 2015; Cronk et al., 2018; Füger et al., 2017; Karlen et al., 2018; Varvel et al., 2012). Blood brain barrier (BBB) breakdown in diseases or after damage does result in peripheral immune infiltration to the CNS parenchyma (Sweeney et al., 2018). The interaction between resident microglia and invading leukocytes remains unclear, as does the fate of these invading cells. It is possible that they are capable of responding to their new environment and transforming into a microglia-like cell (Nau et al., 2006; Varvel et al., 2012), or undergo apoptosis with time and immune resolution, and are then eventually cleared by microglia.

1.1.2 Microglial morphology

Following development, synaptic pruning, and differentiation into mature cells, microglia establish themselves throughout the CNS parenchyma in a non-overlapping fashion. They form a mosaic-like tiling pattern, with each cell establishing a clearly-defined surveillance territory from which it excludes the processes of neighbouring microglia. This suggests that there are mechanisms of contact inhibition in place between microglia during homeostatic functioning (Askew et al., 2017; Zhan et al., 2019). This contact inhibition can be rapidly blocked or over-ridden in response to injury, as microglial processes converge and overlap to block the spread of damage to surrounding cells (Davalos et al., 2005; Hines et al., 2009).

The density of the microglial population varies between brain regions, ranging from as low as 5% of total cells in the cortex, to as high as 12% in the substantia nigra. The exact regional signalling cues leading to this diversity are not clear, but it does not appear to be a simple response to levels of cell death during development (Lawson et al., 1990). There are more microglia found throughout the grey matter than in white matter tracts, with morphological variations across brain regions. Microglia in white matter are radially branched to align mainly in parallel with the fibre tract, with only a few processes extending perpendicularly. Brain regions with a perforated blood-brain barrier contain rounder microglia with only a few thick processes. The classical microglial morphology with elaborate branching of long, thin processes was observed across the cerebral neuropil (Lawson et al., 1990), and are referred to as ‘ramified’ microglia. Sometimes called the resting microglial state, it is now appreciated that these cells are “never-resting”, as they continuously extend their processes into the parenchyma to survey the environment for damage

and infection, or make contact with synapses to regulate neuronal function (Nimmerjahn et al., 2005; Wake et al., 2009).

In response to signals such as ATP or norepinephrine, G-protein coupled receptors result in focal, subcellular gradients of cAMP. It has recently been described that this intracellular cAMP signalling is critical for filopodia formation on microglial processes. Filopodia are small, actin-dependent extrusions off of main microglial processes that move in a random-sensing motion, and dramatically increase the surveillance ability and area of microglia. In response to chemoattractants, such as ATP or ADP, a decrease in local cAMP decreases the outgrowth of filopodia and allows extension of bulbous tips (Bernier et al., 2019). As it was shown that the extension in bulbous tips corresponds with a decrease in presence of actin-dependent filopodia, it is possible that cAMP is interacting with the actin cytoskeleton through the Rho family GTPases, including Rho. This pathway is well established, with evidence of morphological outcomes in other cell types (Pelletier et al., 2005).

Microglial morphology is also exceptionally dynamic, again often in response to local cues from the environment. In response to focal damage, such as vessel leak or cell necrosis, microglia extend their processes to converge at the site of injury (Davalos et al., 2005; Dissing-Olesen et al., 2014; Drew et al., 2010; U. B. Eyo et al., 2015, 2014; Hines et al., 2009; Lou et al., 2016; Nimmerjahn et al., 2005). However, in scenarios of extensive damage, pathogen-associated activation, or chronic neurodegeneration, microglia retract their processes and become amoeboid, a morphology associated with proliferation, migration, and phagocytosis (Doorn et al., 2014; Kloss et al., 2001; Kreutzberg, 1996). Since microglial morphological changes are influenced by the environment,

and are reflective of cellular activity, these contextual changes of microglial shape and process ramification have been used to infer function (Davis et al., 1994; Karperien et al., 2013).

The advancement of single cell proteomics and transcriptomics are now making their way into the microglial field and are vastly expanding the understanding of cell state and function (Hammond et al., 2019). Unfortunately, a major limitation of these techniques is the necessity of isolating microglia cells from brain tissue, which causes a rapid change in cell morphology and function. It is logical that an immune cell, highly sensitive to changes in their local environment, would mount an immediate response to such a dramatic alteration. New methods are currently in development to validate rapid extraction with minimal impact on microglial state. However, at the moment, the gold standard for true, physiological function is *in vivo* imaging through a thinned skull or cranial window preparation (Drew et al., 2010; Shih et al., 2012). While powerful, this technique also suffers from limitations, as the imaging area is restricted and the brain tissue is not readily accessible to manipulation, particularly changes in ion concentration or application of pharmacological manipulators. To address these issues, while maintaining relatively physiological conditions, the microglial field, and neuroscience community more broadly, relies heavily on acute brain slice preparations. It has been validated that microglia in these conditions retain the baseline ramified morphology observed *in vivo*. Two-photon microscopy and genetic identification of microglia (such as the $CX3CR1^{EGFP/EGFP}$ and $CX3CR1^{EGFP/+}$ models (S. Jung et al., 2000)), have allowed the investigation of live microglia in response to environmental manipulations or changes in neuronal activity. A rapid fixation method, known as SNAPSHOT, has also been developed to chemically fix the tissue with paraformaldehyde, allowing immunohistochemical investigations

(Dissing-Olesen & MacVicar, 2015). This has been an invaluable tool to address changes in microglial immune activation, maturation, and phagocytosis in physiological conditions.

1.2 Microglia-neuron communication

In the CNS, cooperation of neuronal and glial activity is essential to allow for proper neuronal development, function, and health. While astrocytes attract much of the focus in this area, microglia also play a large role the maintenance of appropriate connections through synaptic pruning (Hong, Beja-Glasser, et al., 2016; Hong, Dissing-Olesen, et al., 2016; Schafer et al., 2012; Q. Shi et al., 2015; Sipe et al., 2016; Stephan et al., 2012; Stevens et al., 2007), regulation of axonal growth cones to migrate and form synapses (Squarzoni et al., 2014), and fine-tuning of synaptic activity (Béchade et al., 2013; Blank and Prinz, 2013; Eyo and Wu, 2013; Tremblay et al., 2011). Microglia-neuron communication can be parsed into two critical aspects, which will be further discussed: 1) microglia must have the ability to sense local neuronal activity; and 2) microglia can in turn regulate synaptic activity (See Figure 1.1).

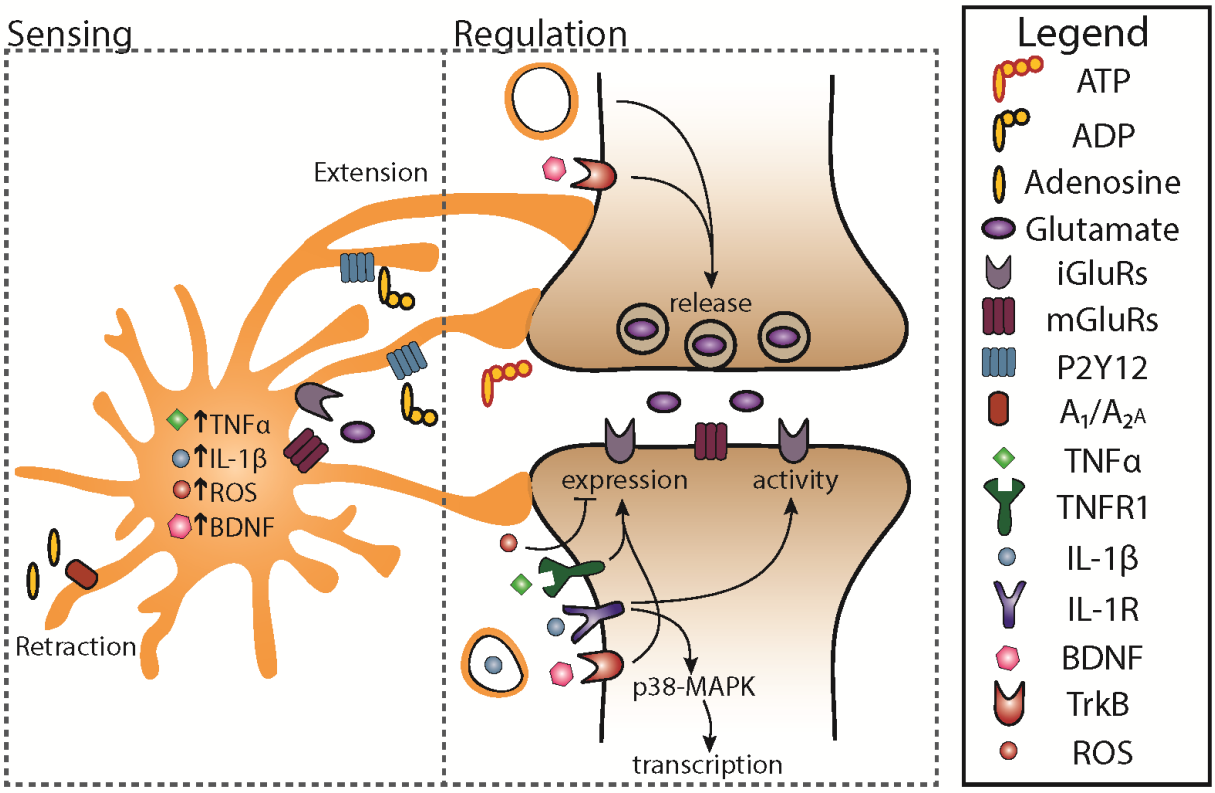

Figure 1.1: Mechanisms of communication between microglia and neurons in the healthy brain to maintain homeostatic activity.

Microglia sense neuronal firing through mGluR and iGluR stimulation by glutamate, as well as detection of activity-induced ATP/ADP, and adenosine levels via P2YRs and adenosine receptors. In response to P2Y12 stimulation, microglia rapidly extend their processes towards the synapse or release EVs, while adenosine signalling triggers process retraction. Cell-cell contact can dampen the activity of neurons through phagocytosis, remodeling of the extracellular matrix, or local release of synaptic modulators. EVs can alter neuronal function either through their packaged messengers, lipid content, or stimulation of neuronal sphingosine metabolism, which enhances presynaptic vesicle release. Glutamate and ATP levels also regulate microglial production of TNF-α, IL-1β, BDNF, and ROS. Decreased glutamate tone stimulates TNF-α release, which binds postsynaptic TNFR1 and increases the surface expression of iGluRs, thus increasing neuronal activity. IL-1β triggers postsynaptic IL-1R activation to increase activity of glutamate receptors, and also increases protein transcription.

1.2.1 Microglia sense neuronal activity

In order to maintain homeostatic activity, microglia must first be able to sense the firing rate of neurons. To accomplish this, microglia express receptors for purines, as well as for many common neurotransmitters to directly sense synaptic communication (Butovsky et al., 2014; Hickman et al., 2013; Y. Zhang et al., 2014).

Glutamate is the major excitatory neurotransmitter used for communication between neurons throughout the CNS. Microglia express both metabotropic (mGluR) and ionotropic (iGluR) glutamate receptors (Domercq et al., 2013; Murugan et al., 2013; Pocock & Kettenmann, 2007). Metabotropic glutamate receptors present on microglia include group I (mGluR5), group II (mGluR2 and 3), and group III (mGluR4, 6, and 8, but not mGluR7). Classically, group I mGluR stimulation activates G_q proteins, whereas group II and III mGluRs are coupled to G_i/G_o proteins (Swanson et al., 2005).

Stimulation of group I and III metabotropic glutamate receptors induces a neuroprotective microglial phenotype (Byrnes et al., 2009; Murugan et al., 2013). In microglia-neuron co-culture, LPS application combined with a group III mGluR agonist significantly reduced neuronal death relative to LPS treatments alone (D L Taylor et al., 2003). This effect may be through stimulated intracellular Ca^{2+} release and activation of the PKC pathway, causing release of nerve growth factor or brain-derived neurotrophic factor (BDNF) (J. Liang et al., 2010). There is also *in vivo* evidence that group III mGluR activation is neuroprotective in models of Parkinson's disease (Betts et al., 2012; Vernon et al., 2007) and traumatic brain injury (Loane, Stoica, et al., 2014).

Conversely, if microglial group II mGluRs are activated, neuronal apoptosis is increased, either in co-culture conditions or after incubation with microglia-conditioned media. Neurotoxicity appears to be mediated through microglial shedding of FasL (death receptor ligand) and release of TNF-α, which triggers neuronal caspase 3 pathways (Deanna L Taylor et al., 2005).

Ionotropic glutamate receptors include α-amino-3-hydroxy-5-methyl-4-isoxazolepropionic acid (AMPA), N-methyl-d-aspartate (NMDA), and kainate receptors. While there is evidence for the expression of these receptors in microglia, whether activation causes microglial currents measured by electrophysiology remains controversial. Results may be dependent on experimental techniques, as there are reports of NMDAR-dependent responses in cultured microglia (Murugan et al., 2011; Noda et al., 2000; Pocock & Kettenmann, 2007); however direct NMDAR-dependent responses have not been recorded *in situ* (Fontainhas et al., 2011; L.-J. Wu & Zhuo, 2008).

Although the mechanism of activation still needs to be elucidated, it is clear that ionotropic glutamate receptors trigger functional changes in microglia – leading most notably to increases in TNF-α, IL-1β, and nitric oxide (NO) release, as well as cytoskeletal rearrangements resulting in changes in morphology and dynamic behaviour (Fontainhas et al., 2011; Murugan et al., 2013, 2011; Noda et al., 2000). Blocking NMDAR activity with the antagonist MK801 reduced expression of TNF-α, IL-1β, and NO in hypoxic microglia cultures, likely by decreasing the NFκB signalling pathway (Murugan et al., 2011). These results suggest a possible role of basal glutamate tone in regulating the activity of microglia, as sensed through both ionotropic and metabotropic receptors.

In addition to synaptically-released glutamate, excitatory neuronal transmission may cause release of ATP through hemichannels (Dissing-Olesen et al., 2014; U. B. Eyo et al., 2015, 2014; Fields & Ni, 2010; Y. Li et al., 2012; Thompson et al., 2008). Once released, ATP can be degraded by ectonucleotidases such as CD37 and CD39 into ADP, which then activates purinergic receptors. ADP is further metabolized into adenosine which activates metabotropic adenosine receptors (Domercq et al., 2013; Robson et al., 2000).

Microglia express purinergic receptors at particularly high levels relative to other cell types in the CNS (Domercq et al., 2013; Pocock & Kettenmann, 2007). These receptors are divided into the metabotropic (P2Y) and ionotropic (P2X) families. Upon P2Y12 receptor stimulation, the major microglial response is to undergo process extension towards the site of release, making ATP/ADP a major 'find me' signal (Dissing-Olesen et al., 2014; U. B. Eyo et al., 2015, 2014; Y. Li et al., 2012; Sipe et al., 2016). This function is important in allowing microglia to detect active synapses in the visual cortex following monocular deprivation (Sipe et al., 2016), during NMDAR activation in hippocampal slices (Dissing-Olesen et al., 2014), or during kainate-induced seizure activity *ex vivo* and *in vivo* (U. B. Eyo et al., 2014). Notably, pharmacologically blocking P2Y12 function or using P2Y12 KO models inhibited microglial process convergence and experience-dependent plasticity (Sipe et al., 2016), and resulted in exacerbated seizure behaviours (U. B. Eyo et al., 2014). As shown by Li et al., neuronal activity caused ATP release, triggering directed microglial process outgrowth, and formation of bulbous tips that contacted neurons, ultimately resulting in decreased neuronal activity (Y. Li et al., 2012).

In contrast to process extension via P2Y12 receptor activation, adenosine stimulation of the A_{1A} or A_{2A} receptors in microglia blunts ATP-induced Ca^{2+} signalling and results in process retraction (Luongo et al., 2014; Orr et al., 2010). Microglial adenosine receptors are upregulated under inflammatory conditions, and may contribute to microglial transformation into an amoeboid morphology (Orr et al., 2010). Therefore, sensing of ATP and its hydrolysis products, ADP and adenosine, may be a mechanism by which microglia monitor the activity of nearby neurons and extend their processes towards areas of increased synaptic activity to allow local synaptic modulation or scaling.

While glutamate and ATP are the most widely studied molecules conveying activity from neurons to microglia, they are not the sole methods of communication. Several additional signals sensed by microglia include serotonin, γ-Aminobutyric acid (GABA), acetylcholine, and CX_3CL1 (fractalkine) (Kettenmann et al., 2011; Pocock & Kettenmann, 2007). Microglia express serotonin receptors, including $5\text{-}HT_{2B}$, and increased serotonin release acts as a chemoattractant for microglial processes (Kolodziejczak et al., 2015), and increases process movement, but not phagocytosis (Krabbe et al., 2012). The neurotransmitter GABA can stimulate microglial $GABA_B$ receptors and cause a reduction in release of cytokines IL-6 and IL-12p40 following LPS activation or facial nerve axotomy (Charles et al., 2003; Kuhn et al., 2004). GABA stimulation appears to inhibit the inflammatory NFκB and p38 MAPK pathways involved in release of interleukins and TNF-α (Lee et al., 2011). Acetylcholine is another neurotransmitter associated with decreasing microglial inflammation, functioning through the α7 nicotinic acetylcholine receptor to inhibit the MAPK pathway and decrease LPS-stimulated TNF-α release (King et al., 2017; Shytle et al., 2004). Finally, neuronal CX3CL1 binds to CX3CR1 expressed on microglia and limits

inflammation, process dynamics, and migration (Cardona et al., 2006; K. J. Liang et al., 2010). Therefore, these signals are able to modulate the microglial response to secondary stimuli, and in physiological conditions, may alter microglial function in synaptic regulation.

1.2.2 Microglia modify neuronal activity

Microglia can contribute to synaptic modulation through microglia-neuron contact, or release of extracellular vesicles and other small signalling molecules. Common microglial-released molecules involved in regulating synaptic plasticity include TNF-α, IL-1β, BDNF, and ROS.

Microglia have been observed to contact both pre- and post-synaptic neuronal elements of active synapses (Kettenmann et al., 2013; Pfeiffer et al., 2016; M. E. Tremblay et al., 2010; Wake et al., 2009) and increase or decrease synaptic firing in order to maintain appropriate activity levels. Through cell-cell contact, microglia likely remodel the extracellular matrix to allow synapse reorganization, or perform phagocytosis of synaptic components (Hong, Beja-Glasser, et al., 2016; Schafer et al., 2012; M. È. Tremblay & Majewska, 2011). Inducing long term potentiation (LTP) increased microglial process number and spine contact duration – a response that could be blocked by inhibiting neuronal activity (Pfeiffer et al., 2016). Occurrence of microglia-synapse contacts have also been shown to increase upon neuronal activity in the zebrafish tectum, again through the concomitant release of ATP. Neurons that were contacted by microglial processes significantly downregulated their activity after 5 minutes, while non-contacted neurons continued their high firing rate (Y. Li et al., 2012). Similarly, in a model of kainate-induced seizure activity, microglia extended their processes to sites of ATP release associated with increased neuronal firing. Strikingly, this microglial response was absent in P2Y12 knockout mice, and P2Y12 deficiency

led to exacerbated seizure behaviours, suggesting that the microglia-neuron contact is neuroprotective in cases of neuronal hyperexcitation (U. B. Eyo et al., 2014). Another study using repeated stimulation to induce depolarization and axonal swelling suggest that neurons release both ATP and glutamate to induce microglial process extension and wrapping. This behaviour may physically shield leaky membranes, release neuroprotective factors, or phagocytose damaged cellular debris, and return axons to their resting membrane potential (Kato et al., 2016). Therefore, direct contact between microglia and neurons appears to be necessary in experience-dependent synaptic remodelling and is neuroprotective to hyperexcitable neurons. Once drawn to a synapse, microglia may provide direct ligand-receptor contact, phagocytose synaptic components and debris, or release small neurotrophic and neuroprotective signalling molecules to regulate neuronal activity.

In addition to extending their processes, microglia also undergo another type of cytoskeletal remodelling to shed extracellular vesicles (EVs), which communicate with neurons through membrane composition or packaged molecules. Microglial EVs caused an increase in visually evoked field potentials in the rat visual cortex (Antonucci et al., 2012). This group also later showed that microglial EVs were able to carry hydrophobic endocannabinoids between cells to stimulate type-1 cannabinoid receptors. This interaction then decreased presynaptic transmission of GABAergic neurons (Gabrielli et al., 2015). In addition to endocannabinoids, ATP-induced microglial EVs have also been shown to contain the cytokine IL-1β (Bianco et al., 2005).

Microglial-derived IL-1β plays a key role in physiological and pathological synaptic regulation. Functionally, IL-1β binds to type I IL-1 receptors (IL-1Rs), which associate with IL-1R accessory

protein (IL-1RAcP) to cause p38 MAPK signalling and gene transcription (Srinivasan, 2004). The IL-1RAcPb isoform was recently identified exclusively in neurons (Y. Huang et al., 2011), activation of which potentiates the NMDAR-dependent Ca^{2+} influx in hippocampal or spinal cord neurons in a dose-dependent fashion (A. K. Clark et al., 2015; Y. Huang et al., 2011). These mechanisms might be responsible for the sensitivity of outcomes to IL-1β concentration, and its effects in both memory acquisition and maintenance.

It has been suggested that an inverted U-shaped relationship exists in the role of IL-1β on memory performance, where either high or low levels of IL-1β signalling impaired fear-conditioned memory (Goshen et al., 2007; Rogers et al., 2011). Twenty-four hours after establishment of fear conditioning, IL-1β expression was increased within the hippocampus, and blocking its function with continuous perfusion or overexpression of Interleukin-1 receptor antagonist (IL-1Ra), impaired memory performance (Goshen et al., 2007). Similarly, in a Y-maze model of spatial learning and memory, an increase in hippocampal IL-1β and neuronal c-fos was observed. No such effect was found in P2X7R KO mice, suggesting P2X7 activation is necessary for IL-1β maturation and release from microglia (Ferrari et al., 2006; Labrousse et al., 2009; Mingam et al., 2008).

However, there are also many accounts detailing the negative impact of IL-1β on hippocampal LTP or promotion of LTD. Bath application of 1 ng/ml IL-1β caused a sustained decrease in basal synaptic transmission in the CA1 region. Following low frequency stimulation (LFS)-induced LTD, addition of IL-1β did not cause a further persistent decrease, and similarly, IL-1β-induced synaptic depression blocked any additional effect of LFS, suggesting they are employing similar mechanisms of action (Ikegaya et al., 2003). Looking instead at synaptic strengthening, IL-1β

incubation (50 pg/ml) inhibited LTP in the mossy fibre-CA3 pathway (Katsuki et al., 1990), and in a dose-dependent manner in CA1 hippocampus which was inhibited by addition of IL-1Ra (Bellinger et al., 1993).

Furthermore, increased IL-1β release following CX3CL1/CX3CR1 disruption was sufficient to impair LTP, hippocampal neurogenesis, motor learning, associative memory, and spatial memory, as these effects could be rescued by the simultaneous infusion of IL-1Ra (Rogers et al., 2011). These results have implications for the increased IL-1β tone following injury or with aging (Murray & Lynch, 1998). These findings highlight the important subtleties in the IL-1β signalling pathway such as location of release, mechanism of action, and dose-response sensitivity.

In addition to IL-1β, another microglial-derived cytokine, tumor necrosis factor α (TNF-α), influences neuronal function through synaptic scaling. Synaptic scaling is a mechanism critical in maintaining homeostatic activity, whereby the overall activity and firing rate of a neuron is adjusted. Decreased glutamate activity increases TNF-α release, which promotes neuronal AMPAR expression. Conversely, an increase in ambient glutamate tone reduces TNF-α release, decreasing additional glutamate receptor expression, and allowing neuronal activity to decline (Aizenman & Pratt, 2008; Beattie et al., 2002; Stellwagen & Malenka, 2006). TNF-α has multiple modes of action, including modifying gene expression (Kraig et al., 2010), and neuronal GABA and glutamate receptor expression (Aizenman & Pratt, 2008; Cingolani et al., 2008; Pribiag & Stellwagen, 2013). Therefore, TNF-α appears to be part of a signalling pathway necessary to allow an increase in synaptic scaling to maintain homeostatic activity.

Additional microglial mechanisms of synaptic influence include brain derived neurotrophic factor (BDNF) and reactive oxygen species (ROS). BDNF has been well-studied in the spinal cord, where microglial release of BDNF causes hyperexcitability of neurons in the dorsal horn and contributes to neuropathic pain (Coull et al., 2005). Within the hippocampus, BDNF also increases LTP through both functional and structural modifications (Leal et al., 2015). The opposite effect is observed with ROS release in the hippocampus. Simultaneous hypoxia and LPS stimulation activate microglial complement receptor 3 (CR3) and induce activity of NADPH oxidase. The increase in extracellular superoxide causes neuronal AMPAR internalization through protein phosphatase 2A and results in long-term depression (J. Zhang et al., 2014).

These studies highlight the importance of microglia-neuron communication in regulating synaptic activity. When this homeostatic signalling is disrupted, there are behavioural manifestations, such as motor learning and memory deficits (Goshen et al., 2007; Labrousse et al., 2009; Parkhurst et al., 2013; Rogers et al., 2011), and exacerbated seizure outcomes (U. B. Eyo et al., 2014), demonstrating the importance of microglia in maintaining proper synaptic homeostasis.

1.3 Key pathways of cellular metabolism

The brain is an extremely energy-demanding organ, in humans making up only 2% of the total body weight, but requiring 20% of the body's oxygen for energy production (Mink et al., 1981). Much of this energy is thought to support neuronal activity through the functioning of the Na^+/K^+ ATPase to maintain polarization, as well as the regulation of other channels, and loading of synaptic vesicles (Harris et al., 2012). However, it is estimated that approximately 50% of the brain's energy is used for non-signalling related purposes. Although the exact uses of this energy

are unclear, it is likely related to both neuronal and glial mitochondrial proton leak, actin and microtubule treadmilling, and protein and lipid synthesis (Engl & Attwell, 2015).

Cellular energy, in the form of adenosine triphosphate (ATP), is produced mainly by the metabolism of glucose through cytoplasmic glycolysis to pyruvate, which is further processed in the tricarboxylic acid (TCA) cycle within the mitochondrial matrix to fuel the electron transport chain (ETC). This mitochondrial metabolism is also referred to as oxidative phosphorylation (OXPHOS), as the addition of organic phosphate to adenosine diphosphate (ADP) requires the oxidation of the electron carriers, nicotinamide adenine dinucleotide (NADH) and flavin adenine dinucleotide ($FADH_2$), as well as a series of redox reactions throughout the ETC. In addition to glycolysis, the TCA cycle, and the ETC, a plethora of other metabolic pathways exist to process different carbon sources (Figure 1.2). These pathways largely overlap, interact, and are redundant, demonstrating the importance of continued metabolic activity for cellular survival. Additional available nutrients include other sugars (fructose), amino acids (glutamate, valine, leucine, and isoleucine), fatty acids (triglycerides and short-chain fatty acids), and monocarboxylates (lactate, pyruvate, and ketone bodies).

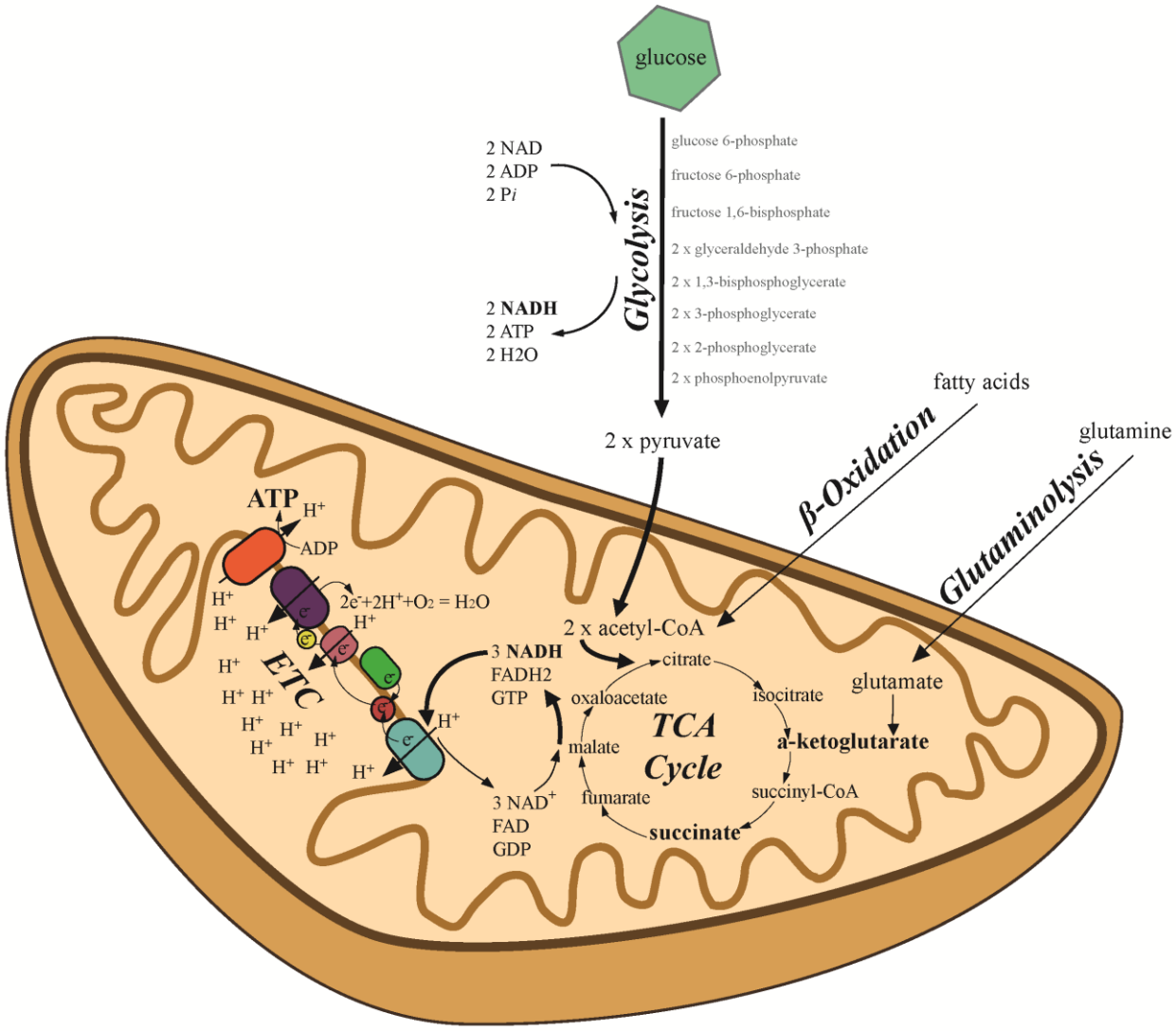

Figure 1.2: Key pathways of cellular metabolism.

Glucose is processed in the cytoplasm via glycolysis to two molecules of pyruvate. Fatty acids are processed via β-oxidation in the mitochondria to multiple molecules of acetyl-CoA, while glutamate is processed via glutaminolysis into α-ketoglutarate. All of these molecules supply carbon to the metabolites of the TCA cycle, whose continued cycling reduces the electron carriers, NADH and $FADH_2$, which supply electrons to the ETC in the inner mitochondrial membrane. The ETC uses the energy of multiple redox reactions to pump protons across the inner mitochondrial membrane, with O_2 being the final electron acceptor. This electrochemical gradient is used to power ATP synthase for phosphorylation of ADP.

While the core metabolic pathways are well understood, very little is known about how the brain regulates, compartmentalizes, and adapts its energy supply. It is largely believed that the brain relies almost entirely on glucose, which is nearly completely oxidized (Magistretti & Allaman, 2008), either through the mitochondria, or by conversion to lactate, which can then be transferred between cells before further mitochondrial processing. While the presence of an astrocyte-neuron lactate shuttle may exist at rest, it is still unclear whether this pathway fuels increased neuronal metabolism following increased activation (Diaz-Garcia et al., 2017; Magistretti & Allaman, 2018).

1.3.1 Glycolysis

Blood glucose levels rise and fall throughout the day, influenced by circadian rhythms, meal times, and hormone release. While the local environment of the brain experiences an additional level of regulation by the BBB, the levels of glucose in the brain fluctuate in a linear relationship to blood glucose (Seaquist et al., 2001; Seaquist & Öz, 2012; van de Ven et al., 2012). Typical brain glucose concentrations in human are around 1 mM during euglycemia, which correspond to concentrations of 4.7 mM in the plasma with small fluctuations depending on fed-fasted states (R Gruetter et al., 1992). To reach neurons, the glucose must be taken up from the blood through a series of glucose transporters. These transporters are divided into two main groups – the sodium-dependent transporters (SGLTs) efflux sodium to power the transport of glucose against its concentration gradient, and the facilitative transporters (GLUTs) that allow the passive flow of glucose. The main forms of transporters present in the brain are GLUT1 and GLUT3 (Duelli & Kuschinsky, 2001).

GLUT1 exists in two isoforms, one of which is 55 kDa and is expressed on the luminal and abluminal surface of endothelial cells to allow initial transport of glucose from the blood (Duelli & Kuschinsky, 2001; Gerhart et al., 1989). The second isoform is 45 kDa and is expressed in astrocytes and oligodendrocytes (Duelli & Kuschinsky, 2001; Yu & Ding, 1998). Upon entry to astrocytes, glucose can be further shuttled into the brain parenchyma for neuronal uptake, or can be processed into glycogen. Astrocytes are the main site of glycogen stores, which comprise one of the only local energy reserves for brain metabolism (Bélanger et al., 2011; Brown & Ransom, 2007). While astrocytic endfeet are estimated to cover 90% of the brain's capillaries, it is not necessary for all glucose to pass through astrocytes before reaching neurons, as there is sufficient room for molecular diffusion to allow glucose to reach neurons directly after passing through the endothelium (Gonçalves et al., 2019).

Once available in the parenchyma, glucose is transported into neurons mainly by GLUT3. While there is evidence of insulin-sensitive GLUT4 expression, this is mainly in the cerebellum and is not thought to contribute notably to glucose handling in the cerebrum (Rayner et al., 1994). GLUT3 has a low Michaelis-Menten constant, which allows neuronal glucose uptake even when it is present at low extracellular concentrations (Duelli & Kuschinsky, 2001). An area still under intensive debate is the role of astrocytes in exporting glucose directly to neurons, or first processing it via glycolysis to lactate before shuttling it to neurons for mitochondrial processing (Diaz-Garcia et al., 2017; Magistretti & Allaman, 2018).

Interestingly, microglia are the sole expressers of the transporter GLUT5 in the brain, which has been suggested to be a microglial-specific marker (Payne et al., 1997). Surprisingly, GLUT5 has a much higher affinity for fructose transport relative to glucose (Douard & Ferraris, 2008). While the basal regulation and diet or hormonal influences on fructose concentration in the brain remain understudied, this may be an area of particular importance in diet-induced obesity and affects of the 'Western diet' rich in high-fructose corn syrup. The relevance of GLUT5 in sensing fructose levels, and perhaps influencing the immune function of microglia, will be exciting areas of future research. While GLUT1 expression is conspicuously absent in microglia (Yu & Ding, 1998), it is possible that they express low levels of GLUT3 (Y. Zhang et al., 2014), although further targeted studies are needed for conclusive evidence of the expression and function of glucose transporters in microglia.

Once present in the cytoplasm, glucose is processed by the first glycolytic enzyme, hexokinase (HK), into glucose-6-phosphate. The rapid conversion of glucose helps to keep the intracellular concentrations low and facilitate further uptake (Miseta et al., 2003). Further processing can occur through either an anabolic or catabolic route. Catabolism refers to the breakdown of glucose through sequential carbon removal for oxidation and energy production. Anabolism is instead the breakdown of glucose to create specific metabolites, which exit glycolysis and are used to fuel biosynthesis of nucleotides or lipids. HK exists as four isoforms, the expression and subcellular localization of which may influence the flux of glucose through catabolic or anabolic metabolism. HKI and HKII are the most commonly expressed isoforms. HKI is mainly localized to the mitochondria where it channels glucose-6-phosphate to catabolic metabolism, while HKII can

move between the cytoplasmic and mitochondrial compartments, thereby influencing the ratio of anabolic and catabolic processing (John et al., 2011).

Glucose-6-phosphate is then processed by phosphofructokinase (PFK), the rate-limiting step of glycolysis. PFK is sensitive to the energy state of the cell, where AMP and ADP are allosteric activators of its activity and phosphoenolpyruvate is an inhibitor (Schirmer & Evans, 1990). PFK represents the first irreversible step of glycolysis, after which the glucose carbons are committed to further glycolytic processing. Prior to PFK activity, glucose-6-phosphate can instead be metabolized through the pentose phosphate pathway (PPP), which is important for supplying ribose-5-phosphate for nucleotide biosynthesis, and NADPH for NADPH oxidase formation of ROS or glutathione reduction for oxidative protection (Bolaños & Almeida, 2010; Cairns et al., 2011; Fan & Lane, 2015; Patra & Hay, 2014). If not used for biosynthesis, the carbons of the PPP can feed back into glycolysis as glyceraldehyde 3-phosphate.

Continued glycolysis in the cytoplasm results in the breakdown of one glucose molecule to produce 2 pyruvate, 2 NADH, and 2 ATP molecules. The ATP can be used directly for energy-consuming processes, and this cytoplasmic ATP production is thought to be important for meeting rapid energy requirements (Pfeiffer et al., 2001; Zheng, 2012). Regulation of ATP localization can also control the function of cytosolic proteins, such as the K_{ATP} channel (Gimenez-Cassina et al., 2012; Martinez-François et al., 2018; Yellen, 2008). The reducing equivalents of NADH generated during glycolysis are transferred to NAD^+ in the mitochondrial compartment through the malate-aspartate shuttle and the glycerol phosphate shuttle (McKenna et al., 2006) where they contribute to ETC function. When glycolytic rates are upregulated, NAD^+ can be resupplied by the

cytoplasmic conversion of pyruvate to lactate, which oxidizes NADH, and allows continued glycolysis in metabolically stimulated tissue. Therefore, it is possible for cells to process glucose to lactate, avoiding the use of mitochondrial metabolism. While this is advantageous in hypoxic conditions, where oxygen is not present as the final ETC electron acceptor, it can also function in normoxia, and is known as aerobic glycolysis or Warburg metabolism (Cairns et al., 2011; Hsu & Sabatini, 2008; López-Lázaro, 2008; Warburg, 1956). This unusual metabolic activity is mainly associated with cancerous tissues, or cells of the immune system activated by pro-inflammatory stimuli. However, most cells under normoxic conditions transport pyruvate across the inner mitochondrial membrane (IMM) by mitochondrial pyruvate carriers (McCommis & Finck, 2015) and continue its metabolism by pyruvate dehydrogenase (PDH) into acetyl-CoA.

1.3.2 Mitochondrial metabolism

Within the mitochondrial matrix, acetyl-CoA is consumed by the TCA cycle, which releases CO_2 as a by-product and reduces the electron carriers NADH and $FADH_2$. As carbon is lost as CO_2, it is necessary for the TCA cycle to be continuously supplied with additional carbon. This carbon is usually incorporated from acetyl-CoA, which can come from pyruvate, or as the product of triglyceride breakdown through fatty acid oxidation, or ketolysis processing of ketone bodies (Houten et al., 2016; D. Huang et al., 2016; Newsholme et al., 1986; O'Neill et al., 2016). Metabolism of branched chain amino acids results in either acetyl-CoA or succinyl-CoA, both of which can be incorporated into the TCA cycle (Adeva-Andany et al., 2017; Yudkoff, 2017).

An additional carbon source with potentially important effects in the brain is the amino acid glutamine, which is kept at high extracellular concentrations in the CNS (385 μM) (Kanamori &

Ross, 2004). Glutamine is deaminated to glutamate by the mitochondrial enzyme glutaminase (GLS), which in the brain is mainly studied in the glutamine-glutamate cycle to resupply the neuronal glutamate pool for maintained excitatory transmission (Schousboe et al., 2014; Tani et al., 2014). However, glutamate can instead be metabolized into α-ketoglutarate (α-KG), which is an intermediate metabolite of the TCA cycle. This conversion takes place mainly by glutamate dehydrogenase (GDH), but can also be carried out by glutamate oxaloacetate transaminase or glutamate pyruvate transaminase.

There is little support for the direct uptake of glutamate by microglia, as they have very low expression of the transporters GLAST (EAAT1) and Glt1 (EAAT2) (Y. Zhang et al., 2014), although these may be upregulated in damage or infection conditions (Chrétien et al., 2002; López-Redondo et al., 2000; Persson et al., 2005). In contrast, there is evidence of microglial glutamine uptake through SLC1A5 (ASCT2) (Scalise et al., 2018) and SLC38A1 (SNAT1) (Kalsbeek et al., 2016; Y. Zhang et al., 2014). The functional role of SNAT1 has been extensively studied, as its microglial-specific overexpression is seen in Rett's syndrome, an autism spectrum disorder. While overexpression leads to excess glutamate release and NMDA excitotoxicity in this condition, there is also an increased rate of microglial oxygen consumption, suggesting that the glutamate is being metabolized (Jin et al., 2015).

In the final pathway of mitochondrial metabolism, NADH and $FADH_2$ donate their electrons to complex I and complex II of the ETC, respectively. This initiates a series of redox reactions in which the energy released by electron transfer is coupled to proton extrusion from the matrix to the intermembrane space. Complex IV transfers the electron to the final acceptor, O_2, which creates

H_2O. The proton gradient established by this pathway generates the electrochemical force used by ATP synthase to power the addition of an organic phosphate to ADP, thereby storing the energy in this bond for use by other cellular processes.

1.3.3 Measuring cellular metabolism in the brain

As transcriptomics and proteomics exist for the RNA and protein level characteristic of a cell, metabolomics is a growing field, aiming to define the complete metabolite profile at the cellular, tissue, or organismal level. While the enzymes and key metabolites of the metabolic pathways are well understood, it is technically very difficult to study the functional activity and rate of metabolism in tissue, particularly heterogeneous organs such as the brain. Most of the limitations in this field stem from a lack of appropriate tools. Current metabolic imaging techniques are limited by the specificity and quality of available sensors, and are sensitive only to the small handful of metabolites being investigated. On the other hand, standard biochemical approaches suffer from poor spatial resolution, measuring metabolites at the whole tissue level and losing the detailed metabolic information of specific cell compartments. In the CNS, where there is a tight regulation of metabolites, extensive metabolic coupling between glia and neurons, and rapid fluctuations following neuronal excitation, definitive metabolic measurements have proven particularly difficult.

Many common approaches to metabolic measurements have been designed for *in vitro* experiments. These include the colorimetric/fluorometric measurements of specific metabolites or ATP directly from cellular homogenates. The MTT assay is often considered to measure cellular viability, but is in fact a direct measure of mitochondrial activity. In this assay, the tetrazolium

dye, MTT, is converted to a purple-coloured formazan by oxidoreductase enzymes (Mosmann, 1983; Stockert et al., 2018). Therefore, the amount of coloured product measured is dependent upon the cellular mitochondrial mass and expression of these metabolic enzymes.

A more recently popularized method is the measurement of extracellular acidification and oxygen consumption by Seahorse technology, indicative of glycolytic and OXPHOS rates, respectively (van der Windt et al., 2016). In this technique, probes sensitive to protons and oxygen measure the change in extracellular acidification rate (ECAR) and oxygen consumption rate (OCR) across time. This technology is particularly advantageous relative to previous methods as it allows rate measurements of the same sample across time, and after the introduction of specific metabolic perturbations. Four drug ports in each well allow the sequential injection of nutrients or toxins to record the metabolic response and determine proton leak, maximal respiration, spare respiratory capacity, and glycolytic reserve. Metabolic dependency on particular nutrients or flexibility of pathways can be determined by the addition or exclusion of metabolites or inhibitors. Seahorse technology has proven particularly valuable in elucidating the rapid metabolic reprogramming underlying immune cell activation (Angelin et al., 2016; Arts, Carvalho, et al., 2016; Gubser et al., 2013; van der Windt et al., 2012).

While excellent for establishing the cell autonomous metabolic pathways present, a main caveat of *in vitro* studies is that it removes the physiological levels of extracellular metabolites, structure, and neuron-glial metabolic communication. To complement these studies, several *in vivo* methods are such as positron emission tomography (PET), stable isotope labeling, and biosensor imaging are also available.

PET is a particularly powerful technique as it is one of the few metabolic measurements that can be performed in humans. Injection of the radiotracer ^{18}F-FDG (fluorodeoxyglucose) allows visualization of brain areas requiring increased glucose uptake, which is associated with synaptic activity (Berti et al., 2014). Nuclear magnetic resonance (NMR) spectroscopy is another useful tool for studying metabolomics in humans. This technique is capable of measuring the abundance of specific metabolites from *in vivo* samples using clinically-available MRI scanners. It is common to pair this measurement with stable isotope labeling to improve signal-to-noise ratio, and target the metabolite or pathway of interest (Befroy & Shulman, 2011; Rolf Gruetter et al., 2003). For experiments requiring higher spatial resolution, this technique can be performed in tissue or cell samples, although the availability and cost of scanners remain largely prohibitive for wider introduction to basic research practices. Thus, while regional differences can be observed with PET imaging and NMR spectroscopy, the cellular types responsible for this signal can not be resolved, and metabolic investigation is limited to the availability of approved tracers or stable isotope inclusion.

Stable isotope labeling is one of the more traditional approaches to studying metabolism, and can be performed at the organism, tissue, or cellular level. It consists of supplying a carbon source, such as glucose or glutamine, which is labelled with a stable isotope, usually ^{13}C, ^{15}N, ^{18}O, or ^{2}H. After feeding cells, tissues, or organisms with the heavy-labelled nutrient, metabolites are collected and analyzed by mass spectrometry. Depending on the labels chosen, specific location of isotope insertion, and timing of incubation, these experiments can be extremely informative of the quantitative rate of a metabolic pathway, and determination of which pathways are active

(Antoniewicz, 2015; Jang et al., 2018; Weindl et al., 2016). Mass spectrometry itself is a useful technique for measuring unlabeled metabolites, however often loses spatial resolution and cellular specificity. The advancements of mass spectrometry imaging (MSI) now allow the nearly complete and unbiased metabolic profile of single 'pixel' locations within tissue at a spatial resolution reaching 5 μm (Rawlins et al., 2015). Mass spectrometry data can be precisely registered onto an optical image of the tissue, allowing investigation of specific regions or cell types of interest. Therefore, data from a specific population of cells can be extracted from mouse brain slices, and their metabolic states identified within their complex native environment. Due to the unique metabolic signature of tumor cells relative to healthy brain tissue, metabolite measurements using MSI have proven powerful in discriminating between clinically similar forms of pediatric brain tumors (A. R. Clark et al., 2018), and can now be used to determine tumor margins and guide intraoperative decisions (Eberlin et al., 2012; Santagata et al., 2014).

To investigate metabolism with higher spatial resolution, specific biosensors are available, which can be imaged by traditional fluorescence microscopy, Förster resonance energy transfer, or fluorescence lifetime imaging. A variety of sensors are now available including PercevalHR for ATP:ADP ratio (Berg et al., 2009), Laconic for lactate (San Martin et al., 2013), and Peredox, RexYFP, and SoNar for NADH:NAD^+ redox state (Bilan et al., 2014; Hung & Yellen, 2014; Zhao et al., 2016). These sensors have greatly advanced our understanding of the brain's metabolic regulation and compartmentalization at the cellular level (Diaz-Garcia et al., 2017; Machler et al., 2016).

In addition to biosensors, it is possible to directly image NADH by autofluorescence. This method is particularly useful as it is a label-free technique and so can be used for clinical applications in which transgenic models or application of biosensors are not feasible (Büttner et al., 2018; Jing et al., 2018; Lombardo et al., 2015). As a product of glycolysis, oxidized NAD^+ becomes reduced to NADH, which is autofluorescent in the blue spectrum (λ_{em} 460 nm). An additional benefit of NADH autofluorescence is its compatibility with fluorescence lifetime imaging (FLIM). This technique compares the time of excitation with the time of emitted photon detection, and can then calculate how long the electron was in an excited state – its fluorescence lifetime. In the free, unbound state, NADH emits photons with a short fluorescence lifetime of 400 ps. However, upon enzymatic binding, such as to complex I of the ETC, NADH is stabilized and its fluorescence lifetime increases to around 2000 ps (Bird et al., 2005; Lakowicz et al., 1992; Schneckenburger et al., 2004; Vergen et al., 2013). Therefore, by comparing the relative contribution of photons from the free or bound NADH pool, it is possible to infer the relative rates of glycolysis and the ETC (Ghukasyan & Kao, 2009). This method, too, is not without its limitations. NADH is not restricted to binding only ETC proteins, and while these measurements are often simplified as mitochondrial metabolism, it is possible that there is also a contribution of photons which are bound to other enzymes, such as lactate dehydrogenase in the cytoplasm. The resulting mean lifetimes are also representations of the ratio of glycolysis to ETC, not a measurement of absolute rate, making it difficult to interpret if a changing lifetime is driven by modifications in the free or bound component. Finally, it is impossible to experimentally distinguish NADH from the closely related nicotinamide adenine dinucleotide phosphate (NADPH) by emission wavelength or lifetime. However, there have been computational methods developed to address this, in which the bound component of NADH and NAD(P)H can be separated, and this ratio is then used to interpret the

contribution of NADPH to the total NADH measurement (Blacker et al., 2014). Without computational separation of these molecules, this limitation is acknowledged by referring to this technique as NAD(P)H-FLIM. Despite these caveats, by pairing NAD(P)H-FLIM with cell-type specific identification, it is possible to measure single cell metabolism while maintaining *in vivo* or *in situ* environments, making this a powerful metabolic technique. It has revealed many biological impacts of cellular metabolism, such as stem cell differentiation, cancer cell metastasis, and immune activation (Alfonso-García et al., 2016; Stringari et al., 2011, 2012, 2015).

1.4 Immunometabolism

The involvement of metabolism in the regulation of immune cell polarization has become an increasingly growing and influential field, known as immunometabolism (Fumagalli et al., 2015; Newton et al., 2016; O'Neill et al., 2016; Rambold & Pearce, 2017). While metabolic pathways are most recognized for the production of ATP, the vast network of enzymes and metabolites involved can also function as sensors and regulators of non-metabolic activities, allowing these pathways to act as signalling platforms. The metabolic components are perfectly situated to integrate extracellular cues with intracellular energy levels, transcription and translation, and biosynthesis, thereby regulating cellular function. Several metabolic mechanisms involved in immune regulation have been elucidated, including activity of glycolytic enzymes, accumulation of TCA cycle metabolites, and repurposing of the mitochondria to increase ROS production (see Table 1.1).

Mechanism	Anti-inflammatory	Pro-inflammatory
ETC:	OXPHOX metabolism ⟷	ROS production
TCA metabolites:	αKG ⟷	Succinate
Fumarate and Citrate:	Mitochondria ⟷	Cytoplasm
GAPDH:	TNFα inhibition ⟷	Glycolysis

Table 1.1 Overview of mechanisms of metabolic reprogramming in immune cells.

The electron transport chain (ETC) can be used for ATP production through OXPHOS, or could be repurposed to support reactive oxygen species (ROS) production. Altered ratios of tricarboxylic acid (TCA) metabolites can regulate the activity or stability of downstream enzymes. αKG:succinate ratios regulate HIF-1α stabilization. Subcellular localization of metabolites, such as fumarate or citrate, can regulate their activity in either energy production (mitochondrial) or epigenetic modifications (cytoplasmic). Activity of metabolic enzymes, including GAPDH, may have anti-inflammatory functions in addition to their metabolic role.

From extensive work in the peripheral immune system, it has become clear in both the innate (macrophage and dendritic cells) and adaptive (T cells and B cells) immune system that a pro-inflammatory stimulus induces aerobic glycolysis while anti-inflammatory signals increase FAO and OXPHOS. Many reports point to the role of mammalian target of rapamycin complexes (mTORC1 and mTORC2) as master regulators coordinating this metabolic reprogramming. In T cells, constitutive mTORC1 activation increased glycolysis and resulted in effector T cell phenotypes that were then incapable of differentiating into a resting T memory cell. Conversely, mTORC1 inhibition resulted in memory T cells which were unable to mount an effector response (Pollizzi et al., 2015). Additional work supports this finding, identifying mTORC1-dependent metabolic reprogramming necessary for T cell exit from quiescence to a T helper cell (K. Yang et al., 2013). In contrast to the effector phenotypes, long-lived memory T cells are associated with

mitochondrial biogenesis, OXPHOS, and mitochondrial spare respiratory capacity (van der Windt et al., 2012). Similar pathways have been identified in macrophages, where LPS stimulation increases aerobic glycolysis and pro-inflammatory polarization (EL Kasmi & Stenmark, 2015; Palsson-McDermott et al., 2015; Tannahill et al., 2013). However, the anti-inflammatory cytokine, interleukin 10, reduced aerobic glycolysis following LPS, and instead promoted OXPHOS metabolism in macrophages (Ip et al., 2017).

1.4.1 Increased aerobic glycolysis

An increased glycolytic rate, even under normoxic conditions and with functional mitochondria, is called aerobic glycolysis, or Warburg metabolism, as it was first described by Otto Warburg as a unique metabolic signature of cancerous tissue (Warburg, 1956). Rather than viewing metabolic shifts as a result of transcription changes or a response to the local environment, Warburg suggested that it was this initial metabolic dysregulation that was one of the oncogenic factors triggering cells to become cancerous. While this result remained unappreciated for several decades, aerobic glycolysis is now recognized as an important regulator of cell function, including stem cell renewal (Stringari et al., 2015), and pro-inflammatory immune activation (Everts et al., 2014; Kornberg et al., 2018; Netea et al., 2017).

An initially suggested outcome of glycolytic increase was a cytosolic ATP burst allowing the associated energy-demanding activities of immune cell activation. While the total ATP contribution from glycolysis is hard to quantify, and the amount of ATP generated in this pathway (2 molecules) is much less than if glucose were to be fully oxidized by the ETC (38 molecules), it is plausible that this is a much faster pathway than incorporating mitochondrial metabolism. The

role of subcellular location of ATP generation may also be important in regulating enzyme-specific activity, such as the neuronal K_{ATP} channel. This transmembrane protein responsible for K^+ efflux is inactivated by ATP. Therefore, cytosolic ATP production via glycolysis decreases its activity, leading to an increased intracellular K^+ concentration, membrane depolarization, and increased firing rates possibly leading to epileptic activity. If ketone bodies are supplied to promote mitochondrial ATP production, there is a release of cytoplasmic ATP inhibition to the K_{ATP} channel, allowing K^+ efflux and membrane polarization, decreasing seizure-like firing rates (Gimenez-Cassina et al., 2012; Martinez-François et al., 2018; Yellen, 2008).

Beyond ATP generation, the flow of carbon through glycolysis or the PPP can regulate cellular redox state and nucleic acid biosynthesis. NADPH reduction through the PPP increases ROS production as it acts as a substrate for the NADPH oxidase (NOX) enzymes to generate superoxide. However, NADPH is also a critical molecule is ROS handling, as it donates a hydrogen to oxidized glutathione (GSSG), regenerating its reduced form (GSH), which can then continue to serve protective effects by neutralizing ROS within the cell. An intermediate metabolite of the PPP is ribose-5-phosphate, which can exit the pathway to be used for nucleotide biosynthesis (Bolaños & Almeida, 2010; Cairns et al., 2011; Fan & Lane, 2015; Patra & Hay, 2014). In immune cell activation, colony proliferation is an important response, and therefore increased nucleotide synthesis is necessary to support mitotic expansion.

The rate of glycolysis can also control the subcellular localization of key enzymes, such as glyceraldehyde 3-phosphate dehydrogenase (GAPDH). In addition to performing the sixth step of glycolysis, GAPDH also serves as a translational inhibitor of pro-inflammatory cytokine, TNF-α,

by binding to its 3' untranslated region (Chang et al., 2013; Millet et al., 2016). When monocytes were kept in a state of low glycolysis, there was an increased binding of GAPDH to the TNF-α mRNA and less association of this mRNA with polysomes. Increasing glycolysis causes GAPDH to be drawn away from the mRNA to meet the demand for its increased metabolic functions. Indeed, either knocking down GAPDH or increasing glycolysis was sufficient to decrease GAPDH binding to TNF-α mRNA. Therefore, the rate of glycolysis and need for GAPDH activity regulates TNF-α translation (Chang et al., 2013; Millet et al., 2016). As further support for the importance of GAPDH, the immunomodulatory drug, dimethyl fumarate (DMF) or endogenous fumarate can irreversibly inhibit the catalytic cysteine of GAPDH. This resulted in anti-inflammatory effects in both mouse and human monocytes and lymphocytes, and in a mouse model of multiple sclerosis, experimental autoimmune encephalomyelitis (EAE), which were mediated by down-regulating the rates of aerobic glycolysis (Kornberg et al., 2018).

1.4.2 Broken TCA cycle

In addition to increased aerobic glycolysis, pro-inflammatory immune stimulation causes inhibition of several TCA cycle metabolites, resulting in a 'broken' TCA cycle. This results in the accumulation of several intermediate metabolites, most notably citrate, fumarate, and succinate, which can then support biosynthesis, induce epigenetic modifications, or regulate protein activity.

Citrate, the first metabolite formed after acetyl-CoA integration is usually converted to isocitrate via the enzyme aconitase. When immune cells are stimulated with pro-inflammatory signals, there is an accumulation of citrate, which can be exported to the cytoplasm by the mitochondrial citrate carrier (Williams & Neill, 2018). The citrate carrier itself is also upregulated following

lipopolysaccharide (LPS) activation and its inhibition decreased nitric oxide (NO), ROS, and prostaglandin production (Infantino et al., 2011). Once in the cytoplasm, citrate can be converted back into oxaloacetate and acetyl-CoA. Through processing of oxaloacetate to pyruvate, NADPH can be generated, which supports the production of ROS by NOX and NO by inducible NO synthase (Infantino et al., 2011).

Citrate that has been processed into acetyl-CoA instead supports the lipogenesis associated with membrane expansion. As with nucleotide biosynthesis, immune stimulation and the following colony expansion requires organelle and membrane generation to support mitosis. Increased protein production, including cytokine translation, will also stimulate endoplasmic reticulum and Golgi expansion, which increases lipogenic demands (Everts et al., 2014; Hatzivassiliou et al., 2005). Citrate-supplied cytoplasmic acetyl-CoA is also necessary for the TNF-α or interferon gamma (IFNγ) induction of prostaglandin production (Infantino et al., 2014). Finally, increased acetyl-CoA from cytoplasmic citrate is a substrate for lysine acetylation of histone and non-histone proteins (Choudhary et al., 2014). By providing acetyl groups, citrate can alter the acetylation status of chromatin, and therefore the epigenetic regulation of immune cells (Kinnaird et al., 2016; Morciano et al., 2009; Wellen et al., 2009). These epigenetic changes in innate immune cells following stimulation is termed ‘trained immunity’ or ‘innate immune memory’ and are protective against a second infection. This occurs even in organisms lacking functional T and B cells of the adaptive immune system, which is classically considered to be the only branch of the immune system to acquire immunological memory (M. G. Netea et al., 2016; Saeed et al., 2014). In a striking experimental example of innate immune memory, initial training by β-glucan stimulation in a mouse model caused an epigenetic shift associated with a maintained increase in aerobic

glycolysis of monocytes, and subsequent protection against lethal *C. albicans* infection or *Staphylococcus aureus* sepsis. This protection could be blocked by treating the mice with inhibitors of the mTOR pathway to block the metabolic reprogramming and increased aerobic glycolysis (Cheng et al., 2014).

In addition to citrate, accumulation of another TCA metabolite, fumarate, can also affect epigenetic modifications. Fumarate can directly inhibit the KDM5 family of histone demethylases, which are known to remove H3K4 acetyl groups (Arts, Novakovic, et al., 2016). Therefore, both citrate and fumarate accumulation will lead to a higher level of histone acetylation, which is associated with chromatin loosening and increased DNA availability for transcription (Verdin & Ott, 2014).

Succinate accumulation in activated immune cells has also become an apparent immunometabolic regulator. Succinate exits the mitochondrial matrix via the dicarboxylic acid transporter (Tannahill et al., 2013). In the cytosol, succinate can influence cellular functions by increasing lysine succinylation, a post-translational modification (E. Mills & O'Neill, 2013; Z. Zhang et al., 2010). One such modified protein is pyruvate kinase M2 (PKM2), which is succinylated in macrophage following LPS activation, increasing its interaction with hypoxia-inducible factor 1α (HIF-1α), nuclear entry, and association with the promoter of IL-1β. In mice with hypersuccinylated PKM2, an increased IL-1β production heightens the vulnerability to dextran sulfate sodium-induced colitis (F. Wang et al., 2017). Interestingly, the expression and posttranslational modifications of PKM2 have been noted to decrease the efficiency of the enzyme in cancer cells displaying Warburg metabolism. This relatively inactive form of the enzyme causes an accumulation of glycolytic intermediate metabolites, which then encourages their flux through anabolic pathways (Prakasam

et al., 2018). The increased anabolic flux may support the phospholipid, amino acid, and macromolecule biosynthesis necessary to support the rapid proliferation of these cells.

Succinate accumulation can also directly stabilize the transcription factor HIF-1α, and thereby increase production of its target genes, including glycolytic enzymes and pro-inflammatory cytokines. As a rapidly inducible and tightly controlled protein, HIF-1α is continuously being transcribed, and then degraded by E3 ubiquitin ligase (Koivunen et al., 2007). It is labeled for degradation by prolyl hydroxylases (PHDs), whose activity is increased by α-KG and decreased by succinate. Thus, the ratio of α-KG and succinate control the stabilization of HIF-1α, where increased succinate causes stabilization. In macrophages, LPS stimulation led to an increased aerobic glycolysis, succinate accumulation, and HIF-1α stabilization, which resulted in the increased production of IL-1β (Tannahill et al., 2013).

Succinate is a particularly interesting metabolite as it is processed by succinate dehydrogenase (SDH), which also serves as complex II in the ETC. SDH therefore serves as a link between TCA and ETC activity. In macrophages, LPS stimulation to a pro-inflammatory state caused an increased aerobic glycolysis, with accumulation of succinate. This succinate fueled the activity of SDH, which caused mitochondrial hyperpolarization and ROS production. Blocking either SDH activity or ROS production decreased the LPS-induced production of pro-inflammatory cytokines (E. L. Mills et al., 2016). This study also highlights another immunometabolic step, which is the repurposing of the mitochondria from ATP production to ROS generation (Chouchani et al., 2014; E. L. Mills et al., 2017). This oxidative burst may serve an important protective role in the antibacterial activity of an activated immune system (West et al., 2011).

1.4.3 Glutaminolysis support of TCA cycle metabolites

As immune activation is associated with aerobic glycolysis, which is converted to lactate rather than pyruvate, and at the same time, an accumulation of TCA cycle metabolites, it is important that an alternative nutrient source supplies the carbon necessary to allow continued TCA cycle function. While several pathways are capable of replenishing the TCA cycle, accumulating evidence across the immunometabolic field points to glutaminolysis as the key pathway fulfilling this role. Through glutaminolysis, glutamine enters the TCA cycle as α-KG.

Continued supply of α-KG via glutaminolysis can support the citrate and fumarate accumulation that are observed in immune activation. When citrate is diverted out of the TCA cycle to contribute to lipogenesis and epigenetic regulation, isocitrate dehydrogenase 2 can convert α-KG into citrate through reductive carboxylation, thereby continuing its supply (Ward et al., 2010). Similarly, in trained immunity, increased glutaminolysis supports fumarate accumulation to mediate the associated epigenetic modifications (Arts, Novakovic, et al., 2016).

A more direct involvement has been shown for glutamine-derived α-KG contribution to succinate accumulation (Tannahill et al., 2013). In these LPS-activated macrophages, there was a marked increase in the amount of succinate derived from stable-isotope labelled glutamine, which was critical for HIF-1α stabilization and IL-1β production. While most of the succinate came from glutaminolysis through α-KG, there was also some contribution of glutamine through the GABA shunt pathway, which bypasses the α-KG step and feeds directly into succinate (Tannahill et al., 2013).

As previously discussed, mTORC1 is involved in pro-inflammatory metabolic reprogramming and increased aerobic glycolysis. Therefore, it is not surprising that it also contributes to the increased rate of glutaminolysis in activated cells. mTORC1-mediated ubiquitination and degradation of CREB2 causes decreased transcription of SIRT4, a mitochondrial sirtuin and inhibitor of glutamate dehydrogenase (GDH). Consequently, increased mTORC1 activity leads to an increase in GDH activity. In glutamine-addicted cancer cells, which are metabolically similar to pro-inflammatory immune cells, SIRT4 levels are reduced and its overexpression decreases proliferation and tumorigenesis (Csibi et al., 2013).

Supply of α-KG via glutaminolysis can also regulate polarization of T cells into helper or regulatory phenotypes. Activation of glutamine-deprived naïve T cells in the presence of cytokines to induce helper cell polarization instead produced T regulatory cells. These cells maintained their suppressor function after *in vivo* adoptive transfer to recipient mice. The effect of glutamine deprivation could be rescued by supplying a cell-permeable α-KG analog. Under these conditions, stimulation was again able to induce T helper cells, as seen in glutamine replete media (Klysz et al., 2015). Therefore, the role of glutamine in supplying TCA cycle metabolites is critical in controlling the survival, proliferation, and polarization of metabolically reprogrammed cells with aerobic glycolysis and a broken TCA cycle.

1.5 Rationale and hypotheses

The influences of microglia on healthy brain development, functioning, and aging are becoming increasingly clear as studies continue to reveal their nuanced functions. Microglia are long-lived

cells, so previous activation or experiences can contribute to the development of later dysfunctional immune responses. A lack of appropriate regulation, or an increase in pro-inflammatory function are associated with many neurodegenerative diseases, including Alzheimer's disease, Parkinson's disease, and Huntington's disease, and are often detectable before behavioural symptoms become evident. A slow increase in dystrophic microglia with aging is associated with inappropriate immune activation in the absence of a known stimulus, leading to mild but chronic release of cytokines, brain swelling, and eventual neuronal toxicity, a term defined as inflammaging. However, in all of these cases, it is still difficult to ascertain the cause or effect nature of these microglial changes. While immune activation is often seen before gross neurodegeneration, it is possible that subtle changes in neuronal health or activity initially trigger this microglial response. It is also possible that accumulation of modifications and decreased health of microglia are the instigating causes of the following neuronal death. This cause-effect relationship has proven extremely difficult to disentangle. Given their association with a broad spectrum of neurodevelopmental and neurodegenerative conditions, as well as in injuries including traumatic brain injury and stroke, it is not surprising that microglia have increasingly become the target of clinical therapeutic interventions. While some treatments are showing promise, at least at the level of animal models or early clinical trials, much work remains to uncover the initial triggers of microglial activation or dysfunction, the mechanistic signalling pathways involved, and the functional outcome of these changes to neuronal activity.

In the experimental investigations of these issues, it is important to remember the intimate relationship between microglia and their environment and neighbouring cells. *In situ* and *in vivo* preparations have demonstrated the elaborate branching of these three-dimensional cells to

facilitate surveillance and synaptic interactions. Alterations in this morphology, including process elongation, loss of contact inhibition, convergence of processes onto an area of damage, or process retraction to create an amoeboid phenotype, are indicative of microglial responses to environmental cues and corresponding changes in cellular function. It follows that analysis of microglial morphology has become a widely-used and informative technique to investigate their function while avoiding overt tissue disruption. Microglia have extensive three-dimensional ramifications, so that most imaging of these cells requires taking z-stacks to capture the entire extent of their processes. However, most morphological analyses of these stacks are either performed by compressing the z information into a two-dimensional image, or manual process tracing in three-dimensions. These methods are prone to user bias, difficult to replicate across experimenters and labs, extremely time-consuming, or result in the loss of valuable three-dimensional information, resulting in an underestimation of branch length and an inability to separate branches that overlap in the z-dimension. Furthermore, only one cell can be imaged at a time, as taking an image stack containing multiple cells would result in an inseparable network of cells, which are actually territorially distinct.

The limitations in these current methods spurred the development of a new technique, 3DMorph (see Figure 1.3), which is a MATLAB-based manuscript to automatically process three-dimensional images of microglia (**Chapter 2**). This novel script maintains the three-dimensional information, allowing accurate separation of branches, or cells in images containing multiple microglia. The implementation of several graphical user interface windows allows user-defined threshold levels and image scaling to allow the program to handle multiple types of imaging parameters. Once these settings are selected, a parameters file is saved, which can be used to batch

process multiple images using the same settings, thus removing the risk of experimenter bias. If the images and parameters files are shared to another lab, the same results will be obtained, enhancing the reproducibility of these results. Importantly, batch processing of files is done automatically, significantly reducing user-input time for image analysis. Raw data for each image is written and saved as an Excel file, which can then be investigated and plotted by the researcher. This script has been published and made freely available online for the download, use, and modification by other labs to meet their research purposes.

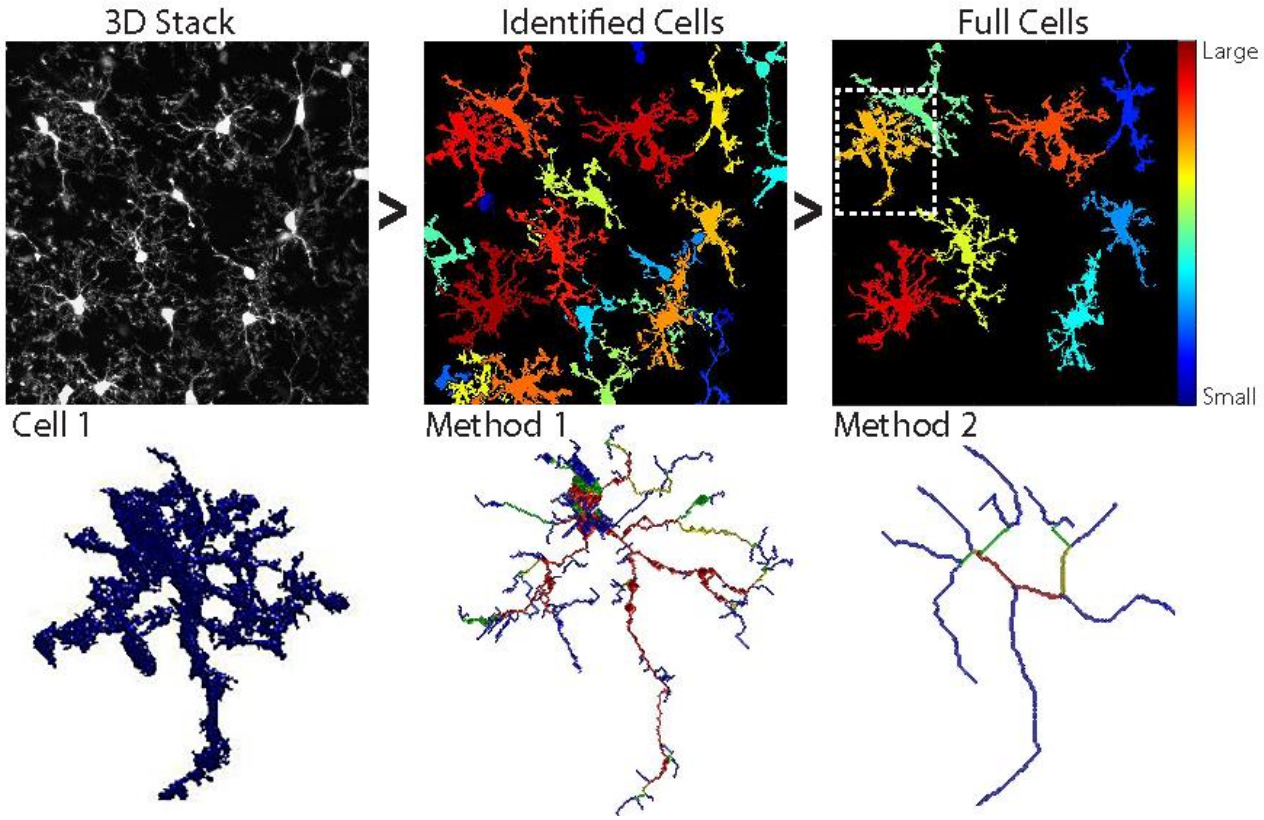

Figure 1.3: Overview of 3DMorph platform.

Using specified settings or a previously-generated parameters file, a 3D imaging stack is processed into individual cells, from which small or out-of-plane processes can be removed, leaving the remaining full cells. Each cell is then individually handled to create a skeleton either including small processes (method 1) or only main branches (method 2). Data from the full image and from each cell are written to an excel file, and specified images of interest are saved.

In parallel to an increasing prevalence of neurodegenerative diseases, there is also a current epidemic of both obesity and malnourishment. The role of nutrient availability and resulting modifications to cellular metabolism have become a field of increasing attention and impact, known as immunometabolism. A long-standing finding linking the metabolic and neurological fields is the observation that untreated diabetes and associated inflammation is a risk factor for developing Alzheimer's disease. Therefore, further investigation to cellular metabolism and its roles in immune function will be important in understanding and treating these complex diseases. Much work has been done in the peripheral immune system, elucidating the roles of glycolysis and TCA cycle metabolites in stimulating and permitting pro-inflammatory immune activation in cells of both the innate and adaptive immune components. In contrast, OXPHOS metabolism is associated with long-lived regulatory cells and anti-inflammatory polarization. A remaining challenge in this field is to determine if these metabolic reprogramming steps also occur in microglia, the resident macrophage of the brain. The brain presents a unique metabolic challenge as its energetic environment is tightly regulated by the BBB and glial cell interactions, and neuronal tissue is extremely sensitive to metabolic disruptions such as lack of oxygen or glucose. With glucose considered as the obligatory fuel source of the brain, it is unclear to what extent each cell type metabolizes alternative carbon sources, the extent of complete oxidation, or any subtle changes reflecting dietary or circadian state, fluctuations in neuronal activity, or tissue health. The brain is also the site of many immune-related dysfunctions throughout development, aging, and disease, about which we are only beginning to understand underlying mechanisms and treatment avenues. Therefore, further investigation of microglial baseline metabolism, as well as metabolic reprogramming in immune stimulation, disease, or aging, will aid in better understanding of

neurological dysfunctions, and potentially provide a promising clinical target with readily accessible and low-risk interventions.

As with morphological considerations, it is also important to investigate microglial metabolism in physiological environments. Many current techniques use *in vitro* measurements, and it is likely that microglia have already undergone massive metabolic reprogramming during the culturing or extraction protocols. While these *in vitro* techniques are useful to address the cell-autonomous microglial effects without confounding factors of metabolic communication with neighbouring cells, it will likely not accurately reflect the true microglial metabolism *in vivo*. Therefore, fluorescence lifetime imaging of NAD(P)H was employed to measure relative rates of glycolysis and the ETC in acute brain slices, which, using two-photon microscopy, can be done in a cell-specific manner. In order to identify microglia within this heterogeneous tissue, the feasibility of pairing NAD(P)H-FLIM with genetic GFP expression (using the CX3CR1$^{EGFP/+}$ mouse line) was tested. It was found that two-photon NAD(P)H imaging conditions excite a protonated form of GFP molecules, which emit in the blue spectrum with a short fluorescence lifetime, experimentally inseparable from that of free NAD(P)H (**Chapter 3**). This is critical information for the metabolic imaging field, as reports using NAD(P)H-FLIM in GFP-expressing tissue have previously been published and incorrectly interpreted as cells with increased glycolysis. Therefore, for the metabolic experiments carried out in this thesis, microglia are visualized with DyLight 594-conjugated tomato lectin, which was experimentally validated to have no effect on NAD(P)H imaging.

Using this NAD(P)H imaging technique, the single-cell metabolic profiles of microglia were measured within the physiological environment of an acute brain slice, both at baseline and in response to nutrient or pharmacological interventions. The purpose of this dissertation was to investigate the following hypotheses:

Hypothesis 1: Microglia are not restricted to glucose catabolism, but are metabolically flexible and can metabolize glutamine upon glucose removal **(Chapter 4)**.

Hypothesis 2: Innate immune stimulation of microglia with LPS will cause an increase in glycolytic rate, resulting in accumulation of HIF-1α, which will increase production of the pro-inflammatory cytokine, IL-1β (**Chapter 5**, see Figure 1.4).

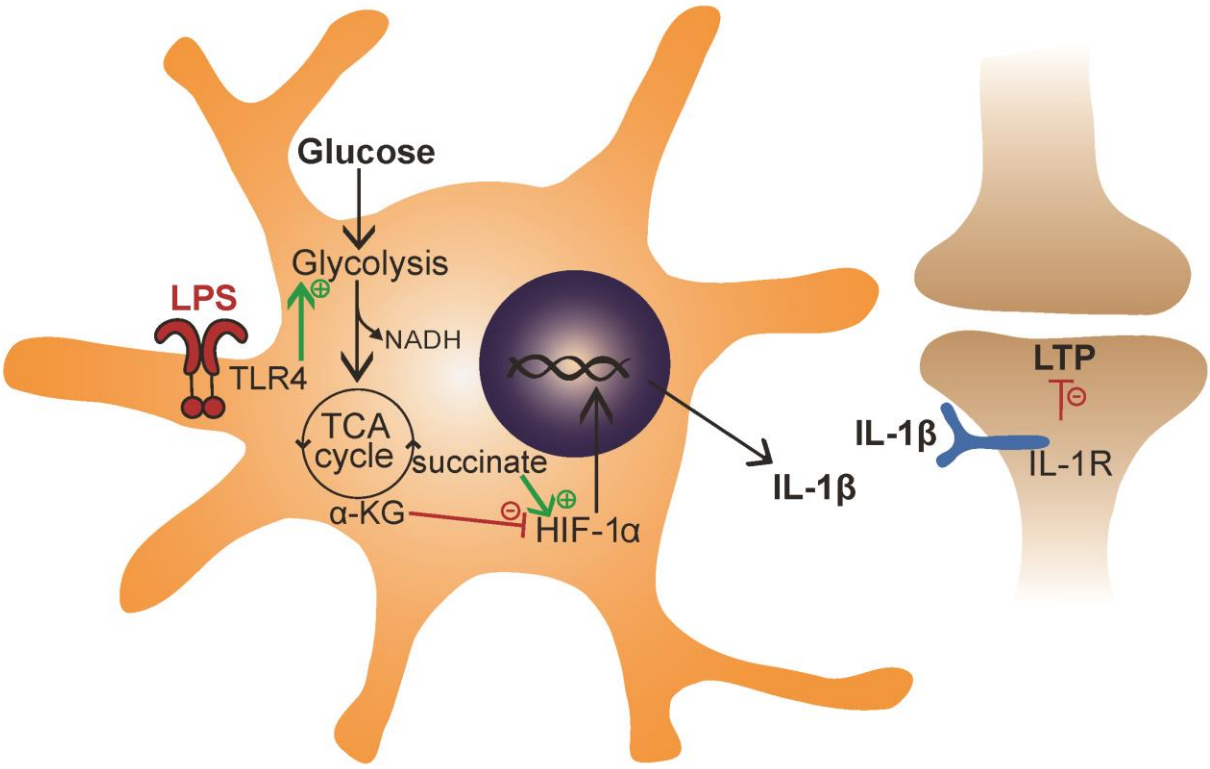

Figure 1.4: Hypothesized microglial metabolic reprogramming.

LPS stimulation of microglial TLR4 causes an increase in glycolytic activity, concomitant break in the TCA cycle, and accumulation of succinate – a stabilizer of the transcription factor, HIF-1α. Increased HIF-1α promotes the transcription and release of the pro-inflammatory cytokine, IL-1β, which activates neuronal IL-1 receptors on synapses and inhibits long-term potentiation.

Chapter 2: 3DMorph automatic analysis of microglial morphology in three dimensions from *ex vivo* and *in vivo* imaging

2.1 Introduction

Microglia, the immune cells of the central nervous system, have small cell bodies and ramified processes that survey the local environment for signs of infection, damage, or disruption of molecular homeostasis (Nimmerjahn et al., 2005). In response to sensing damage, microglia rapidly extend their processes to converge at the site of injury (Davalos et al., 2005; Dissing-Olesen et al., 2014; Drew et al., 2010; U. B. Eyo et al., 2015, 2014; Hines et al., 2009; Lou et al., 2016; Nimmerjahn et al., 2005). Upon extensive damage of surrounding cells or stimulation by pathogen-associated triggers, microglia retract their processes to adopt an amoeboid morphology (Doorn et al., 2014; Kloss et al., 2001; Kreutzberg, 1996).

As a result of these contextual morphological changes, microglial shape and process ramification have been used as correlates of cellular function (Davis et al., 1994; Karperien et al., 2013), with several methods developed to quantify their morphology. Current approaches include manually tracing processes throughout z-stack images (Baron et al., 2014; Takayama et al., 2016), or performing morphological analysis on a 2-dimensional maximum projection (Karperien et al., 2013; Kozlowski & Weimer, 2012; Torres-Platas et al., 2014; Verdonk et al., 2016). The first method is time-intensive and subject to experimenter bias and variability. The second technique loses 3D information, leading to underestimation of process lengths or erroneous connection of processes. Three dimensional reconstructions of microglia cells can be generated using software

such as Imaris (Erny et al., 2015; Perego et al., 2013); however, this is time-intensive and expensive. There is a clear need for a method that performs unbiased and automatic analysis of the 3D microglial structure observed in *ex vivo* and *in vivo* systems.

Here, we describe a method for semi-automatic analysis of microglial morphology in 3D using a custom Matlab script, 3DMorph. The program uses graphical user interfaces to initially define image threshold, noise limits, and cell sizes. Once these settings are selected, a parameters file is saved that can be used to automatically batch process multiple files. From each image, an Excel file is saved with output data from the entire image (volume covered, average centroid distance), as well as from individual cells within the image (territorial volume, cell volume, cell ramification index, number of endpoints and branch points, and average, min, and max branch lengths).

The utility of 3DMorph is validated by analyzing and quantifying typical examples of morphological changes of groups of microglia under control conditions, after hyper-ramification triggered by ATP application, and after retraction of ramifications triggered by inhibiting neuronal AMPA receptors with CNQX and action potentials with TTX. 3DMorph is also shown to process *in vivo* microglial images, as well as other branching cell types such as neurons. Therefore, this analysis software will allow for the automatic and unbiased analysis of microglial morphologies in 3D under several experimental and pathological conditions.

2.2 Materials and Methods

2.2.1 Animal protocols

All housing and experimental procedures were carried out in accordance with University of British Columbia and Canadian Council on Animal Care regulations. $CX3CR1^{EGFP/EGFP}$ or $CX3CR1^{+/EGFP}$ mice on a C57Bl/6 background (S. Jung et al., 2000) were housed in a 12 h light/day cycle with food and water *ad libitum*.

2.2.2 Acute hippocampal slice preparation

Male mice (2 months of age) were anesthetized to surgical plane with isoflurane and decapitated according to protocols approved by the University of British Columbia committee on animal care. Brains were dissected and sliced horizontally with a vibratome (Leica VT1200S) at 300 μm thick in ice-cold NMDG slicing solution containing (in mM): 120 N-methyl-D-glucamine, 2.5 KCl, 25 $NaHCO_3$, 1 $CaCl_2$, 7 $MgCl_2$, 1.2 NaH_2PO_4, 20 D-glucose, 2.4 sodium pyruvate, and 1.3 sodium L-ascorbate, which was constantly oxygenated with 95% O_2 and 5% CO_2. Hippocampal slices were immediately transferred to artificial cerebral spinal fluid (aCSF) continuously oxygenated with 95% O_2 and 5% CO_2, and allowed to recover for 30 minutes at 32 ˚C. Artificial CSF contained (in mM): 126 NaCl, 2.5 KCl, 26 $NaHCO_3$, 2 $CaCl_2$, 2 $MgCl_2$, 1.25 NaH_2PO_4, and 10 D-glucose, pH 7.3–7.4, osmolarity 300 mOsm.

2.2.3 Treatment conditions and SNAPSHOT

Slices were incubated for 10 min at 32 °C in either control aCSF, or aCSF containing 500 μM ATP, or 50 μM CNQX and 1 μM TTX. Slices were then fixed using the SNAPSHOT method (Dissing-Olesen & MacVicar, 2015), which consists of a 2 minute immersion in 4% PFA at 80 ˚C,

rinse in 0.1 M PBS, and storage in clearing solution (0.1M PBS with 20% DMSO, and 2% triton X) at 4 ˚C for one week. GFP fluorescence is well-preserved by this method, and slices were ready for imaging immediately after clearing.

2.2.4 Acute hippocampal slice image acquisition

Fixed hippocampal slices were imaged with a two-photon Coherent Chameleon Ultra II laser with a Zeiss LSM 7 MP microscope. Using a Zeiss 20x-W/1.0 NA objective, GFP was excited at 920 nm, and emission was detected by a photo-multiplier tube (Zeiss LSM BiG) after passing through a 535 ± 25 nm filter. Images were taken in the stratum radiatum of CA1 hippocampus at a depth of 150 µm ± 25 µm. Stacks were imaged at 16-bit, with 1024 x 1024 pixels, 16-line averaging, a zoom of 2.8, and z-step distance of 1 µm. After acquisition, background signal was removed from all images using Fiji's rolling ball (radius = 25 pixels) background subtraction.

2.2.5 Cranial window surgery

Mice were anesthetized using a tricomponent anesthesia (fentanyl, 0.05 mg/kg; midazolam, 5 mg/kg; medetomidine, 0.50 mg/kg), placed on a heating pad, and secured to a stereotactic frame. After the skull was exposed by removing the skin and periosteum, a circle was gently drilled into the skull's surface at 0.5 mm lateral of -0.5 mm bregma. Once this portion of skull was removed, the brain was kept moist using surgical gel sponges in PBS (GelitaSpon). A custom-made 14 mm diameter titanium ring was secured around the cranial window with light-curing dental cement (Heraeus). This ring fits into a custom-made head fixation plate, which secures the skull in the x, y, and z planes during *in vivo* imaging (Hefendehl et al., 2014).

2.2.6 *In Vivo* image acquisition

After cranial window preparation and titanium head ring fixation, anesthetized mice (fentanyl, 0.05 mg/kg; midazolam, 5 mg/kg; medetomidine, 0.50 mg/kg) were imaged on a custom-made two-photon microscope (Rosenegger et al., 2014) using a Coherent Chameleon Ultra II laser and a Zeiss 40X-W/1 NA objective. The head ring is secured to a fixation plate (Hefendehl et al., 2014), which is connected to a motorized x-y stage (Sutter Instruments). EGFP was imaged with 920 nm excitation and detected via non-descanned detectors after passing an ET525/50m-2P emission filter (Chroma Technology). Laser power did not exceed 45 mW throughout the experiment. Z-stack images (z = 40; 1 µm steps) were acquired at 512 x 512 pixels with no averaging, at a depth of 100 - 140 µm. Using a custom-designed perfusion system, aCSF was continuously perfused across the cortical surface at a rate of 3 ml/min. After acquisition, the signal of EGFP in these images was enhanced by increasing the contrast in Fiji, and motion artifacts were corrected with the Gaussian 3D filter.

2.2.7 Neuronal dye loading

Layer 3 neurons from acute cortical slices (P24 rat) were whole-cell patch clamped with borosilicate glass electrodes (3-4 MΩ). The intracellular recording solution consisted of (in mM): 113 K-gluconate, 2 $MgCl_2$, 8 Na-gluconate, 3 KCl, 1 K2-EGTA, 4 K2-ATP, and 0.3 Na3-GTP at pH 7.25 with 10 HEPES. The solution also contained 50 µM Alexa 594 hydrazide (Thermo-Fisher) to visualize the morphology of the dendritic arbour. The example cell was dialysed with dye for 30 minutes before the patch electrode was slowly withdrawn prior to imaging. Images were post-processed in Fiji to subtract background using rolling ball radius, and enhance connectivity while removing speckles using the Gaussian Blur 3D filter and smooth functions.

2.2.8 3DMorph Workflow

The overall workflow of 3DMorph is outlined in Figure 2.1. Once images are acquired and processed as necessary, they should be moved to the Current Folder within Matlab, or the data folder should be added to Matlab's search path. The user first selects 'Interactive Mode' or 'Automatic Mode'. Any time a new batch of images with different threshold settings or xyz scales are being processed, it is necessary to run the program in Interactive Mode. The user inputs the file of interest, its xy and z scale, the number of channels included in the image, and the channel of interest (Figure 2.1A). Either .tiff or .lsm files are accepted. The user then adjusts threshold and size cut-off values (as discussed in detail below; Figure 2.1B-D). Finally, a folder is created to store figures, and an Excel file of results is saved (Figure 2.1E). Output values include data obtained prior to small object removal (average centroid distance between cells, total territorial volume, uncovered volume, percent covered volume), and from individual full cells (cell and territorial volumes, ramification index, number of endpoints and branch points, and average, minimum, and maximum branch lengths). If the user selects the option, a separate Excel file containing a list of all branch lengths can be generated for each cell. Once an Interactive Mode analysis is complete, a parameter file will be created to save relevant input values. This can then be used to batch process a group of files using the same values and settings.

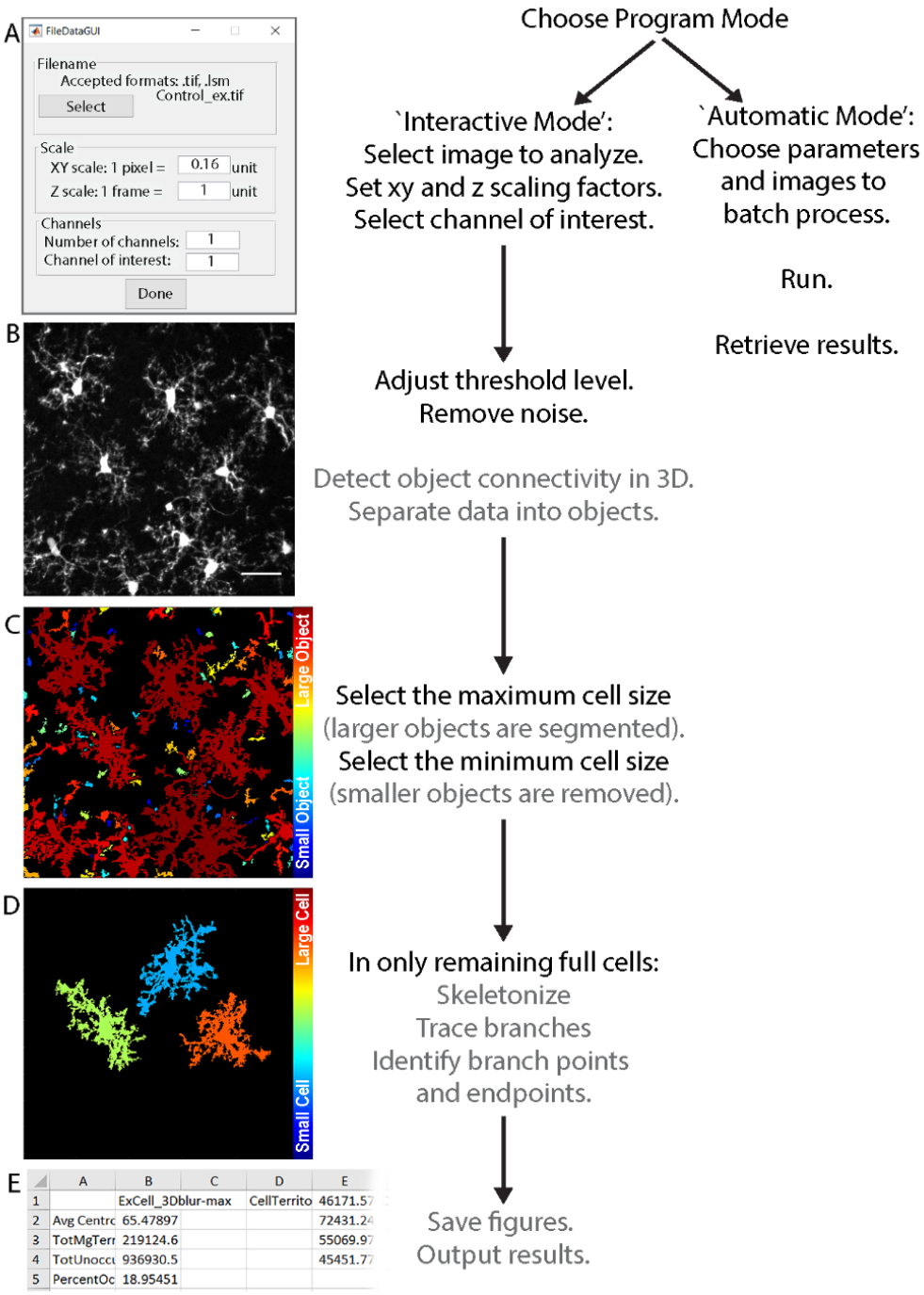

Figure 2.1 3DMorph workflow.

The user selects either Interactive or Automatic mode. Interactive mode must be used first to generate a parameters file. (A) The user then selects the file to analyze, and specifies xy and z scale, number of channels, and the channel of interest. Both .tiff and .lsm files are supported. The original image (B) is loaded and 3D connected components (C)

are automatically detected. (D) Large cells can be selected for segmentation and small objects can be removed. (E) After skeletonization and measurements of remaining cells, 3DMorph saves selected images and generates an Excel results file. Grey text indicates automatic steps.

2.2.9 Threshold images

Images saved as .lsm or .tiff files (Figure 2.2A) are opened using the bfopen, or imread functions, respectively. A threshold value, based on Otsu method (Otsu, 1979) is then set. A new window will appear (Figure 2.2B), showing the middle image of the z-stack, which can be used for a reference in deciding threshold values. A slider on the left sets the threshold level, and an automatically updated image shows the results of selected threshold values. The purpose of this step is to select a threshold level that accurately separates the small processes from background signal. Once an appropriate level is chosen, the 'Try this…' button passes the threshold adjustment value to the noise filter. Again, a slider on the left can be adjusted to decide the minimum size of objects that should be considered noise. This filter functions in 3D, so if a process is removed here, it was likely separated from the cell in the thresholding step. Small cells and processes will be excluded in a later step (Figure 2.2E), so it is not necessary to exclude them as noise here – they contribute to the calculation of total occupied brain volume. If selected, a threshold output image (Figure 2.2C) can be generated, which is a projection of the thresholded z-stack, where the thicker portions of cells (such as somas) are displayed in yellow and thinner portions are in blue. This colour coding is only used to visualize the approximate 3D shape of cells in a 2D image, and can be helpful to ensure the selected threshold value is correctly separating the cell from background signal.

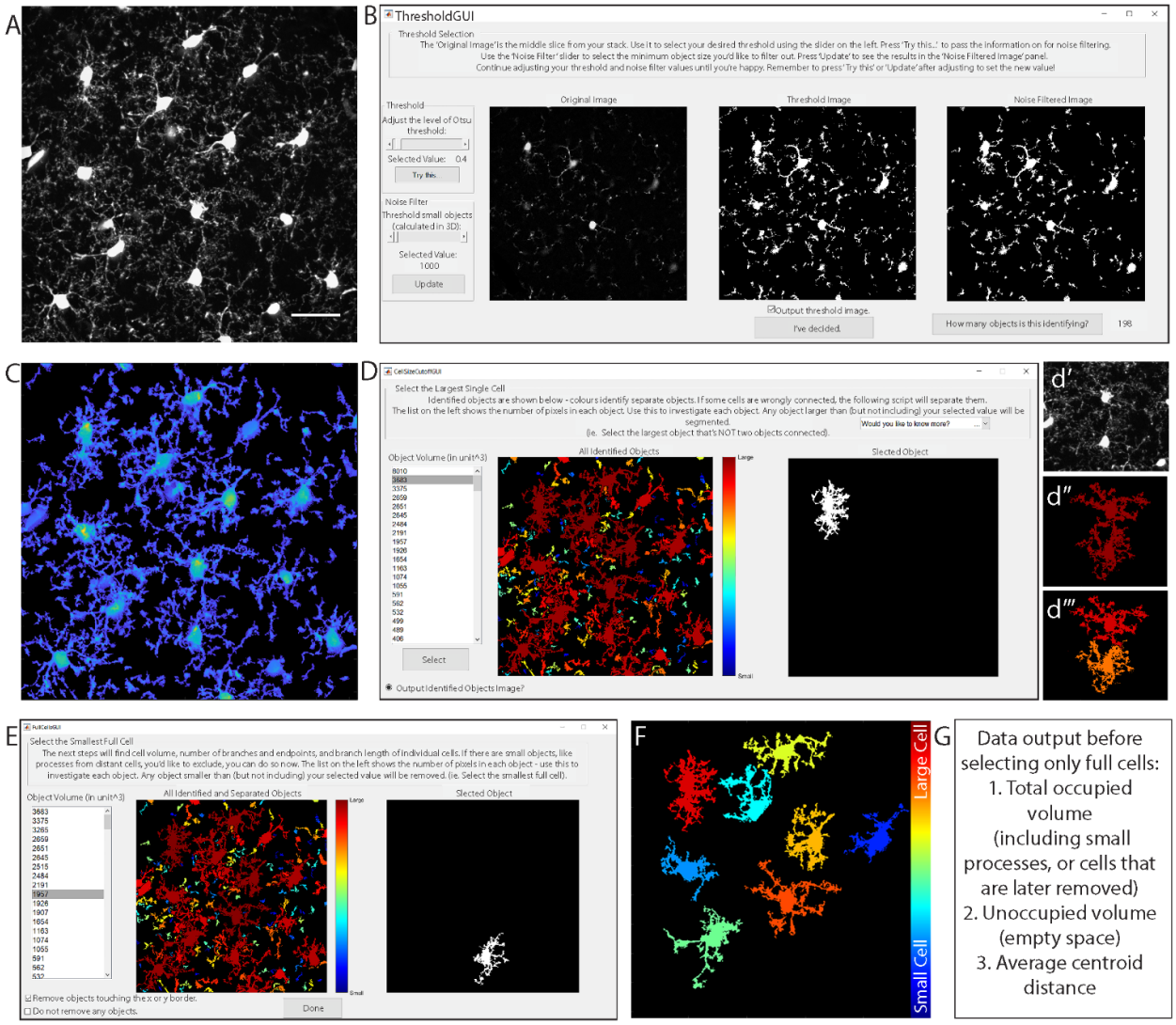

Figure 2.2 Select threshold and identify cells.

(A) Grayscale maximum projection of original stack. Scale bar = 25 µm. (B) Select threshold level, and noise filter value to remove small spots. (C) 'Output Threshold Image' is a 2D projection after threshold and noise filters are applied. To visualize 3D shapes of cells, hotter colours indicate thicker portions of cells. (D) 3DMorph automatically identifies 3D connected components, and the user selects a maximum cell size. Objects larger than this value are considered to be erroneously connected cells (d', d''), and will be segmented into separate objects (d'''). (E) Exclude remaining small cells, out-of-focus processes, or cells touching the xy borders to isolate only full cells (F). (G) At this point, the program records total occupied volume (calculated before excluding small cells, processes, etc.), the unoccupied volume, and the distance between cell centroids.

2.2.10 Identify and segment cells

The resulting thresholded image is separated into objects based on their 3D connectivity. To segment erroneously connected cells, identify the largest cell that is not two cells connected (Figure 2.2D). Any object above this threshold (Figure 2.2d', d'') is automatically segmented by fitting a Gaussian mixture distribution (Matlab function fitgmdist) to the data (Figure 2.2d''').

2.2.11 Total territorial area of microglia

As microglia are highly ramified cells, the volume of brain they survey is greater than the volume of the cell itself. To estimate total territorial volume of microglia, a polygon is created to surround the outside points of each cell, and its volume is measured. All small cells and processes from above or below the image are included here. The amount of unoccupied volume and percentage of volume covered is also determined.

2.2.12 Identify full cells

To get accurate volume and branching data of individual microglia, it is important to eliminate cells that are partially excluded from the image. The user selects the smallest full cell (any smaller objects are removed from further processing), and indicates whether cells touching the xy border should be removed (Figure 2.2E). From the remaining cells (Figure 2.2F), cell volumes and territorial volumes (Figure 2.3A) are recorded. Cell volume is calculated by converting the number of voxels in each object to a real-world unit based on the specified scaling factors. Cell ramification index (or extent) is calculated by territorial volume divided by cell volume. This is a measure of how ramified or amoeboid the cells are. For instance, a small ramified cell and a bushy cell may

have a similar cell volume, but the bushy cell will occupy more of its territorial space, therefore the ramification index measure will be smaller.

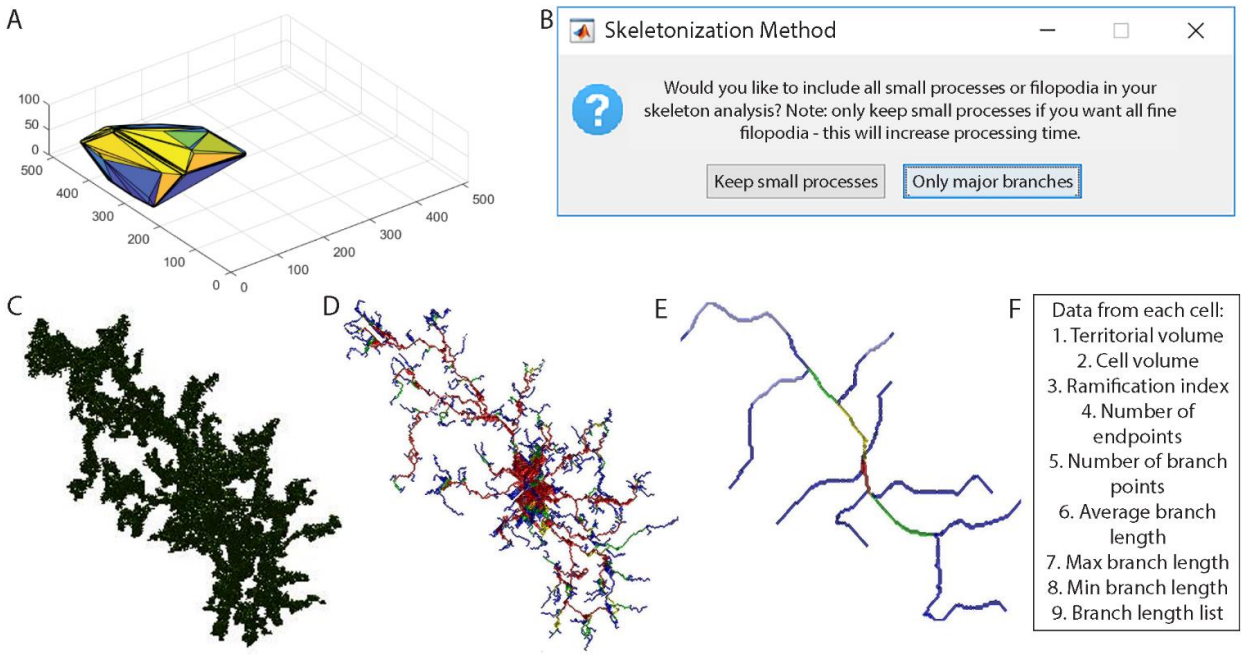

Figure 2.3 Analysis of individual full cells.

(A) Territorial volume of each cell is determined by placing a polygon around all of the extreme points of the cell. (B) The user decides which skeletonization method to use and which images to save (including: original cell, skeleton, branch points, and end points). Each full cell (C) is then processed individually to generate a 3D skeleton, keeping either all branches (D), or only major branches (E). In skeleton figures, colors indicate order of connectivity (red = primary, yellow = secondary, green = tertiary, and blue = connected to endpoint). (F) After processing all cells, the program outputs territorial volume, cell volume, ramification index (calculated as territorial volume / cell volume), number of endpoints and branch points, as well as average, maximum, and minimum branch length for each cell. A complete list of branch lengths for each cell can also be generated.

2.2.13 Distance between cell centroids

Distribution of cells is addressed by measuring the average distance between centroids. Accurate centroids (unbiased by the 'weight' of processes), are determined by eroding the cell to leave only the soma. These coordinates are converted to the unit of interest by multiplying the specified scales, and the distance between them is calculated. The average centroid distance is saved to the final results file.

2.2.14 3D skeletonization and branch tracing

To calculate branch lengths, endpoints, and branch points, a 3D skeleton of each cell is first generated. In 3DMorph, two skeletonization methods are available (Figure 2.3B). The first keeps all small processes (Figure 2.3D). This is ideal for images taken at a high magnification or to investigate differences in small filipodia-like structures. However, this method is also much slower and computationally demanding. This method is accomplished using the Skeleton3D method, developed by Kerschnitzki and colleagues (Kerschnitzki et al., 2013), and is available on File Exchange (https://www.mathworks.com/matlabcentral/fileexchange/43400-skeleton3d). Small extensions remaining on the skeleton, which are not likely to be true processes, are removed using the Graph2Skel3D and Skel2Graph3D (available at https://www.mathworks.com/matlabcentral/fileexchange/43527-skel2graph-3d). The second skeleton method looks only at large branches and ignores smaller structures (Figure 2.3E). This method might be preferred in images with a lower magnification and with several cells per image. It processes the skeleton using the Accurate Fast Marching method (made available by authors at https://www.mathworks.com/matlabcentral/fileexchange/24531-accurate-fast-marching).

Within each skeleton, endpoints are identified as pixels attached to only one other pixel. For each endpoint, a path between the endpoint and the centroid of the cell is traced to create a mask of each branch, from which the length is measured. This method may give a longer average branch length than other methods, as each end is traced to the soma, rather than to the nearest branch point. However, this method is more sensitive to differences in highly ramified vs bushy or amoeboid cells.

By adding the masks of all branches, a colour code is generated with primary branches in red as those that have been traced 4 or more times, secondary branches in yellow have been traced 3 times, tertiary in green have been traced twice, and quaternary in blue have been traced only once (most distal process, which terminate in an endpoint). From this process mask, the number of branch points are calculated by determining points of intersection between primary, secondary, tertiary, or quaternary branches.

If requested, a new folder is generated in the Current Folder titled as '*filename*_figures' to save specified images and branch lengths. 3D representations of original cells (Figure 2.3C), endpoints, branch points, and skeletons (Figure 2.3D, E) can be saved. Images of initial thresholding, identified objects, segmented objects, and full cells will also be saved to this folder if the user chooses to have them generated.

2.2.15 Export data

Finally, the data is written to an Excel file titled 'Results*filename*' and saved to Matlab's Current Folder. For each image, the exported data includes: average centroid distances, total microglial

territory volume, total unoccupied volume, and percentage of volume occupied. For each full cell: territory volume, cell volume, ramification index, number of endpoints and branch points, and average, minimum, and maximum branch lengths are saved.

2.2.16 Statistics

All data was analyzed using a one-way ANOVA and Tukey's multiple comparison post-hoc analysis with a significance level of $p < 0.05$.

2.3 Results

2.3.1 Accuracy of 3DMorph results

To validate our 3DMorph program, we generated a test image to process and compare with current analysis methods (Figure 2.4A,B). The image size is 512 x 512 pixels with 100 slices (0.21 µm/pixel, and 1 µm/slice). We analyzed this image in 3DMorph (Figure 2.4C,D,E), as well as with the 3D-tracing ImageJ plugin, Simple Neurite Tracer (Figure 2.4F), and by freehand tracing of a maximum intensity z-projection image (Figure 2.4G). Features of each method are summarized in Table 2.1.

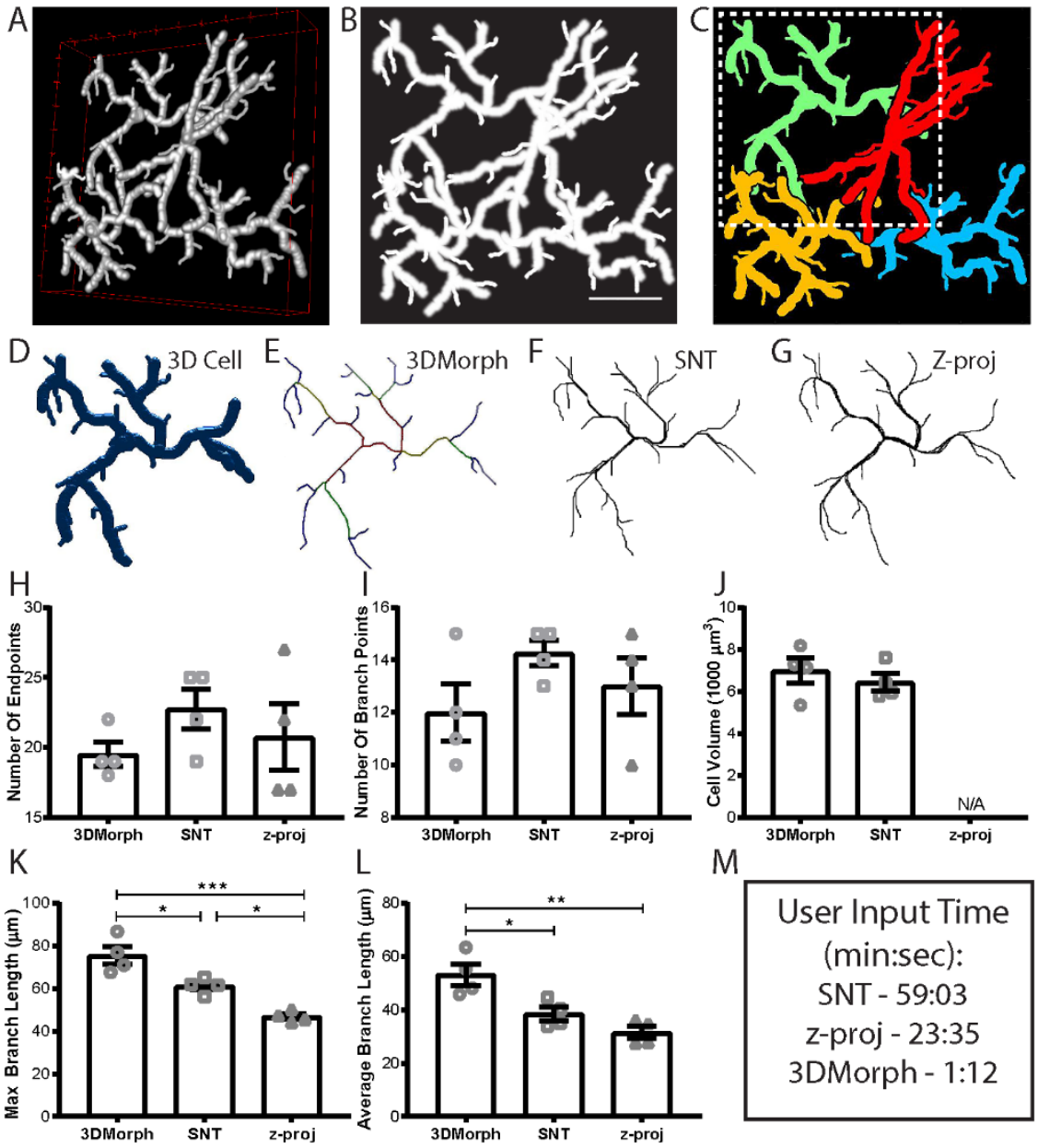

Figure 2.4 Validation and comparison of 3DMorph with current analysis tools.

(A) 3D visualization of a manually-generated test image composed of four cells with overlapping processes. (B) Z-projection of test image. Scale bar = 25 µm. (C) Full cells as identified by 3DMorph. (D) A single full cell from the test image (outlined by dashed box in C). (E) 3D skeleton generated automatically by 3DMorph. (F) 3D skeleton manually drawn using Simple Neurite Tracer (SNT). (G) 2D skeleton manually drawn using freehand tracing of a z-projection of the test image. Based on analysis by 3DMorph, SNT, or z-projection tracing, there is no significant

difference in the number of endpoints (H) or branch points (I) recorded. (J) Cell volume measurements are accurate between 3DMorph and SNT, but unavailable from z-projection analysis. (K) Maximum branch length is significantly longer by 3DMorph and SNT analysis than by z-projection tracing. (L) Average branch lengths are significantly longer by 3DMorph than by SNT or z-projection. (M) Comparison of user input time to measure data. Error bars indicate mean +/- SEM. *p<0.05, **p<0.01, ***p<0.001 by one-way ANOVA.

	3DMorph	Simple Neurite Tracer	Z-Projection Trace
Branch Length	✓	✓	✓
Cell Volume	✓	✓	✘
Territorial Volume	✓	✘	✘
Total Occupied Volume	✓	✘	✘
Ramification Index	✓	✘	✘
# of Endpoints	✓	✓	✓
# of Branch Points	✓	✓	✓
3D Analysis	✓	✓	✘
Automatic Batch Processing	✓	✘	✘
User Input Time	Fastest (min)	Slowest (min-hr)	Intermediate (10s of min)

Table 2.1

3DMorph, Simple Neurite Tracer ImageJ plugin, and freehand tracing of maximum z-projection images. While both 3DMorph and Simple Neurite Tracer process 3D information, only 3DMorph offers an automatic batch processing mode to greatly decrease user input time.

When comparing these techniques, there was no significant difference in the number of endpoints or branch points identified (Figure 2.4H,I). However, process overlap in z-projected images led to greater uncertainty in separating branches of individual cells. Cell volumes were similar between 3DMorph and Simple Neurite Tracer (Figure 2.4J), but are unavailable from z-projected data.

Maximum and average branch lengths were significantly greater when processed by 3DMorph compared to z-projected images (Figure 2.4K,L), confirming the importance of maintaining 3D information. While Simple Neurite Tracer does analyze length in 3D, we found that these values are lower than our 3DMorph analysis. This is likely because 3DMorph measures the length of each endpoint to the soma centroid instead of the distance between an endpoint and its parent branch.

Processing Time of 3DMorph

In addition to providing similar or more accurate measurements, 3DMorph also took considerably less time for the same investigator to complete the analysis of the test image (1 min, 12 s) compared to Simple Neurite Tracer (59 min, 3 s) or z-projection tracing (23 min, 35 s) (Figure 2.4M). While times were measured using Interactive Mode processing on one image, 3DMorph's Automatic Mode processing would be even more advantageous.

Finally, while both Simple Neurite Tracer and z-projections require subjective branch tracing, 3DMorph completes these steps automatically. Therefore, variability between researchers will be greatly decreased, while improving data reproducibility among researchers and between labs.

2.3.2 Microglial morphology changes in response to local cues

We next used 3DMorph to compare conditions which cause or mimic an increase or decrease in neuronal activity. As previously published (Dissing-Olesen et al., 2014), application of ATP triggers microglial process outgrowth, whereas processes retract in the presence of CNQX and TTX (Fontainhas et al., 2011). While the biological pathways leading to these changes are

interesting, here we do not address the biological cause of the process extensions or retractions. Instead we use these pharmacological manipulations only as tools to alter microglial morphology. Acute hippocampal slices from CX3CR1$^{EGFP/+}$ mice were incubated with either control aCSF (Figure 2.5A,B), 500 µM ATP (Figure 2.5C,D), or 50 µM CNQX with 1 µM TTX (Figure 2.5E,F) at 32 °C. Slices were fixed using the SNAPSHOT protocol (Dissing-Olesen & MacVicar, 2015) and imaged by 2-photon microscopy. A 1024 x 1024 image with 50 z-slices was acquired (xy scale: 0.17 µm/pixel; z scale: 1 µm/slice; image dimensions are 174.08 x 174.08 x 50 µm). The same parameter file was used to automatically process images from these three conditions, removing any experimenter bias.

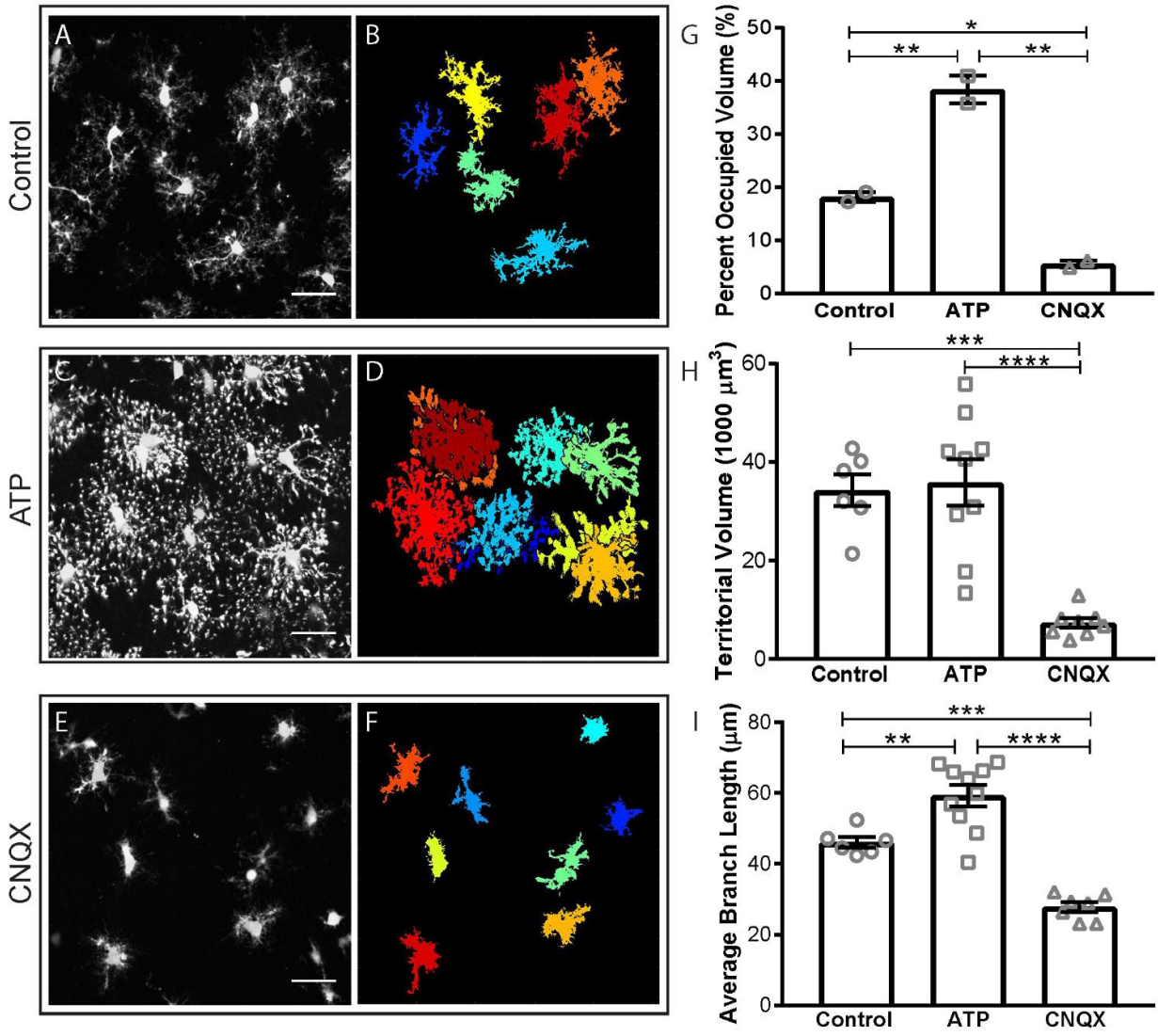

Figure 2.5 Microglia morphology changes in response to local cues.

Microglia are incubated with control aCSF (A, B), 500 µM ATP (C, D), or 50 µM CNQX and 1 µM TTX (E, F) before fixing and imaging (imaging dimensions: 174.08 x 174.08 x 50 µm). Original 3D projections (A, C, E; scale bar = 25 µm), and remaining full cells (B, D, F), are shown. (G) Quantification confirms that microglia cover more volume in ATP than in control conditions, while CNQX/TTX treatment decreases the total surveyed volume. When only full cells are considered, each microglial cell in CNQX/TTX conditions covers a smaller territorial volume (H) and has shorter average branch lengths (I) than control or ATP conditions, while ATP cells have significantly longer branch lengths than control. Error bars represent mean +/- SEM. *p<0.05, **p<0.01, ***p<0.001, ****p<0.0001 by one-way ANOVA.

3DMorph analysis revealed a significant increase in the percentage of brain volume surveyed by microglia in ATP conditions, whereas CNQX/TTX treatment decreased relative to control (Figure 2.5G). When single cells were analyzed, the territorial volume of each cell treated with CNQX/TTX was significantly smaller than in control aCSF (Figure 2.5H), while ATP induced a small increase. Finally, 3DMorph quantification confirmed that there is a significant increase in branch length of ATP-treated microglia, while CNQX/TTX-treated microglia have significantly shorter branches (Figure 2.5I). These results demonstrate the ability of 3DMorph to automatically quantify morphological changes of microglia *in situ* across different conditions in an automatic, unbiased, and reproducible manner.

2.3.3 Microglial morphology *in vivo*

While *in situ* imaging has many advantages, there is a growing push in the scientific field to confirm results using *in vivo* experiments. As 3DMorph requires only one channel containing the microglia image, and does not rely on counterstaining, it is possible to process microglia images from *in vivo* data.

We confirm this by processing microglia images of CX3CR1$^{EGFP/EGFP}$ mice acquired through a cranial window on an *in vivo* 2-photon microscope (Figure 2.6A). Image stacks were taken at 512 x 512 with 40 slices at an interval distance of 1 μm. 3DMorph analysis accurately thresholded (Figure 2.6B), segmented (Figure 2.6C), and skeletonized (Figure 2.6D-G) these images, confirming that 3DMorph is appropriate for analyzing *in vivo* microglial morphology.

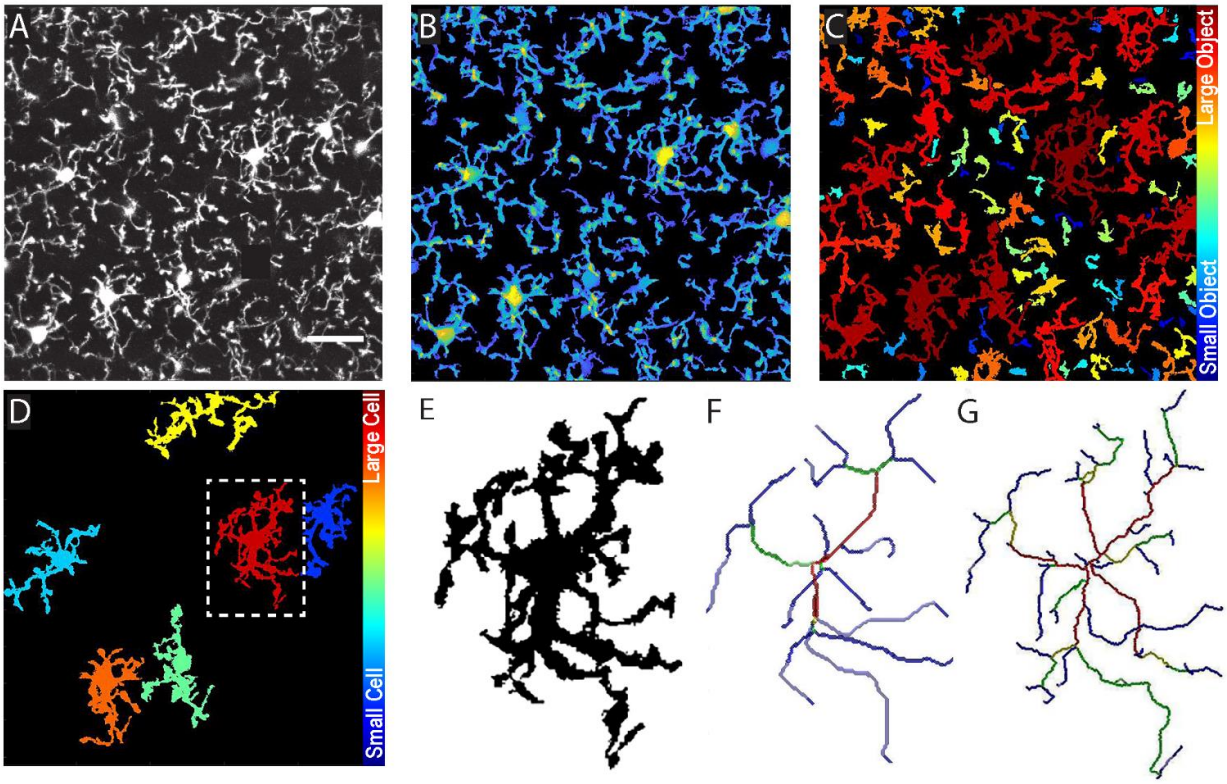

Figure 2.6 Morphology analysis of *in vivo* microglia images.

A) Maximum projection of in vivo image stack. B) 3DMorph threshold image shown as a maximum projection. C) Separation of thresholded image into individual objects, colour-coded based on size of object. D) Remaining full cells after removing small processes from out-of-frame cells. E) Isolated single cell from outlined region in D. F) Skeleton of major branches and G) skeleton maintaining fine processes.

2.3.4 Morphology of neurons

A benefit of 3DMorph's Interactive Mode is that the software is adaptable to work with many types of input data. This makes it possible to process other types of branched cells in addition to microglia, such as neurons, astrocytes, or oligodendrocyte precursor cells. We validate 3DMorph's performance in processing a patched and dye-loaded neuron (Figure 2.7A). 3DMorph accurately identifies and maintains only the neuron (Figure 2.7B), and skeletonizes the processes (Figure

2.7C). Given the size difference between microglia and neurons, we therefore validate that 3DMorph correctly processes images of branched cells other than microglia.

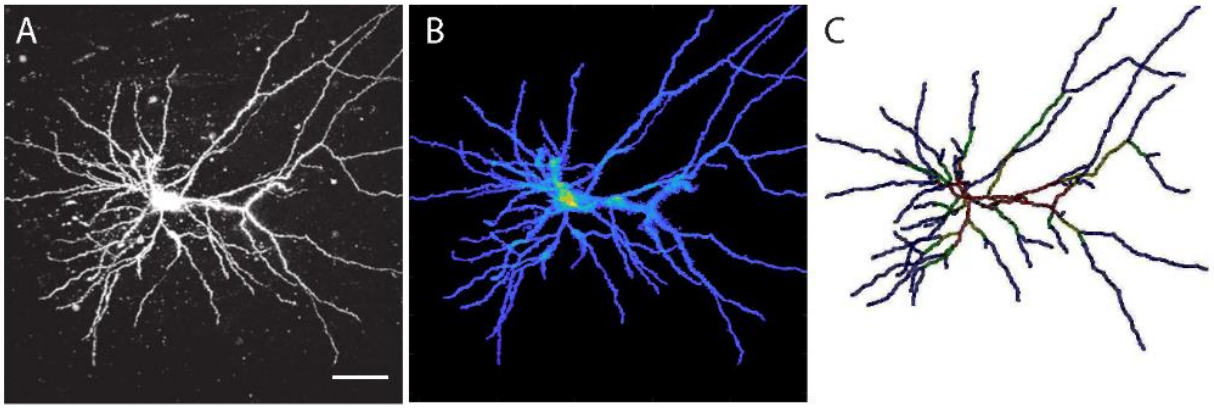

Figure 2.7 Morphology analysis of dye-loaded neuron.

A) Maximum projection of dye-loaded neuron; scale bar = 50 µm. B) Remaining cell following 3DMorph thresholding. C) Skeletonized neuron keeping fine processes.

2.4 Discussion

Here, we present a novel method that allows for rapid and unbiased analysis of microglial morphologies in 3 dimensions. This is an open source script running in Matlab, which is widely available through academic institutions, making 3DMorph free and easily accessible. We have written the program to make it user-friendly and compatible with many imaging settings. Furthermore, the program is well suited for analysis of other branched cells, such as astrocytes or oligodendrocyte precursor cells, in addition to microglia and neurons.

This program is an advancement to the currently available methods, as it relies on minimal user input, making it fast, replicable between experimenters and labs, and not subject to bias. Once

parameters have been chosen, Automatic Mode processes large amounts of data with minimal input time. Importantly, using 3DMorph maintains the 3D information of cells, providing more accurate volume and branch length measurements.

We have validated 3DMorph against two other analysis techniques (Simple Neurite Tracer, and z-projection tracing), and detected alterations in microglial morphology e.g. hyper-ramification triggered by ATP and hypo-ramification triggered by CNQX. Importantly, 3DMorph is compatible with images obtained *in vivo* and images of other branching cell types.

Another automatic 3D microglial analysis program has recently been published (Heindl et al., 2018). While this is a powerful program offering a range of output results, our 3DMorph program offers some key advantages. Most importantly, it does not require a DAPI input image, which removes the necessity for immunostaining and makes 3DMorph capable of handling *in vivo* data. Furthermore, 3DMorph can process .tiff files, which allows the processing of images acquired by multiple types of software. We have also shown here that 3DMorph can manage thick sections of tissue and reliably separate cells that may appear overlapped when z projected. Finally, although a completely automated analysis is available in 3DMorph, we first implement a series of graphical user interfaces that show real-time updates of how chosen settings will process the data. This transparency allows the user to confirm that the program is correctly processing their data.

Another promising analysis tool, ProMoIJ (Inaki Paris, 2018), has been recently published, which looks at microglial process motility. While this method is excellent at analyzing tip extension and retraction, it does not analyze morphology differences of whole-cell images. Microglial

morphology provides a clue to the cell's biological function. Therefore, shape measurements (ie. branch length and estimations of extent) are often used to differentiate healthy microglia from those associated with disease (Baron et al., 2014; Doorn et al., 2014; Kreutzberg, 1996; Perego et al., 2013; Torres-Platas et al., 2014). We encourage the field to use our 3DMorph program to perform their morphological quantifications, and we gladly supply the original code (https://github.com/ElisaYork/3DMorph) so that it can be adapted and improved upon by labs to best meet their needs.

2.5 Troubleshooting

While we have tried to make this program robust, user-friendly, and adaptable, it is possible issues may still occur. We have compiled this list of possible errors to assist with troubleshooting.

2.5.1 Errors when running the script

2.5.1.1 Mex file error, or all output data for full cells is "0":

At the skeletonization step, if the script encounters an error, it will output zeros for this cell and move on to the next cell in the file. If all cells encountered an error, it is likely a mex compiling issue. Some skeletonization functions need to be compiled from C to Matlab. In the original folder, go to: Functions>FastMarching_version3b>compile_c_files. You will need a compatible compiler to run this. If you do not have one, Matlab will provide instructions on installing one.

2.5.1.2 ThresholdGUI:

If you would like to keep the threshold and noise levels set to 0, please increase them, then move them back to 0. Be sure to confirm your adjusted values by pressing the 'Try This' and 'Update' buttons.

2.5.1.3 numObjMg = numel(FullMg):

If you only have one cell in your image, you must choose to keep it during small cell removal by selecting the "Keep all cells" option. If this is not selected, your cell will be removed and pass on a blank image to the next processing step.

2.5.1.4 "waitbar" error:

The program automatically generates waitbars to update you on how long it will take to process each step. It may reach an error if you have closed the waitbar window before it is finished processing.

2.5.1.5 GMModel: nuc must be a positive integer:

During segmentation, the program erodes the connected cells to find nuclei and determine how many cells the object should be segmented into. If cells or nuclei are small (as in low magnifications), they may be eroded completely and a blank image will be passed on. In the first for loop of the Cell Segmentation portion of the script, decrease the value of se=strel('diamond',**4**); This will decrease the amount of erosion.

2.5.2 Unsatisfactory data processing

3DMorph works best on images with high signal to noise ratio. During the image acquisition stage, try using a high magnification of the cells you would like to analyze and decrease the z-slice interval so that branches remain connected in this dimension. If available, deconvolution post-

processing may be helpful. It may also help to remove background before processing. This can be done with Fiji's rolling ball radius subtraction.

If there is too much connectivity, the program will have trouble segmenting properly. Try increasing the threshold level so that fewer branches remain touching in the binary image.

If you observe too much connectivity that cannot be fixed by increasing threshold levels, try using a spatial sampling of 0.166 µm/pixel, for example a 1024x1024 pixel image with a size of 170x170 µm. Your input images can be scaled in ImageJ prior to analysis to match this pixel density. See ImageJ, Image menu scale function.

When batch processing images, it is beneficial to spend time finding parameters that work well for all files. Test a few example images in Interactive Mode to determine which settings are best. To save time, you can run the program until you have chosen a threshold, and large and small cell limit, then exit before it begins measuring skeletons. Once you have chosen suitable parameters, you will need to let the program run fully to generate a Parameters output file to use in your batch processing.

For accurate total image coverage, keep a low noise level so that small processes are still included. Small cells and processes from out-of-frame cells can be removed at a later step.

Chapter 3: Green fluorescent protein emission obscures metabolic fluorescent lifetime imaging of NAD(P)H

3.1 Introduction

Use of label-free imaging techniques are rapidly increasing, with many advantages in both clinical applications and basic research (Büttner et al., 2018; Jing et al., 2018; Lombardo et al., 2015). These imaging strategies typically exploit endogenous tissue properties (e.g. autofluorescence) to circumvent the need for genetically encoded indicators or organic dyes. One such method is fluorescence lifetime imaging (FLIM) of endogenous nicotinamide adenine dinucleotide (NADH) to monitor cellular metabolic changes. This is commonly achieved by time-correlated single photon counting (TCSPC), using 2-photon laser scanning microscopy (2PLSM) of NADH autofluorescence, whose lifetime depends on intermolecular binding states (Figure 3.1). In glycolysis, oxidized, non-fluorescent NAD^+ becomes reduced to fluorescent NADH. In this free, unbound state, NADH emits photons with a short fluorescence lifetime of 400 ps. However, upon enzymatic binding, such as to complex I of the electron transport chain (ETC), NADH is stabilized and its fluorescent lifetime increases to approximately 2000 ps, with reports ranging from 1000 – 5000 ps depending on its binding partner (Bird et al., 2005; Blacker et al., 2014; Lakowicz et al., 1992; Schneckenburger et al., 2004; Vergen et al., 2013; M. a Yaseen et al., 2013) (Figure 3.1d,e). It is therefore possible to distinguish free and bound forms of NADH, and to extrapolate the ratio of glycolysis to ETC metabolism. As NADH is experimentally indistinguishable from the closely related nicotinamide adenine dinucleotide phosphate (NADPH) molecule by excitation and emission spectra or fluorescence lifetimes (though possible to computationally separate *post hoc*

(Blacker et al., 2014)), we refer to them jointly as NAD(P)H. NAD(P)H-FLIM has gleaned important roles of cellular metabolism in stem cell differentiation, cancer cell metastasis, and immune activation (Alfonso-García et al., 2016; Stringari et al., 2011, 2012, 2015; M. a Yaseen et al., 2013).

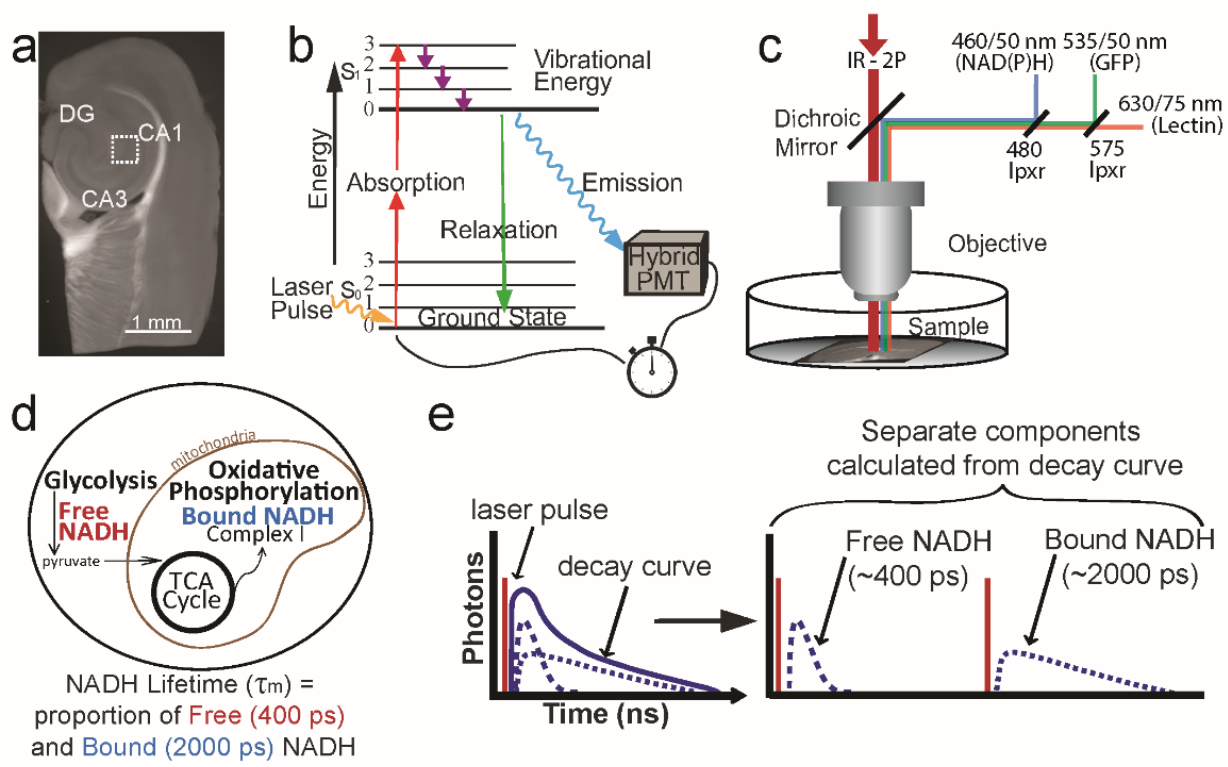

Figure 3.1 NAD(P)H-FLIM.

(a) Experiments were performed in the CA1 region of acute hippocampal slices. (b) A two-photon laser excites electrons of fluorescent molecules. Upon electron decay to ground state, a photon is released and detected by the hybrid PMT. The time of photon arrival is compared to the time of initial laser pulse, and the lifetime of the excited electron is calculated. (c) On a two-photon microscope, emitted light is passed through a series of long-pass dichroic mirrors and filter sets for NAD(P)H (460/50 nm), GFP (535/50 nm), or tomato lectin 594-DyLight (630/75 nm). (d) Endogenous NADH is autofluorescent and has a short lifetime of 400 ps when free, which increases to 2000 ps when

enzymatically bound. (e) Based on photon arrival times, a biexponential curve (solid line is fit to the data to separate photons into free or bound NADH components (dotted lines).

NAD(P)H-FLIM is a label-free technique that allows investigation of metabolically active tissue, thereby making the method applicable to *in vivo* or *ex vivo* preparations, including human samples (Pouli et al., 2017; Skala et al., 2007; Stringari et al., 2015; M. a Yaseen et al., 2013). Since NAD(P)H is ubiquitous across cell types, it is also possible to pair NAD(P)H-FLIM with cell-specific fluorescent markers to investigate metabolism of particular cells within heterogeneous tissue. The most commonly used cell marker in biology is green fluorescent protein (GFP).

GFP itself has also been investigated as a useful FLIM tool to measure intracellular pH, with reports of its lifetime varying from 2000 ps at pH 4.5 to 3000 ps at pH 7.5 (W. Li et al., 2017; Nakabayashi et al., 2008). Additional studies have reported a mean GFP lifetime of 2500 ps (Hess et al., 2003; Stringari et al., 2011; Volkmer et al., 2000). This lifetime is longer than that observed for bound (~2000 ps) or free (~400 ps) NAD(P)H, and the reported GFP emission is also spectrally separate from the blue NAD(P)H emission (510 nm vs 460 nm, respectively). Therefore, it initially appears that these two fluorophores would be compatible to investigate cell-specific metabolism.

In this study, we examined the feasibility of using NAD(P)H-FLIM in brain tissue to measure metabolic states of cells identified by GFP expression. While GFP is well-known to fluoresce within the green spectrum with a peak at 510 nm, there were concerns based on early accounts of weak emission in the blue spectrum (<460 nm) (Chattoraj et al., 1996; G. Jung et al., 2005; Shimomura & Johnson, 1969). To our knowledge, there have been few reports describing the

emission wavelength and lifetimes of this non-canonical blue GFP fluorescence. One such study used 2PLSM with 800 nm excitation to measure GFP emission properties in aqueous solution. They found green emission (514 nm) was well fit by a single exponential decay curve with a lifetime of 3000 ps, as expected and described by others. However, blue emission (456 nm) was better suited to a biexponential decay, where an additional component displayed a lifetime of 200 ps (Volkmer et al., 2000). An additional study found that in cell culture conditions, GFP excitation at 740 nm exhibited blue emission at 450 nm with a triple exponential decay of τ_1: 110 ps, $\tau_{2:}$ 430 ps and τ_3: 2610 ps (Hess et al., 2003).

Although these studies describe the presence of blue GFP emission with short lifetimes, the impact on NAD(P)H-FLIM has not been examined. Pairing GFP identification with NAD(P)H-FLIM would be a powerful technique to measure the metabolic profile of specific cell types within their native, heterogeneous environments. However, the lesser-known blue fluorescence of GFP appears to match the emission spectrum and potentially the fluorescence lifetime of free NAD(P)H. We therefore sought to determine whether blue GFP photons would obscure NAD(P)H-FLIM measurements in GFP-positive cells.

We demonstrate that cellular expression of EGFP leads to nearly complete contamination of the NAD(P)H signal. Using recombinant GFP in a sealed pipette, as well as neuronal and microglial expression of EGFP, we identify GFP and EGFP emission in the blue spectrum (460 nm) with a mean lifetime around 500 ps when excited by NAD(P)H-FLIM parameters. Therefore, GFP or EGFP expression would lead to the erroneous conclusion that cells are glycolytic, which highlights

the necessity of ensuring appropriate cell-specific indicators are used in combination with NAD(P)H-FLIM.

3.2 Materials and Methods

3.2.1 Animal protocols

All housing and experimental procedures were carried out in accordance with Canadian Council on Animal Care (CCAC) regulations. Wild type C57Bl/6 (WT), CX3CR1$^{+/EGFP}$ (Jackson Lab strain 005582 crossed with wild type C57Bl/6), or Thy1-EGFP mice (Jackson Lab strain 007788) on a C57Bl/6 background were housed on a 12 h light/day cycle with food and water *ad libitum*.

3.2.2 Acute hippocampal slice preparation

Adult mice (2 months of age) were anesthetized to surgical plane with isoflurane and decapitated according to protocols approved by the University of British Columbia committee on animal care. Brains were dissected and sliced horizontally with a vibratome (Leica VT1200S) at 300 μm thick in ice-cold NMDG slicing solution containing (in mM): 120 N-methyl-D-glucamine, 2.5 KCl, 25 $NaHCO_3$, 1 $CaCl_2$, 7 $MgCl_2$, 1.2 NaH_2PO_4, 20 D-glucose, 2.4 sodium pyruvate, and 1.3 sodium L-ascorbate, which was constantly oxygenated with 95% O_2 and 5% CO_2. Hippocampal slices were immediately transferred to artificial cerebral spinal fluid (aCSF) continuously oxygenated with 95% O_2 and 5% CO_2, and allowed to recover for 30 minutes at 32 ˚C. Artificial CSF contained (in mM): 126 NaCl, 2.5 KCl, 26 $NaHCO_3$, 2 $CaCl_2$, 2 $MgCl_2$, 1.25 NaH_2PO_4, and 10 D-glucose, pH 7.3–7.4, osmolarity 300 mOsm. For tomato lectin identification of microglia, slices were incubated with tomato lectin-594 DyLight (8 μg/ml; Vector Labs DL-1177) for 45 min at 32 °C.

3.2.3 Recombinant GFP

Recombinant GFP (EMD Millipore 14-392; 35 μM), was loaded into a glass micropipette (outer diameter: 1.5 mm; inner diameter 0.86 mm, sealed at one end with a microforge). The pipette was secured into a manipulator (Luigs & Neumann), and lowered into water for imaging by a water-immersion lens.

3.2.4 Imaging parameters

Hippocampal slices and recombinant GFP were imaged with a Coherent Chameleon Ultra II laser (mode-locked pulse train at 80 MHz) with a Zeiss LSM 7 MP microscope and Zeiss 20x-W/1.0 NA objective. Green and red fluorescence emission were detected by GaAsP photo-multiplier tubes (PMT; Zeiss LSM BiG), while blue NAD(P)H fluorescence lifetime emission was detected by a GaAsP hybrid detector (HPM-100-40 hybrid PMT, Becker and Hickl).

To image NAD(P)H lifetime in GFP-expressing cells, tissue was excited at 750 nm, and emitted light was split using a 480 nm long pass dichroic mirror. Blue NAD(P)H fluorescence passed through a 460/50 nm filter, while longer wavelengths were again split by a 575 nm long pass dichroic mirror (Chroma tech, Bellows Falls, VT). Green fluorescence was collected after passing through a 535/50 nm filter, while red (non-NAD(P)H autofluorescence or tomato lectin) passed through a 630/75 nm filter before detection (Chroma tech, Bellows Falls, VT; Fig 1c). Images were taken in the stratum radiatum of CA1 hippocampus at a depth of 50 μm – 80 μm below the surface of the brain slice.

Recombinant GFP was imaged from 700 to 950 nm excitation, and emission was detected with the TCSPC hybrid-PMT using either an NAD(P)H filter (460/50 nm) for blue emission, or GFP filter (535/50 nm) for green emission. Images were acquired at 256 x 256 (zoom factor 2.8) over 30 seconds to ensure a sufficient number of photons were collected for curve fitting. For cross section measurements of recombinant GFP, laser excitation intensity was adjusted to achieve a consistent power output of 12.5 mW for green emission and 15 mW for blue emission (measured below the objective). Photons were collected for one minute in both cases for lifetime decay curve calculations. Note that it was necessary to use different excitation powers (15 mW for blue emission, and 12.5 mW for green emission) as the blue emission is dimmer across all excitation wavelengths, so the normalized intensities are not directly comparable.

3.2.5 NAD(P)H Fluorescence Lifetime Data

NAD(P)H photons collected by the hybrid-PMT were detected by a TCSPC module (SPC-150, Becker and Hickl, Berlin, Germany) and SPCM software (Becker and Hickl, Berlin, Germany). Laser pulse clock information was simultaneously sent to the SPC-150 module enabling lifetime calculations.

Photon counts were passed to SPC Image (version 7.3), where decay curves for each pixel were calculated using a two-component exponential by the following equation:

$$F(t) = \alpha_1 e^{-t/\tau_1} + \alpha_2 e^{-t/\tau_2} \quad (1)$$

Where α is the amplitude and τ is the lifetime. We processed the data with unfixed τ_1 and τ_2 lifetimes, which correspond to the free and bound forms of NAD(P)H, respectively (Fig 1d, e). The instrument response function (IRF) was automatically calculated by taking the derivative of

the rising edge of the fluorescence signal. SPC Image performed automatic convolution of the decay model with this calculated IRF to best fit the measured data. There was no evidence of continued NAD(P)H emission past the 12 ns acquisition window set by the laser pulse rate, with only background photons detected at the onset of the following acquisition.

The mean lifetime (τ_m) of each pixel is calculated by:

$$\tau_m = \alpha_1\tau_1 + \alpha_2\tau_2 \quad (2)$$

Where $\alpha_1 + \alpha_2 = 1$. The average mean lifetime across the image or mask of a cell was reported.

A spatial bin factor with a radius of 3 pixels was used to attain a photon count >10 at the tail of the curve. Fluorescence lifetime of GFP was calculated as either a one or two-component decay curve, and the τ_m was recorded.

3.2.6 Single-cell NAD(P)H lifetime analysis

To measure NAD(P)H lifetime within single cells, a mask was drawn around the cell using either the EGFP or tomato lectin fluorescence image as a guide. Masks were drawn away from the edge of the cell to avoid any pixels contaminated by photons from the surrounding tissue. The τ_m of the mask was recorded. Results were compared by a Student's t-test or one-way ANOVA as specified, and reported or displayed as mean ± SD.

3.3 Results

3.3.1 Recombinant GFP lifetime under NAD(P)H imaging parameters

GFP is commonly reported to have a mean lifetime of 2500 ps (Hess et al., 2003; Stringari et al., 2011). However, this is measured using excitation and emission wavelengths ideal for GFP (2P

λex: 910 nm, λem: 510 nm). To test if the presence of GFP interferes with metabolic recordings, we first measured GFP emission in the blue spectrum using NAD(P)H imaging parameters (2P λex: 750 nm, λem filter: 460/50 nm). To accomplish this, we measured the fluorescence lifetime of recombinant GFP (35 μM) in a sealed micropipette to circumvent contamination from NAD(P)H, cellular components, and pH changes. The concentration and environment of GFP remained constant while the excitation and emission settings could be adjusted. When imaged at λex 910 nm with 2PSLM, GFP is expected to fluoresce from 470 nm to 650 nm, with a peak at 510 nm (Chalfie et al., 1994). To test the lifetime of both green and blue emission in these excitation parameters, emitted photons were collected by the TCSPC detector using either a green (535/50 nm) or blue (460/50 nm) emission filter. The mean lifetime measured through both emission filters approximated 2500 ps (Figure 3.2a, b). The histograms of each image show a well-defined peak, and both τ1 and τ2 are approximately 2500 ps with an equal split between the contributions of the components (α1 and α2), suggesting these data would fit to a single-component decay curve. The data were processed as a bi-exponential decay curve to match the parameters used for NAD(P)H lifetime calculations. These values correlate well with the previously measured lifetime of GFP (W. Li et al., 2017; Nakabayashi et al., 2008).

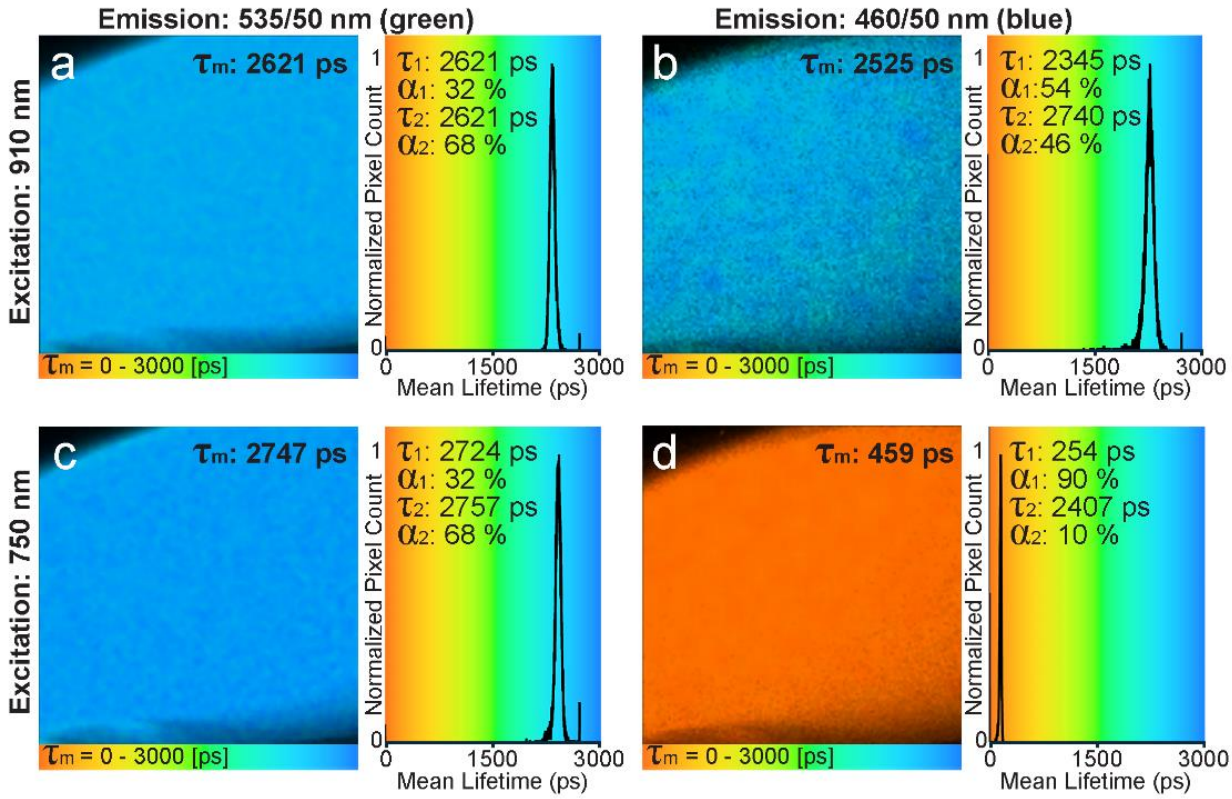

Figure 3.2 Recombinant GFP lifetime across excitation and emission settings.

Recombinant GFP protein in a sealed pipette was imaged with 910 nm or 750 nm excitation wavelengths. Either a green (535/50 nm) or blue (460/50 nm) emission filter was used before collecting light with the FLIM hybrid detector. Mean GFP lifetimes are over 2500 ps using 910 nm excitation with either the green (a), or the blue emission filter (b). Mean lifetime is also over 2500 ps using 750 nm excitation and the green emission filter (c). Using 750 nm excitation and the blue emission filter, the mean lifetime of GFP is 459 ps (d). Distribution of lifetimes are plotted as histograms showing the normalized number of pixels across mean lifetimes.

GFP lifetime was then measured using 750 nm excitation to mimic NAD(P)H imaging conditions. Green emission once again exhibited an expected mean lifetime of 2500 ps (Figure 3.2c). However, the blue emission had a short mean lifetime (τ_m ~500 ps) closely matching that of free NAD(P)H (Figure 3.2d). These data confirm that, in the absence of NAD(P)H autofluorescence,

GFP itself emits blue light with a short lifetime that is detectable with 750 nm, but not 910 nm, excitation.

To further characterize the blue and green GFP lifetimes and intensities, we measured these parameters using recombinant GFP across an excitation spectra of 700 – 950 nm. Blue emission had a short mean lifetime from 700-800 nm due to a predominant τ_1 component (τ_m ~500 ps, α_1: 83-87 %; lifetimes fixed at τ_1: 267 ps, τ_2: 2330 ps based on the average lifetimes from 700-800 nm excitation; Figure 3.3a). At excitation wavelengths over 800 nm, there is a precipitous increase in mean lifetime to 2500 ps. The normalized emission intensity (Figure 3.3b) reveals fewer photons are emitted at lower wavelengths relative to the peak intensity around 900 nm. As expected, the green emission showed a long and stable mean lifetime around 2500 ps (Figure 3.3c), and an emission intensity increasing at longer wavelengths with a shoulder at 800 nm (Figure 3.3d).

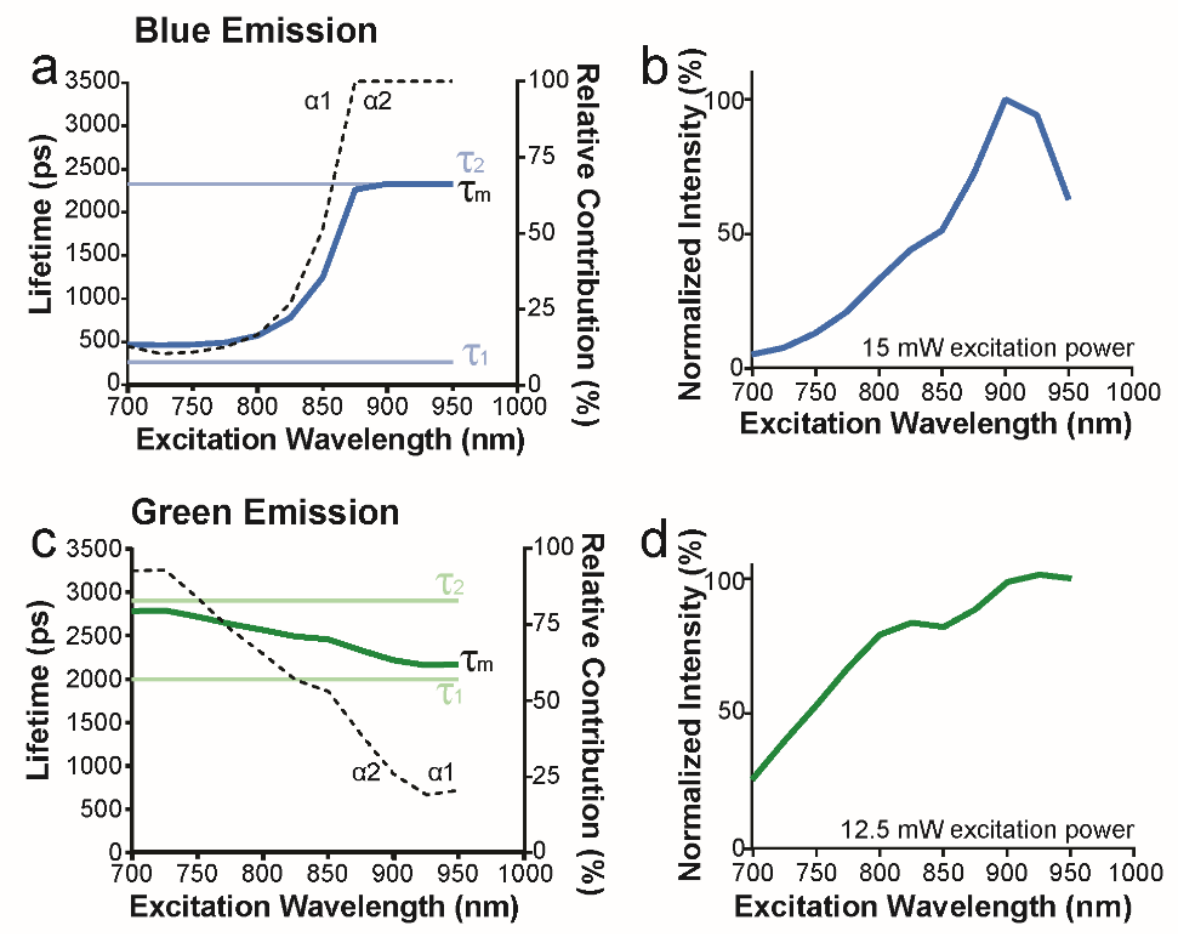

Figure 3.3 Recombinant GFP emission lifetime and intensity spectra.

Recombinant GFP protein in a sealed pipette was imaged from 700 nm to 950 nm excitation wavelengths at intervals of 25 nm. Either a blue (460/50 nm) or green (535/50 nm) emission filter was used before collecting light with the FLIM hybrid detector. Mean GFP lifetimes (τ_m; bold line) and the corresponding short (τ_1) and long (τ_2) lifetimes are shown across excitation lifetimes for blue (a) and green (c) emission. τ_1 and τ_2 lifetimes were fixed based on the average unfixed values from 700 – 825 nm. The relative contribution of the short (α_1) and long (α_2) lifetimes are represented as percentage of the total photons (dashed line). Intensities of blue (b) and green (d) GFP emission were measured across excitation wavelengths as the number of photons collected and normalized to the peak emission intensity.

3.3.2 NAD(P)H measurements in Thy1-EGFP neurons

To investigate the GFP contamination of NAD(P)H fluorescence in a biological system, we turned to Thy1-EGFP mice that express EGFP in a subset of neurons. As an important control, we evaluated the metabolic profile of wild type (WT; non-EGFP) pyramidal neurons in the CA1 region of WT hippocampus. Neurons were identified with transmitted light (Figure 3.4a) and NAD(P)H-FLIM was imaged using 2PLSM tuned to 750 nm. We observed perinuclear NAD(P)H fluorescence with a heterogeneous distribution of lifetimes denoting the abundance of free (glycolytic) and bound (ETC) NAD(P)H, with an average mean lifetime of 1193 ± 44 ps across cells (τ_1: 550 ps, α_1: 70 %; τ_2: 2500 ps, α_2: 30 %; Figure 3.4b).

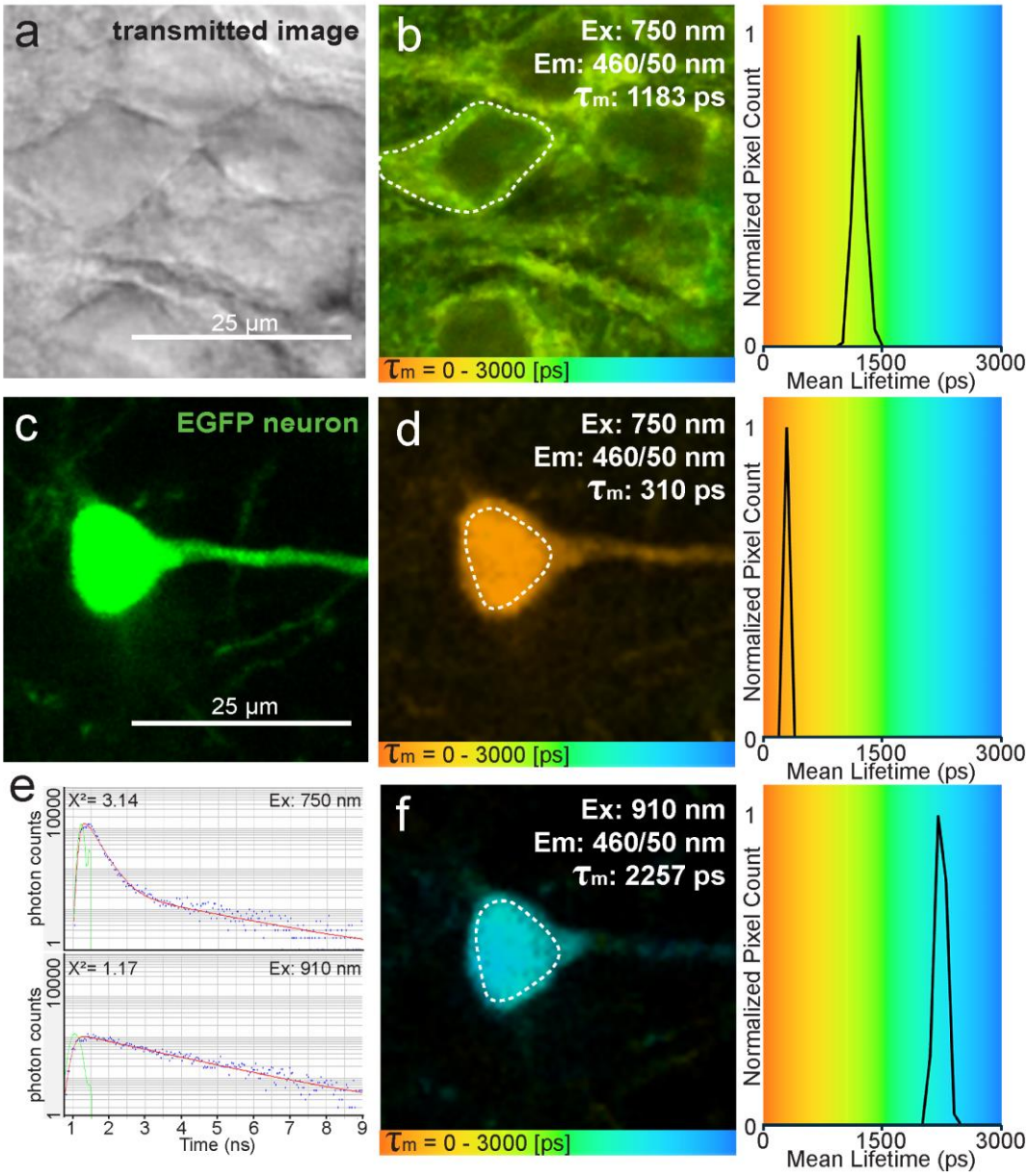

Figure 3.4 NAD(P)H measurements of Thy1-EGFP neurons *in situ*.

(a) Non-EGFP neurons are identified by transmitted light. (b) NAD(P)H mean lifetime is 1183 ps, representing a mix of bound and free NAD(P)H species. Thy1-EGFP neurons (c) were imaged with either 750 nm (d) or 910 nm (f) excitation, using the NAD(P)H (460/50 nm) emission filter. Distribution of lifetimes are plotted as histograms showing the normalized number of pixels across mean lifetimes. Only pixels within the neuron mask (dotted line in b, d, and f) are considered. (e) Decay curves within traced mask generated with 750 nm (top) or 910 nm (bottom) excitation.

In contrast, performing NAD(P)H-FLIM in Thy1-EGFP neurons (Figure 3.4c) revealed a short mean lifetime (τ_m: 290 ± 25 ps; τ_1: 280 ps, α_1: 98 %; τ_2: 2400 ps, α_2: 2 %), incorrectly suggesting a high rate of glycolysis over ETC (Figure 3.4d,e top). As confirmation of the EGFP lifetime in these conditions, excitation of Thy1-EGFP neurons at 910 nm revealed the expected EGFP lifetime near 2500 ps (τ_1: 2000 ps, α_1: 80 %; τ_2: 2500 ps, α_2: 20 %; Figure 3.4e bottom, f). As the blue emission of GFP decreases at lower excitation wavelengths (Figure 3.3b), EGFP-expressing neurons were imaged at 710 nm, 725 nm, and 750 nm excitation. The short EGFP component was observed in all conditions, suggesting EGFP and NAD(P)H cannot be differentiated at shorter excitation wavelengths. Therefore, we have confirmed that the lifetime of EGFP in the blue emission spectrum mimics that of free NAD(P)H in biological tissue, and in this case, overwhelms the endogenous NAD(P)H signal and cannot be confidently separated by experimental conditions.

3.3.3 Cell-specific metabolism in EGFP-negative systems

As an alternative to EGFP expression, exogenous dyes may be used as cell-specific indicators. To test the impact of a red-shifted, externally-applied dye on the NAD(P)H-FLIM signal, we turned to microglia in acute hippocampal slices. It has been previously established that these cells can be identified by incubation with Isolectin-B4, or tomato lectin, which binds to the extracellular surface with no adverse effect on their physiology (Boscia et al., 2013; Schwendele et al., 2012; Streit, 1990). To image EGFP-negative microglia, WT C57Bl/6 acute hippocampal slices were incubated with tomato lectin-594 DyLight (8 µg/ml; Vector Labs DL-1177) for 45 min at 32 °C as previously described (Schwendele et al., 2012). In microglia identified by this method, the NAD(P)H mean lifetime was 837 ps (SD: ± 113 ps; Figure 3.5a, b).

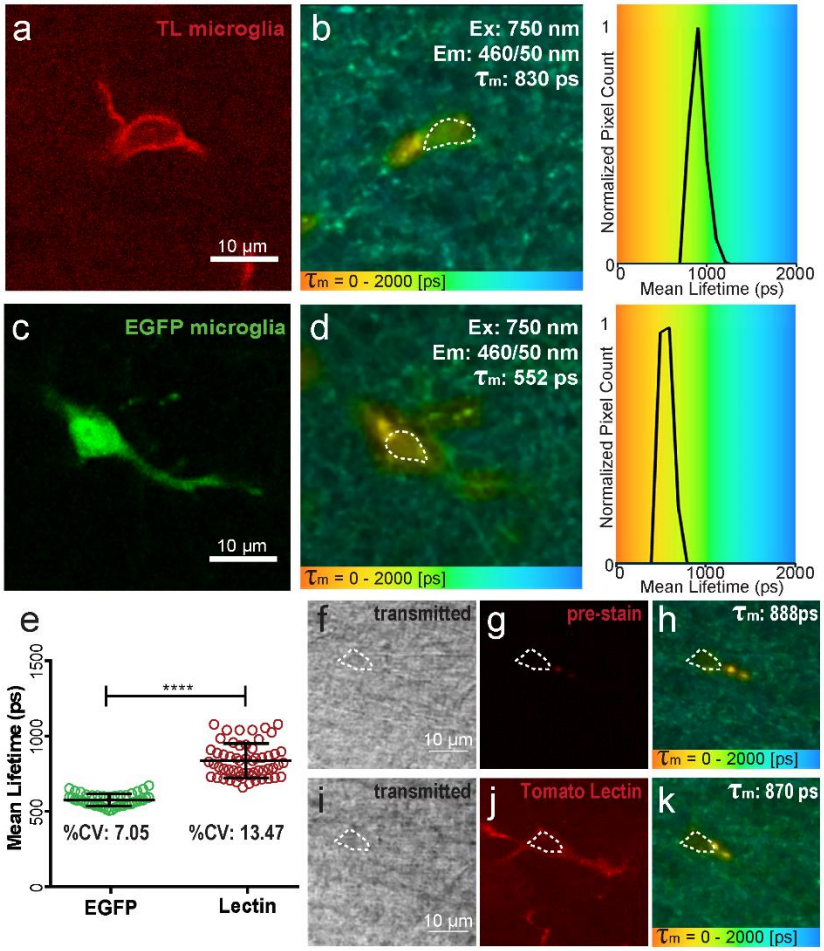

Figure 3.5 EGFP-expressing microglia have shorter NAD(P)H mean lifetimes.

Wild type microglia identified by tomato lectin 594-DyLight (a), and corresponding NAD(P)H lifetime measurement (b). EGFP-expressing microglia imaged at 750 nm excitation with a 535/50 nm filter (c), or 460/50 nm filter to collect NAD(P)H emission (d). Distribution of lifetimes are plotted as histograms showing the normalized number of pixels across mean lifetimes. Only pixels within microglia cell masks (dotted line in b and d) are considered. (e) Comparison of mean NAD(P)H lifetime and coefficients of variation (%CV) from microglia with or without EGFP expression. Microglia were identified by transmitted light and imaged before (f,g,h), and after (i,j,k) tomato lectin application. **** $p < 0.0001$ by Student's t-test; error bars show standard deviation of the mean.

As confirmation that tomato lectin staining does not directly interfere with NAD(P)H-FLIM measurements or change microglial metabolism, microglia were imaged before and after tomato

lectin application. Microglia were initially identified by transmitted light and lipofuscin autofluorescent inclusions to measure NAD(P)H lifetime (Figure 3.5f,g,h). Tomato lectin was then puffed onto the slice to stain microglia, and the NAD(P)H lifetime was again measured (Figure 3.5i,j,k). Pre- and post-lectin images showed no difference in NAD(P)H mean lifetime (τ_m: 912 ± 50 ps pre-tomato lectin; τ_m: 889 ± 50 ps post-tomato lectin, n.s. by one-way ANOVA including EGFP and Tomato-Lectin incubation tissue). Therefore, tomato lectin staining is a reliable way of identifying microglia in heterogeneous *ex vivo* conditions without affecting cell metabolism or NAD(P)H-FLIM measurements.

3.3.4 NAD(P)H measurements in CX3CR1-EGFP microglia

To confirm the effect of EGFP on the NAD(P)H signal within microglia, acute hippocampal slices from CX3CR1$^{+/EGFP}$ mice were imaged. Comparing the NAD(P)H lifetime of several microglia by EGFP expression or tomato lectin staining revealed that EGFP-positive microglia have significantly shorter mean lifetimes (τ_m: 577 ± 41 ps in EGFP-positive cells, Figure 3.5c,d; τ_m: 838 ± 113 ps in EGFP-negative cells), further confirming the bright EGFP emission in the blue spectrum with a short fluorescent lifetime. Microglia identified by tomato lectin also have a larger standard deviation around the mean relative to EGFP-positive cells (coefficient of variation: EGFP 7.05%; tomato lectin 13.47%; Figure 3.5e), which is representative of complex metabolic pathways. This provides further evidence that EGFP expression overwhelms NAD(P)H signals within biological systems.

3.3.5 Reactive oxygen species and protein load on NAD(P)H measurements

While we confirm that recombinant EGFP fluoresces in the blue spectrum with a lifetime around 500 ps in biological systems, it is possible that the altered NAD(P)H-FLIM measurements in EGFP-positive cells is the result of a metabolic alteration caused by EGFP protein expression. Responses to EGFP expression might include reactive oxygen species (ROS) load (Ganini et al., 2017), or cell and endoplasmic reticulum (ER) stress induced by exogenous protein expression (Mandl et al., 2013). To address the concern of increased ROS in EGFP-expressing cells, $CX3CR1^{+/EGFP}$ slices were incubated with the ROS scavengers N-acetyl-cysteine (5 mM) and ascorbic acid (2 mM). Addition of these ROS buffers did not rescue the NAD(P)H measurements of EGFP-positive microglia to tomato lectin levels (τ_m: 619 ± 68 ps in ROS scavenger incubated EGFP microglia; Figure 3.6).

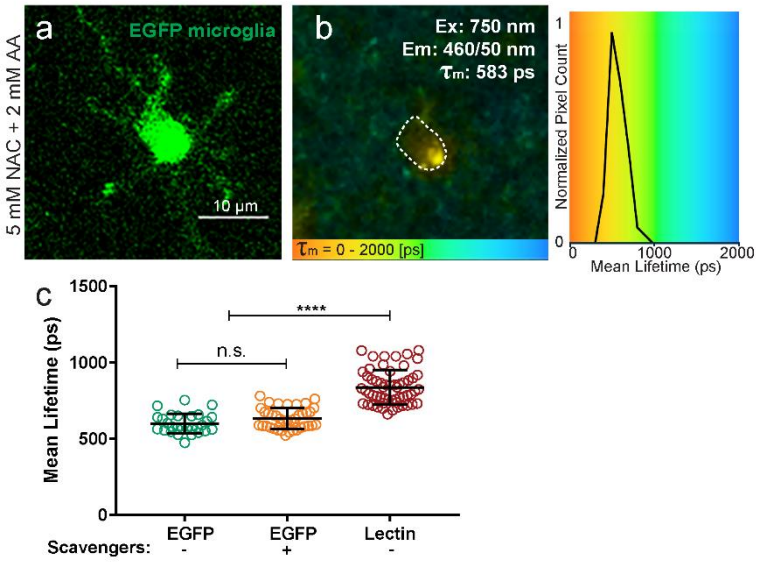

Figure 3.6 ROS scavengers do not increase NAD(P)H lifetimes in EGFP expressing microglia.

Acute hippocampal slices with EGFP-positive microglia were incubated for 1 hour in 5 mM N-acetyl cysteine and 2 mM ascorbic acid before imaging (a). Microglial NAD(P)H lifetime in the presence of ROS scavengers was ~583 ps.

Distribution of lifetimes are plotted as a histogram showing the normalized number of pixels across mean lifetimes. Only pixels within the microglia cell mask (dotted line) are considered (b). ROS scavengers did not significantly increase the mean lifetimes of EGFP-positive microglia, which were still significantly shorter than microglia from wild type slices (c). **** p< 0.0001 by one-way ANOVA; error bars show standard deviation of the mean.

To investigate the role of exogenous protein expression and associated cellular and ER stress, NAD(P)H-FLIM was performed on the CX3CR1-Cre mouse line. In these mice, microglia express the Cre protein under the same promoter as used to drive EGFP in the CX3CR1$^{+/EGFP}$ line. Therefore, if metabolic changes resulted from exogenous protein expression, these cells should also have the short NAD(P)H lifetime seen in EGFP-positive tissue. However, all Cre-expressing microglia showed a similar NAD(P)H measurement to those from WT cells (Cre-microglia τ_m: 998 ps; Figure 3.7). As in WT microglia (Figure 3.5a,b,e), Cre-expressing microglia have a significantly longer mean lifetime, with a greater coefficient of variation when compared to EGFP-positive cells (τ_m: 573 ± 42 ps in EGFP cells; τ_m: 1067 ± 197 ps in Cre cells; Figure 3.7c).

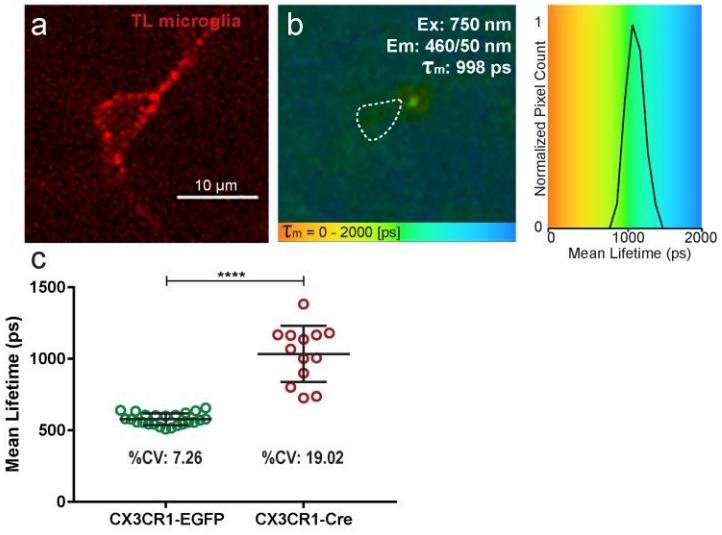

Figure 3.7 Exogenous protein expression does not cause short NAD(P)H lifetime measurements.

Microglia were identified by tomato lectin staining in acute hippocampal slices from mice expressing a Cre protein under the CX3CR1 promoter (a). The NAD(P)H lifetime in these cells was 998 ps (b). Distribution of lifetimes are plotted as a histogram showing the normalized number of pixels across mean lifetimes. Only pixels within the microglia cell mask (dotted line) are considered. (c) NAD(P)H lifetimes in Cre-expressing microglia are significantly higher and with a larger coefficient of variation than microglia from EGFP-positive cells. **** $p < 0.0001$ by Student's t-test; error bars show standard deviation of the mean.

3.4 Discussion

We have tested the possibility that combining NAD(P)H-FLIM with EGFP expression could be used to measure cell-type specific metabolism within heterogeneous tissue preparations. Analyzing NAD(P)H signals with NAD(P)H-FLIM is an effective imaging technique to quantify shifts in metabolic states. However, we show here that despite the spectral separation of reported NAD(P)H and EGFP emissions, exciting either GFP or EGFP at 750 nm yields blue emission at 460 nm that contaminates NAD(P)H fluorescence. This was confirmed both in aqueous solution and *ex vivo* in neurons and microglia. All EGFP-positive cells imaged with NAD(P)H-FLIM parameters possessed an artifactual glycolytic phenotype due to EGFP molecules fluorescing in the blue spectrum with a short lifetime matching free NAD(P)H.

The EGFP and free NAD(P)H components could not be confidently separated using different excitation wavelengths. Further, EGFP expression masked metabolic changes to NAD(P)H, as 10 min exposure to hypoxia had no effect on emission lifetime in the blue spectrum (data not shown). EGFP separation was also attempted by using a three component model to fit the decay curve with fixed τ_1 and τ_2 at the expected free and bound NAD(P)H lifetimes, respectively. While this method uncovers an additional short component with a lifetime matching the τ_1 of recombinant GFP, it is

still unclear if EGFP photons are contributing to the fixed free NAD(P)H component. Based on our experience, this method does not reliably separate the EGFP photons and it cannot be confidently recommended without further validation. The contribution of EGFP and NAD(P)H may change across cell types, expression patterns, or experimental setups, and may therefore be separable under certain conditions. However, the presence of EGFP will nevertheless introduce noise and decrease the dynamic range of the NAD(P)H signal, and in so doing, decrease confidence in the resulting data. It is instead suggested that EGFP-expressing tissue is avoided when performing NAD(P)H-FLIM measurements.

In practice, endogenous NAD(P)H autofluorescence has low emission intensity, while EGFP is bright and often expressed at high levels. Furthering the problem is the unexpectedly high quantum yield of GFP in the blue spectrum after 2PLSM relative to one-photon excitation (Volkmer et al., 2000). Therefore, EGFP contamination of the blue channel is likely to completely obscure the NAD(P)H signal in common experimental preparations. NAD(P)H-FLIM measurements in GFP-expressing cells have been performed previously to investigate macrophage metabolism or metabolic effects of viral infection (Mazumder et al., 2013; Szulczewski et al., 2016). A high rate of glycolysis and low ETC activity in GFP-positive cells was reported (Szulczewski et al., 2016). Indeed, their measurements have little deviation around the mean and are centered at 500 ps, which is what we have observed to be the GFP lifetime under NAD(P)H imaging conditions. Without GFP-negative experiments, the results are difficult to interpret, which underscores the importance of appropriate controls when using FLIM techniques in combination with fluorescent proteins and dyes.

It is well established that the GFP chromophore exists in both anionic deprotonated (R^-), and neutral protonated (RH) states (Chattoraj et al., 1996; Kummer et al., 1996). The deprotonated form is structurally relaxed and emits at a peak around 510 nm with a monoexponential decay curve and lifetime of 3200 ps (G. Jung et al., 2005). However, when protonated, the GFP excitation peak is shifted to ~395 nm from the typical peak at ~475 nm. The protonated form first undergoes excited state proton transfer to a structurally unstable intermediate form, which shows emission at 510 nm, but also a unique blue fluorescence (Chattoraj et al., 1996; G. Jung et al., 2005; Shimomura & Johnson, 1969). To investigate the lifetime of this blue fluorescence, prior studies have used a GFP mutant (T203V) with an increased fraction of protonated protein. Researchers found that fitting a lifetime curve at 515 nm emission revealed a lifetime around 3290 ps. However, fitting the lifetime curve at 460 nm revealed a tri-component decay curve, τ_1 of 70 ps (68%) which falls within the instrument response function, τ_2 of 420 ps (25%), and τ_3 of 1210 ps (7%) (G. Jung et al., 2005). The observation of blue fluorescence with short fluorescence lifetime has also been confirmed using 2P excitation at 740 nm (Hess et al., 2003). Therefore, our work agrees with previously published results that a subset of protonated GFP molecules can emit in the blue spectra with a short fluorescence lifetime. This also reconciles the absence of a short lifetime emission when GFP is imaged at 910 nm, as this is unlikely to excite the protonated chromophore.

There are several other possible mechanisms which could lead to the observed GFP effect in NAD(P)H-FLIM recordings. These include biological effects of GFP expression on cellular metabolism such as ROS production, or protein load and cell stress.

It has been previously reported that the maturation of each GFP molecule releases a hydrogen peroxide molecule (Ganini et al., 2017). While it is speculated that the originating jellyfish species, *Aequorea Victoria*, have evolved ROS scavenging mechanisms to cope with increased oxidative stress, artificial expression in mammalian cells may cause stress and damage. Furthermore, this altered redox state may impair the function of complexes within the ETC and force the cell to rely on glycolysis for energy production (Marcillat et al., 1989). While this should remain a consideration to the health and understanding of biological experiments, it does not appear to be the cause of the short lifetime signal in NAD(P)H-FLIM. Addition of ROS scavengers (N-acetyl-cysteine, and ascorbic acid) did not alter the NAD(P)H signal within EGFP-positive microglia. We cannot, however, experimentally rule-out possible chronic ROS-induced changes to the cytosolic milieu that are not amenable to transient ROS scavenging.

This short lifetime signal in EGFP-positive cells also does not appear to be the result of exogenous protein expression and associated cellular stress (Mandl et al., 2013), as we did not observe a 'glycolytic' shift in lifetimes from CX3CR1-Cre tissue (Fig 7). The absence of a Cre-dependent shift in NAD(P)H lifetimes compared to control cells points toward a technical artifact from EGFP fluorescence, rather than a metabolic effect of EGFP on biological tissue. The clearest example of this is shown in imaging recombinant GFP solution within a micropipette, where there is no confounding effect of metabolic changes or variable cytoplasmic conditions.

While researchers should be aware of these unintended consequences of using genetically encoded indicators, we provide evidence that the EGFP effect on NAD(P)H-FLIM measurements is a result of emission in the blue spectrum with a short lifetime.

In conclusion, we have shown that when either GFP or EGFP are excited at 750 nm, there is a strong emission in the blue spectrum (~460 nm) with a short mean lifetime (~500 ps). This is likely due to excitation and detection of a fraction of molecules in the protonated form. As these are the same imaging parameters used to measure NAD(P)H lifetime, the use of EGFP-expressing cells will lead to incorrect interpretations of cellular metabolism. Instead, to perform cell-specific metabolic measurements, we encourage investigators to use fluorophores with no emission in the blue spectrum. We remind researchers of the importance of testing their fluorescent molecules under NAD(P)H imaging conditions to ensure they are reliably measuring only NAD(P)H metabolism.

Chapter 4: Microglial glutamine metabolism maintains viability and immune surveillance during glucose deprivation

4.1 Introduction

Glucose is often considered to be the main source of metabolic fuel for the brain (Dienel, 2019; Magistretti & Allaman, 2015), with small stores of glycogen kept in astrocytes to support neuronal function during metabolic stress (Bélanger et al., 2011; Brown & Ransom, 2007). However, it has been estimated that glycogen stores can only support neuronal activity for approximately 30 minutes before a metabolic rundown occurs in brain tissue, along with a decrease in neuronal function (Izumi et al., 1994; Ransom & Fern, 1997; Shetty et al., 2013; Waitt et al., 2017). The reliance on continuous oxygen and glucose supply to the brain becomes apparent in stroke (Sims & Muyderman, 2010), and cases of severe hypoglycemia as seen in diabetic management with insulin (Meneilly & Tessier, 2016; Rehni & Dave, 2018). Upon vessel hemorrhage or thrombosis, the resulting occlusion of downstream oxygen and nutrients results in severe metabolic starvation and neuronal death in an area known as the ischemic core. While injury to neurons in this region is apparent and often irreversible, there is at the same time a repopulation of microglia into the region of damage by an invasion from the adjacent penumbra (Alexander & Wolf-Dieter, 2011; Tanaka et al., 2003). It is critical that microglia are able to infiltrate and perform immune protection and debris clearance functions in this damaged area (Denes et al., 2007; Schilling et al., 2005). A more global and chronic metabolic restriction is insulin-induced severe hypoglycemia in diabetic patients. Hypoglycemia is one of the main concerns in the treatment of diabetes, as exogenously-administered insulin levels do not fall naturally with decreasing blood glucose (Cryer et al., 2003).

Given that the brain is particularly sensitive to perturbations in glucose supply, hypoglycemic episodes may result in seizures and neuronal damage in vulnerable regions, including the hippocampus and cortex (Bree et al., 2019), as neuronal metabolic stress leads to the loss of ion gradients and membrane polarization. The number of seizure events have been correlated with the extent of neuronal death, and these events may be the underlying cause of cognitive deficits in individuals with severe or repeated hypoglycemic episodes (Bree et al., 2019).

While the effect of hypoglycemia on neurons has been well-established, the impact of these conditions on microglial viability and function remain unclear. It has been suggested that administration of the anti-inflammatory drug, minocycline, after a hypoglycemic event decreased microglial activation, neuronal death, and cognitive impairment (Won, Kim, et al., 2012). Similarly, treatment with apocynin to decrease reactive oxygen species production reduced microglial activation and oxidative injury of dendrites in response to repeated, moderate hypoglycemia (Won, Yoo, et al., 2012). Therefore, it is plausible that periods of hypoglycemia are altering microglial function without causing overt death, which would suggest that microglia are capable of metabolizing non-glucose carbon sources. Interestingly, such metabolic flexibility has been largely reported for cancerous tissues (Berridge et al., 2010; Boroughs & DeBerardinis, 2015), and cells of the peripheral immune system (Buck et al., 2016; B. Kelly & O'Neill, 2015; Newton et al., 2016). The rapid adaptation to alternative metabolic fuels may provide a key advantage for these cells to maintain viability in altered exogenous environments.

In addition to glycolysis, another key metabolic source might be the metabolism of glutamine, which is found in high concentrations within the brain. Glutamine is typically overlooked as a

metabolic source as its deaminated form, glutamate, is the primary excitatory neurotransmitter in the central nervous system. In a process known as the glutamate-glutamine cycle, synaptically released glutamate is rapidly cleared by astrocytes, where it is converted into glutamine and released back into the parenchyma for neuronal uptake and re-processing to glutamate (Schousboe et al., 2014; Tani et al., 2014). Additionally, glutamine may be taken up and processed through the metabolic pathway of glutaminolysis, in which it is converted into glutamate by glutaminase (GLS), and further processed into α-ketoglutarate by glutamate dehydrogenase (GDH). The α-ketoglutarate can then directly enter the tricarboxylic acid (TCA) cycle to support mitochondrial metabolism. It is possible that in the absence of glucose, such as during stroke or periods of hypoglycemia, microglia rapidly reprogram their metabolic activity to favor the breakdown of glutamine. This metabolic flexibility would make microglia capable of surviving and maintaining their critical immune functions during episodes of glucose deprivation.

Therefore, we aim to address the metabolic flexibility of microglia in the absence of glucose. We find that microglial morphology, baseline motility, and damage responsiveness to a laser-induced lesion are maintained throughout 60 minutes of glucose-free solutions. Furthermore, microglia are able to sustain their mitochondrial metabolism, which we suggest is the result of increased glutaminolysis. Application of glutaminolysis inhibitors decreases microglial viability, phagocytosis, and oxygen consumption *in vitro*, and inhibits mitochondrial metabolism, baseline motility, and immune surveillance of microglia *in situ*. We provide evidence that this metabolic reprogramming is dependent upon the function of mTOR, as the maintained microglial functions in aglycemia could be prevented by mTOR inhibition. We therefore propose that microglia are capable of rapid metabolic flexibility, which would permit their continued survival and immune

surveillance in conditions of vascular impairments, stroke, or periods of insulin-induced hypoglycemia.

4.2 Materials and Methods

4.2.1 Animal protocols

Mouse housing and experimental procedures were performed in accordance with Canadian Council on Animal Care (CCAC) regulations, with protocols approved by the University of British Columbia committee on animal care. Wild type C57Bl/6 (WT) or CX3CR1$^{+/EGFP}$ (Jackson Lab strain 005582 crossed with wild type C57Bl/6) mice were housed on a 12 h light/day cycle with food and water *ad libitum*.

4.2.2 Acute hippocampal slice preparation

Brains from mice 4-6 months of age were dissected and sliced horizontally with a vibratome (Leica VT1200S) to 300 μm thick in ice-cold NMDG slicing solution containing (in mM): 120 N-methyl-D-glucamine, 2.5 KCl, 25 $NaHCO_3$, 1 $CaCl_2$, 7 $MgCl_2$, 1.2 NaH_2PO_4, 20 D-glucose, 2.4 sodium pyruvate, and 1.3 sodium L-ascorbate, which was constantly oxygenated with 95% O_2 and 5% CO_2. Hippocampal slices were immediately transferred to artificial cerebral spinal fluid (aCSF), which was continuously oxygenated with 95% O_2 and 5% CO_2. Artificial CSF contained (in mM): 126 NaCl, 2.5 KCl, 26 $NaHCO_3$, 2 $CaCl_2$, 2 $MgCl_2$, 1.25 NaH_2PO_4, and 10 D-glucose, pH 7.3–7.4, osmolarity 300 mOsm. In aglycemic conditions, glucose was replaced with 10 mM sucrose. Slices were recovered in aCSF at 32 °C for a minimum of 30 minutes before imaging for time-lapse experiments, or were incubated for one hour in specified experimental conditions before imaging or SNAPSHOT fixation.

Using acute slices, NADPH protein was measured by ELISA (K347, BioVision) after 2 hour tissue incubation with or without 100 µM Physcion. Readings were normalized to total protein levels.

4.2.3 Two-photon NAD(P)H imaging

To image NAD(P)H lifetime, microglia in WT slices were identified by a 45-minute incubation with DyLight 594 tomato lectin. $CX3CR1^{+/EGFP}$ mice could not be used, as it was recently confirmed that GFP expression causes an artifact in NAD(P)H measurements (Chapter 3). During imaging, slices were submerged in oxygenated aCSF (at 3 mL/min perfusion speed) in an imaging chamber. Tissue was excited at 750 nm, and emitted light was split using a 480 nm long pass dichroic mirror. Blue NAD(P)H fluorescence passed through a 460/50 nm filter and was detected by a GaAsP hybrid detector (HPM-100-40 hybrid PMT, Becker and Hickl). Longer wavelengths were again split by a 575 nm long pass dichroic mirror. Green fluorescence (non-NAD(P)H autofluorescence) was collected after passing through a 535/50 nm filter to be excluded from lifetime analysis, while red (DyLight 594 tomato lectin) passed through a 630/75 nm filter before detection. All mirrors and filters were purchased from Chroma tech, Bellows Falls, VT. Images were taken in the stratum radiatum of CA1 hippocampus at a depth between 50 µm – 80 µm below the surface of the brain slice. Images were acquired at 256 x 256 (zoom factor 10; 42.51 x 42.51 µm xy scale) over 30 seconds to ensure a sufficient number of photons were collected for curve fitting.

4.2.4 NAD(P)H fluorescence lifetime data

NAD(P)H photons were collected by the hybrid-PMT, and detected by a TCSPC module (SPC-150, Becker and Hickl, Berlin, Germany) and SPCM software (Becker and Hickl, Berlin, Germany). Laser pulse clock information was sent to the SPC-150 module to enable lifetime calculations.

Photon counts were passed to SPC Image, where decay curves for each pixel were calculated using a two-component exponential (representing free and bound NAD(P)H) by the following equation:

$$F(t) = \alpha_1 e^{-t/\tau_1} + \alpha_2 e^{-t/\tau_2} \quad (1)$$

Where α is the amplitude and τ is the lifetime. The data was processed with unfixed τ_1 and τ_2 lifetimes, which correspond to the free and bound forms of NAD(P)H, respectively.

The mean lifetime of each pixel is calculated by:

$$\tau_m = \alpha_1\tau_1 + \alpha_2\tau_2 \quad (2)$$

Where α1 + α2 = 1. A spatial bin factor of 3 was used to attain a photon count >10 at the tail of the curve. A mask around the microglial soma was manually drawn, using the DyLight 594 tomato lectin fluorescence image as a guide, and avoiding neuropil signal contamination at cell edges. The average mean lifetime within a microglial mask was recorded. The data of all microglia in a mouse were averaged and considered as a single biological N.

4.2.5 Primary microglia culture and Seahorse assays

For primary microglial cultures, cortex from embryonic day 18 Sprague Dawley rats were obtained and gently triturated in DMEM culture media containing 10% FBS and 100 units/mL penicillin/streptomycin. Cells were filtered through 22 µm culture inserts, seeded into 100 mm culture dishes, and incubated at 37°C and 5% CO_2 for two weeks. The mixed glia cultures were shaken (Southwest Science SBT300 Digital Orbital Shaker) with a speed of 80 rpm for 4 hours and the detached microglia were plated into a Seahorse 96-well plate at a density of 30K cells/well and left to adhere overnight. Immediately following experimental media application, plates were loaded into the 96-well Seahorse XFe machine. Treatments consisted of full media (10 mM glucose + 4 mM L-glutamine), glucose only (10 mM glucose + 4 mM sucrose), glutamine only (4 mM L-glutamine + 10 mM sucrose), or deplete (14 mM sucrose for osmotic balance). An initial baseline reading was set for a total of four hours to measure the microglial metabolic response to media conditions. After four hours, a mitochondrial stress test was performed, including the sequential injection of Oligomycin (final concentration: 2 µM), FCCP (final concentration: 2 µM), and Rotenone/ Antimycin A (final concentration: 2.5 µM each). Oligomycin inhibits ATP synthase, revealing the amount of OCR used by cells to fuel ATP production. FCCP is a protonophore, which disrupts the inner mitochondrial membrane and thereby dissipates the electrochemical proton gradient. In attempt to restore the gradient, components of the ETC work at maximum rate, and the resulting OCR corresponds to the maximal respiratory capacity of the cells. Finally, Rotenone and Antimycin A inhibit complex I and III of the ETC, respectively. This completely blocks electron flow and any remaining OCR measured after this point is non-mitochondrial respiration, and was subtracted from all values. All OCR data was normalized to the initial baseline reading to control for variability in cell numbers and a minimum of 10 wells

were run per condition in each experiment. The experiment was repeated in two separate plates. Normalized baseline metabolic rates are considered as the average of the last three readings before metabolic drug injection (after a four-hour incubation with treatment media), and maximum respiration is considered as the third measurement following FCCP application.

4.2.6 Reagents

Physcion (19863-50, Cayman Chemical Co.); EGCG (Cayman Chemical Company 70935, 100 µM *in situ*); R162 (EMD Millipore 538098, 200 µM).

4.2.7 Data analysis and statistics

All values shown in the figures are the mean ± standard error of mean. For imaging experiments, data is reported as N indicating a biological replicate, composed of averaged data from multiple cells. Statistical significance was assessed using either One-way ANOVA with Tukey's multiple comparison post-hoc analysis for multiple groups, t-test for comparison of two means, or paired t-test when the same data is reported at 0 and 60-minute time points (*: $p<0.05$; **: $p<0.01$; ***: $p<0.001$, ****: $p<0.0001$).

4.3 Results

4.3.1 Microglia maintain baseline and immune surveillance in 0 mM glucose *in situ*

Microglia are highly dynamic cells, rapidly altering their morphology in response to immune stimuli or cellular damage, which can be used as an indicator of cell health and function. Therefore, we compared the morphology of microglia in acute hippocampal slices of CX3CR1$^{+/EGFP}$ mice following 60 minutes in control (10 mM glucose) or aglycemic (0 mM glucose) artificial

cerebrospinal fluid (aCSF) (Figure A.2.1a,b). By 3DMorph quantification (York et al., 2018), no change was observed in ramification index (control: 6.5±0.92; aglycemia: 6.9±0.44), or number of branch points (control: 5.07±0.36; aglycemia: 5.4±0.24; N=6) between conditions (Figure A.2.1c-f). In addition to rapid morphological changes, microglia also have highly motile processes, important for continuous surveillance of their local environment (Bernier et al., 2019; Nimmerjahn et al., 2005). This function promotes sensing of the parenchyma for damage or pathogen associated molecules, and allows contact with neurons and synapses to regulate neuronal health and activity (Hong, Dissing-Olesen, et al., 2016; A. Miyamoto et al., 2016; Sipe et al., 2016; Y. Wu et al., 2015; York et al., 2017). Between control and aglycemic conditions, there was no detectable change in microglial baseline motility in response to aglycemic onset, or following a 60-minute incubation with control or aglycemic solution (Figure A.2.1g-i). These data demonstrate that after 60 minutes in aglycemia, microglia are able to maintain their baseline morphology and motility, suggesting their basal function is unaltered in the absence of glucose.

While microglial baseline morphology and function were unaffected, it remained possible that microglia would be unable to respond to a site of focal damage. To test this, a laser-induced lesion was created in the tissue, which is well-known to stimulate coordinated microglial process extension (Davalos et al., 2005; Hines et al., 2009). Indeed, microglial processes were able to sense and surround the lesion within 10 minutes after damage in both control and aglycemic conditions (Figure A.2.1k,l). Quantification revealed no difference in speed of process response (Figure A.2.1m) or number of cells responding (control: 96.67 ± 3.33%; aglycemia: 88.48 ± 4.79%; Figure A.2.1n). Therefore, we confirm that in the absence of glucose, microglial baseline surveillance and damage-sensing functions are maintained.

4.3.2 Microglial mitochondrial metabolism is maintained during aglycemia *in situ*

As glucose is often considered the main carbon source for brain metabolism, and it is likely that microglial surveillance and damage-sensing functions are metabolically demanding (Engl & Attwell, 2015), we next examined the metabolic activity of microglia in control and aglycemic conditions. To accomplish metabolic measurements specifically in microglia within their physiological environment, we used fluorescence lifetime imaging of nicotinamide adenine dinucleotide (NAD(P)H-FLIM) (Lakowicz et al., 1992; Vergen et al., 2013). NAD^+ is reduced during glycolysis to NADH, which is autofluorescent (λ_{em}: 460 nm). While in a free molecule state, NADH has a short fluorescence lifetime of 400 ps, however upon enzymatic binding (such as to complex I of the electron transport chain), its lifetime is increased to around 2000 ps (Figure 4.2a). Therefore, by measuring the lifetime of NADH, it is possible to estimate the ratio of glycolysis to mitochondrial metabolism (Bird et al., 2005; Skala et al., 2007; M. O. A. Y. Yaseen et al., 2017). As NADH cannot be experimentally distinguished from the closely related species NADPH (Blacker et al., 2014), we refer to our measurements here as NAD(P)H. To ensure the majority of our signal is from the NADH component, we performed experiments inhibiting NADPH production with 100 μM Physcion (R. Lin et al., 2015) and observed no appreciable change in our imaging intensity (Figure 4.1a). As expected, there was a significant decrease in the NADPH protein level as measured by ELISA, confirming the effect of Physcion (Figure 4.1b).

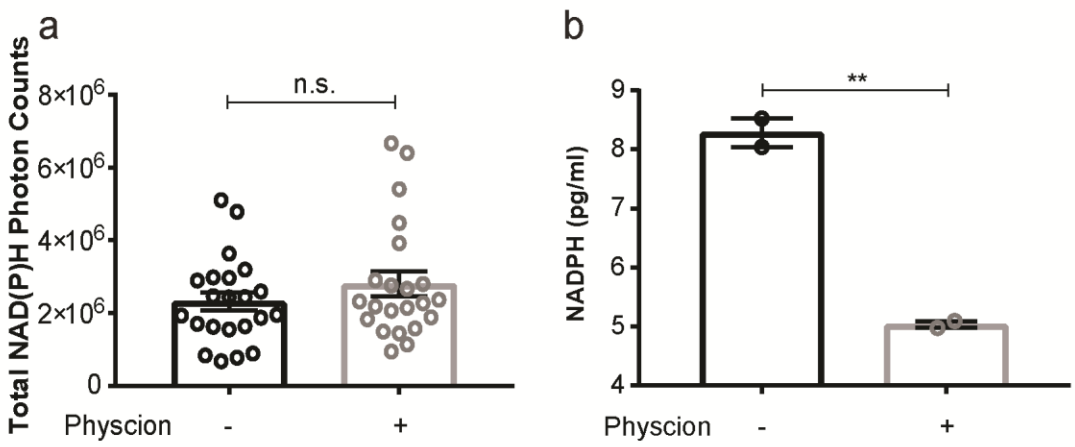

Figure 4.1 NAD(P)H-FLIM photons are mainly from NADH.

a) Total photon counts from NAD(P)H-FLIM images with or without Physcion (N = 3). b) NADPH protein level measurements by ELISA, with or without Physcion (N = 2). Error bars represent mean +/- SEM. **p<0.01, by Student's t-test.

By this technique, it was evident that in control aCSF, microglia have a much shorter mean NADH lifetime than the surrounding neuropil, suggesting that they have a higher rate of glycolysis at baseline (Figure 4.2b). Time-lapse imaging allowed measurements of NAD(P)H lifetime in response to changes in bath-applied solutions. Between control and aglycemic conditions, neuropil tissue showed no difference in the slope of change of NAD(P)H lifetime from 0 to 60 minutes, indicating that while the basal metabolic rates may be changing, this tissue is unable to substantially increase mitochondrial metabolism (Figure 4.2c). In contrast, microglial metabolism adapted to aglycemic conditions by increasing the relative rate of mitochondrial metabolism, as measured by an increase in NAD(P)H lifetime throughout the experiment (Figure 4.2d). The change in metabolism from 0 to 60 minutes is quantified for microglia in control or aglycemic conditions ($p>0.05$ in control from 0 min τ_m 865±21.5 ps to 60 min τ_m 864±10.1 ps; $p<0.05$ in

aglycemia from 0 min τ_m 876±13.5 ps to 60 min τ_m 930±17.0 ps; Figure 4.2e). Representative images of tomato lectin identified microglia and the corresponding mean NAD(P)H lifetime within the microglial mask are presented for 60 minutes in 10 mM or 0 mM glucose (Figure 4.2f,g). These data show a unique capacity of microglia to sustain their mitochondrial metabolism in the absence of glucose, suggesting that they are metabolizing an alternate carbon source to supply TCA metabolites.

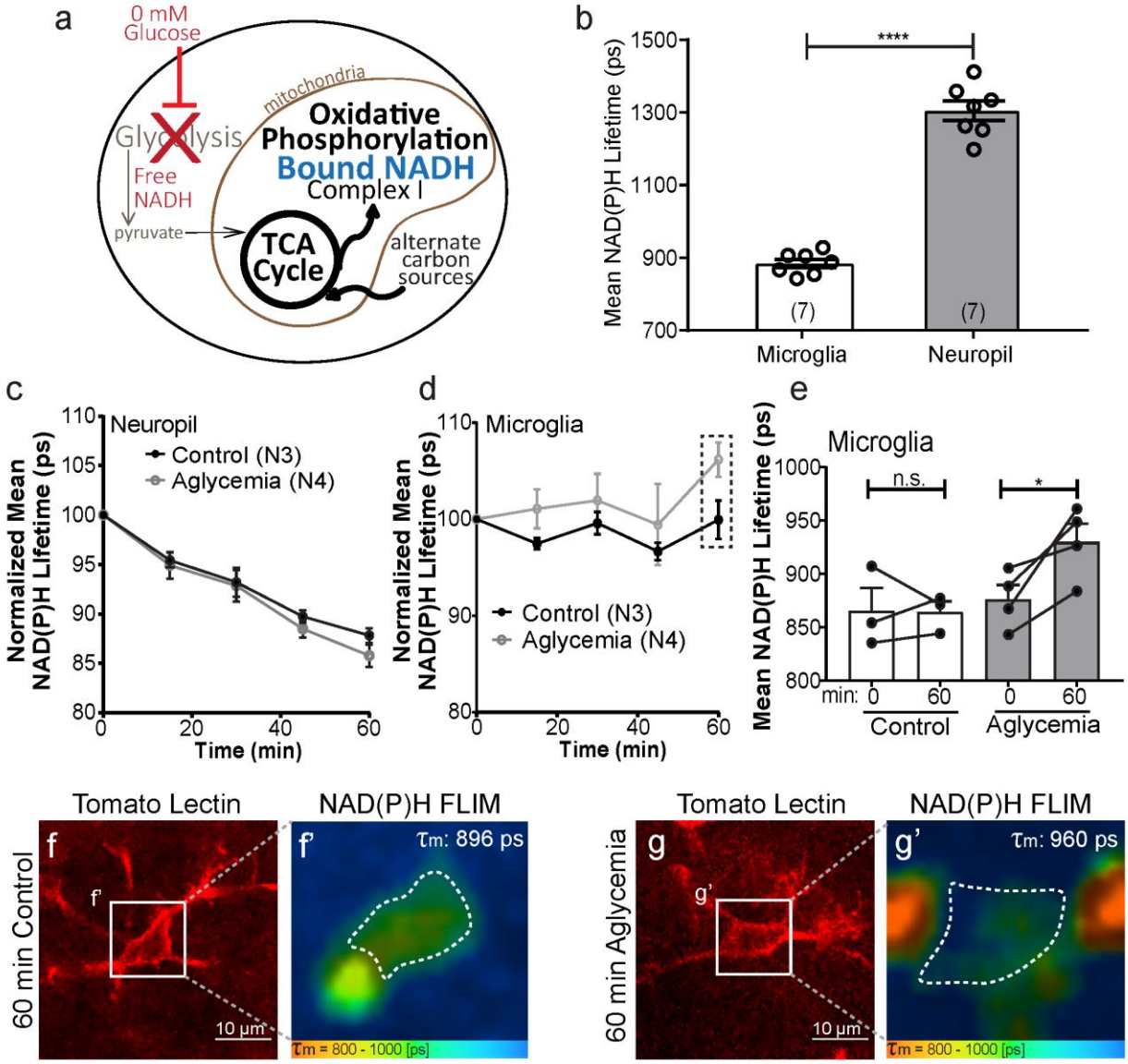

Figure 4.2 Microglia maintain mitochondrial metabolism in 0 mM glucose *in situ*.

a) Schematic showing effects of aglycemia on free (400 ps lifetime) and bound (~2000 ps lifetime) NADH. b) In control conditions, microglia have a significantly shorter lifetime than surrounding neuropil. c) Upon treatment with aglycemia, neuropil tissue does not maintain mitochondrial metabolism, whereas microglia (d) show a significantly increased lifetime after 60 minutes (e). Representative image of microglia identified by tomato lectin and the corresponding NAD(P)H lifetime image in control (f) and aglycemic (g) conditions. Dotted line in NAD(P)H image delineates the area included in the microglial mask. Only those pixels within the mask were included in calculating

the reported mean lifetime. Error bars represent mean +/- SEM. *p<0.05, ****p<0.0001 by paired (e) or unpaired (b) t-test.

4.3.3 Microglia are capable of metabolizing glutamine *in vitro*

As microglial function and metabolism were maintained in the absence of glucose for over 60 minutes, it follows that they must be metabolizing an alternative carbon source. In addition to glucose, amino acids can be used as an energy source. Glutamine is an amino acid found in high concentrations within brain tissue, as its deaminated form, glutamate, is the most prevalent excitatory neurotransmitter. In addition to being processed through the glutamate-glutamine cycle, glutamate can also be directly metabolized into the TCA cycle through glutaminolysis. In this pathway, glutamine is deaminated to glutamate via glutaminase, and subsequently processed by glutamate dehydrogenase (GDH) to α-ketoglutarate, an intermediate metabolite in the TCA cycle. To examine whether microglia could metabolize glutamine in a cell autonomous manner, we used cultures of both the immortalized microglial cell line, SIM-A9 (Nagamoto-Combs et al., 2014) and primary microglial cell cultures.

SIM-A9 cells were incubated for 4 hours in serum-free media containing 10 mM glucose and 4 mM glutamine in control conditions, 10 mM glucose only, 4 mM glutamine only, or sucrose only in depleted conditions. Sucrose was also included in glucose or glutamine only conditions as a non-metabolizable osmotic balance. To investigate the ability of microglia to maintain metabolism and viability, we used the MTT assay, in which the tetrazolium dye, MTT, is converted into an insoluble purple formazan product by NAD(P)H-dependent oxidoreductase enzymes. We observed a significant reduction in MTT metabolism in glucose-only media relative to control

($p<0.001$ glucose only 58.8±4.9% relative to control, N=19). However, there was no significant difference between control and glutamine-only conditions. Interestingly, MTT metabolism in glutamine-only conditions was significantly higher than glucose-only media ($p<0.001$ between glucose and glutamine 95.9±8.35% relative to control levels, N=19). As expected, microglia in deficient media had a significantly reduced MTT metabolism relative to both control and glutamine media ($p<0.001$, deficient=53.9±5.2% of control levels, N=19), which was not significantly lower than glucose-only conditions (Figure A.2.2a). To confirm that microglia were metabolizing glutamine for energy in these conditions, we repeated the experiment in the presence of epigallocatechin gallate (EGCG), which inhibits GDH and therefore, glutaminolysis (Choo et al., 2010; Csibi et al., 2013; C. Li et al., 2006; C. Yang et al., 2014). With glutaminolysis blocked, the amount of MTT metabolism in glutamine-only conditions was reduced, however all conditions remained higher than deficient (relative to normalized EGCG control, glucose-only 67.6±5.2%, glutamine-only 70.2±4.9%, deficient 37.9±8.1% of control levels, N=11 for all conditions; Figure A.2.2a).

As a measurement of function in these culture conditions, a phagocytosis assay was performed, in which SIM-A9 cells were treated with full, glucose, glutamine, or deficient media for 3 hours, followed by a 1-hour incubation with 1 μm fluorescent microspheres. After a brief wash, the number of phagocytosed beads were counted and presented as a percentage of the total number of cells in each condition. Relative to control, the glucose or glutamine conditions were not significantly reduced in their phagocytic ability, however all three conditions were significantly higher than deficient media (full 18.3±3.9%, glucose-only 14.3±2.8%, glutamine-only 14.8±2.4,

deficient 2.3±1.0%, N=4 in all conditions; Figure A.2.2b). Therefore, glutaminolysis can maintain microglial metabolic viability and phagocytic capacity in the absence of glucose.

We also used primary cultures of rat microglia to investigate mitochondrial metabolism of microglia in the presence or absence of glucose and glutamine. Primary rat E18 microglia were plated in 96-well plates for studies using the Seahorse mitochondrial stress test to measure microglial oxygen consumption rate (OCR). Cells were loaded into the Seahorse reader immediately after changing the media to 1) control media, 2) glutamine-deficient media, 3) glucose-deficient media, or to 4) media deficient in both glucose and glutamine (made from Seahorse base media with sucrose included as an osmotic balance). The initial measurement was used to normalize all experimental data for variations in plating densities. Cells were incubated for 4 hours with repeated OCR measurements to visualize metabolic changes over time. After 4 hours, the normalized basal OCR was significantly lower in deficient conditions relative to control, while there was no significant difference in glucose or glutamine only conditions (control 0.58±0.05 N=20, glucose 0.46±0.04 N=19, glutamine 0.42±0.03 N=20, deficient 0.31±0.04 N=20, N indicates number of wells preformed across replicate experiments; Figure 4.3a).

Following a 4-hour incubation in experimental conditions, all wells were injected with oligomycin to inhibit ATP synthase, revealing the amount of oxygen consumption used for ATP synthesis. Thereafter, the protonophore, FCCP was added to dissipate the mitochondrial membrane proton gradient and drive the electron transport chain to maximal respiration. The OCR following FCCP treatment is indicative of the maximum cellular respiratory capacity, and therefore a measure of mitochondrial content and function. Microglia incubated in control conditions had significantly

higher maximal respiratory rates than cells in deficient media. While glucose and glutamine conditions were not significantly different from control or each other, the glutamine-only condition was significantly higher than cells given deficient media (control 0.53±0.08, glucose 0.36±0.05, glutamine 0.43±0.07, deficient 0.17±0.03; Figure 4.3b). These data suggest that microglia given glutamine are able to maintain mitochondrial activity in the absence of glucose.

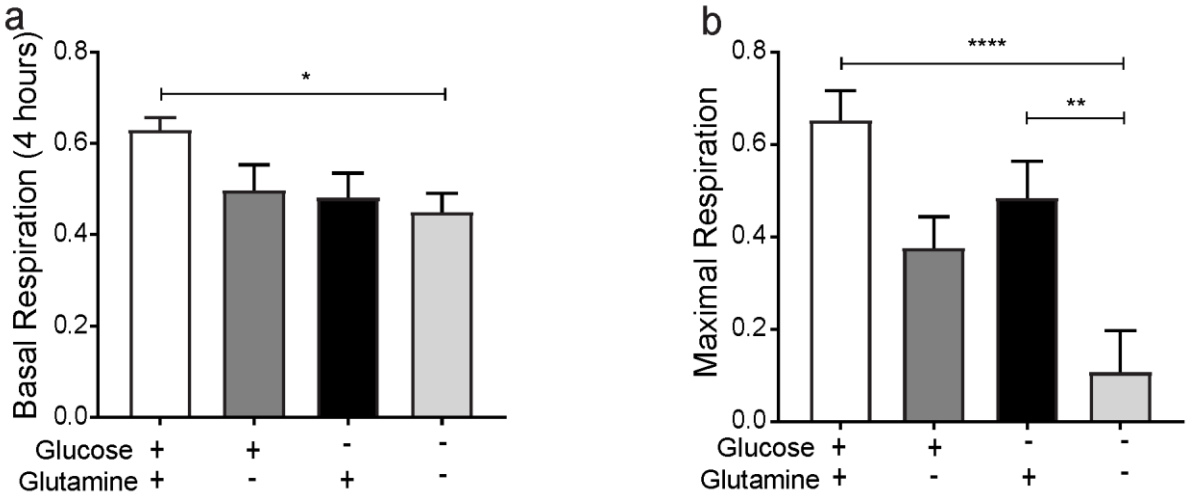

Figure 4.3 Microglia metabolize glutamine *in vitro* to maintain OCR.

Seahorse metabolic assays were performed with primary rat E19 microglia. Basal respiration after 4 hours in experimental media (a), and maximal respiration following addition of FCCP (b) are reported. Data is normalized to initial reading to control for variations in plating density. Error bars represent mean +/- SEM. *p<0.05, ***p<0.001 by One-way ANOVA and Tukey's multiple comparison.

4.3.4 During aglycemia, glutaminolysis supports microglial metabolism *in situ*

Upon confirming microglial metabolism of glutamine *in vitro*, we confirmed these findings *in situ* with acute hippocampal slices. Using NAD(P)H-FLIM and tomato lectin identification of microglia in wild-type tissue, we again confirmed that microglial mean NAD(P)H lifetimes are

increased in conditions of 60 minutes in 0 mM glucose. After 60 minutes in 0 mM glucose with EGCG, the microglia were no longer able to increase their mean NAD(P)H lifetime, again confirming that these cells switch to reliance on glutaminolysis in the absence of glucose (60 minutes aglycemia τ_m 930±17 ps, N=4; 60 minutes EGCG + aglycemia τ_m 794±39.8 ps, N=3; Figure 4.4a-e). To confirm this pharmacological effect, an additional inhibitor of GDH, R162, was tested. These treatments confirmed the effect seen with EGCG, that inhibition of glutaminolysis prevented the mitochondrial metabolism observed in aglycemic solutions (control τ_m 861±1.4 ps, aglycemia τ_m 1027±45 ps, R162 τ_m 859±44 ps, R162+aglycemia τ_m 884±23 ps; N=3; Figure 4.4f). Therefore, microglia are metabolically flexible in the absence of glucose and increase their reliance on glutaminolysis to maintain mitochondrial metabolism.

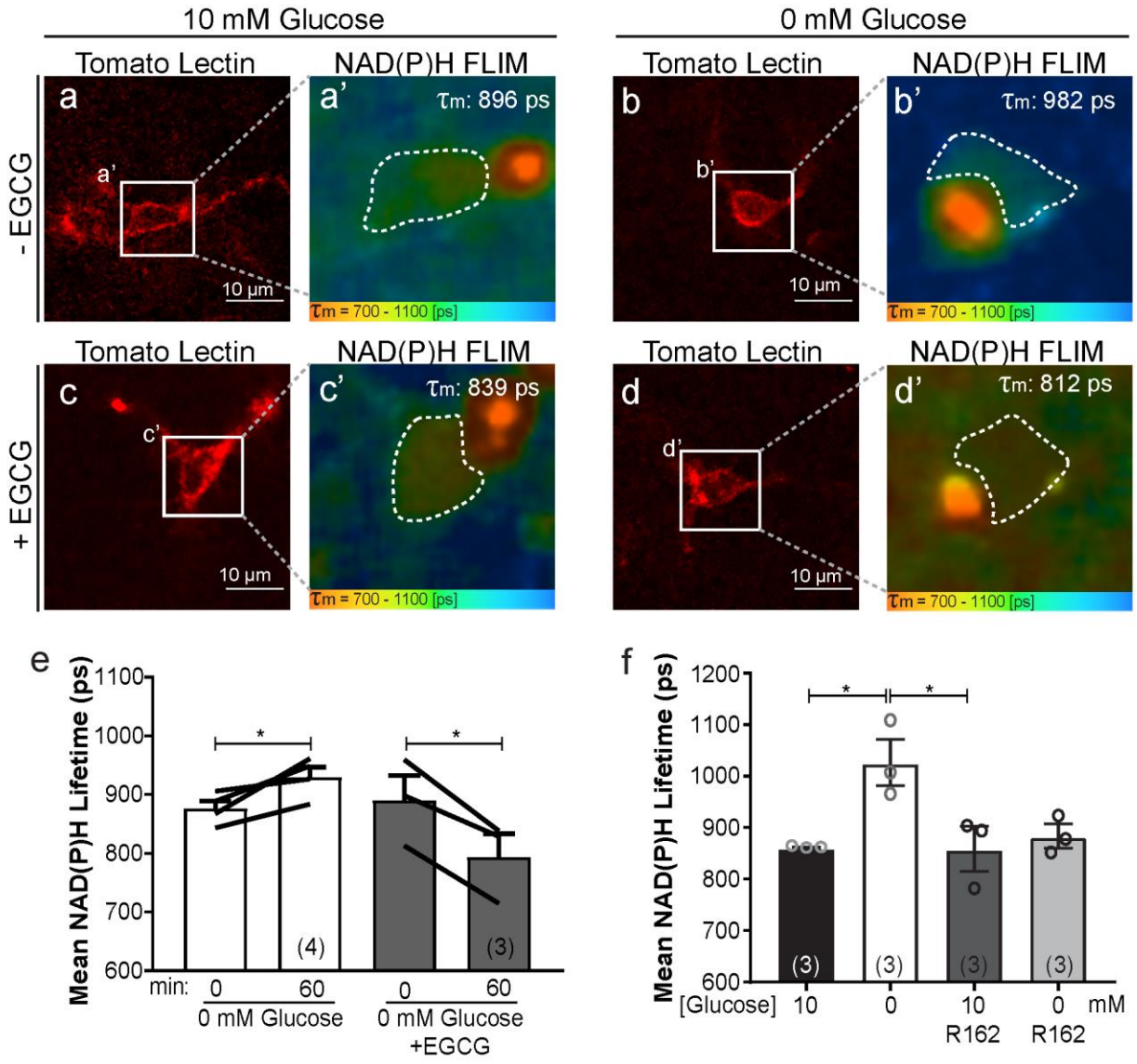

Figure 4.4 Microglia metabolize glutamine *in situ*.

Representative tomato lectin identified microglia and corresponding NAD(P)H lifetime image from acute hippocampal slices incubated for 60 minutes in control (a), aglycemic (b), EGCG (c), or aglycemic and EGCG (d) conditions. Dotted line in NAD(P)H image delineates the area included in the microglial mask. Only those pixels within the mask were included in calculating the reported mean lifetime. e) Mean lifetimes at 0 and 60 minutes are reported for aglycemic, and aglycemic with EGCG conditions. f) Mean lifetimes of microglia after 60 minutes in 0 or 10 mM glucose in the presence or absence of R162. Error bars represent mean +/- SEM. *p<0.05 by paired t-test (e), or One-way ANOVA and Tukey's multiple comparison (f).

4.3.5 Glutaminolysis maintains microglial motility and immune function in 0 mM glucose

As microglial glutaminolysis can support mitochondrial metabolism in the absence of glucose, we next investigated whether glutaminolysis was also responsible for the maintained motility and immune surveillance *in situ* during aglycemic conditions using CX3CR1$^{+/EGFP}$ mice. Relative to aglycemia alone, 60 minutes in aglycemic conditions with EGCG had a dramatic effect on microglial morphology (Figure A.2.3a-d). By 3DMorph quantification, EGCG and aglycemia caused a significant decrease in ramification index (control 7.6±0.2, aglycemia 6.9±0.7, EGCG 3.7±0.2, EGCG + aglycemia 4.6±0.6, N=4; Figure A.2.3e) and number of branch points (control 5.6±0.07, aglycemia 5.5±0.39, EGCG 3.7±0.06, EGCG + aglycemia 3.9±0.23, N=4; Figure A.2.3f). In addition to morphological changes, the addition of EGCG to aglycemic solutions decreased microglial baseline motility (EGCG 0.192±0.014, aglycemia 0.267±0.014, EGCG + aglycemia 0.165±0.018 N=4 slices, Figure A.2.3i).

Upon neighboring damage stimulation by laser-induced lesion, microglia in aglycemic conditions rapidly respond and are able to surround the site of injury within 10 minutes (Figure A.2.3g). With addition of EGCG in aglycemic solution, the microglia no longer responded to the damage and showed very little process extension (Figure A.2.3h). The percentage of microglia reaching the lesion (EGCG 64.17±13.15, aglycemia 77.5±10.31, EGCG + aglycemia 11.81±6.84, N=4 slices; Figure A.2.3j), and process extension, as measured by microglial GFP intensity around the lesion (Figure A.2.3k) were quantified. These data confirm that in the absence of glucose, the microglia rely on glutaminolysis to maintain their metabolism and support baseline and immune surveillance.

4.3.6 Microglial metabolic switch to glutaminolysis is dependent on mTOR

A well-known master regulator of metabolism is the mammalian target of rapamycin (mTOR), which has been confirmed to mediate metabolic flexibility across many cell types (C.-L. Lu et al., 2015; Saxton & Sabatini, 2017; Weichhart et al., 2015). To investigate whether mTOR activity was necessary in microglia to allow the metabolic flexibility between glycolysis and glutaminolysis, we used hippocampal slices from CX3CR1$^{+/EGFP}$ mice throughout 60 minutes of aglycemia in the presence or absence of the mTOR inhibitor, Torin-1 (Carlessi et al., 2017; Thoreen et al., 2009). Matching the morphological response observed in EGCG and aglycemia conditions, addition of Torin-1 caused a dramatically altered microglial morphology relative to aglycemic solutions alone (Figure A.2.4a,b).

Application of Torin-1 in control solution had no affect on baseline microglial motility, confirming that no metabolic switch was needed in the presence of glucose (Torin-1 0.237±0.028, aglycemia 0.236±0.028, Torin-1 + aglycemia 0.149±0.009 N=4 slices; Figure A.2.4e). In addition to baseline motility, immune surveillance was also blunted by Torin-1 treatment in aglycemia (Figure A.2.4c,d) as measured by percentage of responding cells (Torin-1 93.75±6.25, aglycemia 90.83±5.34, Torin-1 + aglycemia 27.50±12.79 N=4 slices; Figure A.2.4f) and intensity of microglial processes around a laser-induced lesion (Figure A.2.4g). Therefore, it appears that mTOR activity is necessary for microglial metabolic flexibility and increased glutaminolysis in aglycemic conditions. This metabolic adaptation is necessary for microglia to perform both their baseline surveillance, as well as damage-sensing functions.

4.4 Discussion

4.4.1 Microglia maintain metabolism, motility, and immune surveillance in the absence of glucose

It has been previously established that neuronal metabolism and synaptic activity rundown after approximately 30 minutes without glucose, likely coinciding with the depletion of limited glycogen stores within neural tissue (Brown & Ransom, 2007; Izumi et al., 1994; Magistretti & Allaman, 2015; Shetty et al., 2013). In dramatic contrast to this finding, we here present the continued surveillance and immune function of microglia for 60 minutes in aglycemic conditions. The absence of a morphological change, and the maintenance of baseline surveillance of the brain parenchyma and directed outgrowth towards damage implies that the microglia remain viable and functional in these conditions. While there is no significant morphological change, it does appear as though aglycemia induces a small increase in process outgrowth and motility. It is likely that alterations in neuronal activity and health result in the release of factors such as ATP, a known chemoattractant for microglial processes (Davalos et al., 2005). This would further support our finding that neuronal functions are being perturbed, while microglial immune surveillance is maintained.

The continued membrane and cytoskeleton dynamics involved in surveillance and process extension are postulated to be energetically-demanding activities (Engl & Attwell, 2015), and thus, it is interesting that they are undisturbed upon the complete removal of glucose. It is therefore evident that an alternative metabolic source must be supplementing the metabolites necessary to maintain energy homeostasis in these cells. By employing NAD(P)H-FLIM, we were able to

validate that microglia are highly glycolytic at baseline in control tissue, but are also metabolically flexible, capable of increasing their mitochondrial metabolism throughout 60 minutes in aglycemia. No such adaptation was observed in the metabolism of the surrounding neuropil tissue, suggesting that cells of the neuropil are largely unable to support mitochondrial metabolism, while microglia are readily flexible.

4.4.2 Microglial glutaminolysis maintains mitochondrial metabolism during aglycemia

An increased reliance on mitochondrial metabolism in the absence of glucose suggests that microglia are metabolizing an alternate carbon source, which would supply metabolites to the TCA cycle and electrons to the electron transport chain (ETC). Using both *in vitro* and *in situ* models, we provide evidence that microglia are able to metabolize glutamine as an alternative metabolic source in the absence of glucose. While the MTT assay is widely used as a measure of viability, it is also a measure of mitochondrial metabolism, as it relies on the activity of oxidoreductase enzymes involved in the ETC. Therefore, this assay reveals not only the microglial viability in glutamine-only conditions, but also that their mitochondrial metabolism remains functional. These results were further confirmed by measurements of oxygen consumption rate (OCR) using Seahorse technology in primary microglia.

The *in vitro* metabolism data were verified *in situ* by measuring the mean NAD(P)H lifetime of microglia in acute hippocampal slices. As previously shown, 60 minutes in aglycemic solution causes an increased mean NAD(P)H lifetime in microglia. In addition, pharmacological inhibition of glutaminolysis with either EGCG or R162 blocked the increase of mean NAD(P)H lifetime in

aglycemic conditions supporting our conclusion that glutaminolysis maintains mitochondrial metabolism.

4.4.3 Glutaminolysis supports microglial surveillance during aglycemia

Upon inhibition of both glycolysis and glutaminolysis, microglia were no longer able to maintain their highly ramified morphology, dynamic baseline motility, or response to tissue insult. The striking affect of glutaminolysis inhibition in aglycemic conditions suggests that it is the main alternative metabolic pathway for these cells in the absence of glucose. This is a likely scenario in brain tissue, where glutamate acts as an excitatory neurotransmitter and is rapidly cleared (3 µM extracellular concentration) (Miele et al., 1996), while glutamine is maintained at high extracellular concentrations (385 µM) (Kanamori & Ross, 2004).

It is possible that microglia may directly take up external glutamate for metabolism, and thereby contribute to protection against excitotoxicity. However, this is not likely to occur at appreciable levels during baseline conditions, as microglia have very low expression of the glutamate transporters, GLAST (EAAT1) and Glt1 (EAAT2) (Y. Zhang et al., 2014). There have been several reports of microglial Glt1 upregulation, although this is in response to viral infection, neuronal damage, or LPS and TNFα stimulation (Chrétien et al., 2002; López-Redondo et al., 2000; Persson et al., 2005). However, there is evidence for the microglial expression of the glutamine transporters, SLC1A5 (ASCT2) (Scalise et al., 2018) and SLC38A1 (SNAT1) (Kalsbeek et al., 2016; Y. Zhang et al., 2014). Functionally, the role of SNAT1 in microglial glutamine transport has been extensively studied in cases of Rett's syndrome, an autism spectrum disorder. In this condition, the deficiency of MeCP2, a microglial-specific transcriptional repressor

of SNAT1, results in an overproduction of glutamate and NMDA-mediated excitotoxicity (Jin et al., 2015). Interestingly, SNAT1 overexpression in these microglia also resulted in a glutamine-dependent increase in OCR (Jin et al., 2015), confirming the microglial uptake and metabolism of glutamine.

Although our evidence and other reports (A. M. Nagy et al., 2018) suggest that microglia are primarily metabolizing glutamine to support metabolic and biosynthetic demands in the absence of glucose, it is possible that there are additional contributions from other energy sources. The metabolism of ketone bodies and branched chain amino acids may also be used by microglia under different energetic or extracellular conditions. Whether these pathways are capable of supporting microglia in aglycemic conditions would require further investigation. Based on our observations, they do not appear sufficient to maintain microglial metabolism and function in conditions of aglycemia or after inhibition of glutaminolysis. Fatty acid oxidation (FAO) is another major metabolic pathway, although it is unlikely to occur in microglia as they lack a key enzyme, Cpt1a (Jernberg et al., 2017). It has also been postulated that FAO occurs only sparingly in brain tissue as it is highly sensitive to the local depletions in oxygen required for this metabolic activity (Schönfeld & Reiser, 2013). Therefore, we propose that glutamine metabolism is the major pathway supporting microglia in aglycemic tissue.

A remaining and interesting question is the role of astrocytes in supporting neuronal and microglial metabolism, and regulating the extracellular glutamine and glutamate environment. Astrocytes are major contributors to synaptic glutamate uptake, and are key players in the glutamine-glutamate cycle (Schousboe et al., 2014; Tani et al., 2014). Whether astrocytes are themselves metabolizing

glutamine during aglycemia, or are influencing the metabolic state of the tissue through release of lactate, glutamine, or ketone bodies remains an unanswered and interesting question.

4.4.4 mTOR-mediated metabolic flexibility

To further explore the mechanisms regulating the rapid metabolic flexibility observed in microglia, the role of the mammalian target of rapamycin (mTOR) was investigated. mTOR is a core component of the multiprotein complexes, mTORC1 and mTORC2, and acts as a master regulator of metabolism and cell proliferation. These mTOR complexes integrate signals of nutrient availability and cellular energy status and in turn regulate protein and lipid synthesis, autophagy, and metabolic flux (Saxton & Sabatini, 2017). mTOR not only increases glycolysis by activating the HIF-1α pathway, it is also critical in stimulating mitochondrial function and promotes tumor cell survival (C.-L. Lu et al., 2015) and immune cell reprogramming (Weichhart et al., 2015). Several cancer cell lines survive irradiation by rapidly relocating mTOR to the mitochondria where it decreases hexokinase-II activity. In this way, mTOR reduces glycolysis and stimulates oxidative phosphorylation (OXPHOS), thereby reversing the classic Warburg metabolism of tumorigenic cells. Inhibition of mTOR blocked this relocation, metabolic alteration, and reduced clonogenic survival following irradiation (C.-L. Lu et al., 2015). mTOR is also able to interact with the transcriptional regulator, Yin Yang 1 (YY1), to increase peroxisome proliferator-activated receptor gamma coactivator 1-alpha (PGC-1α) activity and mitochondrial biogenesis (Morita et al., 2015). In addition to biogenesis, mTOR also stimulates translation of nuclear-encoded mitochondrial genes by inhibiting the eukaryotic translation initiation factor 4E-binding proteins (4E-BPs), to support an increased OXPHOS capacity (Morita et al., 2013, 2015).

Interestingly, there is also evidence that the mTORC1 pathway increases glutaminolysis. This is accomplished by mTORC1-mediated ubiquitination and degradation of CREB2, leading to a downstream decrease in SIRT4 transcription, which is an inhibitor of GDH. Therefore, mTORC1 increases the activity of GDH, the enzyme necessary for conversion of glutamate to α-ketoglutarate (Csibi et al., 2013). Addition of rapamycin to inhibit mTORC1 decreased GDH activity to a similar extent as addition of the established GDH inhibitor, EGCG (Csibi et al., 2013). These results support our own findings, in which mTOR inhibition by Torin-1 blocked microglial motility and lesion response in aglycemic conditions, which is reminiscent of EGCG-treated aglycemic conditions. This further substantiates our finding of microglial metabolic adaptation and reliance on glutaminolysis during periods of aglycemia.

4.4.5 Microglial metabolic flexibility

In conclusion, we have discovered that microglia exhibit remarkably rapid metabolic flexibility to increase glutaminolysis in aglycemic conditions. This switch to glutaminolysis in microglia is sufficient to support their mitochondrial metabolism and maintain both baseline surveillance and morphology, as well as targeted damage sensing and process outgrowth. The metabolic flexibility of microglia was largely unexpected, because brain tissue and neurons in particular, are extremely sensitive to metabolic disruptions such as stroke (Sims & Muyderman, 2010), and diabetic hypoglycemia (Meneilly & Tessier, 2016; Rehni & Dave, 2018). Microglial adaptation to alternative metabolic fuels likely provides a key advantage for their survival and continued function in these damaged or perturbed environments. The maintenance of protection, debris clearance, and immune activation of microglia in these conditions will have key clinical implications for neuronal health and recovery of cognitive function.

Chapter 5: TLR4-mediated increase of microglial glycolysis inhibits expression of LTP through IL-1β

5.1 Introduction

Alterations in synaptic plasticity are major contributors to learning and memory impairments following brain trauma, in disease states, and in advanced aging (Albensi & Janigro, 2009; Burke & Barnes, 2006; Shankar et al., 2008; Spronsen & Hoogenraad, 2010). A common underlying factor in these conditions is an inappropriate or prolonged pro-inflammatory activation of microglia, the main immune component in the central nervous system. Microglia are the first responders to trauma such as stroke (Yenari et al., 2010) and traumatic brain injury (Simon et al., 2017), and are seen in activated or dystrophic states in various neurodegenerative diseases (Salter & Stevens, 2017), such as in Alzheimer's disease (Heppner et al., 2015), Parkinson's disease (Gelders et al., 2018), and Huntington's disease (Crotti & Glass, 2015).

Microglia may modify neural functions through direct contacts or release of pro-inflammatory cytokines, such as tumor necrosis factor α (TNFα) and interleukin 1 β (IL-1β) (Beattie et al., 2002; Goshen et al., 2007; Romana Rizzo et al., 2018; Stellwagen & Malenka, 2006; Yirmiya & Goshen, 2011; York et al., 2017). Neurons express a range of receptors for these cytokines, which in physiological conditions, may be important for synaptic scaling (Stellwagen & Malenka, 2006) or pruning (Schafer et al., 2012) to prevent hypo or hyperexcitation. However, in pathological states, prolonged and excessive release of cytokines may induce synaptic long-term depression (LTD), potentially leading to learning and memory deficits.

As previously shown, microglial stimulation by lipopolysaccharide (LPS; a component of gram-negative bacteria), can act through complement receptor 3 to trigger NADPH oxidase production of reactive oxygen species (ROS), which results in LTD (J. Zhang et al., 2014). However, LPS is also a well-established activator of Toll-like receptor 4 (TLR4), which leads to a robust increase in cytokine production. This effect is mediated via downstream pathways, which may be largely reliant on regulation of cellular metabolism (Everts et al., 2014; Kornberg et al., 2018; Tannahill et al., 2013).

The field of immunometabolism has been making rapid and remarkable progress in understanding the metabolic regulation of peripheral immune cell polarization (E. L. Mills et al., 2017; O'Neill et al., 2016; Weinberg et al., 2015). This includes the roles of enzymes and metabolites involved in glycolysis, the tricarboxylic acid (TCA) cycle, and the electron transport chain (ETC), as well as pathways of amino acid and fatty acid metabolism. Although the details are complex and still under intensive investigation, it has become apparent that increased glycolysis is permissive to pro-inflammatory activation of macrophages (Jha et al., 2015; Tannahill et al., 2013), T-cells (Blagih et al., 2015; Chang et al., 2013; Klysz et al., 2015; L. Z. Shi et al., 2011), and dendritic cells (Everts et al., 2014). Conversely, pathways of fatty acid metabolism and oxidative phosphorylation (OXPHOS) are increased by stimuli to induce T memory cells (van der Windt et al., 2012). Additionally the choice of differentiation into a T effector cell or T regulatory cell is highly dependent on metabolic transitions, and altering these metabolic pathways can drive cell differentiation into either effector or regulatory cell type (Berod et al., 2014; Kornberg et al., 2018;

L. Z. Shi et al., 2011), highlighting the importance of these pathways in both permitting and inducing polarization.

Following pro-inflammatory immune stimulation, a rapid increase in glycolysis may serve many signalling functions. First, a shift in metabolite production is necessary to support the biosynthetic demands of dividing cells and organelle expansion associated with increased protein and cytokine production (Everts et al., 2014; B. Kelly & O'Neill, 2015). Additionally, the glycolytic enzyme, glyceraldehyde 3-phosphate dehydrogenase (GAPDH) can also bind (AU)-rich elements of mRNA 3' untranslated region and act as a post-transcriptional repressor of TNFα and IFNγ (Chang et al., 2013; Millet et al., 2016). Finally, a 'broken' TCA cycle (Cordes et al., 2016; Jha et al., 2015) can allow accumulation of certain metabolites, such as fumarate and citrate, which can cause epigenetic changes resulting in a form of trained immunity (Arts, Novakovic, et al., 2016; Dominguez-Andres et al., 2019; Williams & Neill, 2018), and can be used to fuel *de novo* fatty acid synthesis used for organelle expansion (Everts et al., 2014). There is also an important balance in the ratio of α-ketoglutarate (α-KG) to succinate in regulating hypoxia-inducible factor 1α (HIF-1α). To allow for rapid regulation, HIF-1α is continuously produced and targeted for degradation by prolyl hydroxylases (PHD), which are stimulated by α-KG, and inhibited by succinate (Koivunen et al., 2007). Therefore, an increase in succinate can cause a stabilization in HIF-1α, which is a transcriptional activator of a range of hypoxia response elements, including IL-1β (Tannahill et al., 2013).

Therefore, it is clear that tight metabolic regulation is critical in controlling immune function, and furthermore, that a delicate immune balance is essential for neuronal health and communication.

Here, we show that innate immune stimulation with lipopolysaccharide (LPS) triggers an increase in aerobic glycolysis in microglia, which is associated with an increase in hypoxia-inducible factor 1α (HIF-1α) stabilization and production of pro-inflammatory cytokines, including interleukin-1β (IL-1β). IL-1β release inhibits the induction of long term potentiation (LTP), a neural correlate of memory, following high-frequency stimulation (HFS) – an effect which can be rescued by Interleukin 1 receptor antagonist, or by inhibiting LPS-stimulated glycolysis and IL-1β production with 2-deoxy-D-glucose. These results highlight the importance of both immune and metabolic balance in the maintenance of brain health.

5.2 Materials and Methods

5.2.1 Animal protocols

Mouse housing and experimental procedures were carried out in accordance with Canadian Council on Animal Care (CCAC) regulations, with protocols approved by the University of British Columbia committee on animal care. Wild type C57Bl/6 (WT) and CX3CR1$^{+/EGFP}$ (Jackson Lab strain 005582 crossed with wild type C57Bl/6) were housed on a 12 h light/day cycle with food and water *ad libitum*.

5.2.2 Acute hippocampal slice preparation

For FLIM recordings and microglial imaging, brains from mice 4-6 months of age were quickly dissected and sliced horizontally with a vibratome (Leica VT1200S) at 300 μm thick in ice-cold NMDG slicing solution containing (in mM): 120 N-methyl-D-glucamine, 2.5 KCl, 25 $NaHCO_3$, 1 $CaCl_2$, 7 $MgCl_2$, 1.2 NaH_2PO_4, 20 D-glucose, 2.4 sodium pyruvate, and 1.3 sodium L-ascorbate, which was constantly oxygenated with 95% O_2 and 5% CO_2. Hippocampal slices were

immediately transferred to artificial cerebral spinal fluid (aCSF) continuously oxygenated with 95% O_2 and 5% CO_2. Artificial CSF contained (in mM): 126 NaCl, 2.5 KCl, 26 $NaHCO_3$, 2 $CaCl_2$, 2 $MgCl_2$, 1.25 NaH_2PO_4, and 10 ᴅ-glucose, pH 7.3–7.4, osmolarity 300 mOsm. In LPS conditions, 10 µg/ml was added to aCSF. For 2DG conditions, 5 mM glucose was omitted from aCSF and replaced with 5 mM 2DG (final glucose volume of 5 mM). Slices were incubated in 15 mL chambers for two hours at 32 °C before imaging or tissue collection for pro-inflammatory cytokine measurements.

5.2.3 Primary microglia culture

Cortex from embryonic day 18 Sprague Dawley rats were obtained and gently triturated in DMEM culture media containing 10% FBS and 100 units/mL penicillin/streptomycin. Cells were filtered through 22 µm culture inserts, seeded into 100 mm culture dishes, and incubated at 37°C and 5% CO_2 for two weeks. The mixed glia cultures were shaken (Southwest Science SBT300 Digital Orbital Shaker) with the speed of 80 rpm for 4 hours and the detached microglia were plated into 12-well plates at 1,000,000 cells/well for HIF-1α measurements. One hour after plating, microglia cultures were treated with serum-free DMEM for one hour before treatments were performed. Treatments included addition of 100 ng/ml LPS and/or 5 mM 2DG to serum-free DMEM media.

5.2.4 Two-photon imaging

For morphological analysis, hippocampal slices from $CX3CR1^{+/EGFP}$ mice were incubated for two hours in treatment conditions at 32 °C, then rapidly fixed by SNAPSHOT protocol (Dissing-Olesen & MacVicar, 2015). This includes a two-minute fixation in 4% PFA at 80 ˚C, rinse in 0.1 M PBS, and storage in clearing solution (0.1M PBS with 20% DMSO, and 2% Triton X-100) at 4

˚C. GFP fluorescence is well-preserved by this method, and slices were ready for imaging immediately after clearing. Images were acquired with a Coherent Chameleon Ultra II laser (mode-locked pulse train at 80 MHz at 910 nm) with a Zeiss LSM 7 MP microscope and Zeiss 20x-W/1.0 NA objective. Green fluorescence was detected by a 535/50m filter and GaAsP photo-multiplier tube (PMT; Zeiss LSM BiG). Images were acquired as a z-stack at 1024 x 1024 (zoom factor 2.8; 170.04 x 170.04 µm xy scale) from 125 – 175 µm deep (1 µm slice interval) in the stratum radiatum region of CA1 hippocampus.

To image NAD(P)H lifetime, microglia in WT slices were identified by DyLight 594 tomato lectin incubation. CX3CR1$^{+/EGFP}$ mice could not be used, as GFP expression causes an artifact in NAD(P)H measurements (Chapter 3). During imaging, slices were submerged in oxygenated aCSF (at 3 mL/min perfusion speed) in an imaging chamber. Tissue was excited at 750 nm, and emitted light was split using a 480 nm long pass dichroic mirror. Blue NAD(P)H fluorescence passed through a 460/50 nm filter and was detected by a GaAsP hybrid detector (HPM-100-40 hybrid PMT, Becker and Hickl), while longer wavelengths were again split by a 575 nm long pass dichroic mirror. Green fluorescence (non-NAD(P)H autofluorescence) was collected after passing through a 535/50 nm filter to be excluded from lifetime analysis, while red (DyLight 594 tomato lectin) passed through a 630/75 nm filter before detection. All mirrors and filters were purchased from Chroma tech, Bellows Falls, VT. Images were taken in the stratum radiatum of CA1 hippocampus at a depth between 50 µm – 80 µm below the surface of the brain slice. Images were acquired at 256 x 256 (zoom factor 10; 42.51 x 42.51 µm xy scale) over 30 seconds to ensure a sufficient number of photons were collected for curve fitting.

5.2.5 Microglial morphology analysis

Representative images were acquired from each hippocampal slice, with an experimental N of 3 mice. Multiple cells are analyzed in each image, and the data is analyzed as the average measurement of each image. Images were initially pre-processed in FIJI with a mean filter, background subtraction, and contrast enhancement to better visualize signal-to-noise ratio. All images were processed using the same settings, then loaded into 3DMorph (York et al., 2018) for analysis. A threshold adjustment of 0.4 and noise cut-off of 5000 were used to analyze all images in the batch processing mode.

5.2.6 NAD(P)H fluorescence lifetime data

NAD(P)H photons were collected by the hybrid-PMT, and detected by a TCSPC module (SPC-150, Becker and Hickl, Berlin, Germany) and SPCM software (Becker and Hickl, Berlin, Germany). Laser pulse clock information sent to the SPC-150 software module enabled lifetime calculations.

Photon counts were passed to SPC Image, where decay curves for each pixel were calculated using a two-component exponential by the following equation:

$$F(t) = a_1 e^{-t/\tau_1} + a_2 e^{-t/\tau_2} \quad (1)$$

Where α is the amplitude and τ is the lifetime. We processed the data with unfixed τ_1 and τ_2 lifetimes, which correspond to the free and bound forms of NAD(P)H, respectively.

The mean lifetime of each pixel is calculated by:

$$\tau_m = a_1\tau_1 + a_2\tau_2 \quad (2)$$

Where α1 + α2 = 1. A bin factor of 3 was used to attain a photon count >10 at the tail of the curve. The average mean lifetime within a microglial mask was recorded. The data of all microglia in a mouse are averaged and considered an experimental N of 1 (Control N7, LPS N6, 2DG N5, 2DG+LPS N4).

To measure NAD(P)H lifetime within single microglia, a mask was drawn around the cell using the DyLight 594 tomato lectin fluorescence image as a guide. Masks were drawn away from the edge of the cell to avoid any pixels contaminated by photons from the surrounding tissue.

5.2.7 Pro-inflammatory cytokine, HIF-1α, and NADPH measurement

Cytokines were measured *in situ* by collection of hippocampal slices after a two-hour treatment incubation and homogenization in lysis buffer on ice. Cytokines were measured using the Meso Scale Discovery (MSD) mouse pro-inflammatory 7-plex kit (K15012B-1). The plate was incubated with detection antibody cocktail overnight at 4 °C on a microplate shaker at maximum speed. The plate was then washed three times, and read immediately upon addition of read buffer with the MSD MESO QuickPlex SQ 120 plate reader. An experimental N of 5 was performed for all measurements.

HIF-1α levels were measured in primary microglia cultures using an enzyme-linked immunosorbent assay (ELISA). After treatment, cell lysates were collected for HIF-1α measurements. The LifeSpan BioSciences (LS-F4225) kit was used to measure HIF-1α, according to manufacturer's instructions. Briefly, 100 µl of sample or standard were added to a 96-well plate followed by one-hour incubation at 37 °C. After sequential incubations with detection reagents

and solutions, stop solution was added and the optical density of each well was measured at 450 nm. The concentration of HIF-1α in each sample was calculated according to the standard curve.

5.2.8 Data analysis and statistics

All values shown in the figures are the mean ± standard error of mean. For imaging experiments, data is reported as N indicating a biological replicate, composed of averaged data from multiple cells. Statistical significance was assessed using a Student's t-test, or One-way ANOVA, and differences between means were determined by Tukey's multiple comparison post-hoc analysis. (*: $p<0.05$; **: $p<0.01$; ***: $p<0.001$, ****: $p<0.0001$).

5.2.9 Drugs and reagents

LPS (E. coli 0111:B4, Sigma); DyLight 594 tomato lectin (DL-1177, Vector Laboratories); DMEM (Sigma); FBS (Gibco).

5.3 Results

5.3.1 LPS increases microglial glycolysis, which can be blocked by 2DG

In order to measure the metabolic profile of microglia within their complex, heterogeneous native environment, we employed NAD(P)H fluorescence lifetime imaging (FLIM). Nicotinamide adenine dinucleotide (NAD^+) is reduced to NADH during glycolysis and becomes autofluorescent in the blue spectrum with a short fluorescence lifetime (400 ps). When NADH binds to an enzyme, such as Complex I of the electron transport chain (ETC), its fluorescence lifetime increases to 2000 ps. Therefore, by measuring the mean fluorescence lifetime (τ_m), a ratio of the rates of glycolysis and oxidative phosphorylation (OXPHOS) can be calculated (Bird et al., 2005; Lakowicz et al.,

1992; Vergen et al., 2013). Due to an inability to separate NADH and NADPH autofluorescence by emission spectra or fluorescence lifetime (Blacker et al., 2014), we refer to both species here as NAD(P)H. In these experimental conditions, the majority of imaged signal is from NADH, as Physcion, a PPP inhibitor, had no appreciable change on imaging intensity (Figure 4.1a), while dramatically reducing NADPH levels (Figure 4.1b).

As NAD(P)H is ubiquitous in all metabolically active tissue, we were able to image metabolic rates of acute hippocampal slices from wild-type (WT) mice. In order to identify microglia specifically, slices were co-incubated with DyLight 594 tomato lectin during treatment incubations. Importantly, we could not use GFP-expressing transgenic mouse lines due to an artifact of GFP fluorescence in the blue NAD(P)H channel (Chapter 3). Therefore, this technique allowed us to observe single cell metabolism without removing these highly responsive cells from their physiological environment.

NAD(P)H mean lifetime was recorded in microglia from slices which had been incubated in control, lipopolysaccharide (LPS 10 µg/ml), 2-deoxy-D-glucose (5 mM 2DG + 5 mM glucose), or 2DG and LPS conditions for 2 hours at 32 °C. Relative to control lifetimes, we found a significant decrease in the mean lifetime of microglia exposed to LPS ($p<0.05$ between control τ_m 871±12.4 ps, N=7; and LPS τ_m 822±9.9 ps, N=6), suggesting an increased rate of glycolysis relative to OXPHOS (Figure 5.1a-d). When slices were incubated with 2DG, an increase in mean lifetime was observed ($p<0.0001$ between control and 2DG τ_m 972±12.7 ps, N=5), confirming a decrease in glycolytic capacity and forced reliance on mitochondrial metabolism (Figure 5.1b,e). When slices were stimulated with LPS while in the presence of 2DG, the LPS-induced glycolysis was

inhibited ($p<0.0001$ between LPS and 2DG LPS τ_m 941±10 ps, N=4; Figure 5.1b,f). Therefore, immune stimulation with LPS caused a metabolic shift in microglia to favor aerobic glycolysis, which could be prevented by the glycolytic inhibitor, 2DG.

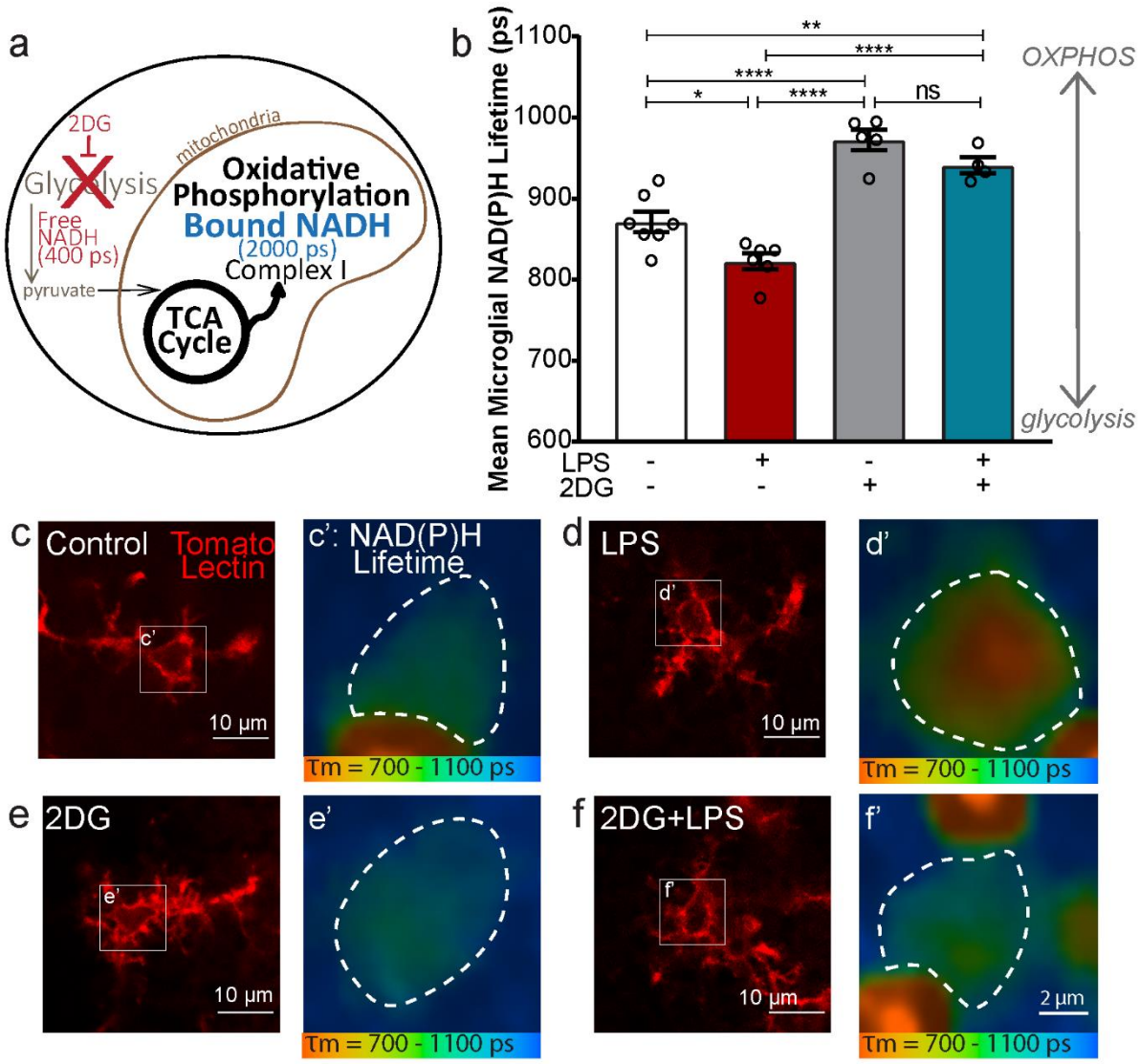

Figure 5.1 LPS increases microglial glycolysis.

a) Schematic of free and bound NADH in 2DG-treated conditions. b) Quantification of mean NAD(P)H lifetime from microglial masks showing increased glycolysis following LPS treatment, and decreased glycolysis in 2DG or

2DG+LPS conditions. Examples of tomato-lectin identified microglia and the corresponding mean NAD(P)H lifetime image in control (c), 10 µg/ml LPS (d), 5 mM 2DG (e), or 2DG+LPS (f). Error bars represent mean +/- SEM. *p<0.05, **p<0.01, ****p<0.0001 by One-way ANOVA and Tukey's multiple comparison.

5.3.2 Metabolic adaptation prior to morphological changes

In microglial cells, cell morphology is a strong indicator of activation status, in which thin ramified processes become retracted and amoeboid upon stimulation (Kettenmann et al., 2011; Stence et al., 2001). Previous papers have shown that a morphological change is observed in microglia beginning 40 minutes after incubation with 40 µg/ml LPS (Hines et al., 2013). To test if our 10 µg/ml LPS treatments were inducing a morphological change, we incubated slices from CX3CR1$^{+/EGFP}$ mice in control, LPS, 2DG, or LPS and 2DG conditions before fixing them by SNAPSHOT for detailed two-photon imaging (N=3; Figure 5.2a). Interestingly, after automatic morphological analysis by 3DMorph (York et al., 2018), there was no apparent difference in morphology assessed across various parameters, including cell territorial volume (Figure 5.2b), number of endpoints (Figure 5.2c), or average branch length (Figure 5.2d). Therefore, this lower dose incubation of LPS is sufficient to drive an alteration in microglial cellular metabolism without inducing an overt morphological transformation. This may suggest that metabolism is more acutely sensitive to immunological triggers or precedes large-scale cellular rearrangement.

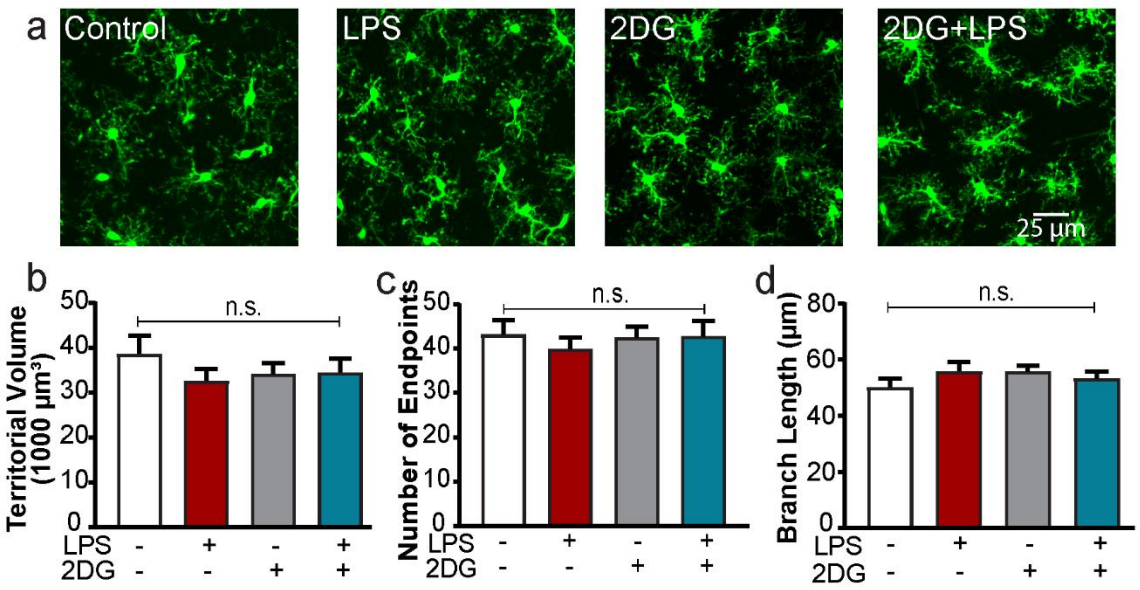

Figure 5.2 LPS increases microglial glycolysis prior to morphological changes.

a) EGFP-expressing microglia were imaged in all four conditions for morphological analysis. After a two-hour incubation, there was no significant difference in territorial volume (b), number of endpoints (c), or average branch length (d). Error bars represent mean +/- SEM. *p<0.05, **p<0.01, ****p<0.0001 by One-way ANOVA and Tukey's multiple comparison.

5.3.3 LPS stabilizes HIF-1α through glycolysis-mediated pathways

One downstream mechanism of immunometabolic adaptations is a 'broken' tricarboxylic acid (TCA) cycle (Cordes et al., 2016; Jha et al., 2015). The result is an alteration in the concentration of certain metabolites, such as α-ketoglutarate (α-KG) and succinate. The balance of these metabolites is critical in regulating the stabilization of hypoxia inducible factor 1 α (HIF-1α) (Tannahill et al., 2013), which is continually being produced, and targeted for degradation by prolyl hydroxylases (PHD) (Koivunen et al., 2007). Succinate inhibits PHD, whereas α-KG promotes it, therefore an increase in the succinate:α-KG ratio results in decreased PHD activity, and an accumulation of HIF-1α protein.

To test the level of HIF-1α, specifically in microglia, primary microglial cultures were grown and treated with LPS (100 ng/ml) ± 2DG for two hours. By ELISA, a small increase in HIF-1α was measured upon LPS stimulation ($p = 0.1464$ between control 0.13±0.009 pg/ml, $N = 5$; and LPS 0.16±0.008 pg/ml, $N=5$, which was blocked by co-application of 2DG ($p<0.05$ between LPS and 2DG LPS 0.1148±0.01 pg/ml, $N=5$; Figure 5.3a). These data suggest that a downstream effect of the immunometabolic adaptation and glycolysis increase is a stabilization of HIF-1α protein.

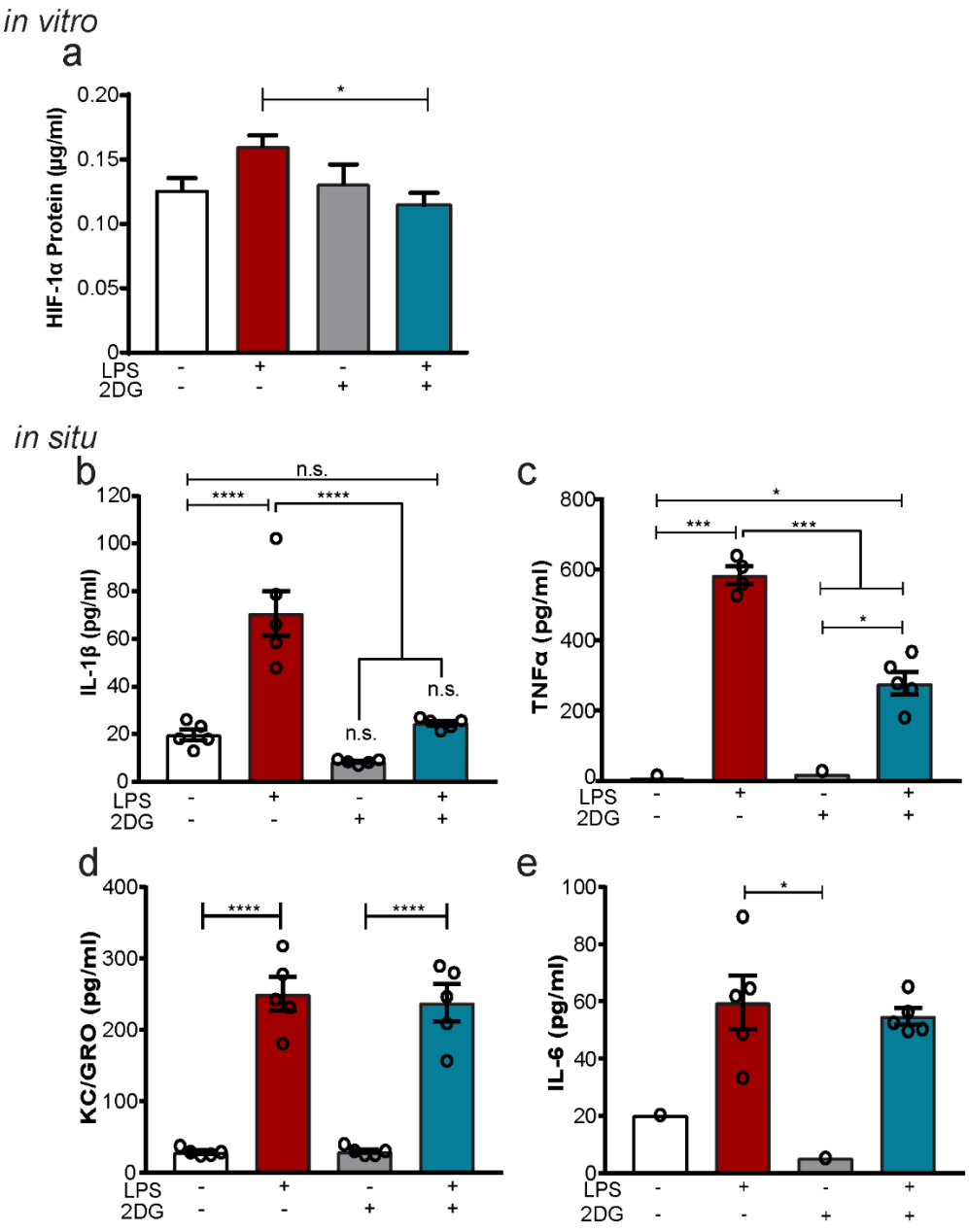

Figure 5.3 LPS stabilizes HIF-1α and increases pro-inflammatory production through glycolysis-mediated pathways.

In primary microglial cultures, HIF-1α protein shows a trend to stabilize with LPS and is inhibited by 2DG (a). In acute hippocampal slices, LPS increased production of both IL-1β (b) and TNFα (c), which were inhibited by co-incubation with 5 mM 2DG. Both KC/GRO (d) and IL-6 (e) were increased by LPS stimulation, but their regulation

was independent of glycolytic inhibition by 2DG. Error bars represent mean +/- SEM. *p<0.05, ***p<0.001, ****p<0.0001 by One-way ANOVA and Tukey's multiple comparison.

5.3.4 LPS triggers glycolysis-dependent pro-inflammatory cytokine production

Once accumulated in the cell, HIF-1α can translocate to the nucleus where it acts as a transcriptional activator of several genes, including the pro-inflammatory cytokine, interleukin-1 β (IL-1β) (Tannahill et al., 2013). To measure the effect of LPS and 2DG on cytokine production, a pro-inflammatory Meso Scale Discovery kit was used on WT acute hippocampal slices. This analysis confirmed that LPS increases IL-1β production, which is inhibited by 2DG (control 19.70±2.29 pg/ml, N=5; LPS 70.63±9.35 pg/ml, N=5; 2DG 8.44±0.45 pg/ml, N=5; 2DG LPS 25.54±1.01 pg/ml, N=5; Figure 5.3b). A similar effect was seen with TNFα, which is also increased by LPS and inhibited by 2DG co-application (control 7.55 pg/ml, N=5; LPS 584.80±25.38 pg/ml; N=5, 2DG 21.11 pg/ml, N=5; 2DG LPS 277.90±31.80 pg/ml, N=5; Figure 5.3c). Interestingly, it has been shown that TNFα is also a metabolically regulated cytokine, as it is post-transcriptionally inhibited by GAPDH (Millet et al., 2016). Upon an increased glycolytic demand (such as seen in LPS treatment), GAPDH is flooded with its substrate, glyceraldehyde 3-phosphate, and can no longer bind the inhibitory 3' UTR of TNFα mRNA, thus allowing translation to proceed (Millet et al., 2016; E. Nagy et al., 2000). The pro-inflammatory cytokines KC/GRO (control 28.52±2.37 pg/ml, N=5; LPS 250.30±23.87 pg/ml, N=5; 2DG 29.85±2.68 pg/ml, N=5; 2DG LPS 237.80±26.55 pg/ml, N=5; Figure 5.3d) and IL-6 (control 20.33 pg/ml, N=5; LPS 59.59±9.33 pg/ml, N=5; 2DG 5.27 pg/ml, N=5; 2DG LPS 54.78±2.83 pg/ml, N=5; Figure 5.3e) are also increased in LPS conditions, but insensitive to the addition of 2DG. Levels of IFNγ, IL-10, and IL-12p70 remained below detection limit in all conditions (data not shown). Therefore, we confirm

that LPS-increased glycolysis is important in causing an accumulation of HIF-1α protein and increased production of both IL-1β and TNFα.

5.3.5 LPS inhibits LTP in acute hippocampal slices

An important function of cytokines in the brain is the regulation of neuronal communication by modulating synaptic plasticity, such as long term potentiation (LTP) (York et al., 2017). To assess the impact of LPS-induced cytokines on LTP formation, electrophysiological recordings were performed in Schaffer collaterals of the CA1 region of rat acute hippocampal slices. Slices were recovered at least one hour in control aCSF before incubation with LPS (10 µg/mL unless otherwise indicated) for one hour before recording. The same concentration of LPS was also included in the recording solution throughout the experiment. Baseline synaptic responses were established by evoking field excitatory postsynaptic potentials (fEPSPs) every 30 seconds for at least 20 minutes. In this study, stable baselines were obtained from all slices that have been preincubated in LPS, indicating a lack of influence on basal synaptic transmission by LPS pre-incubation, in line with results reported in our previous work (J. Zhang et al., 2014).

To determine whether LPS can modulate synaptic plasticity, high frequency stimulation (HFS, 100 Hz stimulation for one second, three times, at 30 second intervals) was applied to induce LTP. HFS induced a stable LTP of fEPSP in control slices (fEPSP slope 138.4 ± 2.3% of baseline 40 min after HFS, N=6). In LPS-treated slices, HFS only succeeded in inducing a normal post-tetanic potentiation (PTP), but failed to induce any LTP (fEPSP slope 101.8±3.9% of baseline 40 min after HFS; $p<0.05$ compared to control, N=6; Figure B.2.1a,f). To investigate the effect of higher LPS treatments, 25 µg/mL LPS was also tested. At this concentration, PTP was reduced from

186.9±8.8% to 151.7±4.7% four minutes after HFS, a depression not observed in 10 µg/mL LPS treatment. However, 25 µg/mL LPS reduced LTP to the same level as 10 µg/mL LPS, resulting in an fEPSP 100.3±6.4% of baseline ($p>0.05$ compared to 10 µg/mL LPS and $p<0.001$ compared to control, N=6) 40 minutes after HFS. Therefore, the inhibiting effect of LPS on LTP was already saturated at 10 µg/mL, and we conclude that LPS does not alter basal synaptic transmission, but selectively inhibits expression of LTP in the hippocampal CA1 region. From here, 10 µg/ml LPS was used in all following experiments unless otherwise stated.

5.3.6 LPS inhibits LTP through IL-1β signalling

As previously shown, IL-1β is significantly increased *in situ* by LPS stimulation within the same timeframe as the observed LPS-induced inhibition of LTP. Furthermore, other groups have suggested a key role of IL-1β in LPS-impaired LTP, and memory deficits, after *in vivo* LPS stimulation (Cunningham & Sanderson, 2008; A. Kelly et al., 2003; Vereker et al., 2000). Therefore, the direct effect of IL-1β on LTP was tested in acute hippocampal slices.

When IL-1β (20 ng/mL) was bath-applied in the recording chamber for 15 minutes prior to HFS, LTP induction was reduced to 113.6±5.9% of baseline ($p<0.01$ compared to control, $p>0.05$ compared to LPS alone, N=6; Figure B.2.1b,f). This effect matches that observed with LPS treatment, suggesting that acute application of IL-1β can directly mimic the effect of LPS on LTP in hippocampal slices.

To determine the contribution of IL-1β to the impairment of LTP by LPS, the IL-1β pathway was blocked with interleukin-1 receptor antagonist (IL-1ra) (Loscher et al., 2003; Ross et al., 2003).

When IL-1ra (100 ng/ml) was included in the pre-incubation and bath perfusion, the LPS-inhibited LTP was rescued, resulting in a potentiation 154.6±6.9% of baseline (N=6, $p>0.05$ compared to IL-1ra alone, 156.0±4.9% of baseline, N=5; Figure B.2.1c,f). Taken together, our results suggest that LPS-induced blockage of LTP is mediated by IL-1β.

5.3.7 LPS-induced LTP impairment is mediated by the TLR4 pathway

LPS is well-known to trigger microglial stimulation by activating toll-like receptor 4 (TLR4), leading to downstream pro-inflammatory cytokine production (Kettenmann et al., 2011; Olson & Miller, 2004). To determine if LPS is directly activating microglia through TLR4 stimulation, fEPSP recordings were repeated in TLR4 knockout (TLR4 KO) mice. In acute hippocampal slices from these mice, HFS in control conditions induced an LTP 144.6±6.7% of baseline (N=6), similar to that seen in WT slices. In conditions of LPS stimulation in TLR4 KO slices, HFS was able to induce LTP, resulting in an LTP 149.9±5.7% of baseline ($p>0.05$ compared to TLR4 KO control, N=5; Figure B.2.1d,f). These results suggest an important role of TLR4 in mediating the LPS-induced inhibition of LTP in WT slices.

5.3.8 LPS inhibition of LTP is mediated by metabolically regulated IL-1β

As we have previously illustrated, LPS increases microglial glycolysis, which is necessary for HIF-1α stabilization and IL-1β production, and either LPS or IL-1β itself inhibit LTP formation in acute hippocampal slices. Therefore, the role of metabolism in mediating the LTP-inhibiting effects of LPS were tested. 2DG (5 mM) was applied on slices one hour before exposure to LPS and maintained throughout experiments. 2DG at this concentration, and in the presence of 5 mM glucose did not completely block metabolism in slices, resulting in a normal LTP 149.0±8.6% of

baseline (N=6). When applied together with LPS, 2DG prevented the inhibition of LTP, resulting in an LTP 156.1±9.2% of baseline ($p>0.05$ compared to 2-DG alone, N=5; Figure B.2.1e,f). This suggests that an LPS-stimulated increase in glycolysis stabilizes HIF-1α and increases IL-1β production, which inhibits induction of LTP. This effect can be rescued by directly blocking the IL-1R or by inhibiting excessive glycolysis.

5.4 Discussion

5.4.1 Microglial metabolism is important for proper response to immune stimulation by LPS

Using NAD(P)H-FLIM, we measured a significant increase in microglial glycolysis in acute hippocampal slices stimulated with LPS, as has been previously reported in macrophages (Jha et al., 2015; Tannahill et al., 2013). Increased glycolysis, and potentially pentose-phosphate pathway activity, may be needed to supply metabolites necessary for the increased biosynthetic demands of stimulated immune cells. These include nucleic acid and organelle production for proliferating colonies, and the expansion of ER and Golgi networks to facilitate increased protein and cytokine production (Everts et al., 2014; B. Kelly & O'Neill, 2015). However, glycolysis may also be necessary to supply a rapid ATP supply for increased energy demands, and to compensate for decreased oxidative phosphorylation. Upon immune stimulation, it is likely that some mitochondrial potential is used to drive a ROS burst (E. L. Mills et al., 2016), particularly following bacterial or innate immune stimuli, and altered enzymatic activity induces a 'broken' TCA cycle (Cordes et al., 2016; Jha et al., 2015). The multi-purpose of TCA metabolites to function as signalling molecules may allow them to act as indicators of mitochondrial activity (Murphy & Neill, 2018). Citrate, malate, and fumarate can accumulate inside the cytoplasm, which

may contribute to organelle expansion through *de novo* fatty acid synthesis, or altered epigenetic state, resulting in 'trained' innate immunity (Arts, Novakovic, et al., 2016; Dominguez-Andres et al., 2019; Williams & Neill, 2018). Succinate is also able to exit the mitochondrial matrix via the dicarboxylic acid transporter (Tannahill et al., 2013). Once in the cytoplasm, succinate can inhibit the activity of prolyl hydroxylases (PHDs). This decreases the ability of PHDs to label HIF-1α for degradation by E3 ubiquitin ligase (Koivunen et al., 2007), and allows the protein to accumulate. Upon binding its partner, HIF-1β, these proteins act as transcriptional regulators of hypoxia-responsive elements (HREs), which include glycolytic enzymes and pro-inflammatory cytokines, among others (Koivunen et al., 2007).

Indeed, measuring HIF-1α protein levels in primary microglial cultures, we found that LPS caused a small increase. This culture data implies that the LPS effect on microglia is cell autonomous, and does not rely on intercellular communication or signalling molecules. To confirm the effect of increased HIF-1α, IL-1β was measured in acute hippocampal slices. LPS-stimulation increases the production of IL-1β, as well as another pro-inflammatory cytokine, TNFα, while the levels of IFNγ, IL-10, and IL-12p70 remained below detection limit in all conditions.

As an increase in glycolysis and associated downstream signalling have been reported as necessary for induction of effector cell phenotypes (Berod et al., 2014; Kornberg et al., 2018; L. Z. Shi et al., 2011), we tested the effects of the glycolytic inhibitor, 2-deoxy-D-glucose, on microglial metabolism and cytokine response. By NAD(P)H-FLIM, 5 mM 2DG in the presence of 5 mM glucose reduced microglial glycolysis, as expected, but without causing overt cell death.

Interestingly, adding 2DG to LPS conditions resulted in a lower level of glycolysis than in LPS-only conditions, suggesting that 2DG is able to block the LPS-induced glycolytic response.

Confirming the importance of this glycolytic shift to LPS-induced immune response, 2DG also significantly decreased HIF-1α stabilization relative to LPS only conditions, and showed a similar decrease in IL-1β *in situ*. These data suggest the necessity of glycolysis to allow increased microglial production of IL-1β in response to LPS stimulation.

Interestingly, TNFα also showed an LPS-induced increase *in situ*, which was blocked by addition of 2DG. Therefore, this pro-inflammatory cytokine may also be regulated via metabolic pathways. Indeed, it has been reported that GAPDH, an important glycolytic enzyme, can act as a post-transcriptional repressor of TNFα and IFNγ. Upon increased glycolytic flux, GAPDH is pulled away from the 3'UTR of TNFα mRNA, thereby allowing its expression (Chang et al., 2013; Millet et al., 2016). Two additional cytokines, KC/GRO and IL-6, showed an LPS-dependent increase, which was not affected by addition of 2DG, perhaps suggesting that these cytokines are regulated in a glycolysis-independent manner.

In addition to production of cytokines, microglia also respond to immune insults by a dramatic morphological shift from a small cell body with fine, ramified processes, to a large amoeboid-like cell with retracted processes (Kettenmann et al., 2011; Stence et al., 2001). It has been shown previously that acute hippocampal slice incubation with LPS causes microglial process retraction beginning at 20 minutes (Hines et al., 2013). We did not observe any morphological changes in our conditions out to 2 hours of incubation. However, an important difference is that the previous

study used 40 µg/ml LPS, whereas our study used 10 µg/ml LPS. Therefore, at this lower concentration, a longer incubation may be necessary before overt morphological changes occur. Importantly, we were able to detect changes in metabolism and cytokine production in these conditions, suggesting that these are more sensitive measures of microglial activation than morphology, which may be a better indicator of more dramatic or chronic activation.

5.4.2 LPS inhibits LTP through an IL-1β dependent pathway

As we have confirmed that LPS increases microglial glycolysis, HIF-1α stabilization, and IL-1β production, we next investigated the impact of this pathway on neuronal function. Using fEPSP recordings in CA1 following stimulation of the Schaffer collateral pathway, we were able to measure the strength of synaptic connections in this region. HFS induces a strengthening of these connections, which results in a potentiated fEPSP response, known as long-term potentiation (LTP) (Miller & Mayford, 1999; Nicoll, 2017). Under control conditions, a strong LTP was induced, but was completely absent in the presence of LPS. This result was replicated by IL-1β application itself, and rescued by the IL-1 receptor antagonist, suggesting that the LPS-inhibition of LTP is acting through release of IL-1β.

Microglial cytokines have previously been shown to affect neuronal communication, and IL-1β is well-known to inhibit hippocampal LTP (Prieto & Cotman, 2018; Rogers et al., 2011; York et al., 2017). Importantly, hippocampal neurons express high levels of both IL-1 receptor type-1 and its accessory proteins (Farrar et al., 1987; Prieto et al., 2015; Smith et al., 2009), making them likely targets for released IL-1β. Although the downstream mechanisms of IL-1 receptor stimulation to

LTP impairment are yet to be elucidated, it is clear that the IL-1β receptor is necessary, as blocking this step rescues the inhibitory effects of LPS.

5.4.3 LPS stimulation inhibits LTP through TLR4-mediated IL-1β release

LPS stimulation is classically thought to act through binding and dimerization of TLR4 receptors at the immune cell surface, which then causes downstream effects through MyD88-dependent or MyD88-independent pathways (Esen & Kielian, 2006; Everts et al., 2014; Y. Lu et al., 2008). To confirm that the LTP inhibition by LPS is a result of TLR4 signalling, we show that the LPS effect is rescued in TLR4 KO mice. This is strong evidence of a necessary function of TLR4 in mediating this pathway.

The downstream pathways in microglia from TLR4 stimulation to increased glycolysis remain to be elucidated. In dendritic cells, Everts et al., showed that glycolytic increase occurred rapidly after LPS stimulation, and was therefore not likely due to transcriptional increase of glycolytic enzymes. Instead, they propose a mechanism whereby TLR4 stimulation activates Tank-binding kinase-1 (TBK1) and I kappa B kinase-epsilon (IKKε). These kinases phosphorylate and activate Akt, which promotes the interaction of the glycolysis enzyme, hexokinase-II (HK-II), with voltage-dependent anion channels on the outer mitochondrial matrix. This direct link to mitochondrial ATP may increase the activity of HK-II, and therefore glycolytic flux (Everts et al., 2014; John et al., 2011; S. Miyamoto et al., 2007). Inhibitors of TBK1 and IKKε decreased Akt phosphorylation and blunted the glycolytic response *in vitro*. Inhibition of this early glycolytic response *in vivo* with 2-NBDG impaired dendritic cell activation and their ability to prime T cells after LPS stimulation (Everts et al., 2014). As these are similar to our observed results of

glycolytic-dependent microglial activation, it is possible that TBK1, IKKε, and Akt mediate the glycolysis increase following TLR4 stimulation.

5.4.4 LPS-mediated LTP inhibition is rescued by blocking increased glycolysis

As further confirmation of the importance of LPS-stimulated glycolysis, there was a striking rescue of LTP induction by the co-application of the glycolytic inhibitor, 2DG, with LPS treatment. As previously established, this same treatment was able to block the microglial glycolytic increase, HIF-1α stabilization, and IL-1β production following LPS treatment.

In conclusion, we define a mechanism whereby LPS stimulation leads to LTP impairment through TLR4-mediated IL-1β production, in a manner dependent on increased microglial glycolysis and HIF-1α stabilization. These results underscore the importance of an appropriate immune and metabolic balance to regulate microglial function and promote proper neuronal communication. Disturbances to both metabolism and immune regulation are seen in a range of brain traumas, cognitive diseases, and in advanced aging, and we encourage clinical researchers in this field to consider metabolic intervention as part of a possible therapeutic approach.

Chapter 6: Conclusion

6.1 Summary of research findings

The principal objectives throughout the work presented in this dissertation were to elucidate the metabolic flexibility and immunometabolic reprogramming of microglia, while advancing the current tools available to the fields of microglial and metabolic research.

6.1.1 3DMorph microglial morphology analysis

Chapter 2, describes the development of 3DMorph, a useful tool for microglia research that allows the 3D analysis of microglial morphology. Numerous studies, including my own, have shown that microglial morphology is remarkably dynamic and sensitive to changes in the extracellular environment, presence of local damage, or neuronal health. Due to the rapid responsiveness of process outgrowth and retraction, changes in microglial morphology are often used to infer microglial protective or immunological activities (Davis et al., 1994; Karperien et al., 2013). However, these ramified cells have elaborate arbours extending in 3D throughout the neural tissue, and current morphological analyses have been limited to either image compression to 2D, or time-consuming and biased manual process tracing (Baron et al., 2014; Karperien et al., 2013; Kozlowski & Weimer, 2012; Takayama et al., 2016; Torres-Platas et al., 2014; Verdonk et al., 2016). Therefore, there was a need in the field for a method of analyzing microglial morphologies in 3D using an unbiased and reproducible approach. The work of Chapter 2 details 3DMorph's ability to measure the total territorial volume occupied by microglia in an image, as well as their density, and the branch length, endpoints, branch points, and cell and territorial volume of individual cells within a single image. Maintenance of 3D information ensures that cells and branches can be accurately separated, even if overlapped in the z dimension, whereas these would

be difficult or impossible to distinguish in an image compressed to 2D. Furthermore, this method does not rely on counterstaining, allowing it to be performed on *in vivo* images. It has also been validated to successfully quantify the morphology of other branching cell types, such as neurons. The inclusion of graphical user interfaces allows scalability for diverse imaging techniques, and the output of a parameters file permits the automatic batch processing of multiple images. The 3DMorph script has been made publicly available for free download and use. This tool is currently in use by microglial labs internationally, and has been published by our lab in the description of microglial filopodia (Bernier et al., 2019).

During the period of publishing this method, several other similar techniques were made available, highlighting the importance of this approach (Heindl et al., 2018; Kyriazis et al., 2018; Iñaki Paris et al., 2018). While all of these methods address the 3D or automatic quantification of microglia, each has advantages and limitations. It will further advance the field to have such diversity available so the most appropriate method can be employed for each of the individual and specific research questions asked by microglial researchers.

6.1.2 GFP contamination of NAD(P)H-FLIM

In continuation with the advancement of current techniques, Chapter 3 outlines the discovery that excitation of GFP or EGFP fluorophores with a 750 nm 2P laser causes emission of photons in the blue spectrum (460 nm) with a short fluorescence lifetime (500 ps). While the presence of blue fluorescence from GFP had previously been described (Chattoraj et al., 1996; G. Jung et al., 2005; Shimomura & Johnson, 1969), the impact of these photons on metabolic measurements of NAD(P)H-FLIM had not been investigated. As GFP is commonly used as a genetically-encoded

cell type specific marker, the combination of GFP expression and NAD(P)H-FLIM measurements is an attractive experimental design to investigate single-cell metabolism within heterogeneous tissues. The findings presented in Chapter 3 confirm the surprising finding that cellular EGFP expression obscures endogenous NAD(P)H fluorescence, resulting in a false measurement that can be incorrectly interpreted as a highly glycolytic cell. As metabolic imaging by NAD(P)H-FLIM gains popularity as a research tool, it is important that the field is aware of the contamination by GFP photons. Therefore, these results have been published in addition to the validation that alternative dyes are compatible with the NAD(P)H-FLIM technique. Verification that exogenously applied 594-DyLight tomato lectin identifies microglia without interfering with NAD(P)H-FLIM measurements has proven to be a powerful technique. This allows the metabolic measurement of single microglia while they are maintained in the relatively physiological state of acute brain slice preparations, or potentially during *in vivo* imaging of the intact brain.

Using both 3DMorph and NAD(P)H-FLIM of tomato lectin identified microglia, the metabolic flexibility of microglia in aglycemic conditions and the immunometabolic reprogramming of LPS-stimulated microglia were investigated.

6.1.3 Microglial metabolic flexibility

Nutrient availability necessary to meet the metabolic requirements of the brain are critical for neuronal health and function. Action potential firing requires the activity of the Na^+/K^+ ATPase to restore membrane potentials and the ionic gradients required for active transport of neurotransmitters (Harris et al., 2012). These processes in particular make neuronal activity extremely energy demanding. In addition to a high energy requirement, the nutrient environment

of the neural parenchyma is subject to an additional level of regulation by the blood brain barrier (BBB). Thus, the availability of nutrients is limited by transporter expression and dynamics. For instance, glucose is described as the obligate energy source for the brain, and is transported across the endothelium and astrocytic endfeet by GLUT1. Brain glucose concentrations fluctuate in a linear relationship to the concentration in the blood, but remain lower, typically at 1 mM in the brain, when blood glucose is 4.7 mM (R Gruetter et al., 1992). In addition to this limitation, it is hypothesized that the brain does not metabolize an appreciable level of fatty acids, as this pathway consumes high levels of oxygen, possibly leading to local hypoxic domains to which neurons are extremely sensitive (Schönfeld & Reiser, 2013). Furthermore, the only source of local energy storage in the brain is astrocytic glycogen. The brain thus represents an organ of extreme energy demand, but at the same time is subject to unique nutrient restrictions.

The importance of a continuous glucose supply to the brain is apparent in studies measuring synaptic transmission in aglycemic conditions. Neuronal activity decreases progressively over 30 minutes following glucose removal, which corresponds to a run down in cellular energy and depletion of astrocytic glycogen stores (Izumi et al., 1994; Ransom & Fern, 1997; Shetty et al., 2013; Waitt et al., 2017). While these results clearly demonstrate the sensitivity of neuronal activity to changes in nutrient availability, there are estimates that 50% of the brain's energy demand is used for non-synaptic activities (Engl & Attwell, 2015). While some of this energy may be used for cellular functions in neurons, the energetic requirements of glia remain largely unknown. In particular, there are currently no studies addressing the metabolic activities of microglia, which have highly motile processes both during baseline surveillance and in response

to damage sensing. Such dramatic and constant membrane and cytoskeletal turnover is likely to require a substantial energy supply.

In contrast to the vulnerability and death of neurons in the ischemic core following stroke, microglia have been observed to migrate into the area of damage (Alexander & Wolf-Dieter, 2011; Tanaka et al., 2003). Additionally, diabetes-associated hypoglycemia results in neuronal seizure activity, which has been correlated with neuronal death (Bree et al., 2019). However, the metabolic sensitivity of microglia to nutrient restriction is unknown.

The work presented in Chapter 4 describes the metabolic flexibility of microglia that allows these cells to metabolize glutamine in aglycemic conditions to maintain viability and function. Initial baseline measurements revealed the surprising finding that microglia have a higher rate of glycolysis than electron transport chain (ETC) relative to neuropil tissue. Interestingly, removal of glucose from the artificial cerebrospinal fluid (aCSF) resulted in a steady increase in the microglial NAD(P)H lifetime over 60 minutes, corresponding to a decrease of the glycolysis to ETC rate – a result that was not observed in the surrounding neuropil. Therefore, the electrons necessary to maintain ETC metabolism must be supplied by a continued tricarboxylic acid (TCA) cycle. Since carbon is lost from the TCA cycle as CO_2, in the absence of glucose, TCA metabolites must be supported by an alternative carbon source.

Glutamine was a likely candidate for support of microglial metabolism because it is maintained at high extracellular concentrations of around 385 μM in the brain (Kanamori & Ross, 2004), and can be metabolized by glutaminolysis into α-ketoglutarate (α-KG). Oxygen consumption rates of

primary microglia in control, glucose only, glutamine only, or deficient media suggested that microglia are autonomously capable of metabolizing glutamine. Confirming this finding *in situ,* microglial NAD(P)H lifetime did not increase after 60 minutes in aglycemic solution if either of the glutaminolysis inhibitors, EGCG or R162, were present. Instead, the mean lifetime remained at control levels or showed a small decrease reflecting a simultaneous decrease in both glycolysis and ETC rates.

This work is the first example directly measuring the metabolic flexibility of microglia to consume glutamine in the absence of glucose. A specific mutation causing upregulation of a microglial glutamine transporter, SNAT1, is a known genetic variant associated with Rett's disease, an autism spectrum disorder (Jin et al., 2015). To what extent microglia metabolize glutamine in the presence of glucose is unclear, although in our experimental paradigm, addition of R162 had no affect on NAD(P)H lifetime in control solutions. This will be an important and interesting area to investigate, as microglia may be contributing to the glutamate-glutamine cycle and glutamate homeostasis of the parenchyma, which can regulate neuronal firing rates. It also remains unknown whether the rate of glutaminolysis modulates microglial function.

6.1.4 Immunometabolic reprogramming of microglia

Immunometabolism, largely pioneered in the fields of cancer biology and the peripheral immune system, proposes that metabolic pathways act as signalling platforms in addition to producing energy. The elaborate network of enzymes and metabolites involved are ideal candidates for the integration of external signals, particularly nutrient availability, and corresponding alterations to cellular function. An overarching finding is that aerobic glycolysis, also known as Warburg

metabolism, is dominant in tumorigenic (Berridge et al., 2010; Boroughs & DeBerardinis, 2015) and pro-inflammatory cells (Buck et al., 2016; B. Kelly & O'Neill, 2015; Newton et al., 2016). This metabolic signature consists of high glycolytic rates, even in the presence of oxygen and with functional mitochondria. In contrast, cells with anti-inflammatory functions are associated with oxidative phosphorylation (OXPHOS). Incredibly, regulating specific metabolic pathways is sufficient to induce regulatory T cells during activation with cytokines which typically drive T helper cell differentiation (Klysz et al., 2015).

While aerobic glycolysis may be necessary for meeting the rapid ATP demand associated with immune cell activation, additional mechanisms of regulation continue to be discovered. Production of ribose 5-phosphate contributes to nucleotide biosynthesis to allow DNA replication and cell proliferation, while NADPH regulates cellular redox state. Increased glycolytic activity of GAPDH also decreases its binding to the mRNA of TNFα, thereby permitting translation (Chang et al., 2013; Millet et al., 2016). In addition, there is a preferential removal of key TCA metabolites from the mitochondria, leading to their accumulation in the cytoplasm. Increased cytoplasmic citrate is important for lipid production associated with organelle expansion and increased protein production (Everts et al., 2014; Hatzivassiliou et al., 2005), and fumarate regulates epigenetic modifications and innate immune training (Arts, Novakovic, et al., 2016). Finally, accumulation of succinate can drive mitochondrial ROS production (E. L. Mills et al., 2016), as well as stabilize HIF-1α to increase IL-1β production (Tannahill et al., 2013).

Although microglia are immune cells, they are not of hematopoietic origin, and are maintained in the nutrient-strict conditions of the brain. Therefore, it is unknown whether they are subject to

immunometabolic reprogramming to control cellular functions. As the work in Chapter 4 confirmed that microglia are metabolically flexible, the impact of metabolic activities on cellular function was further explored.

Several reports have suggested that lipopolysaccharide (LPS) stimulation induces glycolysis in microglia (Gimeno-Bayón et al., 2014; Voloboueva et al., 2013), however these studies rely on cultured cells, which are likely already perturbed with respect to both metabolism and state of immune activation. The aim of chapter 5 was to address the immunometabolic reprogramming of microglia in a physiological context. Using tomato lectin identification of microglia paired with FLIM of endogenous NAD(P)H, single cell metabolism was measured within acute hippocampal slices.

Application of 2-deoxy-D-glucose (2DG) to block glycolysis increased microglial mean NAD(P)H lifetime, confirming a decrease in glycolysis relative to ETC rates, as was seen in aglycemic conditions in Chapter 4. 2DG was chosen in this set of experiments, as it will preferentially be taken up by those cells with an increased glycolytic rate, which we predict will largely be microglia, based on their measurements of baseline metabolism. Therefore, 2DG is theorized to act in a more cell-specific manner than using aglycemic solutions, which will indiscriminately alter the metabolic rates of all cells in the tissue.

Although microglia are more glycolytic than the surrounding neuropil at baseline, a further decrease in NAD(P)H lifetime was observed upon application of LPS, suggesting an increase in glycolysis and/or decrease in ETC rates. Upon LPS stimulation in the presence of 2DG, microglial

metabolism more closely resembled control than LPS rates. Interestingly, these metabolic alterations occurred before any detectable modifications to microglial morphology, suggesting that metabolic pathways may be more sensitive and rapidly adjustable.

As downstream metabolic reprogramming to increased aerobic glycolysis has been shown to result in production of pro-inflammatory cytokines (Chang et al., 2013; Millet et al., 2016; Tannahill et al., 2013), these were measured from acute hippocampal slices with or without LPS stimulation and 2DG application. As expected, LPS significantly increased the cytokines IL-1β, TNFα, and KC/GRO, while a small but insignificant increase in IL-6 was also detected. Strikingly, both IL-1β and TNFα levels after LPS stimulation were significantly reduced with co-application of 5 mM 2DG to block the increase in glycolytic rate. Interestingly, the production of neither KC/GRO nor IL-6 were affected by 2DG. Both IL-1β and TNFα have proven links to metabolic regulation, through reducing GAPDH translational repression (Chang et al., 2013; Millet et al., 2016) or HIF-1α stabilization and transcriptional activation (Tannahill et al., 2013). Using primary microglial cultures, a small increase in HIF-1α protein was detected upon LPS stimulation, which was significantly reduced in the presence of 2DG.

Since microglial release of cytokines can impact synaptic transmission and neuronal activity, a collaboration with a post-doctoral fellow, Jingfei Zhang, revealed that the LPS-stimulated glycolytic increase and IL-1β production by microglia inhibited the formation of long-term potentiation. This effect could be rescued by 2DG, emphasizing the importance of microglial metabolic reprogramming to neuronal function. These findings point to interesting clinical

applications as many metabolic or mitochondrial disorders and immune activation, are associated with dysfunction and disease.

6.2 Overall significance

Metabolic perturbations to the brain and consequential immune activation lead to neuronal toxicity in cases including stroke, insulin-induced hypoglycemia, and diet-induced obesity or malnourishment. Additionally, mitochondrial dysfunction and microglial toxicity are associated with a variety of neurodegenerative diseases such as Parkinson's, Alzheimer's, and Huntington's diseases. Although immediate immune response may be important for protection, damage clearance, and prevention of secondary damage, the persistent immune activation and inflammation often seen in these cases can result in more neuronal harm than benefit. Appropriately timed immune resolution is equally important to brain health as is initial activation. Therefore, a better understanding of the immunometabolic reprogramming of microglia will facilitate the discovery of novel therapeutic avenues for disease prevention and treatment to promote neuronal health and recovery in both acute and chronic metabolic disruptions, as well as in neurodegenerative diseases.

6.2.1 Microglia in acute metabolic disruptions

Impaired neuronal health and alterations in microglial function are apparent in acute metabolic disruptions, such as stroke or insulin-induced hypoglycemia.

During stroke, brain vessel hemorrhage or occlusion by thrombosis results in a deprivation of oxygen and glucose supply to tissues downstream of the afflicted area. This immediately inhibits

tissue metabolism as both glycolysis and mitochondrial ATP production are blocked. Neurons are extremely sensitive to this disruption and there is an immediate neuronal death in the ischemic core, followed by additional neuronal toxicity and death around the lesion penumbra. While the neuronal death in the ischemic core is often irreversible, there is a migration of microglial cells into this area to perform protective and damage clearance functions (Alexander & Wolf-Dieter, 2011; Denes et al., 2007; Schilling et al., 2005; Tanaka et al., 2003). While microglia may be metabolically flexible and able to survive in these nutrient deprived conditions, the impact of such a metabolic shift on microglial activity is unknown. Although damage clearance is necessary to inhibit spread of secondary injury, there is an associated and prolonged microglial activation and upregulation of pro-inflammatory cytokines that can cause sustained neuronal toxicity long after the initial insult (Yenari et al., 2010).

An additional form of acute metabolic disruption is hypoglycemia, often triggered by high insulin levels in the treatment of diabetes. This exogenously-administered insulin does not fall naturally, and can lead to dangerously low blood glucose levels (Cryer et al., 2003). For the nutrient-sensitive neurons, this glucose depletion can induce seizure activity, which is correlated with neuronal death and may represent the cellular underpinnings of cognitive deficits in these individuals (Bree et al., 2019). Again, it is likely that microglia are viable in these conditions, although the massive metabolic reprogramming is likely to alter their immune function. Indeed, there is evidence of toxic cytokine and ROS release, as treatment with minocycline or apocynin decrease extent of microglial activation and neuronal damage (Won, Kim, et al., 2012; Won, Yoo, et al., 2012).

Therefore, the ability to regulate microglial activation and pro-inflammatory activities is a promising strategy to promote neuronal health and recovery at later time points after acute metabolic disruption. It is possible that metabolic reprogramming of microglia would result in a form of trained innate immunity, as seen in the epigenetic modifications of monocytes after β-glucan stimulation (Arts, Novakovic, et al., 2016; Cheng et al., 2014). This microglial immune training may increase cytokine release and neurotoxicity even after damage resolution and return of the tissue to nutrient homeostasis. The metabolic regulation of microglia in these circumstances remains largely unexplored, and is likely to uncover promising therapeutic interventions.

6.2.2 Microglia in chronic metabolic disruptions

In addition to acute metabolic disruptions, microglial functions are likely to be altered by dietary nutrient content on the order of months, years, or an entire lifespan. The world is currently experiencing a unique metabolic crisis with some regions severely affected by malnutrition at the same time as an obesity epidemic (James, 2009; Perez-Escamilla et al., 2018). Both of these extreme conditions can result in metabolic disorders that affect the whole body as well as causing cognitive dysfunction, particularly if present during the early developmental years. Early childhood malnourishment has been associated with learning disabilities, as well as a predisposition for developmental of neuropsychiatric disorders. (Akman et al., 2004; Hoeijmakers et al., 2015; Pérez-García et al., 2016). There have been reports of decreased levels of brain-derived neurotrophic factor (BDNF) resulting in decreased hippocampal neurogenesis (Pérez-García et al., 2016). Although not directly studied, changes in synaptic pruning during this critical period could impact both learning and memory, and have been associated with the development of psychiatric

disorders such as schizophrenia (Sellgren et al., 2019). In addition, long-term implications of early childhood malnutrition on neuronal health and microglial activity are unknown.

In contrast to malnutrition, childhood and adult obesity are growing concerns, especially in Westernized societies. In addition to the quantity of calories consumed, the composition is particularly high in fats, salt, and simple sugars. While these are well-known to affect vascular tension, heart health, and increase the risk of type-II diabetes (Ballal et al., 2010; D. et al., 2000; Hu et al., 2001), the impact on the brain is only beginning to be revealed. Chronic hypertension and diabetes are both risk factors for the development of Alzheimer's disease (AD) (Profenno et al., 2010), and diet-induced obesity has been associated with increased brain inflammation (Graham et al., 2016; Guillemot-Legris & Muccioli, 2017). Therefore, diet-induced microglial activation may cause a low-grade, chronic state of inflammation which is initially subclinical, but eventually progresses into a debilitating disease. Interestingly, a component notably high in the Western diet is high-fructose corn syrup (HFCS), and microglia are the sole expressers of GLUT5 in the brain, which is a fructose-specific transporter (Douard & Ferraris, 2008; Payne et al., 1997). The reason for this unique sensitivity of microglia to fructose is unknown and may provide interesting results with respect to the impact of HFCS on chronic neuroinflammation.

Finally, aging presents another chronic situation associated with metabolic alterations. Rather than a change in diet, aging is associated with decreased mitochondrial function, giving rise to the mitochondrial theory of aging (Kauppila et al., 2017; Ziegler et al., 2015). This states that impaired mitochondrial health results in mitochondrial DNA mutations, a decrease in OXPHOS, and concomitant increase in ROS production, all of which contribute to cellular damage. Interestingly,

another theory, termed ‘inflammaging’, suggests that there is a chronic and mild increase in inflammation throughout aging that can result in cellular senescence and disease (Chinta et al., 2015; Franceschi et al., 2017). While all metabolic tissues will be affected by decreased mitochondrial health, it is possible that the decreased OXPHOS capacity of microglia results in a shift towards a pro-inflammatory phenotype resulting in the observed brain inflammation.

Therefore, understanding how mild, chronic metabolic stressors from diet content and quantity impact microglial inflammation may help unravel cellular causes of cognitive impairment. Whether these related neurological effects can be rescued by introduction of a healthy diet remains an important direction of study. Further investigations are also necessary into the mitochondrial health of immune cells influencing aging-associated inflammation, and if preventative measures, such as healthy diet and exercise, contribute in a meaningful way to maintenance of metabolic health and immune quiescence.

6.2.3 Microglia and metabolism in neurodegenerative diseases

Microglial dysfunction or aberrant activation, and mitochondrial mutations are both associated with various neurodegenerative diseases, although the cause-effect relationship with cognitive decline and time course of disease progression remains to be clearly separated.

Alzheimer’s disease (AD) is identified by the presence of amyloid-β plaques and neurofibrillary tangles, with widespread and progressive neurodegeneration beginning in the medial temporal lobes. Traditionally, research on this disease has been focused on the neuronal component and preventing the creation of toxic amyloid with β-secretase 1 inhibitors. Much of this work is able

to prevent or delay signs of cognitive impairment in mouse models of AD, but are failing in clinical trials. Microglia have long been associated with amyloid plaques and often thought to be in a dystrophic state, adding to the toxicity of the brain while unable to phagocytose and clear the accumulated protein (Streit, 2004; Streit et al., 2004). This idea largely stemmed from the increased pro-inflammatory profile of AD brains, and the observation that microglia surround plaques, but show no signs of clearance. It is now suggested that these microglia surround plaques, much as they do a site of damage or vessel leakage, to contain the protein aggregates and prevent the spread of damage. Microglia may also be involved in the initial onset and progression of the disease, as 'senescent' phenotypes are present before tau pathology (Streit et al., 2009), and microglial training or tolerance can impact amyloid accumulation (Wendeln et al., 2018).

Also early in AD is an accumulation of structurally and functionally damaged mitochondria, which are more suited to ROS generation than ATP production (X. Wang et al., 2014). ROS accumulation and cytoplasmic damage are apparent in susceptible neuronal populations and are much higher than in healthy aging controls. ROS accumulation can cause mitochondrial DNA mutations, ETC inhibition, and further ROS production, resulting in damage to neuronal macromolecules (Hirai et al., 2001; M. T. Lin & Beal, 2006; X. Wang et al., 2014). The extent and timing of mitochondrial damage and ROS accumulation in microglia is unclear relative to the onset of neuronal mitochondrial involvement. It is feasible to speculate that early microglial metabolic reprogramming due to damaged mitochondria and ROS accumulation potentiate further neuronal toxicity.

Huntington's disease (HD), caused by an expansion of CAG repeats results in the mutant Huntington protein (mtHtt). This mutation triggers neurotoxicity of the striatum causing movement disorders, such as chorea, and also spreads throughout the cortex with impacts on cognitive functioning. Mitochondrial involvement in this disease is becoming increasingly evident, as altered mitochondrial dynamics and morphology are seen in the striatum early in HD (Costa & Scorrano, 2012). A decrease in mitochondrial fusion, or increased fission, may impair the mixing of organelle components for mitochondrial replenishment with healthy enzymes and segregation of damaged organelles for mitophagy. mtHtt may also impair nuclear transcription of mitochondrial proteins, decrease mitochondrial biogenesis, or alter organelle trafficking (Bossy-Wetzel et al., 2008; Guedes-Dias et al., 2016). Increasing mitochondrial biogenesis by stimulating the PGC-1α signalling pathway rescued motor deficits and striatal neuropathology in the R6/2 HD mouse model carrying a truncated huntingtin protein (Johri et al., 2011), as well as in the BACHD mouse model expressing full length human mtHtt (Chandra et al., 2016). In addition to inhibiting biogenesis, mtHtt may increase mitophagy through binding to valosin-containing protein (VCP) and causing its accumulation on mitochondria, tagging the organelle for destruction. Addition of an interference peptide to disrupt this interaction inhibits VCP's mitochondrial accumulation and rescues behavior and neuropathology (Guo et al., 2016). Further evidence of a metabolic link to HD pathology was recently described in a study which found that due to low glucose availability, astrocytes in the striatum are forced to metabolize fatty acids. The resulting accumulation in reactive oxygen species may contribute to neuronal toxicity primarily in the striatum, and may suggest a mechanism behind the region-specific degeneration early in disease (Polyzos et al., 2019).

Again, although mitochondrial function and dynamics in HD microglia are unknown, there is evidence that microglia contribute to disease. Pro-inflammatory cytokines can be detected in the CSF and plasma of humans ~15 years before HD symptom onset, suggesting a microglial role early in this disease. Interestingly, expression of mtHtt exclusively in microglia causes increased pro-inflammatory gene expression, implying that microglial activation is not solely a result of neuronal damage or death (Crotti & Glass, 2015). It would be interesting to test the metabolic signature of microglia and neurons throughout disease progression, and determine if mitochondrial impairments in microglia result in the initiation of a pro-inflammatory cascade.

Finally, the neurodegenerative disease most clearly linked with mitochondrial abnormalities is Parkinson's disease (PD). Impaired mitochondrial quality control is associated with familial, sporadic, and environmental forms of the disease. PINK1 (PTEN-induced kinase 1) and Parkin (E3 ubiquitin ligase) are the primary proteins identified in familial PD linking neurodegeneration to mitochondrial dysfunction. PINK1 targets to the mitochondrial membrane, where in healthy mitochondria, it is cleaved and its N-terminal is degraded. However, in dysfunctional mitochondria, PINK1 is not cleaved and accumulates on the mitochondrial membrane. There, it recruits Parkin, which ubiquitinates the mitochondrial membrane for selective mitophagy. Due to PINK1 and Parkin mutations observed in PD, there is a decrease in removal of damaged mitochondria, and an increase in mitochondrial damage, likely functioning in a positive feedback loop (Pickrell & Youle, 2015). While the affects of PINK1 and Parkin proteins are primarily studied in neurons, it is also possible that microglia express these proteins and will be impacted by mutations and dystrophic mitochondrial accumulation (Y. Zhang et al., 2014). Rotenone, paraquat, and MPP+ (the metabolized form of MPTP) are all chemical inducers of PD, now widely used as

animal models of the disease, and all involve mitochondrial disruption, including complex I inhibition, superoxide formation, or impaired trafficking.

As in AD and HD, there is also a strong link between neurodegeneration and microglial pro-inflammatory profiles. Mitochondrial inhibition in microglial cell cultures using rotenone and tebufenpyrad enhanced the LPS-stimulated NLRP3 inflammasome and IL-1β production. Rotenone-treated cells also showed lysosomal damage, energy deficiencies, and increased mitochondrial ROS production. Interestingly, conditioned media from microglia treated with mitochondrial inhibitors and LPS was toxic to cultures of dopaminergic neurons (Sarkar et al., 2017). Additionally, PINK1 and Parkin have been identified as inhibitors of immune-stimulated inflammation through blockade of mitochondrial antigen presentation. Loss of PINK1 and Parkin activity, as in PD, may thus result in a heightened inflammatory response (Matheoud et al., 2016). Finally, an additional mutation commonly associated with PD is in Leucine-rich repeat kinase 2 (LRRK2), causing hyperactivation of its kinase activity. LRRK2 is seen in both familial and idiopathic PD, is involved in mitochondrial morphology and autophagy, and is highly expressed in immune cells (Alessi & Sammler, 2018). In microglia, mutated LRRK2 induces mitochondrial fission, process retraction, and production of the activation markers CD68 and TNFα (Ho et al., 2018). Therefore, a role for both mitochondria and microglia are clearly associated with the appearance of PD. Further investigations into the early involvement of microglial mitochondria and associated inflammatory profiles will be interesting, and perhaps a potential target to reduce further neurotoxicity and degeneration.

Taken together, the work presented in this dissertation is widely applicable to neuronal health in cases of acute or chronic metabolic disruptions, as well as in many neurodegenerative diseases. Further investigations will be necessary to conclusively define the cause-effect relationship as well as the timing of microglial and neuronal involvement. Metabolic alterations associated with microglial reprogramming and inflammatory profiles may be an attractive therapeutic intervention. Possibly more exciting is the possibility that regulating mitochondrial health, metabolism, and immune activation might be a powerful preventative method to combat neurodegeneration. Exercise, calorie restriction, and healthy diets have long been recognized as protective lifestyles for enhanced cognitive functioning and lifespan elongation. Importantly, while these present druggable targets, they are also readily accessible through safe lifestyle modifications with little or no negative side effects.

6.3 Future Directions

6.3.1 Mechanistic investigation of microglial metabolic reprogramming

While the data presented in this dissertation clearly support microglial metabolic flexibility and reprogramming to regulate immune activation, the mechanistic underpinnings involved remain to be fully defined. A first important question is to measure the membrane expression of glutamine and glutamate receptors and transporters on microglia at baseline, and if these levels are dynamically regulated upon metabolic or immune challenge. Based on mRNA levels, microglia are expected to have only low expression of the glutamate transporters, GLAST (EAAT1) and Glt1 (EAAT2) (Y. Zhang et al., 2014), although these may be upregulated with immune activation (Chrétien et al., 2002; López-Redondo et al., 2000; Persson et al., 2005). Whether aglycemic

conditions would also trigger an upregulation of glutamate transporters in microglia is unknown. These findings would have important implications both for microglial metabolism of glutamate directly in these conditions, as well as for describing the neuroprotective role of microglia in clearing excess glutamate following stroke or hypoglycemia-induced seizure activity. More supporting evidence exists for microglial glutamine transporters, SLC1A5 (ASCT2) (Scalise et al., 2018), and SLC38A1 (SNAT1) (Kalsbeek et al., 2016; Y. Zhang et al., 2014) both in transcriptional studies and in association with Rett's syndrome (Jin et al., 2015). Investigating the dynamic expression and role of these glutamine transporters in supporting microglial metabolism under hypoglycemic conditions remains to be investigated.

The signalling pathway linking immune activation to microglial metabolic reprogramming also remains to be further defined. In dendritic cells, there is a proposed mechanism where LPS stimulation of TLR4 causes activation of Tank-binding kinase-1 (TBK1) and I kappa B kinase-epsilon (IKKε), which phosphorylate Akt. This increase in Akt activity promotes hexokinase-II interaction with mitochondrial voltage-dependent anion channels, directly linking it to ATP supply, which allows a higher activity rate and glycolytic flux (Everts et al., 2014; John et al., 2011; S. Miyamoto et al., 2007). The presence of this pathway and its role in microglial immunometabolism is unknown. As the results presented in Chapter 5 link LPS stimulation of TLR4 to glycolytic increase, the involvement of TBK1, IKKε, and Akt would be interesting to study.

Finally, while the work presented here, and in much of the literature is focused on the classical immune activation by LPS, the role of other immune stimuli may be interesting and more

physiologically relevant. While LPS can cross the BBB during peripheral immune activation and BBB breakdown, it should normally be excluded from accessing the parenchyma (Banks & Robinson, 2010). The impact of viral infection, such as herpes simplex virus, or cell debris as would be present following stroke or traumatic brain injury, may be more relevant stimuli for microglia, and it would be interesting to see similarities or differences in the ability of these cues to trigger metabolic reprogramming and immune activation. The type of cue presented will likely have large affects on the microglial activation profile, as brain invasion of bacteria or virus will call for a pro-inflammatory attack response, whereas damage associated patterns will likely require anti-inflammatory and protective activities.

6.3.2 A role for astrocytes in metabolic regulation

While microglia are the key immune cells of the brain, astrocytes are another subtype of glial cell that have important roles in metabolic regulation. Astrocytes are estimated to cover 90% of the brain's capillaries, and both they and endothelial cells express the glucose transporter, GLUT1 to transport blood glucose into the brain (Duelli & Kuschinsky, 2001; Yu & Ding, 1998). Astrocytes may directly shuttle glucose to the parenchyma, or process it to glycogen, which is one of the only local energy reserves for brain metabolism (Bélanger et al., 2011; Brown & Ransom, 2007). Astrocytic regulation of metabolism is most well-studied in the glutamate-glutamine cycle, where neuronally released glutamate is rapidly sequestered by astrocytes, which process it to glutamine for transport back to neurons, where it again becomes glutamate for continued neurotransmission (Schousboe et al., 2014; Tani et al., 2014). The astrocyte-neuron lactate shuttle is another astrocytic means of metabolic regulation, although its role in supporting neuronal activity during periods of intense activation remain hotly debated (Diaz-Garcia et al., 2017; Magistretti & Allaman, 2018).

Astrocytes are also the main expressers of carnitine palmitoyltransferase 1a (Cpt1a) in the brain, making them capable of fatty acid oxidation (Jernberg et al., 2017; Y. Zhang et al., 2014). Furthermore, astrocytes can produce the ketone bodies, acetoacetate and β-hydroxybutyrate (Cullingford et al., 2002; Takahashi et al., 2014), which not only maintain neuronal viability during metabolic challenges (Chowdhury et al., 2014; Prins, 2008), but may also regulate neuronal activity. Interestingly, microglia can import and metabolize both lactate and ketone bodies (Ghosh et al., 2017; Y. Zhang et al., 2014), therefore astrocytes may be regulating microglial metabolism as well as neuronal. The type of metabolite released by astrocytes in times of rest or intense neuronal activation, as well as the controlled microdomain release sites may have important consequences in the activity of specific cell types. In the acute hippocampal slice data presented in Chapter 4 and 5, it is important to remember that astrocytes are also present and will be affected by our solution of pharmacological manipulations, such as aglycemia or glutaminolysis inhibition. The involvement of astrocytes in regulating glutamine, lactate, and ketone bodies as means of metabolic communication with both neurons and microglia will be a promising area of future study.

6.3.3 Clinical relevance

This work demonstrates microglial metabolic flexibility and immunometabolic regulation at the cellular level. While interesting and important in their own right, these findings support the further investigation into the clinical relevance and therapeutic approaches for treatment of human conditions. As discussed, these include a wide range of neurodegenerative diseases, including AD, HD, and PD, where both microglial activation and metabolic function appear dysregulated early

in disease. Microglial metabolism following stroke, hypoglycemic episodes, and traumatic brain injury may also result in effective treatments for enhanced neuroprotection and cognitive recovery. Perhaps most exciting, is the potential preventative or reversal abilities of exercise and diet regulation to control metabolism and therefore inflammation. This will be particularly important in individuals affected by malnourishment, or a diet enriched in fats and sugars causing diabetes and obesity, and may also suggest lifestyle changes to promote healthy aging. The impact of these chronic changes to metabolic milieus in regulating immune activity, and particularly brain health and function, are an exciting and promising area of future investigation.

References

Adeva-Andany, M. M., López-Maside, L., Donapetry-García, C., Fernández-Fernández, C., & Sixto-Leal, C. (2017). Enzymes involved in branched-chain amino acid metabolism in humans. *Amino Acids*, *49*(6), 1005–1028. https://doi.org/10.1007/s00726-017-2412-7

Aizenman, C. D., & Pratt, K. G. (2008). There's More Than One Way to Scale a Synapse. *Neuron*, *58*(5), 651–653. https://doi.org/10.1016/j.neuron.2008.05.017

Ajami, B., Bennett, J. L., Krieger, C., Tetzlaff, W., & Rossi, F. M. V. (2007). Local self-renewal can sustain CNS microglia maintenance and function throughout adult life. *Nature Neuroscience*, *10*(12), 1538–1543. https://doi.org/10.1038/nn2014

Akman, C., Zhao, Q., Liu, X., & Holmes, G. L. (2004). Effect of food deprivation during early development on cognition and neurogenesis in the rat. *Epilepsy & Behavior*, *5*(4), 446–454. https://doi.org/https://doi.org/10.1016/j.yebeh.2004.03.008

Albensi, B. C., & Janigro, D. (2009). Traumatic brain injury and its effects on synaptic plasticity. *Brain Injury*, *9052*. https://doi.org/10.1080/0269905031000107142

Alessi, D. R., & Sammler, E. (2018). LRRK2 kinase in Parkinson's disease. *Science*, *360*(6384), 36 LP – 37. https://doi.org/10.1126/science.aar5683

Alexander, T., & Wolf-Dieter, H. (2011). Imaging of Microglia Activation in Stroke. *Stroke*, *42*(2), 507–512. https://doi.org/10.1161/STROKEAHA.110.598821

Alfonso-García, A., Smith, T. D., Datta, R., Luu, T. U., Gratton, E., Potma, E. O., & Liu, W. F. (2016). Label-free identification of macrophage phenotype by fluorescence lifetime imaging microscopy. *Journal of Biomedical Optics*, *21*(4), 046005. https://doi.org/10.1117/1.JBO.21.4.046005

Allison, D. J., & Ditor, D. S. (2015). Immune dysfunction and chronic inflammation following

spinal cord injury. *Spinal Cord*, *53*(1), 14–18. https://doi.org/10.1038/sc.2014.184

Angelin, A., Gil-de-Gomez, L., Dahiya, S., Jiao, J., Guo, L., Levine, M. H., … Beier, U. H. (2016). Foxp3 Reprograms T Cell Metabolism to Function in Low-Glucose, High-Lactate Environments. *Cell Metabolism*, 1282–1293. https://doi.org/10.1016/j.cmet.2016.12.018

Antoniewicz, M. R. (2015). Methods and advances in metabolic flux analysis: a mini-review. *Journal of Industrial Microbiology & Biotechnology*, *42*(3), 317–325. https://doi.org/10.1007/s10295-015-1585-x

Antonucci, F., Turola, E., Riganti, L., Caleo, M., Gabrielli, M., Perrotta, C., … Verderio, C. (2012). Microvesicles released from microglia stimulate synaptic activity via enhanced sphingolipid metabolism. *The EMBO Journal*, *31*(5), 1231–1240. https://doi.org/10.1038/emboj.2011.489

Arts, R. J. W., Carvalho, A., La Rocca, C., Palma, C., Rodrigues, F., Silvestre, R., … Netea, M. G. (2016). Immunometabolic Pathways in BCG-Induced Trained Immunity. *Cell Reports*, *17*(10), 2562–2571. https://doi.org/10.1016/j.celrep.2016.11.011

Arts, R. J. W., Novakovic, B., ter Horst, R., Carvalho, A., Bekkering, S., Lachmandas, E., … Netea, M. G. (2016). Glutaminolysis and Fumarate Accumulation Integrate Immunometabolic and Epigenetic Programs in Trained Immunity. *Cell Metabolism*, 807–819. https://doi.org/10.1016/j.cmet.2016.10.008

Askew, K., Li, K., Olmos-Alonso, A., Garcia-Moreno, F., Liang, Y., Richardson, P., … Gomez-Nicola, D. (2017). Coupled Proliferation and Apoptosis Maintain the Rapid Turnover of Microglia in the Adult Brain. *Cell Reports*, *18*(2), 391–405. https://doi.org/10.1016/j.celrep.2016.12.041

Ballal, K., Wilson, C. R., Harmancey, R., & Taegtmeyer, H. (2010). Obesogenic high fat western diet induces oxidative stress and apoptosis in rat heart. *Molecular and Cellular Biochemistry*,

344(1), 221–230. https://doi.org/10.1007/s11010-010-0546-y

Banks, W. A., & Robinson, S. M. (2010). Minimal penetration of lipopolysaccharide across the murine blood–brain barrier. *Brain, Behavior, and Immunity*, *24*(1), 102–109. https://doi.org/https://doi.org/10.1016/j.bbi.2009.09.001

Baron, R., Babcock, A. A., Nemirovsky, A., Finsen, B., & Monsonego, A. (2014). Accelerated microglial pathology is associated with Abeta plaques in mouse models of Alzheimer's disease. *Aging Cell*, *13*(4), 584–595. https://doi.org/10.1111/acel.12210

Beattie, E. C., Stellwagen, D., Morishita, W., Bresnahan, J. C., Ha, B. K., Von Zastrow, M., … Malenka, R. C. (2002). Control of Synaptic Strength by Glial TNFalpha. *Science*, *295*(5563), 2282–2285. https://doi.org/10.1126/science.1067859

Béchade, C., Cantaut-Belarif, Y., & Bessis, A. (2013). Microglial control of neuronal activity. *Frontiers in Cellular Neuroscience*, *7*(March), 1–7. https://doi.org/10.3389/fncel.2013.00032

Befroy, D. E., & Shulman, G. I. (2011). Magnetic resonance spectroscopy studies of human metabolism. *Diabetes*, *60*(5), 1361–1369. https://doi.org/10.2337/db09-0916

Bélanger, M., Allaman, I., & Magistretti, P. J. (2011). Brain energy metabolism: Focus on Astrocyte-neuron metabolic cooperation. *Cell Metabolism*, *14*(6), 724–738. https://doi.org/10.1016/j.cmet.2011.08.016

Bellinger, F. P., Madamba, S., & Siggins, G. R. (1993). Interleukin 1β inhibits synaptic strength and long-term potentiation in the rat CA1 hippocampus. *Brain Research*, *628*(1), 227–234. https://doi.org/https://doi.org/10.1016/0006-8993(93)90959-Q

Berg, J., Hung, Y. P., & Yellen, G. (2009). A genetically encoded fluorescent reporter of ATP:ADP ratio. *Nature Methods*, *6*(2), 161–166. https://doi.org/10.1038/NMETH.1288

Bernier, L.-P., Bohlen, C. J., York, E. M., Choi, H. B., Kamyabi, A., Dissing-Olesen, L., …

MacVicar, B. A. (2019). Nanoscale Surveillance of the Brain by Microglia via cAMP-Regulated Filopodia. *Cell Reports*, *27*(10), 2895–2908. https://doi.org/10.1016/j.celrep.2019.05.010

Berod, L., Friedrich, C., Nandan, A., Freitag, J., Hagemann, S., Harmrolfs, K., … Sparwasser, T. (2014). De novo fatty acid synthesis controls the fate between regulatory T and T helper 17 cells. *Nature Medicine*, *20*(11), 1327–1333. https://doi.org/10.1038/nm.3704

Berridge, M. V, Herst, P. M., & Tan, A. S. (2010). Metabolic flexibility and cell hierarchy in metastatic cancer. *Mitochondrion*, *10*(6), 584–588. https://doi.org/https://doi.org/10.1016/j.mito.2010.08.002

Berti, V., Mosconi, L., & Pupi, A. (2014). Brain: normal variations and benign findings in fluorodeoxyglucose-PET/computed tomography imaging. *PET Clinics*, *9*(2), 129–140. https://doi.org/10.1016/j.cpet.2013.10.006

Betts, M. J., O'Neill, M. J., & Duty, S. (2012). Allosteric modulation of the group III mGlu4 receptor provides functional neuroprotection in the 6-hydroxydopamine rat model of Parkinson's disease. *British Journal of Pharmacology*, *166*(8), 2317–2330. https://doi.org/10.1111/j.1476-5381.2012.01943.x

Bianco, F., Pravettoni, E., Colombo, A., Schenk, U., Moller, T., Matteoli, M., & Verderio, C. (2005). Astrocyte-Derived ATP Induces Vesicle Shedding and IL-1 Release from Microglia. *The Journal of Immunology*, *174*(11), 7268–7277. https://doi.org/10.4049/jimmunol.174.11.7268

Bilan, D. S., Matlashov, M. E., Gorokhovatsky, A. Y., Schultz, C., Enikolopov, G., & Belousov, V. V. (2014). Genetically encoded fluorescent indicator for imaging NAD+/NADH ratio changes in different cellular compartments. *Biochimica et Biophysica Acta - General*

Subjects, *1840*(3), 951–957. https://doi.org/10.1016/j.bbagen.2013.11.018

Bird, D. K., Yan, L., Vrotsos, K. M., Eliceiri, K. W., Vaughan, E. M., Keely, P. J., … Ramanujam, N. (2005). Metabolic mapping of MCF10A human breast cells via multiphoton fluorescence lifetime imaging of the coenzyme NADH. *Cancer Research*, *65*(19), 8766–8773. https://doi.org/10.1158/0008-5472.CAN-04-3922

Blacker, T. S., Mann, Z. F., Gale, J. E., Ziegler, M., Bain, A. J., Szabadkai, G., & Duchen, M. R. (2014). Separating NADH and NADPH fluorescence in live cells and tissues using FLIM. *Nature Communications*, *5*(May), 3936. https://doi.org/10.1038/ncomms4936

Blagih, J., Coulombe, F., Vincent, E. E., Dupuy, F., Galicia-Vázquez, G., Yurchenko, E., … Jones, R. G. (2015). The Energy Sensor AMPK Regulates T Cell Metabolic Adaptation and Effector Responses In Vivo. *Immunity*, *42*(1), 41–54. https://doi.org/10.1016/j.immuni.2014.12.030

Blank, T., & Prinz, M. (2013). Microglia as modulators of cognition and neuropsychiatric disorders. *Glia*, *61*(1), 62–70. https://doi.org/10.1002/glia.22372

Bolaños, J. P., & Almeida, A. (2010). The pentose-phosphate pathway in neuronal survival against nitrosative stress. *IUBMB Life*, *62*(1), 14–18. https://doi.org/10.1002/iub.280

Boroughs, L. K., & DeBerardinis, R. J. (2015). Metabolic pathways promoting cancer cell survival and growth. *Nature Cell Biology*, *17*, 351. Retrieved from https://doi.org/10.1038/ncb3124

Boscia, F., Esposito, C. L., Casamassa, A., De Franciscis, V., Annunziato, L., & Cerchia, L. (2013). The isolectin IB4 binds RET receptor tyrosine kinase in microglia. *Journal of Neurochemistry*, *126*(4), 428–436. https://doi.org/10.1111/jnc.12209

Bossy-Wetzel, E., Petrilli, A., & Knott, A. B. (2008). Mutant huntingtin and mitochondrial dysfunction. *Trends in Neurosciences*, *31*(12), 609–616. https://doi.org/10.1016/j.tins.2008.09.004

Bree, A. J., Puente, E. C., Daphna-iken, D., & Fisher, S. J. (2019). Diabetes increases brain damage caused by severe hypoglycemia. *Am J Physiol Endocrinol Metab*, *297*, 194–201. https://doi.org/10.1152/ajpendo.91041.2008.

Brown, A. M., & Ransom, B. R. (2007). Astrocyte Glycogen and Brain Energy Metabolism. *Glia*, *1271*(June), 1263–1271. https://doi.org/10.1002/glia

Bruttger, J., Karram, K., Wörtge, S., Regen, T., Marini, F., Hoppmann, N., … Waisman, A. (2015). Genetic Cell Ablation Reveals Clusters of Local Self-Renewing Microglia in the Mammalian Central Nervous System. *Immunity*, *43*(1), 92–106. https://doi.org/10.1016/j.immuni.2015.06.012

Buck, M. D., O'Sullivan, D., Geltink, R. I. K., Curtis, J. D., Chang, C.-H., Sanin, D. E., … Pearce, E. L. (2016). Mitochondrial Dynamics Controls T Cell Fate Through Metabolic Programming. *Cell*, *166*(1), 63–76. https://doi.org/10.1016/j.cell.2016.05.035.Mitochondrial

Buck, M. D., O'Sullivan, D., & Pearce, E. L. (2015). T cell metabolism drives immunity. *Journal of Experimental Medicine*, *212*(9), 1345–1360. https://doi.org/10.1084/jem.20151159

Buckley, C. D., Gilroy, D. W., & Serhan, C. N. (2014). Proresolving Lipid Mediators and Mechanisms in the Resolution of Acute Inflammation. *Immunity*, *40*(3), 315–327. https://doi.org/10.1016/j.immuni.2014.02.009

Burke, S. N., & Barnes, C. A. (2006). Neural plasticity in the ageing brain. *Nature Reviews Neuroscience*, *7*(January), 30–40. https://doi.org/10.1038/nrn1809

Butovsky, O., Jedrychowski, M. P., Moore, C. S., Cialic, R., Lanser, A. J., Gabriely, G., … Weiner, H. L. (2014). Identification of a unique TGF-beta-dependent molecular and functional signature in microglia. *Nat Neurosci*, *17*(1), 131–143. https://doi.org/10.1038/nn.3599nn.3599 [pii]

Büttner, P., Galli, R., Husser, D., & Bollmann, A. (2018). Label-free imaging of myocardial remodeling in atrial fibrillation using nonlinear optical microscopy: A feasibility study. *Journal of Atrial Fibrillation*, *10*(5), 3–7.

Byrnes, K. R., Stoica, B., Loane, D. J., Riccio, A., Davis, M. I., & Faden, A. I. (2009). Metabotropic glutamate receptor 5 activation inhibits microglial associated inflammation and neurotoxicity. *Glia*, *57*(5), 550–560. https://doi.org/10.1002/glia.20783

Cairns, R. A., Harris, I. S., & Mak, T. W. (2011). Regulation of cancer cell metabolism. *Nature Reviews Cancer*, *11*(2), 85–95. https://doi.org/10.1038/nrc2981

Cardona, A. E., Pioro, E. P., Sasse, M. E., Kostenko, V., Cardona, S. M., Dijkstra, I. M., … Ransohoff, R. M. (2006). *Control of microglial neurotoxicity by the fractalkine receptor*. *9*(7), 917–924. https://doi.org/10.1038/nn1715

Carlessi, R., Chen, Y., Rowlands, J., Cruzat, V. F., Keane, K. N., Egan, L., … Newsholme, P. (2017). GLP-1 receptor signalling promotes β-cell glucose metabolism via mTOR-dependent HIF-1α activation. *Scientific Reports*, *7*(1), 2661. https://doi.org/10.1038/s41598-017-02838-2

Chalfie, M., Tu, Y., Euskirchen, G., & Ward, W. W. (1994). *Green Fluorescent Protein as a Marker for Gene Expression*. *263*(5148), 802–805.

Chang, C.-H., Curtis, J. D., Maggi, L. B., Faubert, B., Villarino, A. V., O'Sullivan, D., … Pearce, E. L. (2013). Posttranscriptional Control of T Cell Effector Function by Aerobic Glycolysis. *Cell*, *153*(6), 1239–1251. https://doi.org/10.1016/j.cell.2013.05.016

Charles, K. J., Deuchars, J., Davies, C. H., & Pangalos, M. N. (2003). *GABA B receptor subunit expression in glia*. *24*, 214–223. https://doi.org/10.1016/S1044-7431(03)00162-3

Chattoraj, M., King, B. A., Bublitz, G. U., & Boxer, S. G. (1996). Ultra-fast excited state dynamics

in green fluorescent protein: multiple states and proton transfer. *Proc. Natl. Acad. Sci. USA*, *93*(16), 8362–8367. https://doi.org/10.1073/pnas.93.16.8362

Cheng, S.-C., Quintin, J., Cramer, R. a., Shepardson, K. M., Saeed, S., Kumar, V., … Netea, M. G. (2014). mTOR- and HIF-1 -mediated aerobic glycolysis as metabolic basis for trained immunity. *Science*, *345*(6204), 1250684–1250684. https://doi.org/10.1126/science.1250684

Chinta, S. J., Woods, G., Rane, A., Demaria, M., Campisi, J., & Andersen, J. K. (2015). Cellular senescence and the aging brain. *Experimental Gerontology*, *68*, 3–7. https://doi.org/https://doi.org/10.1016/j.exger.2014.09.018

Choo, A. Y., Kim, S. G., Vander Heiden, M. G., Mahoney, S. J., Vu, H., Yoon, S.-O., … Blenis, J. (2010). Glucose addiction of TSC null cells is caused by failed mTORC1-dependent balancing of metabolic demand with supply. *Molecular Cell*, *38*(4), 487–499. https://doi.org/10.1016/j.molcel.2010.05.007

Chouchani, E. T., Pell, V. R., Gaude, E., Aksentijević, D., Sundier, S. Y., Robb, E. L., … Murphy, M. P. (2014). Ischaemic accumulation of succinate controls reperfusion injury through mitochondrial ROS. *Nature*, *515*(7527), 431–435. https://doi.org/10.1038/nature13909

Choudhary, C., Weinert, B. T., Nishida, Y., Verdin, E., & Mann, M. (2014). The growing landscape of lysine acetylation links metabolism and cell signalling. *Nature Reviews Molecular Cell Biology*, *15*, 536. Retrieved from https://doi.org/10.1038/nrm3841

Chowdhury, G. M. I., Jiang, L., Rothman, D. L., & Behar, K. L. (2014). The contribution of ketone bodies to basal and activity-dependent neuronal oxidation in vivo. *Journal of Cerebral Blood Flow and Metabolism*, *34*(7), 1233–1242. https://doi.org/10.1038/jcbfm.2014.77

Chrétien, F., Vallat-Decouvelaere, A.-V., Bossuet, C., Rimaniol, A.-C., Le Grand, R., Le Pavec, G., … Gras, G. (2002). Expression of excitatory amino acid transporter-2 (EAAT-2) and

glutamine synthetase (GS) in brain macrophages and microglia of SIVmac251-infected macaques. *Neuropathology and Applied Neurobiology*, *28*(5), 410–417. https://doi.org/10.1046/j.1365-2990.2002.00426.x

Cingolani, L. A., Thalhammer, A., Yu, L. M. Y., Catalano, M., Ramos, T., Colicos, M. A., & Goda, Y. (2008). Activity-Dependent Regulation of Synaptic AMPA Receptor Composition and Abundance by β3 Integrins. *Neuron*, *58*(5), 749–762. https://doi.org/10.1016/j.neuron.2008.04.011

Clark, A. K., Gruber-Schoffnegger, D., Drdla-Schutting, R., Gerhold, K. J., Malcangio, M., & Sandkuhler, J. (2015). Selective Activation of Microglia Facilitates Synaptic Strength. *Journal of Neuroscience*, *35*(11), 4552–4570. https://doi.org/10.1523/JNEUROSCI.2061-14.2015

Clark, A. R., Calligaris, D., Regan, M. S., Pomeranz Krummel, D., Agar, J. N., Kallay, L., … Sengupta, S. (2018). Rapid discrimination of pediatric brain tumors by mass spectrometry imaging. *Journal of Neuro-Oncology*, *140*(2), 269–279. https://doi.org/10.1007/s11060-018-2978-2

Cordes, T., Wallace, M., Michelucci, A., Divakaruni, A. S., Sapcariu, S. C., Sousa, C., … Metallo, C. M. (2016). Immunoresponsive gene 1 and itaconate inhibit succinate dehydrogenase to modulate intracellular succinate levels. *Journal of Biological Chemistry*, *291*(27), jbc.M115.685792. https://doi.org/10.1074/jbc.M115.685792

Costa, V., & Scorrano, L. (2012). Shaping the role of mitochondria in the pathogenesis of Huntington's disease. *The EMBO Journal*, *31*(8), 1853 LP – 1864. https://doi.org/10.1038/emboj.2012.65

Coull, J. a M., Beggs, S., Boudreau, D., Boivin, D., Tsuda, M., Inoue, K., … De Koninck, Y.

(2005). BDNF from microglia causes the shift in neuronal anion gradient underlying neuropathic pain. *Nature*, *438*(7070), 1017–1021. https://doi.org/10.1038/nature04223

Cronk, J. C., Filiano, A. J., Louveau, A., Marin, I., Marsh, R., Ji, E., … Kipnis, J. (2018). Peripherally derived macrophages can engraft the brain independent of irradiation and maintain an identity distinct from microglia. *The Journal of Experimental Medicine*, *215*(6), 1627 LP – 1647. https://doi.org/10.1084/jem.20180247

Crotti, A., & Glass, C. K. (2015). The choreography of neuroinflammation in Huntington's disease. *Trends in Immunology*, *36*(6), 364–373. https://doi.org/10.1016/j.it.2015.04.007

Cryer, P. E., Davis, S. N., & Shamoon, H. (2003). Hypoglycemia in Diabetes. *Diabetes Care*, *26*(6), 1902 LP – 1912. https://doi.org/10.2337/diacare.26.6.1902

Csibi, A., Fendt, S., Li, C., Poulogiannis, G., Choo, A. Y., Chapski, D. J., … Blenis, J. (2013). The mTORC1 Pathway Stimulates Glutamine Metabolism and Cell Proliferation by Repressing SIRT4. *Cell*, *153*, 840–854. https://doi.org/10.1016/j.cell.2013.04.023

Cullingford, T. E., Eagles, D. A., & Sato, H. (2002). The ketogenic diet upregulates expression of the gene encoding the key ketogenic enzyme mitochondrial 3-hydroxy-3-methylglutaryl-CoA synthase in rat brain. *Epilepsy Research*, *49*, 99–107.

Cunningham, C., & Sanderson, D. J. (2008). Malaise in the water maze: Untangling the effects of LPS and IL-1β on learning and memory. *Brain, Behavior, and Immunity*, *22*(8), 1117–1127. https://doi.org/https://doi.org/10.1016/j.bbi.2008.05.007

D., D. A., J., D. M., L., P. R., & J., L. T. (2000). Development of Hypertension in a Rat Model of Diet-Induced Obesity. *Hypertension*, *35*(4), 1009–1015. https://doi.org/10.1161/01.HYP.35.4.1009

Daulatzai, M. A. (2017). Cerebral hypoperfusion and glucose hypometabolism: Key

pathophysiological modulators promote neurodegeneration, cognitive impairment, and Alzheimer's disease. *Journal of Neuroscience Research*, *95*(4), 943–972. https://doi.org/10.1002/jnr.23777

Davalos, D., Grutzendler, J., Yang, G., Kim, J. V., Zuo, Y., Jung, S., … Gan, W. B. (2005). ATP mediates rapid microglial response to local brain injury in vivo. *Nature Neuroscience*, *8*(6), 752–758. https://doi.org/10.1038/nn1472

David, S., & Kroner, A. (2011). Repertoire of microglial and macrophage responses after spinal cord injury. *Nature Reviews. Neuroscience*, Vol. 12, pp. 388–399. https://doi.org/10.1038/nrn3053

Davis, E. J., Foster, T. D., & Thomas, W. E. (1994). Cellular forms and functions of brain microglia. *Brain Research Bulletin*, *34*(1), 73–78. https://doi.org/10.1016/0361-9230(94)90189-9

Denes, A., Vidyasagar, R., Feng, J., Narvainen, J., McColl, B. W., Kauppinen, R. A., & Allan, S. M. (2007). Proliferating Resident Microglia after Focal Cerebral Ischaemia in Mice. *Journal of Cerebral Blood Flow & Metabolism*, *27*(12), 1941–1953. https://doi.org/10.1038/sj.jcbfm.9600495

Diaz-Garcia, C. M., Mongeon, R., Lahmann, C., Koveal, D., Zucker, H., & Yellen, G. (2017). Neuronal stimulation triggers neuronal glycolysis and not lactate uptake. *Cell Metab*, *26*(2), 361–374. https://doi.org/10.1016/j.cmet.2017.06.021

Dienel, G. A. (2019). Brain Glucose Metabolism: Integration of Energetics with Function. *Physiological Reviews*, *99*, 949–1045. https://doi.org/10.1152/physrev.00062.2017

Dissing-Olesen, L., LeDue, J. M., Rungta, R. L., Hefendehl, J. K., Choi, H. B., & MacVicar, B. a. (2014). Activation of Neuronal NMDA Receptors Triggers Transient ATP-Mediated

Microglial Process Outgrowth. *Journal of Neuroscience*, *34*(32), 10511–10527. https://doi.org/10.1523/JNEUROSCI.0405-14.2014

Dissing-Olesen, L., & MacVicar, B. A. (2015). Fixation and Immunolabeling of Brain Slices: SNAPSHOT Method. *Current Protocols in Neuroscience*, *71*(1), 1.23.1-1.23.12. https://doi.org/10.1002/0471142301.ns0123s71

Domercq, M., Vázquez-Villoldo, N., & Matute, C. (2013). Neurotransmitter signaling in the pathophysiology of microglia. *Frontiers in Cellular Neuroscience*, *7*(April), 1–17. https://doi.org/10.3389/fncel.2013.00049

Dominguez-Andres, J., Joosten, L. A. B., & Mihai, N. G. (2019). Induction of innate immune memory : the role of cellular metabolism Jorge Domı. *Current Opinion in Immunology*, *56*, 10–16. https://doi.org/10.1016/j.coi.2018.09.001

Doorn, K. J., Goudriaan, A., Blits-Huizinga, C., Bol, J. G. J. M., Rozemuller, A. J., Hoogland, P. V. J. M., … Van Dam, A. M. (2014). Increased amoeboid microglial density in the Olfactory Bulb of Parkinson's and Alzheimer's Patients. *Brain Pathology*, *24*(2), 152–165. https://doi.org/10.1111/bpa.12088

Douard, V., & Ferraris, R. P. (2008). Regulation of the fructose transporter GLUT5 in health and disease. *AJP: Endocrinology and Metabolism*, *295*(2), E227–E237. https://doi.org/10.1152/ajpendo.90245.2008

Drew, P. J., Shih, A. Y., Driscoll, J. D., Knutsen, P. M., Blinder, P., Davalos, D., … Kleinfeld, D. (2010). Chronic optical access through a polished and reinforced thinned skull_supp. *Nature Methods*, *7*(12), 981–984. https://doi.org/10.1038/nmeth.1530

Duelli, R., & Kuschinsky, W. (2001). Brain Glucose Transporters: Relationship to Local Energy Demand. *Physiology*, *16*(2), 71–76. https://doi.org/10.1152/physiologyonline.2001.16.2.71

Eberlin, L. S., Norton, I., Dill, A. L., Golby, A. J., Ligon, K. L., Santagata, S., … Agar, N. Y. R. (2012). Classifying Human Brain Tumors by Lipid Imaging with Mass Spectrometry. *Cancer Research*, *72*(3), 645–654. https://doi.org/10.1124/dmd.106.012823.Detection

EL Kasmi, K. C., & Stenmark, K. R. (2015). Contribution of metabolic reprogramming to macrophage plasticity and function. *Seminars in Immunology*, 1–9. https://doi.org/10.1016/j.smim.2015.09.001

Engl, E., & Attwell, D. (2015). Non-signalling energy use in the brain. *The Journal of Physiology*, *593*(16), 3417–3429. https://doi.org/10.1113/jphysiol.2014.282517

Erny, D., Hrabě de Angelis, A. L., Jaitin, D., Wieghofer, P., Staszewski, O., David, E., … Prinz, M. (2015). Host microbiota constantly control maturation and function of microglia in the CNS. *Nature Neuroscience*, *18*(7). https://doi.org/10.1038/nn.4030

Esen, N., & Kielian, T. (2006). Central role for MyD88 in the responses of microglia to pathogen-associated molecular patterns. *Journal of Immunology (Baltimore, Md. : 1950)*, *176*(11), 6802–6811. Retrieved from https://www.ncbi.nlm.nih.gov/pubmed/16709840

Everts, B., Amiel, E., Huang, S. C.-C., Smith, A. M., Chang, C.-H., Lam, W. Y., … Pearce, E. J. (2014). TLR-driven early glycolytic reprogramming via the kinases TBK1-IKKε supports the anabolic demands of dendritic cell activation. *Nature Immunology*, *15*(4), 323–332. https://doi.org/10.1038/ni.2833

Eyo, U. B., Gu, N., De, S., Dong, H., Richardson, J. R., & Wu, L.-J. (2015). Modulation of Microglial Process Convergence Toward Neuronal Dendrites by Extracellular Calcium. *Journal of Neuroscience*, *35*(6), 2417–2422. https://doi.org/10.1523/JNEUROSCI.3279-14.2015

Eyo, U. B., Peng, J., Swiatkowski, P., Mukherjee, A., Bispo, A., & Wu, L.-J. (2014). Neuronal

Hyperactivity Recruits Microglial Processes via Neuronal NMDA Receptors and Microglial P2Y12 Receptors after Status Epilepticus. *Journal of Neuroscience*, *34*(32), 10528–10540. https://doi.org/10.1523/JNEUROSCI.0416-14.2014

Eyo, Ukpong B., & Wu, L. J. (2013). Bidirectional microglia-neuron communication in the healthy brain. *Neural Plasticity*, *2013*. https://doi.org/10.1155/2013/456857

Fan, T. W.-M., & Lane, A. N. (2015). Regulation of mammalian nucleotide metabolism and biosynthesis. *Nucleic Acids Research*, *43*(4), 2466–2485. https://doi.org/10.1093/nar/gkv047

Farrar, W. L., Kilian, P. L., Ruff, M. R., Hill, J. M., & Pert, C. B. (1987). Visualization and characterization of interleukin 1 receptors in brain. *The Journal of Immunology*, *139*(2), 459 LP – 463. Retrieved from http://www.jimmunol.org/content/139/2/459.abstract

Ferrari, D., Pizzirani, C., Adinolfi, E., Lemoli, R. M., Curti, A., Idzko, M., … Di Virgilio, F. (2006). The P2X7 Receptor: A Key Player in IL-1 Processing and Release. *The Journal of Immunology*, *176*(7), 3877–3883. https://doi.org/10.4049/jimmunol.176.7.3877

Fields, R. D., & Ni, Y. (2010). Nonsynaptic Communication Through ATP Release from Volume-Activated Anion Channels in Axons. *Science Signaling*, *3*(142), ra73–ra73. https://doi.org/10.1126/scisignal.2001128

Fontainhas, A. M., Wang, M., Liang, K. J., Chen, S., Mettu, P., Damani, M., … Wong, W. T. (2011). Microglial morphology and dynamic behavior is regulated by ionotropic glutamatergic and GABAergic neurotransmission. *PLoS ONE*, *6*(1). https://doi.org/10.1371/journal.pone.0015973

Franceschi, C., Garagnani, P., Vitale, G., Capri, M., & Salvioli, S. (2017). Inflammaging and 'Garb-aging.' *Trends in Endocrinology & Metabolism*, *28*(3), 199–212. https://doi.org/https://doi.org/10.1016/j.tem.2016.09.005

Füger, P., Hefendehl, J. K., Veeraraghavalu, K., Wendeln, A.-C., Schlosser, C., Obermüller, U., … Jucker, M. (2017). Microglia turnover with aging and in an Alzheimer's model via long-term in vivo single-cell imaging. *Nature Neuroscience*, *20*, 1371. Retrieved from https://doi.org/10.1038/nn.4631

Fumagalli, S., Perego, C., Pischiutta, F., Zanier, E. R., & De Simoni, M.-G. (2015). The Ischemic Environment Drives Microglia and Macrophage Function. *Frontiers in Neurology*, *6*(April), 1–19. https://doi.org/10.3389/fneur.2015.00081

Gabrielli, M., Battista, N., Riganti, L., Prada, I., Antonucci, F., Cantone, L., … Verderio, C. (2015). Active endocannabinoids are secreted on extracellular membrane vesicles. *EMBO Reports*, *16*(2), 213–220. https://doi.org/10.15252/embr.201439668

Ganini, D., Leinisch, F., Kumar, A., Jiang, J., Tokar, E. J., Malone, C. C., … Mason, R. P. (2017). Fluorescent proteins such as eGFP lead to catalytic oxidative stress in cells. *Redox Biology*, *12*(March), 462–468. https://doi.org/10.1016/j.redox.2017.03.002

Gelders, G., Baekelandt, V., & Perren, A. Van der. (2018). Linking Neuroinflammation and Neurodegeneration in Parkinson's Disease. *Journal of Immunology Research*.

Gerhart, D. Z., Levasseur, R. J., Broderius, M. A., & Drewes, L. R. (1989). Glucose transporter localization in brain using light and electron immunocytochemistry. *Journal of Neuroscience Research*, *22*(4), 464–472. https://doi.org/10.1002/jnr.490220413

Ghosh, S., Castillo, E., Frias, E. S., & Swanson, R. A. (2017). Bioenergetic regulation of microglia. *Glia*, (October), 1–13. https://doi.org/10.1002/glia.23271

Ghukasyan, V. V, & Kao, F. (2009). Monitoring Cellular Metabolism with Fluorescence Lifetime of Reduced Nicotinamide Adenine Dinucleotide †. *The Journal of Physical Chemistry C*, *113*(27), 11532–11540. https://doi.org/10.1021/jp810931u

Gimenez-Cassina, A., Ramon Martinez-Francois, J., Fisher, J. K., Szlyk, B., Polak, K., Wiwczar, J., … Danial, N. N. (2012). BAD-Dependent Regulation of Fuel Metabolism and K ATP Channel Activity Confers Resistance to Epileptic Seizures. *Neuron*, 719–730. https://doi.org/10.1016/j.neuron.2012.03.032

Gimeno-Bayón, J., López-López, a., Rodríguez, M. J., & Mahy, N. (2014). Glucose pathways adaptation supports acquisition of activated microglia phenotype. *Journal of Neuroscience Research*, *92*(6), 723–731. https://doi.org/10.1002/jnr.23356

Ginhoux, F., Greter, M., Leboeuf, M., Nandi, S., See, P., Gokhan, S., … Merad, M. (2010). Fate Mapping Analysis Reveals that Adult Microglia Derive from Primitive Macrophages. *Science*, *701*(November), 841–846.

Gonçalves, C.-A., Rodrigues, L., Bobermin, L. D., Zanotto, C., Vizuete, A., Quincozes-Santos, A., … Leite, M. C. (2019). Glycolysis-Derived Compounds From Astrocytes That Modulate Synaptic Communication . *Frontiers in Neuroscience* , Vol. 12, p. 1035. Retrieved from https://www.frontiersin.org/article/10.3389/fnins.2018.01035

Goshen, I., Kreisel, T., Ounallah-Saad, H., Renbaum, P., Zalzstein, Y., Ben-Hur, T., … Yirmiya, R. (2007). A dual role for interleukin-1 in hippocampal-dependent memory processes. *Psychoneuroendocrinology*, *32*(8–10), 1106–1115. https://doi.org/10.1016/j.psyneuen.2007.09.004

Graham, L. C., Harder, J. M., Soto, I., de Vries, W. N., John, S. W. M., & Howell, G. R. (2016). Chronic consumption of a western diet induces robust glial activation in aging mice and in a mouse model of Alzheimer's disease. *Scientific Reports*, *6*, 21568. https://doi.org/10.1038/srep21568

Gruetter, R, Novotny, E. J., Boulware, S. D., Rothman, D. L., Mason, G. F., Shulman, G. I., …

Tamborlane, W. V. (1992). Direct measurement of brain glucose concentrations in humans by 13C NMR spectroscopy. *Proceedings of the National Academy of Sciences of the United States of America*, *89*(3), 1109–1112. Retrieved from https://www.ncbi.nlm.nih.gov/pubmed/1736294

Gruetter, Rolf, Adriany, G., Choi, I.-Y., Henry, P.-G., Lei, H., & Oz, G. (2003). Localized in vivo 13C NMR spectroscopy of the brain. *NMR in Biomedicine*, *16*(6–7), 313–338. https://doi.org/10.1002/nbm.841

Gubser, P. M., Bantug, G. R., Razik, L., Fischer, M., Dimeloe, S., Hoenger, G., … Hess, C. (2013). Rapid effector function of memory CD8+ T cells requires an immediate-early glycolytic switch. *Nature Immunology*, *14*(10), 1064–1072. https://doi.org/10.1038/ni.2687

Guedes-Dias, P., Pinho, B. R., Soares, T. R., de Proença, J., Duchen, M. R., & Oliveira, J. M. A. (2016). Mitochondrial dynamics and quality control in Huntington's disease. *Neurobiology of Disease*, *90*, 51–57. https://doi.org/https://doi.org/10.1016/j.nbd.2015.09.008

Guillemot-Legris, O., & Muccioli, G. G. (2017). Obesity-Induced Neuroinflammation: Beyond the Hypothalamus. *Trends in Neurosciences*, *40*(4), 237–253. https://doi.org/https://doi.org/10.1016/j.tins.2017.02.005

Guo, X., Sun, X., Hu, D., Wang, Y.-J., Fujioka, H., Vyas, R., … Qi, X. (2016). VCP recruitment to mitochondria causes mitophagy impairment and neurodegeneration in models of Huntington's disease. *Nature Communications*, *7*, 12646. Retrieved from https://doi.org/10.1038/ncomms12646

Hammond, T. R., Dufort, C., Dissing-Olesen, L., Giera, S., Young, A., Wysoker, A., … Stevens, B. (2019). Single-Cell RNA Sequencing of Microglia throughout the Mouse Lifespan and in the Injured Brain Reveals Complex Cell-State Changes. *Immunity*, *50*(1), 253-271.e6.

https://doi.org/10.1016/j.immuni.2018.11.004

Harris, J. J., Jolivet, R., & Attwell, D. (2012). Review Synaptic Energy Use and Supply. *Neuron*, *75*(5), 762–777. https://doi.org/10.1016/j.neuron.2012.08.019

Hatzivassiliou, G., Zhao, F., Bauer, D. E., Andreadis, C., Shaw, A. N., Dhanak, D., … Thompson, C. B. (2005). ATP citrate lyase inhibition can suppress tumor cell growth. *Cancer Cell*, *8*(4), 311–321. https://doi.org/10.1016/j.ccr.2005.09.008

Hefendehl, J. K., Neher, J. J., Suhs, R. B., Kohsaka, S., Skodras, A., & Jucker, M. (2014). Homeostatic and injury-induced microglia behavior in the aging brain. *Aging Cell*, *13*(1), 60–69. https://doi.org/10.1111/acel.12149

Heindl, S., Gesierich, B., Benakis, C., Llovera-Garcia, G., Duering, M., & Liesz, A. (2018). Automated Morphological Analysis of Microglia After Stroke. *Frontiers in Cellular Neuroscience*, *12*(April), 106. https://doi.org/10.3389/FNCEL.2018.00106

Heppner, F. L., Ransohoff, R. M., & Becher, B. (2015). Immune attack: the role of inflammation in Alzheimer disease. *Nature Reviews Neuroscience*, *16*(6), 358–372. https://doi.org/10.1038/nrn3880

Hess, S. T., Sheets, E. D., Wagenknecht-Wiesner, A., & Heikal, A. A. (2003). Quantitative analysis of the fluorescence properties of intrinsically fluorescent proteins in living cells. *Biophysical Journal*, *85*(4), 2566–2580. https://doi.org/10.1016/S0006-3495(03)74679-7

Hickman, S. E., Kingery, N. D., Ohsumi, T. K., Borowsky, M. L., Wang, L. C., Means, T. K., & El Khoury, J. (2013). The microglial sensome revealed by direct RNA sequencing. *Nat Neurosci*, *16*(12), 1896–1905. https://doi.org/10.1038/nn.3554nn.3554 [pii]

Hines, D. J., Choi, H. B., Hines, R. M., Phillips, A. G., & MacVicar, B. A. (2013). Prevention of LPS-induced microglia activation, cytokine production and sickness behavior with TLR4

receptor interfering peptides. *PloS One*, *8*(3), e60388. https://doi.org/10.1371/journal.pone.0060388

Hines, D. J., Hines, R. M., Mulligan, S. J., & Macvicar, B. A. (2009). Microglia processes block the spread of damage in the brain and require functional chloride channels. *Glia*, *57*(15), 1610–1618. https://doi.org/10.1002/glia.20874

Hirai, K., Aliev, G., Nunomura, A., Fujioka, H., Russell, R. L., Atwood, C. S., … Smith, M. A. (2001). Mitochondrial Abnormalities in Alzheimer's Disease. *The Journal of Neuroscience*, *21*(9), 3017 LP – 3023. https://doi.org/10.1523/JNEUROSCI.21-09-03017.2001

Ho, D. H., Je, A. R., Lee, H., Son, I., Kweon, H.-S., Kim, H.-G., & Seol, W. (2018). LRRK2 Kinase Activity Induces Mitochondrial Fission in Microglia via Drp1 and Modulates Neuroinflammation. *Exp Neurobiol*, *27*(3), 171–180. Retrieved from https://doi.org/10.5607/en.2018.27.3.171

Hoeijmakers, L., Lucassen, P. J., & Korosi, A. (2015). The interplay of early-life stress, nutrition, and immune activation programs adult hippocampal structure and function . *Frontiers in Molecular Neuroscience* , Vol. 7, p. 103. Retrieved from https://www.frontiersin.org/article/10.3389/fnmol.2014.00103

Hong, S., Beja-Glasser, V. F., Nfonoyim, B. M., Frouin, A., Li, S., Ramakrishnan, S., … Stevens, B. (2016). Complement and microglia mediate early synapse loss in Alzheimer mouse models. *Science*, *352*(6286), 712–716.

Hong, S., Dissing-Olesen, L., & Stevens, B. (2016). New insights on the role of microglia in synaptic pruning in health and disease. *Current Opinion in Neurobiology*, *36*, 128–134. https://doi.org/10.1016/j.conb.2015.12.004

Houten, S. M., Violante, S., Ventura, F. V, & Wanders, R. J. A. (2016). The Biochemistry and Physiology of Mitochondrial Fatty Acid β-Oxidation and Its Genetic Disorders. *Annual Review of Physiology*, *78*(1), 23–44. https://doi.org/10.1146/annurev-physiol-021115-105045

Hsu, P. P., & Sabatini, D. M. (2008). Cancer Cell Metabolism: Warburg and Beyond. *Cell*, *134*(5), 703–707. https://doi.org/https://doi.org/10.1016/j.cell.2008.08.021

Hu, F. B., van Dam, R. M., & Liu, S. (2001). Diet and risk of Type II diabetes: the role of types of fat and carbohydrate. *Diabetologia*, *44*(7), 805–817. https://doi.org/10.1007/s001250100547

Huang, D., Li, T., Wang, L., Zhang, L., Yan, R., Li, K., … Zhang, H. (2016). Hepatocellular carcinoma redirects to ketolysis for progression under nutrition deprivation stress. *Cell Research*, *26*, 1112. Retrieved from https://doi.org/10.1038/cr.2016.109

Huang, Y., Smith, D. E., Ibanez-Sandoval, O., Sims, J. E., & Friedman, W. J. (2011). Neuron-Specific Effects of Interleukin-1b Are Mediated by a Novel Isoform of the IL-1 Receptor Accessory Protein. *Journal of Neuroscience*, *31*(49), 18048–18059. https://doi.org/10.1523/JNEUROSCI.4067-11.2011

Hung, Y. P., & Yellen, G. (2014). Live cell imaging of cytosolic NADH-NAD+ redox state using a genetically encoded fluorescent biosensor. *Methods Mol Biol*, *1071*(4), 49–58. https://doi.org/10.1007/978-1-62703-622-1

Ikegaya, Y., Delcroix, I., Iwakura, Y., Matsuki, N., & Nishiyama, N. (2003). Interleukin-1β abrogates long-term depression of hippocampal CA1 synaptic transmission. *Synapse*, *47*(1), 54–57. https://doi.org/10.1002/syn.10154

Infantino, V., Convertini, P., Cucci, L., Panaro, M. A., Di Noia, M. A., Calvello, R., … Iacobazzi, V. (2011). The mitochondrial citrate carrier: a new player in inflammation. *Biochemical*

Journal, *438*(3), 433 LP – 436. https://doi.org/10.1042/BJ20111275

Infantino, V., Iacobazzi, V., Menga, A., Avantaggiati, M. L., & Palmieri, F. (2014). A key role of the mitochondrial citrate carrier (SLC25A1) in TNFα- and IFNγ-triggered inflammation. *Biochimica et Biophysica Acta (BBA) - Gene Regulatory Mechanisms*, *1839*(11), 1217–1225. https://doi.org/https://doi.org/10.1016/j.bbagrm.2014.07.013

Ip, W. K. E., Hoshi, N., Shouval, D. S., & Snapper, S. (2017). Anti-inflammatory Effect of IL-10 Mediated by Metabolic Reprogramming of Macrophages. *Science*, *519*(May), 513–519.

Izumi, Y., Benz, A. M., Zorumski, C. F., & Olney, J. W. (1994). Effects of lactate and pyruvate on glucose deprivation in rat hippocampal slices. *Neuroreport*, Vol. 5, pp. 617–620.

James, W. P. T. (2009). WHO recognition of the global obesity epidemic. *International Journal Of Obesity*, *32*, S120. Retrieved from https://doi.org/10.1038/ijo.2008.247

Jang, C., Chen, L., & Rabinowitz, J. D. (2018). Metabolomics and Isotope Tracing. *Cell*, *173*(4), 822–837. https://doi.org/10.1016/j.cell.2018.03.055

Jernberg, J. N., Bowman, C. E., Wolfgang, M. J., & Scafidi, S. (2017). Developmental regulation and localization of carnitine palmitoyltransferases (CPTs) in rat brain. *Journal of Neurochemistry*, *142*(3), 407–419. https://doi.org/10.1111/jnc.14072

Jha, A. K., Huang, S. C., Sergushichev, A., Lampropoulou, V., Ivanova, Y., Loginicheva, E., … Artyomov, M. N. (2015). Network Integration of Parallel Metabolic and Transcriptional Data Reveals Metabolic Modules that Regulate Macrophage Polarization. *Immunity*, *42*(3), 419–430. https://doi.org/10.1016/j.immuni.2015.02.005

Jin, L.-W., Horiuchi, M., Wulff, H., Liu, X.-B., Cortopassi, G. a., Erickson, J. D., & Maezawa, I. (2015). Dysregulation of Glutamine Transporter SNAT1 in Rett Syndrome Microglia: A Mechanism for Mitochondrial Dysfunction and Neurotoxicity. *Journal of Neuroscience*,

35(6), 2516–2529. https://doi.org/10.1523/JNEUROSCI.2778-14.2015

Jing, Y., Wang, Y., Wang, X., Song, C., Ma, J., Xie, Y., … Mi, L. (2018). Label-free imaging and spectroscopy for early detection of cervical cancer. *Journal of Biophotonics*, *11*(5), 1–8. https://doi.org/10.1002/jbio.201700245

John, S., Weiss, J. N., & Ribalet, B. (2011). Subcellular Localization of Hexokinases I and II Directs the Metabolic Fate of Glucose. *PLOS ONE*, *6*(3), e17674. Retrieved from https://doi.org/10.1371/journal.pone.0017674

Jung, G., Wiehler, J., & Zumbusch, A. (2005). The Photophysics of Green Fluorescent Protein : Influence of the Key Amino Acids at Positions 65 , 203 , and 222. *Biophysical Journal*, *88*(March), 1932–1947. https://doi.org/10.1529/biophysj.104.044412

Jung, S., Aliberti, J., Graemmel, P., Sunshine, M. J., Kreutzberg, G. W., Sher, A., & Littman, D. R. (2000). Analysis of fractalkine receptor CX(3)CR1 function by targeted deletion and green fluorescent protein reporter gene insertion. *Mol Cell Biol*, *20*(11), 4106–4114. Retrieved from http://www.ncbi.nlm.nih.gov/pubmed/10805752

Kalsbeek, M. J. T., Mulder, L., & Yi, C.-X. (2016). Microglia energy metabolism in metabolic disorder. *Molecular and Cellular Endocrinology*, 1–9. https://doi.org/10.1016/j.mce.2016.09.028

Kanamori, K., & Ross, B. D. (2004). Quantitative determination of extracellular glutamine concentration in rat brain , and its elevation in vivo by system A transport inhibitor , a - (methylamino) isobutyrate. *Journal of Neurochemistry*, *90*, 203–210. https://doi.org/10.1111/j.1471-4159.2004.02478.x

Kaneko, M., Stellwagen, D., Malenka, R. C., & Stryker, M. P. (2010). *Tumor Necrosis Factor-α mediates one component of competitive, experience-dependent plasticity in developing visual*

cortex. *58*(5), 673–680. https://doi.org/10.1016/j.neuron.2008.04.023.Tumor

Karlen, S. J., Miller, E. B., Wang, X., Levine, E. S., Zawadzki, R. J., & Burns, M. E. (2018). Monocyte infiltration rather than microglia proliferation dominates the early immune response to rapid photoreceptor degeneration. *Journal of Neuroinflammation*, *15*(1), 344. https://doi.org/10.1186/s12974-018-1365-4

Karperien, A., Ahammer, H., & Jelinek, H. F. (2013). Quantitating the subtleties of microglial morphology with fractal analysis. *Frontiers in Cellular Neuroscience*, *7*(January), 1–18. https://doi.org/10.3389/fncel.2013.00003

Kato, G., Inada, H., Wake, H., Akiyoshi, R., Miyamoto, A., Eto, K., … Nabekura, J. (2016). Microglial Contact Prevents Excess Depolarization and Rescues Neurons from Excitotoxicity. *ENeuro*, *3*(3), 1–9. https://doi.org/10.1523/ENEURO.0004-16.2016

Katsuki, H., Nakai, S., Hirai, Y., Akaji, K., Kiso, Y., & Satoh, M. (1990). Interleukin-1β inhibits long-term potentiation in the CA3 region of mouse hippocampal slices. *European Journal of Pharmacology*, *181*(3), 323–326. https://doi.org/https://doi.org/10.1016/0014-2999(90)90099-R

Kauppila, T. E. S., Kauppila, J. H. K., & Larsson, N.-G. (2017). Mammalian Mitochondria and Aging: An Update. *Cell Metabolism*, *25*(1), 57–71. https://doi.org/https://doi.org/10.1016/j.cmet.2016.09.017

Kelly, A., Vereker, E., Nolan, Y., Brady, M., Barry, C., Loscher, C., … Lynch, M. (2003). Activation of p38 Plays a Pivotal Role in the Inhibitory Effect of Lipopolysaccharide and Interleukin-1 on Long Term Potentiation in Rat Dentate Gyrus. In *The Journal of biological chemistry* (Vol. 278). https://doi.org/10.1074/jbc.M301938200

Kelly, B., & O'Neill, L. A. (2015). Metabolic reprogramming in macrophages and dendritic cells

in innate immunity. *Cell Research*, *25*(7), 771–784. https://doi.org/10.1038/cr.2015.68

Kerschnitzki, M., Kollmannsberger, P., Burghammer, M., Duda, G. N., Weinkamer, R., Wagermaier, W., & Fratzl, P. (2013). Architecture of the osteocyte network correlates with bone material quality. *Journal of Bone and Mineral Research*, *28*(8), 1837–1845. https://doi.org/10.1002/jbmr.1927

Kettenmann, H., Hanisch, U.-K., Noda, M., & Verkhratsky, A. (2011). Physiology of microglia. *Physiological Reviews*, *91*(2), 461–553. https://doi.org/10.1152/physrev.00011.2010

Kettenmann, H., Kirchhoff, F., & Verkhratsky, A. (2013). Microglia: New Roles for the Synaptic Stripper. *Neuron*, *77*(1), 10–18. https://doi.org/10.1016/j.neuron.2012.12.023

King, J. R., Gillevet, T. C., & Kabbani, N. (2017). A G protein-coupled a 7 nicotinic receptor regulates signaling and TNF- a release in microglia. *FEBS Open Bio*, *7*, 1350–1361. https://doi.org/10.1002/2211-5463.12270

Kinnaird, A., Zhao, S., Wellen, K. E., & Michelakis, E. D. (2016). Metabolic control of epigenetics in cancer. *Nature Reviews Cancer*, *16*, 694. Retrieved from https://doi.org/10.1038/nrc.2016.82

Kloss, C. U. A., Bohatschek, M., Kreutzberg, G. W., & Raivich, G. (2001). Effect of lipopolysaccharide on the morphology and integrin immunoreactivity of ramified microglia in the mouse brain and in cell culture. *Experimental Neurology*, *168*(1), 32–46. https://doi.org/10.1006/exnr.2000.7575

Klysz, D., Tai, X., Robert, P. A., Craveiro, M., Cretenet, G., Oburoglu, L., … Taylor, N. (2015). Glutamine-dependent alpha-ketoglutarate production regulates the balance between T helper 1 cell and regulatory T cell generation. *Sci Signal*, *8*(396), ra97. https://doi.org/10.1126/scisignal.aab2610

Koivunen, P., Hirsila, M., Remes, A. M., Hassinen, I. E., Kivirikko, K. I., & Myllyharju, J. (2007). Inhibition of Hypoxia-inducible Factor (HIF) Hydroxylases by Citric Acid Cycle Intermediates. *The Journal of Biological Chemistry*, *282*(7), 4524–4532. https://doi.org/10.1074/jbc.M610415200

Kolodziejczak, M., B??chade, C., Gervasi, N., Irinopoulou, T., Banas, S. M., Cordier, C., … Maroteaux, L. (2015). Serotonin Modulates Developmental Microglia via 5-HT2B Receptors: Potential Implication during Synaptic Refinement of Retinogeniculate Projections. *ACS Chemical Neuroscience*, *6*(7), 1219–1230. https://doi.org/10.1021/cn5003489

Kornberg, M. D., Bhargava, P., Kim, P. M., Putluri, V., Snowman, A. M., Putluri, N., … Snyder, S. H. (2018). Dimethyl fumarate targets GAPDH and aerobic glycolysis to modulate immunity. *Science*, *453*(April), 449–453.

Kozlowski, C., & Weimer, R. M. (2012). An automated method to quantify microglia morphology and application to monitor activation state longitudinally in vivo. *PLoS ONE*, *7*(2), 1–9. https://doi.org/10.1371/journal.pone.0031814

Krabbe, G., Matyash, V., Pannasch, U., Mamer, L., Boddeke, H. W. G. M., & Kettenmann, H. (2012). Activation of serotonin receptors promotes microglial injury-induced motility but attenuates phagocytic activity. *Brain, Behavior, and Immunity*, *26*(3), 419–428. https://doi.org/10.1016/j.bbi.2011.12.002

Kraig, R. P., Mitchell, H. M., Christie-Pope, B., Kunkler, P. E., White, D. M., Tang, Y. P., & Langan, G. (2010). TNF-α and microglial hormetic involvement in neurological health & migraine. *Dose-Response*, *8*(4), 389–413. https://doi.org/10.2203/dose-response.09-056.Kraig

Kreutzberg, G. W. (1996). Microglia: A sensor for pathological events in the CNS. *Trends in Neurosciences*, *19*(8), 312–318. https://doi.org/10.1016/0166-2236(96)10049-7

Kuhn, S. A., Landeghem, F. K. H. Van, Zacharias, R., Fa, K., Rappert, A., Pavlovic, S., … Kettenmann, H. (2004). *Microglia express GABA B receptors to modulate interleukin release*. *25*, 312–322. https://doi.org/10.1016/j.mcn.2003.10.023

Kumar, A., & Loane, D. J. (2012). Neuroinflammation after traumatic brain injury: Opportunities for therapeutic intervention. *Brain, Behavior, and Immunity*, *26*(8), 1191–1201. https://doi.org/10.1016/j.bbi.2012.06.008

Kummer, H. L. A., Heinecke, R., Kompa, F. P. C., Bieser, G., Jonsson, T., Silva, C. M., … Michel-beyerle, M. E. (1996). Time-resolved spectroscopy of wild-type and mutant Green Fluorescent Proteins reveals excited state deprotonation consistent with fluorophore-protein interactions. *Chemical Physics*, *213*.

Kyriazis, A. D., Noroozizadeh, S., Refaee, A., Choi, W., Chu, L. T., Bashir, A., … Nir, G. (2018). An End-to-end System for Automatic Characterization of Iba1 Immunopositive Microglia in Whole Slide Imaging. *Neuroinformatics*. https://doi.org/10.1007/s12021-018-9405-x

Labrousse, V. F., Costes, L., Aubert, A., Darnaudéry, M., Ferreira, G., Amédée, T., & Layé, S. (2009). Impaired interleukin-1β and c-Fos expression in the hippocampus is associated with a spatial memory deficit in P2X7 receptor-deficient mice. *PLoS ONE*, *4*(6). https://doi.org/10.1371/journal.pone.0006006

Lakowicz, J. R., Szmacinski, H., Nowaczyk, K., & Johnson, M. L. (1992). Fluorescence lifetime imaging of free and protein-bound NADH. *Proceedings of the National Academy of Sciences of the United States of America*, *89*(4), 1271–1275. https://doi.org/10.1073/pnas.89.4.1271

Lawson, L. J., Perry, V. H., Dri, P., & Gordon, S. (1990). Heterogeneity in the distribution and

morphology of microglia in the normal adult mouse brain. *Neuroscience*, *39*(1), 151–170. https://doi.org/0306-4522(90)90229-W [pii]

Leal, G., Afonso, P. M., Salazar, I. L., & Duarte, C. B. (2015). Regulation of hippocampal synaptic plasticity by BDNF. *Brain Research*, *1621*, 82–101. https://doi.org/10.1016/j.brainres.2014.10.019

Lee, M., Schwab, C., & Mcgeer, P. L. (2011). *Astrocytes Are GABAergic Cells That Modulate Microglial Activity*. *165*(June 2010), 152–165. https://doi.org/10.1002/glia.21087

Lehnardt, S. (2009). Innate immunity and neuroinflammation in the CNS: The role of microglia in Toll-like receptor-mediated neuronal injury. *Glia*, *263*(August 2009), NA-NA. https://doi.org/10.1002/glia.20928

Lehrman, E. K., Wilton, D. K., Litvina, E. Y., Welsh, C. A., Chang, S. T., Frouin, A., … Stevens, B. (2018). CD47 Protects Synapses from Excess Microglia-Mediated Pruning during Development. *Neuron*, *100*(1), 120-134.e6. https://doi.org/10.1016/j.neuron.2018.09.017

Li, C., Allen, A., Kwagh, J., Doliba, N. M., Qin, W., Najafi, H., … Smith, T. J. (2006). Green Tea Polyphenols Modulate Insulin Secretion by Inhibiting Glutamate Dehydrogenase. *Journal of Biological Chemistry* , *281*(15), 10214–10221. https://doi.org/10.1074/jbc.M512792200

Li, W., Houston, K. D., & Houston, J. P. (2017). Shifts in the fluorescence lifetime of EGFP during bacterial phagocytosis measured by phase-sensitive flow cytometry. *Scientific Reports*, *7*(December 2016), 1–11. https://doi.org/10.1038/srep40341

Li, Y., Du, X. F., Liu, C. S., Wen, Z. L., & Du, J. L. (2012). Reciprocal Regulation between Resting Microglial Dynamics and Neuronal Activity In Vivo. *Developmental Cell*, *23*(6), 1189–1202. https://doi.org/10.1016/j.devcel.2012.10.027

Liang, J., Takeuchi, H., Jin, S., Noda, M., Li, H., Doi, Y., … Suzumura, A. (2010). Glutamate

induces neurotrophic factor production from microglia via protein kinase C pathway. *Brain Research*, *1322*, 8–23. https://doi.org/10.1016/j.brainres.2010.01.083

Liang, K. J., Lee, J. E., Wang, Y. D., Ma, W., Aurora, M., Fariss, R. N., & Wong, W. T. (2010). Regulation of Dynamic Behavior of Retinal Microglia by CX3CR1 Signaling. *Invest Ophthalmol Vis Sci*, *50*(9), 4444–4451. https://doi.org/10.1167/iovs.08-3357.Regulation

Lin, H., Lee, E., Hestir, K., Leo, C., Huang, M., Bosch, E., … Williams, L. T. (2008). Discovery of a Cytokine and Its Receptor by Functional Screening of the Extracellular Proteome. *Science*, *320*(5877), 807 LP – 811. https://doi.org/10.1126/science.1154370

Lin, M. T., & Beal, M. F. (2006). Mitochondrial dysfunction and oxidative stress in neurodegenerative diseases. *Nature*, *443*(7113), 787–795. https://doi.org/10.1038/nature05292

Lin, R., Elf, S., Shan, C., Kang, H.-B., Ji, Q., Zhou, L., … Chen, J. (2015). 6-Phosphogluconate dehydrogenase links oxidative PPP, lipogenesis and tumour growth by inhibiting LKB1-AMPK signalling. *Nature Cell Biology*, *17*(11), 1484–1496. https://doi.org/10.1038/ncb3255

Loane, D. J., Kumar, A., Stoica, B. A., Cabatbat, R., & Faden, A. I. (2014). Progressive neurodegeneration after experimental brain trauma: association with chronic microglial activation. *Journal of Neuropathology and Experimental Neurology*, *73*(1), 14–29. https://doi.org/10.1097/NEN.0000000000000021

Loane, D. J., Stoica, B. A., Tchantchou, F., Kumar, A., Barrett, J. P., Akintola, T., … Faden, A. I. (2014). Novel mGluR5 Positive Allosteric Modulator Improves Functional Recovery, Attenuates Neurodegeneration, and Alters Microglial Polarization after Experimental Traumatic Brain Injury. *Neurotherapeutics*, *11*(4), 857–869. https://doi.org/10.1007/s13311-014-0298-6

Lombardo, M., Merino, D., Loza-Alvarez, P., & Lombardo, G. (2015). Translational label-free nonlinear imaging biomarkers to classify the human corneal microstructure. *Biomedical Optics Express*, *6*(8), 2803. https://doi.org/10.1364/BOE.6.002803

López-Lázaro, M. (2008). The warburg effect: why and how do cancer cells activate glycolysis in the presence of oxygen? *Anti-Cancer Agents in Medicinal Chemistry*, *8*(3), 305–312. https://doi.org/10.2174/187152008783961932

López-Redondo, F., Nakajima, K., Honda, S., & Shinichi Kohsaka. (2000). Glutamate transporter GLT-1 is highly expressed in activated microglia following facial nerve axotomy. *Molecular Brain Research*, *76*(2), 429–435. https://doi.org/https://doi.org/10.1016/S0169-328X(00)00022-X

Loscher, C. E., Mills, K. H. G., & Lynch, M. A. (2003). Interleukin-1 receptor antagonist exerts agonist activity in the hippocampus independent of the interleukin-1 type I receptor. *Journal of Neuroimmunology*, *137*(1), 117–124. https://doi.org/10.1016/S0165-5728(03)00072-9

Lou, N., Takano, T., Pei, Y., Xavier, A. L., Goldman, S. A., & Nedergaard, M. (2016). Purinergic receptor P2RY12-dependent microglial closure of the injured blood–brain barrier. *Proceedings of the National Academy of Sciences*, *113*(4), 1074–1079. https://doi.org/10.1073/pnas.1520398113

Lu, C.-L., Qin, L., Liu, H.-C., Candas, D., Fan, M., & Li, J. J. (2015). Tumor Cells Switch to Mitochondrial Oxidative Phosphorylation under Radiation via mTOR-Mediated Hexokinase II Inhibition - A Warburg-Reversing Effect. *PLOS ONE*, *10*(3), e0121046. Retrieved from https://doi.org/10.1371/journal.pone.0121046

Lu, Y., Yeh, W., & Ohashi, P. S. (2008). *LPS / TLR4 signal transduction pathway*. *42*, 145–151. https://doi.org/10.1016/j.cyto.2008.01.006

Luongo, L., Guida, F., Imperatore, R., Napolitano, F., Gatta, L., Cristino, L., … Maione, S. (2014). *The A1 Adenosine Receptor as a New Player in Microglia Physiology*. https://doi.org/10.1002/glia.22592

Machler, P., Wyss, M. T., Elsayed, M., Stobart, J., Gutierrez, R., von Faber-Castell, A., … Weber, B. (2016). In Vivo Evidence for a Lactate Gradient from Astrocytes to Neurons. *Cell Metabolism*, *23*, 94–102. https://doi.org/10.1016/j.cmet.2015.10.010

Magistretti, P. J., & Allaman, I. (2008). Brain Energy Metabolism. In *Brain Energy Metabolism. In Fundamental Neuroscience, 3rd edition* (pp. 271–293). https://doi.org/10.1007/978-1-4614-1997-6

Magistretti, P. J., & Allaman, I. (2015). A Cellular Perspective on Brain Energy Metabolism and Functional Imaging. *Neuron*, *86*(4), 883–901. https://doi.org/10.1016/j.neuron.2015.03.035

Magistretti, P. J., & Allaman, I. (2018). Lactate in the brain: From metabolic end-product to signalling molecule. *Nature Reviews Neuroscience*, *19*(4), 235–249. https://doi.org/10.1038/nrn.2018.19

Mandl, J., Mészáros, T., Bánhegyi, G., & Csala, M. (2013). Minireview: Endoplasmic Reticulum Stress: Control in Protein, Lipid, and Signal Homeostasis. *Molecular Endocrinology*, *27*(3), 384–393. https://doi.org/10.1210/me.2012-1317

Marcillat, O., Zhang, Y., & Davies, K. J. (1989). Oxidative and non-oxidative mechanisms in the inactivation of cardiac mitochondrial electron transport chain components by doxorubicin. *Biochem J*, *259*(1), 181-9. https://doi.org/10.1042/bj2590181

Martinez-François, J. R., Fernández-Agüera, M. C., Nathwani, N., Lahmann, C., Burnham, V. L., Danial, N. N., & Yellen, G. (2018). BAD and KATPchannels regulate neuron excitability and epileptiform activity. *ELife*, *7*, 1–25. https://doi.org/10.7554/eLife.32721

Matheoud, D., Sugiura, A., Bellemare-Pelletier, A., Laplante, A., Rondeau, C., Chemali, M., … Desjardins, M. (2016). Parkinson's Disease-Related Proteins PINK1 and Parkin Repress Mitochondrial Antigen Presentation. *Cell*, *166*(2), 314–327. https://doi.org/https://doi.org/10.1016/j.cell.2016.05.039

Mazumder, N., Lyn, R. K., Singaravelu, R., Ridsdale, A., Moffatt, D. J., Hu, C. W., … Pezacki, J. P. (2013). Fluorescence Lifetime Imaging of Alterations to Cellular Metabolism by Domain 2 of the Hepatitis C Virus Core Protein. *PLoS ONE*, *8*(6). https://doi.org/10.1371/journal.pone.0066738

McCommis, K. S., & Finck, B. N. (2015). Mitochondrial pyruvate transport: a historical perspective and future research directions. *The Biochemical Journal*, *466*(3), 443–454. https://doi.org/10.1042/BJ20141171

McKenna, M. C., Waagepetersen, H. S., Schousboe, A., & Sonnewald, U. (2006). Neuronal and astrocytic shuttle mechanisms for cytosolic-mitochondrial transfer of reducing equivalents: Current evidence and pharmacological tools. *Biochemical Pharmacology*, *71*(4), 399–407. https://doi.org/https://doi.org/10.1016/j.bcp.2005.10.011

Meneilly, G. S., & Tessier, D. M. (2016). Diabetes, Dementia and Hypoglycemia. *Canadian Journal of Diabetes*, *40*(1), 73–76. https://doi.org/https://doi.org/10.1016/j.jcjd.2015.09.006

Miele, M., Berners, M., Boutelle, M. G., Kusakabe, H., & Fillenz, M. (1996). The determination of the extracellular concentration of brain glutamate using quantitative microdialysis. *Brain Research*, *707*(1), 131–133. https://doi.org/https://doi.org/10.1016/0006-8993(95)01371-7

Miller, S., & Mayford, M. (1999). Cellular and molecular mechanisms of memory: the LTP connection. *Current Opinion in Genetics & Development*, *9*(3), 333–337. https://doi.org/https://doi.org/10.1016/S0959-437X(99)80050-1

Millet, P., Vachharajani, V., McPhail, L., Yoza, B., & McCall, C. E. (2016). GAPDH Binding to TNF-α mRNA Contributes to PostTranscriptional Repression in Monocytes. *The Journal of Immunology*, 2541–2551.

Mills, E. L., Kelly, B., Logan, A., Costa, A. S. H., Varma, M., Bryant, C. E., … O'Neill, L. A. (2016). Succinate Dehydrogenase Supports Metabolic Repurposing of Mitochondria to Drive Inflammatory Macrophages. *Cell*, *167*(2), 457-470.e13. https://doi.org/10.1016/j.cell.2016.08.064

Mills, E. L., Kelly, B., & O'Neill, L. A. J. (2017). Mitochondria are the powerhouses of immunity. *Nature Immunology*, *18*(5), 488–498. https://doi.org/10.1038/ni.3704

Mills, E., & O'Neill, L. a J. (2013). Succinate: a metabolic signal in inflammation. *Trends in Cell Biology*, *24*(5), 313–320. https://doi.org/10.1016/j.tcb.2013.11.008

Mingam, R., Smedt, V. De, Amédée, T., Bluthé, R.-M., Kelley, K. W., Dantzer, R., & Layé, S. (2008). In vitro and in vivo evidence for a role of the P2X7 receptor in the release of IL-1β in the murine brain. *Brain, Behavior, and Immunity*, *22*(2), 234–244. https://doi.org/10.1016/j.bbi.2007.08.007

Mink, J. W., Blumenschine, R. J., & Adams, D. B. (1981). Ratio of central nervous system to body metabolism in vertebrates: its constancy and functional basis. *American Journal of Physiology-Regulatory, Integrative and Comparative Physiology*, *241*(3), R203–R212.

Miseta, A., Tökés-Füzesi, M., Aiello, D. P., & Bedwell, D. M. (2003). A Saccharomyces cerevisiae Mutant Unable To Convert Glucose to Glucose-6-Phosphate Accumulates Excessive Glucose in the Endoplasmic Reticulum due to Core Oligosaccharide Trimming. *Eukaryotic Cell*, *2*(3), 534 LP – 541. https://doi.org/10.1128/EC.2.3.534-541.2003

Miyamoto, A., Wake, H., Ishikawa, A. W., Eto, K., Shibata, K., Murakoshi, H., … Nabekura, J.

(2016). Microglia contact induces synapse formation in developing somatosensory cortex. *Nature Communications*, *7*, 12540. Retrieved from https://doi.org/10.1038/ncomms12540

Miyamoto, S., Murphy, A. N., & Brown, J. H. (2007). Akt mediates mitochondrial protection in cardiomyocytes through phosphorylation of mitochondrial hexokinase-II. *Cell Death And Differentiation*, *15*, 521. Retrieved from https://doi.org/10.1038/sj.cdd.4402285

Morciano, P., Cenci, G., Carrisi, C., Capobianco, L., De Benedetto, G. E., Mannini, L., … Cestra, G. (2009). A conserved role for the mitochondrial citrate transporter Sea/SLC25A1 in the maintenance of chromosome integrity. *Human Molecular Genetics*, *18*(21), 4180–4188. https://doi.org/10.1093/hmg/ddp370

Morita, M., Gravel, S.-P., Chénard, V., Sikström, K., Zheng, L., Alain, T., … Sonenberg, N. (2013). mTORC1 Controls Mitochondrial Activity and Biogenesis through 4E-BP-Dependent Translational Regulation. *Cell Metabolism*, *18*(5), 698–711. https://doi.org/https://doi.org/10.1016/j.cmet.2013.10.001

Morita, M., Gravel, S.-P., Hulea, L., Larsson, O., Pollak, M., St-Pierre, J., & Topisirovic, I. (2015). mTOR coordinates protein synthesis, mitochondrial activity and proliferation. *Cell Cycle*, *14*(4), 473–480. https://doi.org/10.4161/15384101.2014.991572

Mosmann, T. (1983). Rapid colorimetric assay for cellular growth and survival: Application to proliferation and cytotoxicity assays. *Journal of Immunological Methods*, *65*(1), 55–63. https://doi.org/https://doi.org/10.1016/0022-1759(83)90303-4

Murphy, M. P., & Neill, L. A. J. O. (2018). Krebs Cycle Reimagined : The Emerging Roles of Succinate and Itaconate as Signal Transducers. *Cell*, *174*(4), 780–784. https://doi.org/10.1016/j.cell.2018.07.030

Murray, C. A., & Lynch, M. A. (1998). Evidence That Increased Hippocampal Expression of the

Cytokine Interleukin-1β Is a Common Trigger for Age- and Stress-Induced Impairments in Long-Term Potentiation. *The Journal of Neuroscience*, *18*(8), 2974 LP – 2981. https://doi.org/10.1523/JNEUROSCI.18-08-02974.1998

Murugan, M., Ling, E., & Kaur, C. (2013). Glutamate Receptors in Microglia. *CNS & Neurological Disorders*, *12*, 773–784.

Murugan, M., Sivakumar, V., Lu, J., Ling, E. A., & Kaur, C. (2011). Expression of N-methyl D-aspartate receptor subunits in amoeboid microglia mediates production of nitric oxide via NF-κB signaling pathway and oligodendrocyte cell death in hypoxic postnatal rats. *Glia*, *59*(4), 521–539. https://doi.org/10.1002/glia.21121

Nagamoto-Combs, K., Kulas, J., & Combs, C. K. (2014). A novel cell line from spontaneously immortalized murine microglia. *Journal of Neuroscience Methods*, *233*, 187–198. https://doi.org/10.1016/j.jneumeth.2014.05.021

Nagy, A. M., Fekete, R., Horvath, G., Koncsos, G., Kriston, C., Sebestyen, A., … Tretter, L. (2018). Versatility of microglial bioenergetic machinery under starving conditions. *Biochimica et Biophysica Acta - Bioenergetics*, *1859*(3), 201–214. https://doi.org/10.1016/j.bbabio.2017.12.002

Nagy, E., Henics, T., Eckert, M., Miseta, A., Lightowlers, R. N., & Kellermayer, M. (2000). Identification of the NAD+-Binding Fold of Glyceraldehyde-3-Phosphate Dehydrogenase as a Novel RNA-Binding Domain. *Biochemical and Biophysical Research Communications*, *275*(2), 253–260. https://doi.org/https://doi.org/10.1006/bbrc.2000.3246

Nakabayashi, T., Wang, H.-P., Kinjo, M., & Ohta, N. (2008). Application of fluorescence lifetime imaging of enhanced green fluorescent protein to intracellular pH measurements. *Photochemical & Photobiological Sciences*, *7*(6), 668. https://doi.org/10.1039/b800391b

Nau, R., Djukic, M., Mildner, A., Schmidt, H., Prinz, M., Brück, W., … Priller, J. (2006). Circulating monocytes engraft in the brain, differentiate into microglia and contribute to the pathology following meningitis in mice. *Brain*, *129*(9), 2394–2403. https://doi.org/10.1093/brain/awl206

Netea, M. G., Joosten, L. A. B., Latz, E., Mills, K. H. G., Natoli, G., Stunnenberg, H. G., … Xavier, R. J. (2016). Trained immunity: A program of innate immune memory in health and disease. *Science*, *352*(6284), aaf1098–aaf1098. https://doi.org/10.1126/science.aaf1098

Netea, Mihai G, Balkwill, F., Chonchol, M., Cominelli, F., Donath, M. Y., Giamarellos-Bourboulis, E. J., … Dinarello, C. A. (2017). A guiding map for inflammation. *Nature Immunology*, *18*(8), 826–831. https://doi.org/10.1038/ni.3790

Newsholme, P., Curi, R., Gordon, S., & Newsholme, E. A. (1986). Metabolism of glucose, glutamine, long-chain fatty acids and ketone bodies by murine macrophages. *Biochemical Journal*, *239*(1), 121 LP – 125. https://doi.org/10.1042/bj2390121

Newton, R., Priyadharshini, B., & Turka, L. A. (2016). Immunometabolism of regulatory T cells. *Nat Immunol*, *17*(6), 618–625. https://doi.org/10.1038/ni.3466

Nicoll, R. A. (2017). A Brief History of Long-Term Potentiation. *Neuron*, *93*(2), 281–290. https://doi.org/10.1016/j.neuron.2016.12.015

Nimmerjahn, A., Kirchhoff, F., & Helmchen, F. (2005). *Resting Microglial Cells Are Highly Dynamic Surveillants of Brain Parenchyma in Vivo*. *308*(May), 1314–1319. https://doi.org/10.1126/science.1110647

Noda, M., Nakanishi, H., Nabekura, J., & Akaike, N. (2000). AMPA-kainate subtypes of glutamate receptor in rat cerebral microglia. *The Journal of Neuroscience : The Official Journal of the Society for Neuroscience*, *20*(1), 251–258. Retrieved from

http://www.ncbi.nlm.nih.gov/pubmed/10627602

O'Neill, L. A. J., Kishton, R. J., & Rathmell, J. C. (2016). A guide to immunometabolism for immunologists. *Nature Reviews. Immunology*. https://doi.org/10.1038/nrmicro.2016.15

Olson, J. K., & Miller, S. D. (2004). Microglia Initiate Central Nervous System Innate and Adaptive Immune Responses through Multiple TLRs. *The Journal of Immunology*, *173*(6), 3916 LP – 3924. https://doi.org/10.4049/jimmunol.173.6.3916

Orr, A. G., Orr, A. L., Li, X., Gross, R. E., & Traynelis, S. F. (2010). Adenosine A2A receptor mediates microglial process retraction. *Nature Neuroscience*, *12*(7), 872–878. https://doi.org/10.1038/nn.2341.Adenosine

Otsu, N. (1979). A threshold selection method from gray-level histograms. *IEEE Transactions on Systems, Man, and Cybernetics*, *9*(1), 62–66. https://doi.org/10.1109/TSMC.1979.4310076

Palsson-McDermott, E. M., Curtis, A. M., Goel, G., Lauterbach, M. A. R., Sheedy, F. J., Gleeson, L. E., … O'Neill, L. A. J. (2015). Pyruvate Kinase M2 Regulates Hif-1α Activity and IL-1β Induction and Is a Critical Determinant of the Warburg Effect in LPS-Activated Macrophages. *Cell Metabolism*, *21*(1), 65–80. https://doi.org/10.1016/j.cmet.2014.12.005

Paolicelli, R. C., Bolasco, G., Pagani, F., Maggi, L., Scianni, M., Panzanelli, P., … Gross, C. T. (2011). Synaptic Pruning by Microglia Is Necessary for Normal Brain Development. *Science*, *333*(6048), 1456–1458. https://doi.org/10.1126/science.1202529

Paris, Inaki. (2018). *ProMoIJ : a new tool for automatic three-dimensional analysis of microglial processes motility*.

Paris, Iñaki, Savage, J. C., Escobar, L., Abiega, O., Gagnon, S., Hui, C. W., … Valero, J. (2018). ProMoIJ: A new tool for automatic three-dimensional analysis of microglial process motility. *Glia*, Vol. 66, pp. 828–845. https://doi.org/10.1002/glia.23287

Parkhurst, C. N., Yang, G., Ninan, I., Savas, J. N., Yates, J. R., Lafaille, J. J., … Gan, W.-B. (2013). Microglia Promote Learning-Dependent Synapse Formation through Brain-Derived Neurotrophic Factor. *Cell*, *155*(7), 1596–1609. https://doi.org/10.1016/j.cell.2013.11.030

Patra, K. C., & Hay, N. (2014). The pentose phosphate pathway and cancer. *Trends in Biochemical Sciences*, *39*(8), 347–354. https://doi.org/https://doi.org/10.1016/j.tibs.2014.06.005

Payne, J., Maher, F., Simpson, I., Mattice, L., & Davies, P. (1997). Glucose transporter Glut 5 expression in microglial cells. *Glia*, *21*(3), 327–331. https://doi.org/10.1002/(SICI)1098-1136(199711)21:3<327::AID-GLIA7>3.0.CO;2-1

Pelletier, S., Julien, C., Popoff, M. R., Lamarche-Vane, N., & Meloche, S. (2005). Cyclic AMP induces morphological changes of vascular smooth muscle cells by inhibiting a rac-dependent signaling pathway. *Journal of Cellular Physiology*, *204*(2), 412–422. https://doi.org/10.1002/jcp.20308

Perego, C., Fumagalli, S., & De Simoni, M.-G. (2013). Three-dimensional Confocal Analysis of Microglia/macrophage Markers of Polarization in Experimental Brain Injury. *Journal of Visualized Experiments*, (79), 1–7. https://doi.org/10.3791/50605

Perez-Escamilla, R., Bermudez, O., Buccini, G. S., Kumanyika, S., Lutter, C. K., Monsivais, P., & Victora, C. (2018). Nutrition disparities and the global burden of malnutrition. *BMJ*, *361*, k2252. https://doi.org/10.1136/bmj.k2252

Pérez-García, G., Guzmán-Quevedo, O., Da Silva Aragão, R., & Bolaños-Jiménez, F. (2016). Early malnutrition results in long-lasting impairments in pattern-separation for overlapping novel object and novel location memories and reduced hippocampal neurogenesis. *Scientific Reports*, *6*, 21275. Retrieved from https://doi.org/10.1038/srep21275

Perez-Pouchoulen, M., VanRyzin, J. W., & McCarthy, M. M. (2015). Morphological and

Phagocytic Profile of Microglia in the Developing Rat Cerebellum. *ENeuro*, *2*(4), ENEURO.0036-15.2015. https://doi.org/10.1523/ENEURO.0036-15.2015

Perry, V. H., & Holmes, C. (2014). Microglial priming in neurodegenerative disease. *Nature Reviews Neurology*, *10*(4), 217–224. https://doi.org/10.1038/nrneurol.2014.38

Persson, M., Brantefjord, M., Hansson, E., & Rönnbäck, L. (2005). Lipopolysaccharide increases microglial GLT-1 expression and glutamate uptake capacity in vitro by a mechanism dependent on TNF-α. *Glia*, *51*(2), 111–120. https://doi.org/10.1002/glia.20191

Pfeiffer, T., Avignone, E., & Nägerl, U. V. (2016). Induction of hippocampal long-term potentiation increases the morphological dynamics of microglial processes and prolongs their contacts with dendritic spines. *Scientific Reports*, *6*(1), 32422. https://doi.org/10.1038/srep32422

Pfeiffer, T., Schuster, S., & Bonhoeffer, S. (2001). Cooperation and Competition in the Evolution of ATP-Producing Pathways. *Science*, *292*(5516), 504 LP – 507. https://doi.org/10.1126/science.1058079

Phani, S., Loike, J. D., & Przedborski, S. (2012). Neurodegeneration and Inflammation in Parkinson's disease. *Parkinsonism & Related Disorders*, *18*, S207–S209. https://doi.org/10.1016/S1353-8020(11)70064-5

Pickrell, A. M., & Youle, R. J. (2015). The Roles of PINK1, Parkin, and Mitochondrial Fidelity in Parkinson's Disease. *Neuron*, *85*(2), 257–273. https://doi.org/https://doi.org/10.1016/j.neuron.2014.12.007

Pocock, J. M., & Kettenmann, H. (2007). Neurotransmitter receptors on microglia. *Trends in Neurosciences*, *30*(10), 527–535. https://doi.org/10.1016/j.tins.2007.07.007

Pollizzi, K. N., Patel, C. H., Sun, I., Oh, M., Waickman, A. T., Wen, J., … Powell, J. D. (2015).

mTORC1 and mTORC2 selectively regulate CD8 + T cell differentiation. *Journal of Clinical Investigation*, *125*(5), 1–19. https://doi.org/10.1172/JCI77746DS1

Polyzos, A. A., Lee, D. Y., Datta, R., Hauser, M., Budworth, H., Holt, A., … McMurray, C. T. (2019). Metabolic Reprogramming in Astrocytes Distinguishes Region-Specific Neuronal Susceptibility in Huntington Mice. *Cell Metabolism*, 1258–1273. https://doi.org/10.1016/j.cmet.2019.03.004

Pouli, D., Balu, M., Alonzo, C. A., Liu, Z., Quinn, K. P., Harris, R. M., … Tromberg, B. J. (2017). Imaging mitochondrial dynamics in human skin reveals depth- dependent hypoxia and malignant potential for diagnosis. *Sci. Translational Medicine*, *8*(367), 367ra169-367ra169. https://doi.org/10.1126/scitranslmed.aag2202.Imaging

Prakasam, G., Iqbal, M. A., Bamezai, R. N. K., & Mazurek, S. (2018). Posttranslational Modifications of Pyruvate Kinase M2: Tweaks that Benefit Cancer. *Frontiers in Oncology*, *8*, 22. https://doi.org/10.3389/fonc.2018.00022

Pribiag, H., & Stellwagen, D. (2013). TNF-a Downregulates Inhibitory Neurotransmission through Protein Phosphatase 1-Dependent Trafficking of GABAA Receptors. *Journal of Neuroscience*, *33*(40), 15879–15893. https://doi.org/10.1523/JNEUROSCI.0530-13.2013

Prieto, G. A., & Cotman, C. W. (2018). Cytokines and cytokine networks target neurons to modulate long-term potentiation. *Cytokine Growth Factor Rev*, *34*(949), 27–33. https://doi.org/10.1016/j.cytogfr.2017.03.005.Cytokines

Prieto, G. A., Snigdha, S., Baglietto-Vargas, D., Smith, E. D., Berchtold, N. C., Tong, L., … Cotman, C. W. (2015). Synapse-specific IL-1 receptor subunit reconfiguration augments vulnerability to IL-1β in the aged hippocampus. *Proceedings of the National Academy of Sciences*, *112*(36), E5078 LP-E5087. https://doi.org/10.1073/pnas.1514486112

Prins, M. L. (2008). Cerebral metabolic adaptation and ketone metabolism after brain injury. *Journal of Cerebral Blood Flow and Metabolism*, *28*(1), 1–16. https://doi.org/10.1038/sj.jcbfm.9600543

Prinz, M., & Priller, J. (2014). Microglia and brain macrophages in the molecular age: from origin to neuropsychiatric disease. *Nature Reviews. Neuroscience*, *15*(5), 300–312. https://doi.org/10.1038/nrn3722

Profenno, L. A., Porsteinsson, A. P., & Faraone, S. V. (2010). Meta-Analysis of Alzheimer's Disease Risk with Obesity, Diabetes, and Related Disorders. *Biological Psychiatry*, *67*(6), 505–512. https://doi.org/https://doi.org/10.1016/j.biopsych.2009.02.013

Rambold, A. S., & Pearce, E. L. (2017). Mitochondrial Dynamics at the Interface of Immune Cell Metabolism and Function. *Trends in Immunology*, *xx*, 1–13. https://doi.org/10.1016/j.it.2017.08.006

Ransom, B. R., & Fern, R. (1997). Does astrocytic glycogen benefit axon function and survival in CNS white matter during glucose deprivation? *Glia*, *21*(1), 134–141. https://doi.org/10.1002/(SICI)1098-1136(199709)21:1<134::AID-GLIA15>3.0.CO;2-T

Rawlins, C. M., Salisbury, J. P., Feldman, D. R., Isim, S., Agar, N. Y. R., Luther, E., & Agar, J. N. (2015). Imaging and Mapping of Tissue Constituents at the Single-Cell level using MALDI MSI and quantitative laser scanning cytometry. *Methods Mol Biol*, *1346*, 133–149. https://doi.org/10.1016/j.copbio.2011.11.023

Rayner, D. V., Thomas, M., & Trayhurn, P. (1994). Glucose transporters (GLUTs 1-4) and their mRNAs in regions of the rat brain: insulin-sensitive transporter expression in the cerebellum. *Canadian Journal of Physiology and Pharmacology*, *72*(5), 476–479.

Rehni, A. K., & Dave, K. R. (2018). Impact of Hypoglycemia on Brain Metabolism During

Diabetes. *Molecular Neurobiology*, (January), 9075–9088.

Réu, P., Khosravi, A., Bernard, S., Mold, J. E., Salehpour, M., Alkass, K., … Frisen, J. (2017). The Lifespan and Turnover of Microglia in the Human Brain. *Cell Reports*, *20*, 779–784. https://doi.org/10.1016/j.celrep.2017.07.004

Robson, S. C., Enjyoji, K., Guckelberger, O., Hammer, K., Braun, N., Se, J., … Zimmermann, H. (2000). *Assignment of ecto-nucleoside triphosphate diphosphohydrolase-1 / cd39 expression to microglia and vasculature of the brain*. *12*, 4357–4366.

Rogers, J. T., Morganti, J. M., Bachstetter, A. D., Hudson, C. E., Peters, M. M., Grimmig, B. A., … Gemma, C. (2011). CX3CR1 Deficiency Leads to Impairment of Hippocampal Cognitive Function and Synaptic Plasticity. *Journal of Neuroscience*, *31*(45), 16241–16250. https://doi.org/10.1523/JNEUROSCI.3667-11.2011

Romana Rizzo, F., Musella, A., Vito, F. De, Fresegna, D., Bullitta, S., Vanni, V., … Gentile, A. (2018). Tumor Necrosis Factor and Interleukin-1β Modulate Synaptic Plasticity during Neuroinflammation. *Neural Plasticity*.

Rosenegger, D. G., Tran, C. H. T., LeDue, J., Zhou, N., & Gordon, G. R. (2014). A high performance, cost-effective, open-source microscope for scanning two-photon microscopy that is modular and readily adaptable. *PLoS ONE*, *9*(10). https://doi.org/10.1371/journal.pone.0110475

Ross, F. M., Allan, S. M., Rothwell, N. J., & Verkhratsky, A. (2003). A dual role for interleukin-1 in LTP in mouse hippocampal slices. *Journal of Neuroimmunology*, *144*(1), 61–67. https://doi.org/10.1016/j.jneuroim.2003.08.030

Roumier, A., Pascual, O., Béchade, C., Wakselman, S., Poncer, J.-C., Réal, E., … Bessis, A. (2008). Prenatal Activation of Microglia Induces Delayed Impairment of Glutamatergic

Synaptic Function. *PLoS ONE*, *3*(7), e2595. https://doi.org/10.1371/journal.pone.0002595

Saeed, S., Quintin, J., Kerstens, H. H. D., Rao, N. A., Aghajanirefah, A., Matarese, F., … Stunnenberg, H. G. (2014). Epigenetic programming of monocyte-to-macrophage differentiation and trained innate immunity. *Science*, *345*(6204), 1251086. https://doi.org/10.1126/science.1251086

Salter, M. W., & Stevens, B. (2017). Microglia emerge as central players in brain disease. *Nature Medicine*, *23*, 1018. Retrieved from https://doi.org/10.1038/nm.4397

San Martin, A., Ceballo, S., Ruminot, I., Lerchundi, R., Frommer, W. B., & Barros, L. F. (2013). A Genetically Encoded FRET Lactate Sensor and Its Use To Detect the Warburg Effect in Single Cancer Cells. *PloS One*, *8*(2). https://doi.org/10.1371/journal.pone.0057712

Santagata, S., Eberlin, L. S., Norton, I., Calligaris, D., Feldman, D. R., Ide, J. L., … Agar, N. Y. R. (2014). Intraoperative mass spectrometry mapping of an onco-metabolite to guide brain tumor surgery. *Proceedings of the National Academy of Sciences*, *111*(30), 11121–11126. https://doi.org/10.1073/pnas.1404724111

Sarkar, S., Malovic, E., Harishchandra, D. S., Ghaisas, S., Panicker, N., Charli, A., … Kanthasamy, A. G. (2017). Mitochondrial impairment in microglia amplifies NLRP3 inflammasome proinflammatory signaling in cell culture and animal models of Parkinson's disease. *Npj Parkinson's Disease*, *3*(1), 30. https://doi.org/10.1038/s41531-017-0032-2

Saxton, R. A., & Sabatini, D. M. (2017). mTOR Signaling in Growth, Metabolism, and Disease. *Cell*, *168*(6), 960–976. https://doi.org/10.1016/j.cell.2017.02.004

Scalise, M., Pochini, L., Console, L., Losso, M. A., & Indiveri, C. (2018). The Human SLC1A5 (ASCT2) Amino Acid Transporter : From Function to Structure and Role in Cell Biology. *Frontiers in Cell and Developmental Biology*, *6*(September), 1–17.

https://doi.org/10.3389/fcell.2018.00096

Schafer, D. P., Lehrman, E. K., Kautzman, A. G., Koyama, R., Mardinly, A. R., Yamasaki, R., … Stevens, B. (2012). Microglia Sculpt Postnatal Neural Circuits in an Activity and Complement-Dependent Manner. *Neuron*, *74*(4), 691–705. https://doi.org/10.1016/j.neuron.2012.03.026

Schilling, M., Besselmann, M., Müller, M., Strecker, J. K., Ringelstein, E. B., & Kiefer, R. (2005). Predominant phagocytic activity of resident microglia over hematogenous macrophages following transient focal cerebral ischemia: An investigation using green fluorescent protein transgenic bone marrow chimeric mice. *Experimental Neurology*, *196*(2), 290–297. https://doi.org/https://doi.org/10.1016/j.expneurol.2005.08.004

Schirmer, T., & Evans, P. R. (1990). Structural basis of the allosteric behaviour of phosphofructokinase. *Nature*, *343*(6254), 140–145. https://doi.org/10.1038/343140a0

Schneckenburger, H., Wagner, M., Weber, P., Strauss, W. S. L., & Sailer, R. (2004). Autofluorescence lifetime imaging of cultivated cells using a UV picosecond laser diode. *Journal of Fluorescence*, *14*(5), 649–654. https://doi.org/10.1023/B:JOFL.0000039351.09916.cc

Schönfeld, P., & Reiser, G. (2013). Why does brain metabolism not favor burning of fatty acids to provide energy? - Reflections on disadvantages of the use of free fatty acids as fuel for brain. *Journal of Cerebral Blood Flow & Metabolism*, *33*(10), 1493–1499. https://doi.org/10.1038/jcbfm.2013.128

Schousboe, A., Scafidi, S., Bak, L. K., Waagepetersen, H. S., & McKenna, M. C. (2014). Glutamate Metabolism in the Brain Focusing on Astrocytes - Glutamate and ATP at the Interface of Metabolism and Signaling in the Brain. In V. Parpura, A. Schousboe, & A.

Verkhratsky (Eds.), *Glutamate and ATP at the Interface of Metabolism and Signaling in the Brain* (pp. 13–30). https://doi.org/10.1007/978-3-319-08894-5_2

Schwendele, B., Brawek, B., Hermes, M., & Garaschuk, O. (2012). High-resolution in vivo imaging of microglia using a versatile nongenetically encoded marker. *European Journal of Immunology*, Vol. 42, pp. 2193–2196. https://doi.org/10.1002/eji.201242436

Seaquist, E. R., Damberg, G. S., Tkac, I., & Gruetter, R. (2001). The Effect of Insulin on In Vivo Cerebral Glucose Concentrations and Rates of Glucose Transport/Metabolism in Humans. *Diabetes*, *50*(10), 2203 LP – 2209. https://doi.org/10.2337/diabetes.50.10.2203

Seaquist, E. R., & Öz, G. (2012). Sweet and Low: Measuring Brain Glucose During Hypoglycemia. *Diabetes*, *61*(8), 1918 LP – 1919. https://doi.org/10.2337/db12-0571

Sellgren, C. M., Gracias, J., Watmuff, B., Biag, J. D., Thanos, J. M., Whittredge, P. B., … Perlis, R. H. (2019). Increased synapse elimination by microglia in schizophrenia patient-derived models of synaptic pruning. *Nature Neuroscience*, *22*(3), 374–385. https://doi.org/10.1038/s41593-018-0334-7

Shankar, G. M., Li, S., Mehta, T. H., Garcia-Munoz, A., Shepardson, N. E., Smith, I., … Selkoe, D. J. (2008). Amyloid-β protein dimers isolated directly from Alzheimer's brains impair synaptic plasticity and memory.pdf. *Nature Medicine*, *14*(8), 837–842.

Shetty, P. K., Sadgrove, M. P., Galeffi, F., & Turner, D. A. (2013). Pyruvate Incubation Enhances Glycogen Stores and Sustains Neuronal Function during Subsequent Glucose Deprivation. *Neurobiology of Disease*, *45*(1), 177–187. https://doi.org/10.1016/j.nbd.2011.08.002.Pyruvate

Shi, L. Z., Wang, R., Huang, G., Vogel, P., Neale, G., Green, D. R., & Chi, H. (2011). HIF1a - dependent glycolytic pathway orchestrates a metabolic checkpoint for the differentiation of

TH17 and Treg cells. *Journal of Experimental Medicine*, *208*(7), 1367–1376. https://doi.org/10.1084/jem.20110278

Shi, Q., Colodner, K. J., Matousek, S. B., Merry, K., Hong, S., Kenison, J. E., … Lemere, C. A. (2015). Complement C3-Deficient Mice Fail to Display Age-Related Hippocampal Decline. *Journal of Neuroscience*, *35*(38), 13029–13042. https://doi.org/10.1523/JNEUROSCI.1698-15.2015

Shih, A. Y., Mateo, C., Drew, P. J., Tsai, P. S., & Kleinfeld, D. (2012). A polished and reinforced thinned-skull window for long-term imaging of the mouse brain. *Journal of Visualized Experiments : JoVE*, (61), 3742. https://doi.org/10.3791/3742

Shimomura, O., & Johnson, F. H. (1969). Properties of the Bioluminescent Protein Aequorin. *Biochemistry*, *8*(10), 3991–3997. https://doi.org/10.1021/bi00838a015

Shytle, R. D., Mori, T., Townsend, K., Vendrame, M., Sun, N., Zeng, J., … Tan, J. (2004). Cholinergic modulation of microglial activation by a 7 nicotinic receptors. *Journal of Neurochemistry*, *89*, 337–343. https://doi.org/10.1046/j.1471-4159.2004.02347.x

Simon, D. W., Mcgeachy, M. J., Bayır, H., Clark, R. S. B., Loane, D. J., & Kochanek, P. M. (2017). The far-reaching scope of neuroinflammation after traumatic brain injury. *Nature Reviews Neurology*, *13*, 171–191. https://doi.org/10.1038/nrneurol.2017.13

Sims, N. R., & Muyderman, H. (2010). Mitochondria, oxidative metabolism and cell death in stroke. *Biochimica et Biophysica Acta (BBA) - Molecular Basis of Disease*, *1802*(1), 80–91. https://doi.org/https://doi.org/10.1016/j.bbadis.2009.09.003

Sipe, G. O., Lowery, R. L., Tremblay, M.-È., Kelly, E. a, Lamantia, C. E., & Majewska, a K. (2016). Microglial P2Y12 is necessary for synaptic plasticity in mouse visual cortex. *Nature Communications*, *7*, 10905. https://doi.org/10.1038/ncomms10905

Skala, M. C., Riching, K. M., Bird, D. K., Gendron-fitzpatrick, A., Eickhoff, J., Eliceiri, K. W., … Ramanujam, N. (2007). In vivo Multiphoton Fluorescence Lifetime Imaging of Protein-bound and Free NADH in Normal and Pre-cancerous Epithelia. *Journal of Biomedical Optics*, *12*(2), 1–19. https://doi.org/10.1117/1.2717503.In

Smith, D. E., Lipsky, B. P., Russell, C., Ketchem, R. R., Kirchner, J., Hensley, K., … Sims, J. E. (2009). A central nervous system-restricted isoform of the interleukin-1 receptor accessory protein modulates neuronal responses to interleukin-1. *Immunity*, *30*(6), 817–831. https://doi.org/10.1016/j.immuni.2009.03.020

Spronsen, M. Van, & Hoogenraad, C. C. (2010). Synapse Pathology in Psychiatric and Neurologic Disease. *Curr Neurol Neurosci Rep*, *10*(March), 207–214. https://doi.org/10.1007/s11910-010-0104-8

Squarzoni, P., Oller, G., Hoeffel, G., Pont-Lezica, L., Rostaing, P., Low, D., … Garel, S. (2014). Microglia Modulate Wiring of the Embryonic Forebrain. *Cell Reports*, *8*(5), 1271–1279. https://doi.org/10.1016/j.celrep.2014.07.042

Srinivasan, D. (2004). Cell Type-Specific Interleukin-1b Signaling in the CNS. *Journal of Neuroscience*, *24*(29), 6482–6488. https://doi.org/10.1523/JNEUROSCI.5712-03.2004

Stellwagen, D., Beattie, E. C., Seo, J. Y., & Malenka, R. C. (2005). Differential Regulation of AMPA Receptor and GABA Receptor Trafficking by Tumor Necrosis Factor- a. *Journal of Neuroscience*, *25*(12), 3219–3228. https://doi.org/10.1523/JNEUROSCI.4486-04.2005

Stellwagen, D., & Malenka, R. C. (2006). Synaptic scaling mediated by glial TNF-α. *Nature*, *440*(7087), 1054–1059. https://doi.org/10.1038/nature04671

Stence, N., Waite, M., & Dailey, M. E. (2001). Dynamics of microglial activation: A confocal time-lapse analysis in hippocampal slices. *Glia*, *33*(3), 256–266.

https://doi.org/10.1002/1098-1136(200103)33:3<256::AID-GLIA1024>3.0.CO;2-J

Stephan, A. H., Barres, B. A., & Stevens, B. (2012). The Complement System: An Unexpected Role in Synaptic Pruning During Development and Disease. *Annual Review of Neuroscience*, *35*(1), 369–389. https://doi.org/10.1146/annurev-neuro-061010-113810

Stevens, B., Allen, N. J., Vazquez, L. E., Howell, G. R., Christopherson, K. S., Nouri, N., … Barres, B. A. (2007). The Classical Complement Cascade Mediates CNS Synapse Elimination. *Cell*, *131*(6), 1164–1178. https://doi.org/10.1016/j.cell.2007.10.036

Stockert, J. C., Horobin, R. W., Colombo, L. L., & Blázquez-Castro, A. (2018). Tetrazolium salts and formazan products in Cell Biology: Viability assessment, fluorescence imaging, and labeling perspectives. *Acta Histochemica*, *120*(3), 159–167. https://doi.org/https://doi.org/10.1016/j.acthis.2018.02.005

Streit, W. J. (1990). An Improved Staining Method for Rat Microglial Cells Using the Lectin from Griffonia simplicifolia. *Journal of Histochemistry and Cytochemistry*, *38*(11), 1683–1686.

Streit, W. J. (2004). Microglia and Alzheimer's disease pathogenesis. *J Neurosci Res*, *77*(1), 1–8. https://doi.org/10.1002/jnr.20093

Streit, W. J., Braak, H., Xue, Q. S., & Bechmann, I. (2009). Dystrophic (senescent) rather than activated microglial cells are associated with tau pathology and likely precede neurodegeneration in Alzheimer's disease. *Acta Neuropathol*, *118*(4), 475–485. https://doi.org/10.1007/s00401-009-0556-6

Streit, W. J., Sammons, N. W., Kuhns, A. J., & Sparks, D. L. (2004). Dystrophic microglia in the aging human brain. *Glia*, *45*(2), 208–212. https://doi.org/10.1002/glia.10319

Stringari, C., Cinquin, A., Cinquin, O., Digman, M. a, Donovan, P. J., & Gratton, E. (2011). Phasor approach to fluorescence lifetime microscopy distinguishes different metabolic states of germ

cells in a live tissue. *Proceedings of the National Academy of Sciences of the United States of America*, *108*(33), 13582–13587. https://doi.org/10.1073/pnas.1108161108

Stringari, C., Nourse, J. L., Flanagan, L. a., & Gratton, E. (2012). Phasor Fluorescence Lifetime Microscopy of Free and Protein-Bound NADH Reveals Neural Stem Cell Differentiation Potential. *PLoS ONE*, *7*(11). https://doi.org/10.1371/journal.pone.0048014

Stringari, C., Wang, H., Geyfman, M., Crosignani, V., Kumar, V., Takahashi, J. S., … Gratton, E. (2015). In Vivo Single-Cell Detection of Metabolic Oscillations in Stem Cells. *Cell Reports*, *10*(1), 1–7. https://doi.org/10.1016/j.celrep.2014.12.007

Swanson, C. J., Bures, M., Johnson, M. P., Linden, A.-M., Monn, J. A., & Schoepp, D. D. (2005). Metabotropic glutamate receptors as novel targets for anxiety and stress disorders. *Nature Reviews Drug Discovery*, *4*(2), 131–144. https://doi.org/10.1038/nrd1630

Sweeney, M. D., Sagare, A. P., & Zlokovic, B. V. (2018). Blood–brain barrier breakdown in Alzheimer disease and other neurodegenerative disorders. *Nature Reviews Neurology*, *14*, 133. Retrieved from https://doi.org/10.1038/nrneurol.2017.188

Szulczewski, J. M., Inman, D. R., Entenberg, D., Ponik, S. M., Aguirre-Ghiso, J., Castracane, J., … Keely, P. J. (2016). In Vivo Visualization of Stromal Macrophages via label-free FLIM-based metabolite imaging. *Scientific Reports*, *6*, 25086. https://doi.org/10.1038/srep25086

Takahashi, S., Iizumi, T., Mashima, K., Abe, T., & Suzuki, N. (2014). Roles and Regulation of Ketogenesis in Cultured Astroglia and Neurons Under Hypoxia and Hypoglycemia. *American Society for Neurochemistry*. https://doi.org/10.1177/1759091414550997

Takayama, F., Hayashi, Y., Wu, Z., Liu, Y., & Nakanishi, H. (2016). Diurnal dynamic behavior of microglia in response to infected bacteria through the UDP-P2Y 6 receptor system. *Scientific Reports*, *6*(July), 1–10. https://doi.org/10.1038/srep30006

Takeuchi, O., & Akira, S. (2010). Pattern Recognition Receptors and Inflammation. *Cell*, *140*(6), 805–820. https://doi.org/10.1016/j.cell.2010.01.022

Tanaka, R., Komine-Kobayashi, M., Mochizuki, H., Yamada, M., Furuya, T., Migita, M., … Urabe, T. (2003). Migration of enhanced green fluorescent protein expressing bone marrow-derived microglia/macrophage into the mouse brain following permanent focal ischemia. *Neuroscience*, *117*(3), 531–539. https://doi.org/https://doi.org/10.1016/S0306-4522(02)00954-5

Tani, H., Dulla, C. G., Farzampour, Z., Taylor-Weiner, A., Huguenard, J. R., & Reimer, R. J. (2014). A Local Glutamate-Glutamine Cycle Sustains Synaptic Excitatory Transmitter Release. *Neuron*, *81*(4), 888–900. https://doi.org/https://doi.org/10.1016/j.neuron.2013.12.026

Tannahill, G. M., Curtis, a M., Adamik, J., Palsson-McDermott, E. M., McGettrick, a F., Goel, G., … O'Neill, L. a J. (2013). Succinate is an inflammatory signal that induces IL-1β through HIF-1α. *Nature*, *496*(7444), 238–242. https://doi.org/10.1038/nature11986

Taylor, D L, Diemel, L. T., & Pocock, J. M. (2003). Activation of microglial group III metabotropic glutamate receptors protects neurons against microglial neurotoxicity. *J Neurosci*, *23*(6), 2150–2160. https://doi.org/23/6/2150 [pii]

Taylor, Deanna L, Jones, F., Kubota, E. S. F. C. S., & Pocock, J. M. (2005). Stimulation of Microglial Metabotropic Glutamate Receptor mGlu2 Triggers Tumor Necrosis Factor α-Induced Neurotoxicity in Concert with Microglial-Derived Fas Ligand. *The Journal of Neuroscience*, *25*(11), 2952–2964. https://doi.org/10.1523/JNEUROSCI.4456-04.2005

Thompson, R. J., Jackson, M. F., Olah, M. E., Rungta, R. L., Hines, D. J., Beazely, M. A., … Macvicar, B. A. (2008). *Hemichannels Augments Aberrant Bursting in the Hippocampus*.

319(December), 1555–1560.

Thoreen, C. C., Kang, S. A., Chang, J. W., Liu, Q., Zhang, J., Gao, Y., … Gray, N. S. (2009). *An ATP-competitive Mammalian Target of Rapamycin Inhibitor Reveals Rapamycin-resistant Functions*. *284*(12), 8023–8032. https://doi.org/10.1074/jbc.M900301200

Torres-Platas, S. G., Comeau, S., Rachalski, A., Bo, G. D., Cruceanu, C., Turecki, G., … Mechawar, N. (2014). Morphometric characterization of microglial phenotypes in human cerebral cortex. *Journal of Neuroinflammation*, *11*. https://doi.org/10.1186/1742-2094-11-12

Tremblay, M.-E., Stevens, B., Sierra, A., Wake, H., Bessis, A., & Nimmerjahn, A. (2011). The Role of Microglia in the Healthy Brain. *Journal of Neuroscience*, *31*(45), 16064–16069. https://doi.org/10.1523/JNEUROSCI.4158-11.2011

Tremblay, M. E., Lowery, R. L., & Majewska, A. K. (2010). Microglial interactions with synapses are modulated by visual experience. *PLoS Biology*, *8*(11). https://doi.org/10.1371/journal.pbio.1000527

Tremblay, M. È., & Majewska, A. K. (2011). A role for microglia in synaptic plasticity? *Communicative and Integrative Biology*, *4*(2), 220–222. https://doi.org/10.4161/cib.4.2.14506

van der Windt, G. J. W., Everts, B., Chang, C.-H., Curtis, J. D., Freitas, T. C., Amiel, E., … Pearce, E. L. (2012). Mitochondrial Respiratory Capacity Is a Critical Regulator of CD8+ T Cell Memory Development. *Immunity*, *36*(1), 68–78. https://doi.org/10.1016/j.immuni.2011.12.007

van de Ven, K. C. C., van der Graaf, M., Tack, C. J., Heerschap, A., & de Galan, B. E. (2012). Steady-State Brain Glucose Concentrations During Hypoglycemia in Healthy Humans and Patients With Type 1 Diabetes. *Diabetes*, *61*(8), 1974 LP – 1977.

https://doi.org/10.2337/db11-1778

van der Windt, G. J. W., Chang, C.-H., & Pearce, E. L. (2016). Measuring Bioenergetics in T Cells Using a Seahorse Extracellular Flux Analyzer. *Current Protocols in Immunology*, *113*(1), 3.16B.1-3.16B.14. https://doi.org/10.1002/0471142735.im0316bs113

Varvel, N. H., Grathwohl, S. A., Baumann, F., Liebig, C., Bosch, A., Brawek, B., … Jucker, M. (2012). Microglial repopulation model reveals a robust homeostatic process for replacing CNS myeloid cells. *Proceedings of the National Academy of Sciences of the United States of America*, *109*(44), 18150–18155. https://doi.org/10.1073/pnas.1210150109

Verdin, E., & Ott, M. (2014). 50 years of protein acetylation: from gene regulation to epigenetics, metabolism and beyond. *Nature Reviews Molecular Cell Biology*, *16*, 258. Retrieved from https://doi.org/10.1038/nrm3931

Verdonk, F., Roux, P., Flamant, P., Fiette, L., Bozza, F. A., Simard, S., … Danckaert, A. (2016). Phenotypic clustering: A novel method for microglial morphology analysis. *Journal of Neuroinflammation*, *13*(1). https://doi.org/10.1186/s12974-016-0614-7

Vereker, E., Campbell, V., Roche, E., McEntee, E., & Lynch, M. A. (2000). Lipopolysaccharide Inhibits Long Term Potentiation in the Rat Dentate Gyrus by Activating Caspase-1. *Journal of Biological Chemistry* , *275*(34), 26252–26258. https://doi.org/10.1074/jbc.M002226200

Vergen, J., Hecht, C., Zholudeva, L. V, Marquardt, M. M., & Nichols, M. G. (2013). *Metabolic imaging using two-photon excited NADH intensity and fluorescence lifetime imaging*. *18*(4). https://doi.org/10.1017/S1431927612000529.Metabolic

Vernon, A. C., Zbarsky, V., Datla, K. P., Dexter, D. T., & Croucher, M. J. (2007). *Selective Activation of Group III Metabotropic Glutamate Receptors by L - (2) -2-Amino-4-phosphonobutryic Acid Protects the Nigrostriatal System against 6-Hydroxydopamine*

Toxicity in Vivo. *320*(1), 397–409. https://doi.org/10.1124/jpet.106.108159.and/or

Volkmer, A., Subramaniam, V., Birch, D. J., & Jovin, T. M. (2000). One- and two-photon excited fluorescence lifetimes and anisotropy decays of green fluorescent proteins. *Biophysical Journal*, *78*(3), 1589–1598. https://doi.org/10.1016/S0006-3495(00)76711-7

Voloboueva, L. a., Emery, J. F., Sun, X., & Giffard, R. G. (2013). Inflammatory response of microglial BV-2 cells includes a glycolytic shift and is modulated by mitochondrial glucose-regulated protein 75/mortalin. *FEBS Letters*, *587*(6), 756–762. https://doi.org/10.1016/j.febslet.2013.01.067

Waitt, A. E., Reed, L., Ransom, B. R., & Brown, A. M. (2017). Emerging Roles for Glycogen in the CNS. *Frontiers in Molecular Neuroscience*, *10*(March), 1–10. https://doi.org/10.3389/fnmol.2017.00073

Wake, H., Moorhouse, A. J., Jinno, S., Kohsaka, S., & Nabekura, J. (2009). Resting Microglia Directly Monitor the Functional State of Synapses In Vivo and Determine the Fate of Ischemic Terminals. *Journal of Neuroscience*, *29*(13), 3974–3980. https://doi.org/10.1523/JNEUROSCI.4363-08.2009

Walberer, M., Jantzen, S. U., Backes, H., Rueger, M. a, Keuters, M. H., Neumaier, B., … Schroeter, M. (2014). In-vivo detection of inflammation and neurodegeneration in the chronic phase after permanent embolic stroke in rats. *Brain Research*, *1581*, 80–88. https://doi.org/10.1016/j.brainres.2014.05.030

Wang, F., Wang, K., Xu, W., Zhao, S., Ye, D., Wang, Y., … Yu, H. (2017). SIRT5 Desuccinylates and Activates Pyruvate Kinase M2 to Block Macrophage IL-1b Production and to Prevent DSS-Induced Colitis in Mice. *Cell Reports*, *19*(11), 2331–2344. https://doi.org/10.1016/j.celrep.2017.05.065

Wang, X., Wang, W., Li, L., Perry, G., Lee, H., & Zhu, X. (2014). Oxidative stress and mitochondrial dysfunction in Alzheimer's disease. *Biochimica et Biophysica Acta (BBA) - Molecular Basis of Disease*, *1842*(8), 1240–1247. https://doi.org/https://doi.org/10.1016/j.bbadis.2013.10.015

Warburg, O. (1956). On the Origin of Cancer Cells. *Science*, *123*(3191), 309 LP – 314. https://doi.org/10.1126/science.123.3191.309

Ward, P. S., Patel, J., Wise, D. R., Abdel-Wahab, O., Bennett, B. D., Coller, H. A., … Thompson, C. B. (2010). The Common Feature of Leukemia-Associated IDH1 and IDH2 Mutations Is a Neomorphic Enzyme Activity Converting α-Ketoglutarate to 2-Hydroxyglutarate. *Cancer Cell*, *17*(3), 225–234. https://doi.org/https://doi.org/10.1016/j.ccr.2010.01.020

Wei, S., Nandi, S., Chitu, V., Yeung, Y.-G., Yu, W., Huang, M., … Stanley, E. R. (2010). Functional overlap but differential expression of CSF-1 and IL-34 in their CSF-1 receptor-mediated regulation of myeloid cells. *Journal of Leukocyte Biology*, *88*(3), 495–505. https://doi.org/10.1189/jlb.1209822

Weichhart, T., Hengstschläger, M., & Linke, M. (2015). Regulation of innate immune cell function by mTOR. *Nature Reviews Immunology*, *15*(10), 599–614. https://doi.org/10.1038/nri3901

Weinberg, S. E., Sena, L. a, & Chandel, N. S. (2015). Mitochondria in the Regulation of Innate and Adaptive Immunity. *Immunity*, *42*(3), 406–417. https://doi.org/10.1016/j.immuni.2015.02.002

Weindl, D., Cordes, T., Battello, N., Sapcariu, S. C., Dong, X., & Wegner, A. (2016). Bridging the gap between non-targeted stable isotope labeling and metabolic flux analysis. *Cancer & Metabolism*, 1–14. https://doi.org/10.1186/s40170-016-0150-z

Wellen, K. E., Hatzivassiliou, G., Sachdeva, U. M., Bui, T. V, Cross, J. R., & Thompson, C. B.

(2009). ATP-Citrate Lyase Links Cellular Metabolism to Histone Acetylation. *Science*, *324*(5930), 1076 LP – 1080. https://doi.org/10.1126/science.1164097

Wendeln, A., Degenhardt, K., Kaurani, L., Gertig, M., Ulas, T., Jain, G., … Staufenbiel, M. (2018). Innate immune memory in the brain shapes neurological disease hallmarks. *Nature*. https://doi.org/10.1038/s41586-018-0023-4

West, A. P., Brodsky, I. E., Rahner, C., Woo, D. K., Erdjument-Bromage, H., Tempst, P., … Ghosh, S. (2011). TLR signalling augments macrophage bactericidal activity through mitochondrial ROS. *Nature*, *472*, 476. Retrieved from https://doi.org/10.1038/nature09973

Williams, N. C., & Neill, L. A. J. O. (2018). A Role for the Krebs Cycle Intermediate Citrate in Metabolic Reprogramming in Innate Immunity and Inflammation. *Frontiers in Immunology*, *9*(February), 1–11. https://doi.org/10.3389/fimmu.2018.00141

Won, S. J., Kim, J. H., Yoo, B. H., Sohn, M., Kauppinen, T. M., Park, M.-S., … Suh, S. W. (2012). Prevention of hypoglycemia-induced neuronal death by minocycline. *Journal of Neuroinflammation*, *9*(1), 225. https://doi.org/10.1186/1742-2094-9-225

Won, S. J., Yoo, B. H., Kauppinen, T. M., Choi, B. Y., Kim, J. H., Jang, B. G., … Suh, S. W. (2012). Recurrent / moderate hypoglycemia induces hippocampal dendritic injury , microglial activation , and cognitive impairment in diabetic rats. *Journal of Neuroinflammation*, *9*, 1–12.

Wu, L.-J., & Zhuo, M. (2008). Resting microglial motility is independent of synaptic plasticity in mammalian brain. *Journal of Neurophysiology*, *99*(February 2008), 2026–2032. https://doi.org/10.1152/jn.01210.2007

Wu, Y., Dissing-Olesen, L., MacVicar, B. a., & Stevens, B. (2015). Microglia: Dynamic Mediators of Synapse Development and Plasticity. *Trends in Immunology*, *36*(10), 605–613.

https://doi.org/10.1016/j.it.2015.08.008

Yang, C., Ko, B., Hensley, C. T., Jiang, L., Wasti, A. T., Kim, J., … DeBerardinis, R. J. (2014). Glutamine oxidation maintains the TCA cycle and cell survival during impaired mitochondrial pyruvate transport. *Molecular Cell*, *56*(3), 414–424. https://doi.org/10.1016/j.molcel.2014.09.025

Yang, K., Shrestha, S., Zeng, H., Karmaus, P. W. F., Neale, G., Vogel, P., … Chi, H. (2013). T Cell Exit from Quiescence and Differentiation into Th2 Cells Depend on Raptor-mTORC1-Mediated Metabolic Reprogramming. *Immunity*, *39*(6), 1043–1056. https://doi.org/10.1016/j.immuni.2013.09.015

Yaseen, M. a, Sakadžić, S., Wu, W., Becker, W., Kasischke, K. a, & Boas, D. a. (2013). In vivo imaging of cerebral energy metabolism with two-photon fluorescence lifetime microscopy of NADH. *Biomedical Optics Express*, *4*(2), 307–321. https://doi.org/10.1364/BOE.4.000307

Yaseen, M. O. A. Y., Utin, J. A. S., Eicheng, W. W. U., Uyin, B. F. U., Hlirova, H. A. N. A. U., Evor, A. N. N. A. D., … Akadži, S. Ć. (2017). *Fluorescence lifetime microscopy of NADH distinguishes alterations in cerebral metabolism in vivo*. *89*(May), 1271–1275. https://doi.org/10.1364/BOE.8.002368

Yellen, G. (2008). Ketone bodies, glycolysis, and KATP channels in the mechanism of the ketogenic diet. *Epilepsia*, *49*(Suppl 8), 80–82. https://doi.org/10.1111/j.1528-1167.2008.01843.x.Ketone

Yenari, M. A., Kauppinen, T. M., & Swanson, R. A. (2010). Microglial Activation in Stroke : Therapeutic Targets. *Neurotherapeutics*, *7*(4), 378–391. https://doi.org/10.1016/j.nurt.2010.07.005

Yirmiya, R., & Goshen, I. (2011). Brain , Behavior , and Immunity Immune modulation of learning

, memory , neural plasticity and neurogenesis. *Brain Behavior and Immunity*, *25*(2), 181–213. https://doi.org/10.1016/j.bbi.2010.10.015

York, E. M., Bernier, L., & MacVicar, B. A. (2017). Microglial Modulation of Neuronal Activity in the Healthy Brain. *Developmental Neurobiology*, (2011). https://doi.org/10.1002/dneu.22571

York, E. M., Ledue, J. M., Bernier, L., & Macvicar, B. A. (2018). 3DMorph Automatic Analysis of Microglial Morphology in Three Dimensions from Ex Vivo and In Vivo Imaging. *ENeuro*, *5*(December), 1–12.

Yu, S., & Ding, W.-G. (1998). The 45 kDa form of glucose transporter 1 (GLUT1) is localized in oligodendrocyte and astrocyte but not in microglia in the rat brain. *Brain Research*, *797*(1), 65–72. https://doi.org/https://doi.org/10.1016/S0006-8993(98)00372-2

Yudkoff, M. (2017). Interactions in the Metabolism of Glutamate and the Branched-Chain Amino Acids and Ketoacids in the CNS. *Neurochemical Research*, *42*(1), 10–18. https://doi.org/10.1007/s11064-016-2057-z

Zhan, L., Krabbe, G., Du, F., Jones, I., Reichert, M. C., Telpoukhovskaia, M., … Gan, L. (2019). Proximal recolonization by self-renewing microglia re-establishes microglial homeostasis in the adult mouse brain. *PLOS Biology*, *17*(2), e3000134. Retrieved from https://doi.org/10.1371/journal.pbio.3000134

Zhang, J., Malik, A., Choi, H. B., Ko, R. W. Y., Dissing-Olesen, L., & MacVicar, B. a. (2014). Microglial CR3 activation triggers long-term synaptic depression in the hippocampus via NADPH oxidase. *Neuron*, *82*(1), 195–207. https://doi.org/10.1016/j.neuron.2014.01.043

Zhang, Y., Chen, K., Sloan, S. A., Bennett, M. L., Scholze, A. R., O'Keeffe, S., … Wu, J. Q. (2014). An RNA-Sequencing Transcriptome and Splicing Database of Glia, Neurons, and

Vascular Cells of the Cerebral Cortex. *Journal of Neuroscience*, *34*(36), 11929–11947. https://doi.org/10.1523/JNEUROSCI.1860-14.2014

Zhang, Z., Tan, M., Xie, Z., Dai, L., Chen, Y., & Zhao, Y. (2010). Identification of lysine succinylation as a new post-translational modification. *Nature Chemical Biology*, *7*, 58. Retrieved from https://doi.org/10.1038/nchembio.495

Zhao, Y., Wang, A., Zou, Y., Su, N., Loscalzo, J., & Yang, Y. (2016). In vivo monitoring of cellular energy metabolism using SoNar, a highly responsive sensor for NAD+/NADH redox state. *Nature Protocols*, *11*(8), 1345–1359. https://doi.org/10.1038/nprot.2016.074

Zheng, J. (2012). Energy metabolism of cancer: Glycolysis versus oxidative phosphorylation. *Oncology Letters*, *4*(6), 1151–1157. https://doi.org/10.3892/ol.2012.928

Ziegler, D. V, Wiley, C. D., & Velarde, M. C. (2015). Mitochondrial effectors of cellular senescence: beyond the free radical theory of aging. *Aging Cell*, *14*(1), 1–7. https://doi.org/10.1111/acel.12287

Zusso, M., Methot, L., Lo, R., Greenhalgh, A. D., David, S., & Stifani, S. (2012). Regulation of postnatal forebrain amoeboid microglial cell proliferation and development by the transcription factor Runx1. *J Neurosci*, *32*(33), 11285–11298. https://doi.org/10.1523/JNEUROSCI.6182-11.201232/33/11285 [pii]

Appendices

Appendix A

A.1 Chapter 4 additional methods

Two-photon imaging

For morphological analysis, hippocampal slices from CX3CR1$^{+/EGFP}$ mice were incubated in treatment conditions, then rapidly fixed by SNAPSHOT protocol (Dissing-Olesen & MacVicar, 2015). This includes a two-minute fixation in 4% PFA at 80 ˚C, rinse in 0.1 M PBS, and storage in clearing solution (0.1M PBS with 20% DMSO, and 2% Triton X-100) at 4 ˚C. EGFP fluorescence is well-preserved by this method, and slices were ready for imaging immediately after clearing. Images were acquired with a Coherent Chameleon Ultra II laser (mode-locked pulse train at 80 MHz at 920 nm) with a Zeiss LSM 7 MP microscope and Zeiss 20x-W/1.0 NA objective. Green fluorescence was detected by a 520/60 nm filter (Chroma tech) and GaAsP photo-multiplier tube (PMT; Zeiss LSM BiG). Images were acquired as a z-stack at 1024 x 1024 (zoom factor 1.5; 283.12 x 283.12 µm xy scale, 16-line averaging) from 125 – 175 µm deep (2 µm slice interval) in the stratum radiatum region of CA1 hippocampus. Multiple cells are analyzed in each image, and the data is analyzed as the average measurement of all cells in a single animal (biological replicate). All images were loaded into 3DMorph (York et al., 2018) for analysis and processed using the same parameters file to avoid experimenter bias.

Images for time-lapse analysis were collected from live slices at 512 × 512 pixels using 8-line averaging and acquired as a time series of stacks of 15 optical sections with a step size of 2 µm in the z-axis. Lesions were induced by exposure of high laser power illumination to a restricted area.

SIM-A9 culture, MTT, and phagocytosis assays

SIM-A9 cells were cultured with DMEM F12 media with 10% FBS and 1% penicillin/streptomycin in a 96-well plate at 20K cells/well. For MTT assays, cells were incubated overnight before media was carefully aspirated and cells were washed with deficient media (0 mM glucose, 0 mM glutamine). Experimental media was added for a four-hour incubation, followed by addition of freshly prepared MTT solution. After a 20-minute incubation, MTT solution was replaced by DMSO, and the plate was agitated for two minutes. DMSO extract (80 µl) was transferred to a fresh 96-well plate and OD measured at 540 nm.

For phagocytosis assays, SIM-A9 cells were plated at 100K cells/well and left in full media overnight. Cells were then washed in deficient media and incubated in experimental media for three hours, at which point, fluorescent microspheres (Polysciences Inc, cat# 17154) were added to the media using a 1:10 000 dilution. Following a one-hour incubation, media was removed and non-phagocytosed beads removed with a gentle wash with deficient media. The number of cells containing phagocytosed beads were counted using an Evos FL microscope, and normalized to the total number of cells.

Reagents

EGCG (Cayman Chemical Company 70935, 50 µM *in vitro*); Torin-1 (Tocris 4247, 10 µM).

A.2 Chapter 4 additional figures

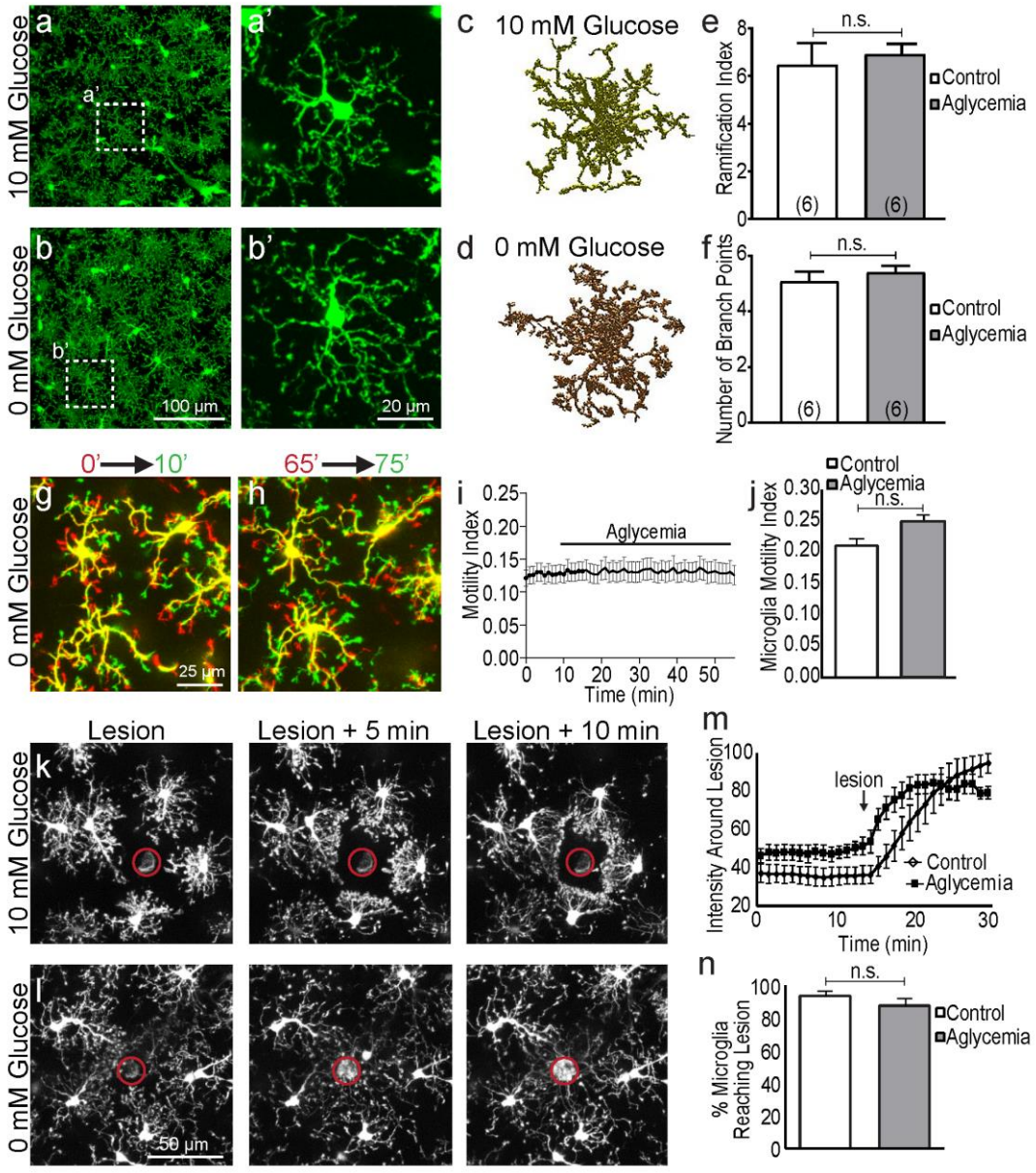

Figure A.2.1 Microglia maintain baseline and immune surveillance in 0 mM glucose *in situ*.

Microglial morphology in acute hippocampal slices after 60 minutes in control (a), or aglycemic (b) conditions. Microglial 3D representation by 3DMorph (c,d) and quantification of ramification index (e) and number of branch points (f). g) Microglial baseline motility represented as initial image (red) overlaid on an image 10 minutes later (green). Yellow areas show static portions of the cell throughout 10 minutes. There is no change in microglial surveillance during aglycemia relative to control (i,j). Following a laser-induced lesion (red circle), microglia in

control (k) or aglycemic (l) solutions respond within 10 minutes. There is no difference in speed of extension (m) or percentage of responsive cells (n). Error bars represent mean +/- SEM. Statistical differences determined by unpaired t-test.

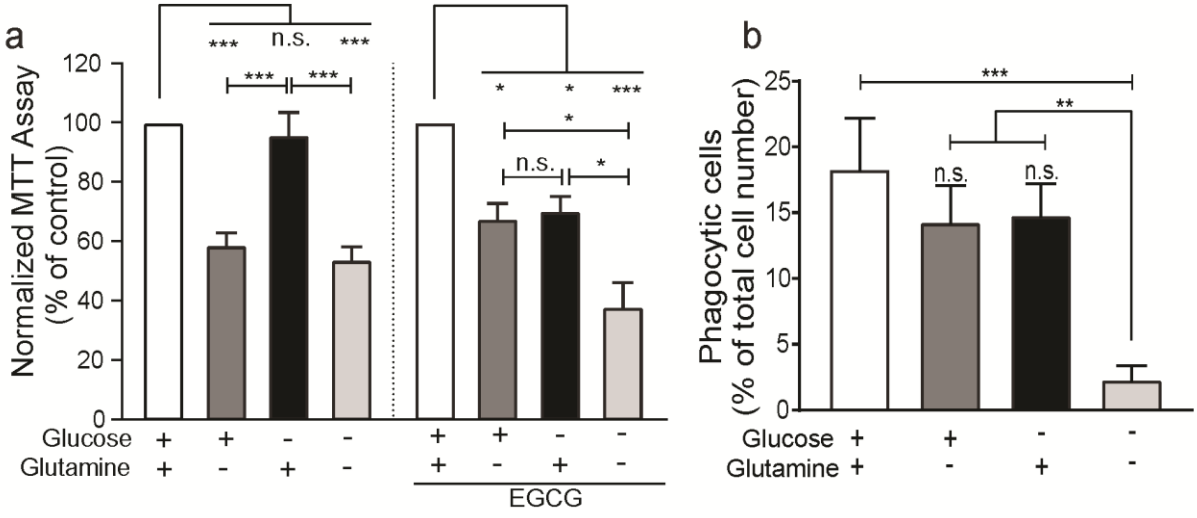

Figure A.2.2 Microglia metabolize glutamine *in vitro* to maintain viability and function.

a) SIM-A9 metabolic viability was assessed by MTT assay after 4 hours in control, glucose only, glutamine only, or deficient media. EGCG was added to inhibit glutaminolysis. b) Phagocytic capacity was measured in SIM-A9 cells following 4 hours in experimental conditions. Error bars represent mean +/- SEM. *p<0.05, **p<0.01, ***p<0.001 by One-way ANOVA and Tukey's multiple comparison.

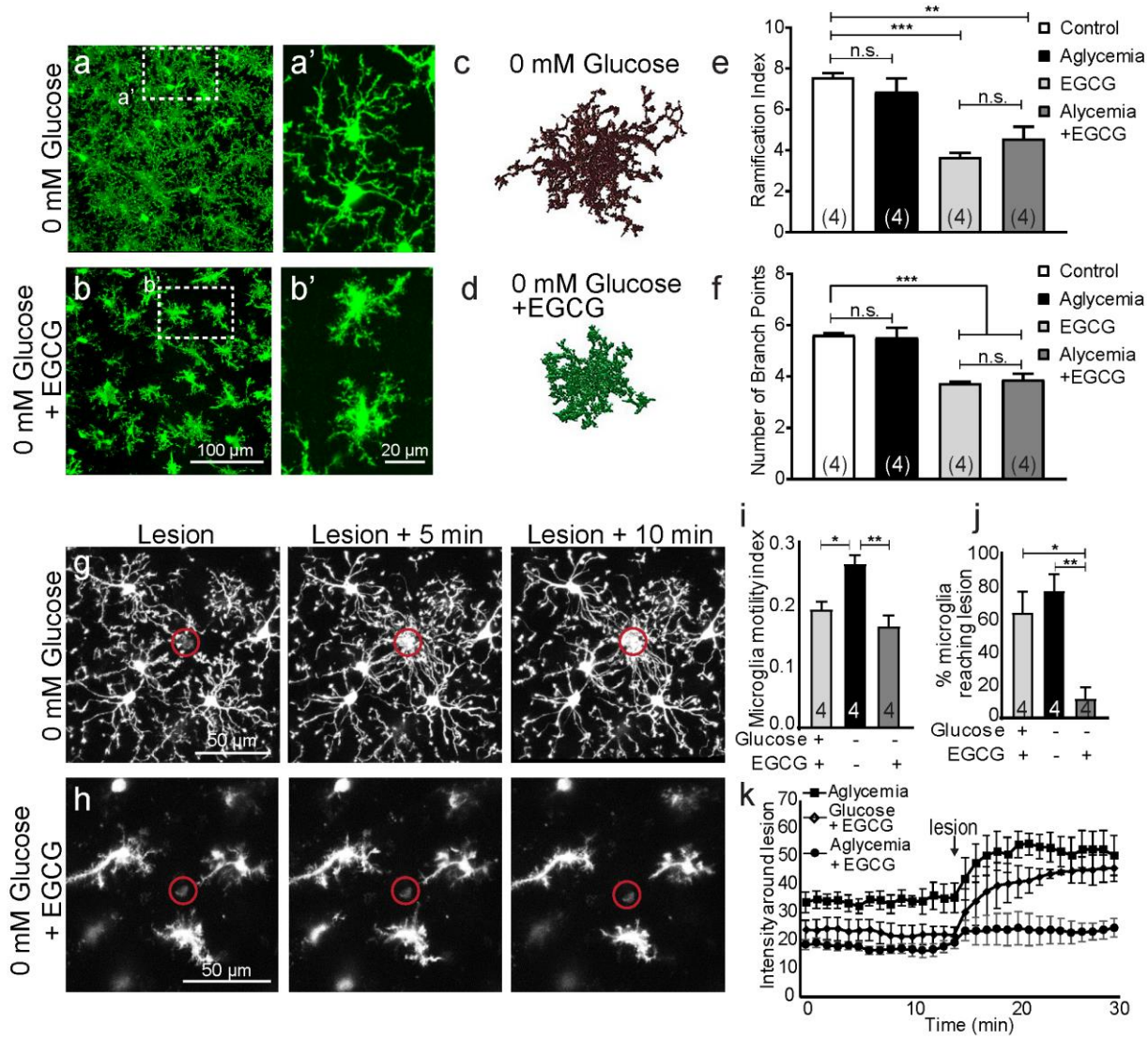

Figure A.2.3 Microglial motility and immune surveillance are supported by glutaminolysis in 0 mM glucose.

Microglial morphology from acute hippocampal slices incubated for 60 minutes in 0 mM glucose (a), or 0 mM glucose with EGCG (b). Microglial 3D representation by 3DMorph (c,d) and quantification of ramification index (e) and number of branch points (f). g) Following a laser-induced lesion (red circle), microglia in aglycemic solutions reach the site of injury within 10 minutes, while those in aglycemic and EGCG solutions (h) do not show process outgrowth. Baseline motility index (i), percentage of responsive cells to injury (j), and the rate of microglial process extension to lesion (k) are quantified. Error bars represent mean +/- SEM. *p<0.05, **p<0.01, ***p<0.001 by One-way ANOVA and Tukey's multiple comparison.

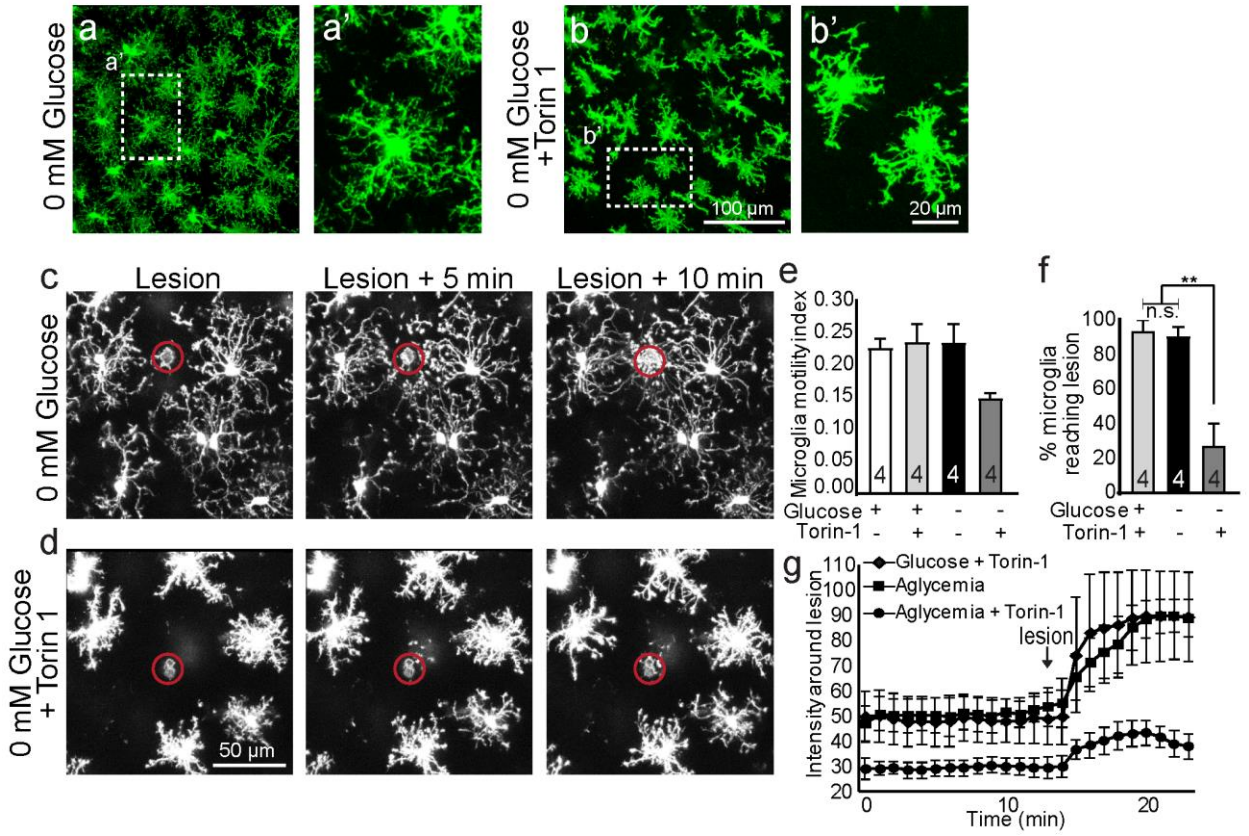

Figure A.2.4 Microglial metabolic switch to glutaminolysis is dependent on mTOR.

Microglial morphology from acute hippocampal slices incubated for 60 minutes in 0 mM glucose (a), or 0 mM glucose with Torin-1 (b). c) Following a laser-induced lesion (red circle), microglia in aglycemic solutions reach the site of injury within 10 minutes, while those in aglycemic and Torin-1 solutions (d) do not reach the lesion. Baseline motility index (e), percentage of responsive cells to injury (f), and the rate of microglial process extension to lesion (g) are quantified. Error bars represent mean +/- SEM. Statistical differences determined by One-way ANOVA and Tukey's multiple comparison, **p<0.01.

Appendix B

B.1 Chapter 5 additional methods

Animal protocols

Mouse and rat housing and experimental procedures were carried out in accordance with Canadian Council on Animal Care (CCAC) regulations, with protocols approved by the University of British Columbia committee on animal care. TLR4 KO (Jackson Lab strain B6.B10ScN-Tlr4lps-del/JthJ), and Sprague Dawley rats were housed on a 12 h light/day cycle with food and water *ad libitum*.

Acute hippocampal slice preparation

For electrophysiological recordings, brains of Sprague Dawley rats (postnatal day 18 to 23) or C57BL/6 mice (1-3 months old) were rapidly removed and placed into ice-cold aCSF slush saturated with 95% O_2 and 5% CO_2. Artificial CSF contained (in mM): 119 NaCl, 26 $NaHCO_3$, 2.5 KCl, 10 glucose, 1.25 NaH_2PO_4, 1.3 $MgSO_4$, 2.5 $CaCl_2$. Transverse hippocampal slices, 400 µm thick, were recovered in aCSF at room temperature for at least one hour prior to experimental incubations.

Field recording

After recovery, slices were submerged in a recording chamber at room temperature (22-25 ^oC). The bath solution (aCSF) was perfused at a rate of 1.5-2 mL/min. Field excitatory postsynaptic potentials (fEPSPs) were evoked by orthodromic stimulation of the Schaffer collateral pathway using a concentric stimulating electrode (Frederick Haer Co.), and were recorded in CA1 stratum radiatum by glass micropipettes filled with aCSF (resistance 3-5 MΩ). Population spikes (PS) were recorded in CA1 pyramidal layer synchronously with fEPSP. Field EPSP and PS signals were

amplified 1000 times with an AC amplifier (Molecular Devices), bandpass filtered at 1000 Hz, digitized at 10 kHz using a Digidata 1440A interface board (Axon Instruments), and transferred to a computer with Clampex 10.0 (Molecular Devices). Results were analyzed using Clampfit 10.0 (Molecular Devices). Baseline synaptic responses were established by evoking fEPSPs every 30 s (0.033 Hz) for 20 min. Field EPSP and PS were quantified by initial slope and amplitude respectively. The fEPSP slope was normalized to the mean of baseline. The mean normalized fEPSP slope was plotted as a function of time with every dot representing the average of 4 sweeps (2 minutes) and error bars representing SEM. Statistics were based on mean values of 8 sweeps within 4 minutes around the chosen time point.

Data analysis and statistics

All values shown are the mean ± standard error of mean. For field recording data, baselines or controls are set as 100%, and N is the number of experiments conducted. One hippocampal slice was used for each experiment. Statistical significance was assessed using One-way ANOVA, and differences between means were determined by Tukey's multiple comparison post-hoc analysis. (*: $p<0.05$; **: $p<0.01$; ***: $p<0.001$, ****: $p<0.0001$).

Drugs and Reagents

LPS (E. coli 0111:B4, Sigma); IL-1β from rat (Peprotech Inc.); IL1ra (Sigma); 2DG (D8375-5G, Sigma).

B.2 Chapter 5 additional figures

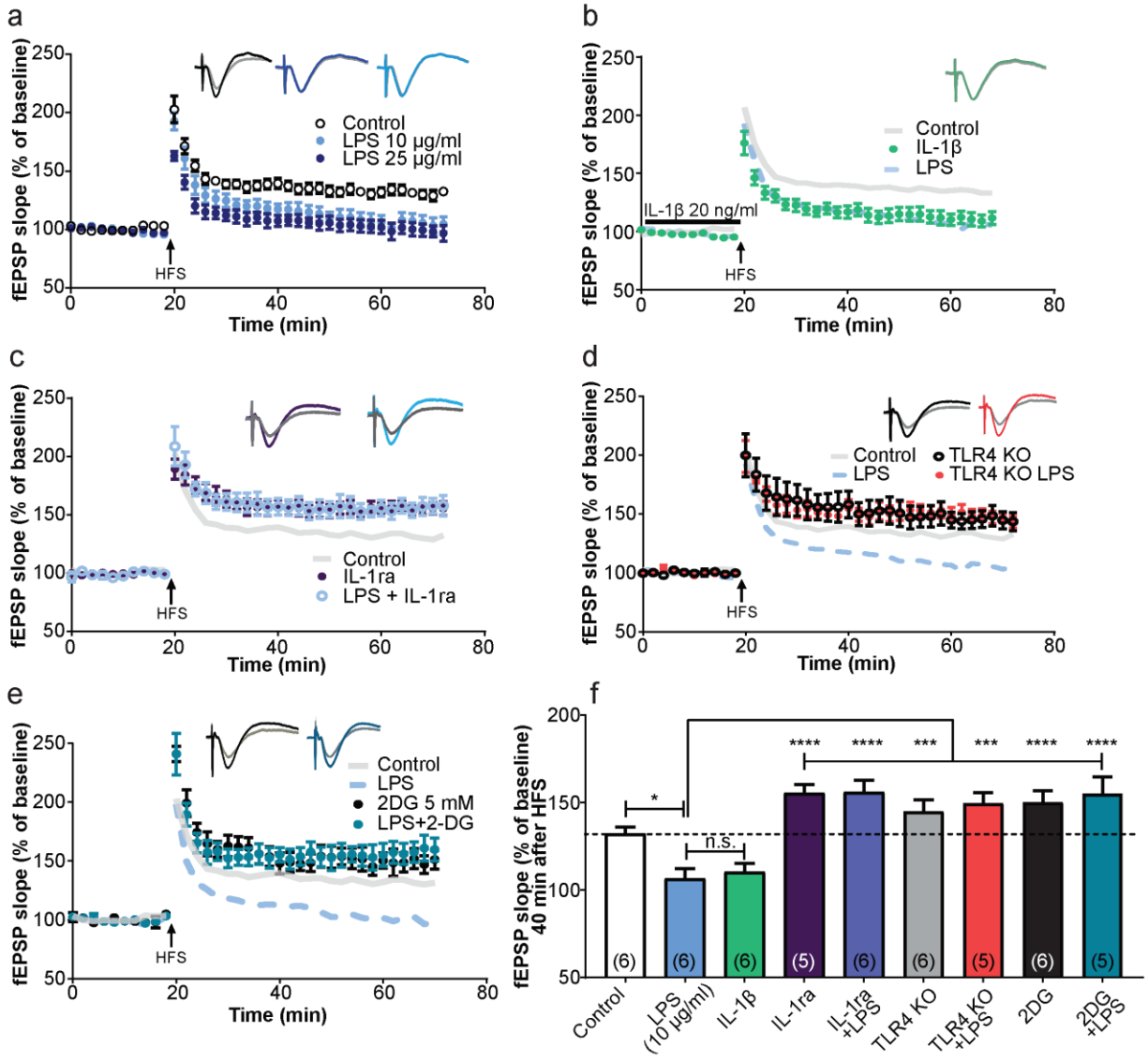

Figure B.2.1 LPS inhibits LTP through IL-1β in a TLR4-mediated and metabolically-dependent manner.

(a) In conditions of 10 or 25 µg/ml LPS, acute hippocampal slices no longer undergo LTP from high-frequency stimulation (HFS). Insets show fEPSP responses before (gray trace), or after (colored trace) HFS-induced LTP. LPS-inhibition of LTP is replicated by direct application of IL-1β (b), and is rescued by IL-1R antagonist (c). (d) In TLR4 KO mice, LPS-induced inhibition of LTP is rescued to control levels. (e) Application of 5 mM 2DG also prevents the LPS inhibition of LTP. (f) Quantification of fEPSP slope 40 minutes after HFS-induced LTP. Numbers represent N

values, error bars are mean +/- SEM. *p<0.05, ***p<0.001, ****p<0.0001 by One-way ANOVA and Tukey's multiple comparison.